Hydrologic Budget of the Harney Basin Groundwater System, Southeastern Oregon

Scientific Investigations Report 2021–5128
Version 1.1, November 2022

Cover:
Background: Steens Mountain near the basin divide, as seen looking southwest near Steens Mountain summit, Harney Basin, southeastern Oregon. Photograph by Hank Johnson, U.S. Geological Survey, July 2017.

Foreground:
Top Left: Harney Basin lowlands as seen looking west from the Stinkingwater Mountains, Harney Basin, southeastern Oregon. Photograph by Amanda Garcia, U.S. Geological Survey, April 2018. **Top right:** Silver Creek At McCanlies Road as seen looking downstream (southwest), Harney Basin, southeastern Oregon. Photograph by Amanda Garcia, U.S. Geological Survey, October, 2016. **Bottom left:** Groundwater evapotranspiration area, Warm Springs Valley, Harney Basin, southeastern Oregon. Photograph by Hank Johnson, U.S. Geological Survey, July 2017. **Bottom right:** Barnyard Spring as seen looking east, OO Ranch, Harney Basin, southeastern Oregon. Photograph by Hank Johnson, U.S. Geological Suvey, July 2017.

Hydrologic Budget of the Harney Basin Groundwater System, Southeastern Oregon

By C. Amanda Garcia, Nicholas T. Corson-Dosch, Jordan P. Beamer, Stephen B. Gingerich, Gerald H. Grondin, Brandon T. Overstreet, Jonathan V. Haynes, and Mellony D. Hoskinson

Scientific Investigations Report 2021–5128
Version 1.1, November 2022

U.S. Department of the Interior
U.S. Geological Survey

U.S. Geological Survey, Reston, Virginia: 2022

Acknowledgments

Contents

Figures

Tables

Conversion Factors

U.S. customary units to International System of Units

Multiply	By	To obtain
Length		
inch (in.)	2.54	centimeter (cm)
foot (ft)	0.3048	meter (m)
mile (mi)	1.609	kilometer (km)
Area		
acre	4,047	square meter (m^2)
acre	0.004047	square kilometer (km^2)
square foot (ft^2)	929.0	square centimeter (cm^2)
square mile (mi^2)	259.0	hectare (ha)
Volume		
gallon (gal)	3.785	liter (L)
cubic foot (ft^3)	28.32	cubic decimeter (dm^3)
acre-foot (acre-ft)	1,233	cubic meter (m^3)
Flow rate		
acre-foot per day (acre-ft/d)	0.01427	cubic meter per second (m^3/s)

Multiply	By	To obtain
acre-foot per year (acre-ft/yr)	0.00138128	cubic meter per year (m^3/yr)
foot per day (ft/d)	0.3048	meter per day (m/d)
foot per year (ft/yr)	0.3048	meter per year (m/yr)
cubic foot per second (ft^3)	0.02832	cubic meter per second (m^3/s)
cubic foot per day (ft^3/d)	0.02832	cubic meter per day (m^3/d)
Hydraulic conductivity		
foot per day (ft/d)	0.3048	meter per day (m/d)
Transmissivity		
foot squared per day (ft^2/d)	0.09290	meter squared per day (m^2/d)

International System of Units to U.S. customary units

Multiply	By	To obtain
Length		
centimeter (cm)	0.3937	inch (in.)
millimeter (mm)	0.03937	inch (in.)
meter (m)	3.281	foot (ft)
kilometer (km)	0.6214	mile (mi)
Area		
square meter (m^2)	0.0002471	acre
hectare (ha)	2.471	acre

Temperature in degrees Fahrenheit (°F) may be converted to degrees Celsius (°C) as follows:

$$°C = (°F - 32) / 1.8.$$

Datums

Vertical coordinate information is referenced to the North American Vertical Datum of 1988 (NAVD 88).

Horizontal coordinate information is referenced to the North American Datum of 1983 (NAD 83).

Elevation, as used in this report, refers to distance above the vertical datum.

Supplemental Information

Transmissivity: The standard unit for transmissivity is cubic foot per day per square foot times foot of aquifer thickness [(ft^3/d)/ft^2]ft. In this report, the mathematically reduced form, foot squared per day (ft^2/d), is used for convenience.

Specific conductance is given in microsiemens per centimeter at 25 degrees Celsius (µS/cm at 25 °C).

Concentrations of chemical constituents in water are given in either milligrams per liter (mg/L) or micrograms per liter (µg/L).

Stable-isotope ratios are reported as delta (δ) values, which are parts per thousand or permil (‰) difference(s) from a standard.

Abbreviations

BFI	base-flow index
BFI-LF$_{ave}$	average of base-flow index and low-flow base-flow estimates
BLM	Bureau of Land Management
bls	below land surface
COOP	Cooperative Observer Network
EROS	Earth Resources Observation and Science
ET	evapotranspiration
ET$_c$	corrected evapotranspiration
ET$_g$	groundwater evapotranspiration
ET$_{irr}$	evapotranspiration of irrigation water
ET$_{net}$	net evapotranspiration
ETN+	Enhanced Thematic Mapper Plus (Landsat 7 dataset)
ET$_o$	grass-reference evapotranspiration
ET$_r$	alfalfa-reference evapotranspiration
ET$_{sw}$	surface-water evapotranspiration
ET*	normalized net evapotranspiration
EVI	Enhanced Vegetation Index
GETA	groundwater evapotranspiration area
GridMET	the gridded meteorological data of Abatzoglou (2013)
LaSRC	Land Surface Reflectance Code
LEDAPS	Landsat Ecosystem Disturbance Adaptive Processing System
METRIC	Mapping Evapotranspiration using high Resolution and Internalized Calibration
MNDWI	modified normalized difference water index
MNWR	Malheur National Wildlife Refuge
NAIP	National Agricultural Imagery Program
NDMI	normalized difference moisture index
NDVI	normalized difference vegetation index
ORBIC	Oregon Biodiversity Information Center
OLI	Operational Land Imager
OWRD	Oregon Water Resources Department
PEST	Parameter ESTimation
PRISM	Parameter-elevation Regressions on Independent Slopes Model
r^2	coefficient of determination
RMS	root-mean-square

SNOTEL	Snowpack Telemetry Network
SWB	Soil-Water-Balance model
SWE	snow-water equivalent
TM	Thematic Mapper
TOA	top of atmosphere
USFS	U.S. Forest Service
USGS	U.S. Geological Survey
USFWS	U.S. Fish and Wildlife Service
WRS2	Worldwide Reference System-2
WY	water year (The 12-month period from October 1 of any given year through September 30 of the following year. The water year is designated by the calendar year in which it ends.)

Hydrologic Budget of the Harney Basin Groundwater System, Southeastern Oregon

By C. Amanda Garcia[1], Nicholas T. Corson-Dosch[1], Jordan P. Beamer[2], Stephen B. Gingerich[1], Gerald H. Grondin[2], Brandon T. Overstreet[1], Jonathan V. Haynes[1], Mellony D. Hoskinson[2]

Abstract

Groundwater-level declines and limited quantitative knowledge of the groundwater-flow system in the Harney Basin prompted a cooperative study between the U.S. Geological Survey and the Oregon Water Resources Department to evaluate the groundwater-flow system and budget. This report provides a hydrologic budget of the Harney Basin groundwater system that includes separate groundwater budgets for upland and lowland areas to avoid double counting water that recharges in the uplands, discharges to streams and springs in the uplands, flows downstream to the lowlands, and recharges the lowland groundwater system. Lowlands generally represent the conterminous valleys within the center of the basin, including floodplains of the major streams and uplands represent all other areas in the basin.

The upland groundwater budget is minimally affected by groundwater development and generally represents the budget of the natural system. In upland areas during 1982–2016, mean-annual recharge totaled 288,000 acre-feet (acre-ft) and mean-annual discharge totaled 239,000 acre-ft, resulting in a net recharge of 49,000 acre-ft. Upland groundwater recharge occurs as infiltration of precipitation and snowmelt and was estimated using the USGS Soil-Water-Balance model calibrated to estimates of runoff, evapotranspiration (ET), base flow, and snow-water equivalent. Groundwater discharge to streams is the predominant discharge mechanism in upland areas and was estimated as 225,000 acre-feet per year (acre-ft/yr) during 1982–2016 using hydrograph separation and summer low-flow estimates in streamgaged watersheds and a linear relation between estimated streamflow and base flow in ungaged watersheds. The remaining upland discharge occurs through springs (14,000 acre-ft/yr) that either emerge down-gradient of locations where groundwater discharge to streams was estimated or are routed to irrigated areas. Spring discharge was estimated as a compilation of current and historical measurements. The net upland recharge, which is 17 percent of total upland recharge, ultimately recharges lowland areas as groundwater flow from uplands to lowlands.

The lowland groundwater budget for the Harney Basin represents a combination of natural conditions and human activity as more than 99 percent of groundwater development has occurred either inside or within 2 miles of the lowland boundary. In lowland areas during 1982–2016, mean annual groundwater recharge totaled 173,000 acre-ft and groundwater discharge totaled 283,000 acre-ft, indicating discharge exceeded recharge by more than 60 percent.

Excluding groundwater pumping, the lowland groundwater budget is more in balance with a mean annual recharge of 165,000 acre-ft and a mean annual discharge of 131,000 acre-ft during 1982–2016. The 23-percent difference between non-pumping recharge and discharge mostly represents the cumulative uncertainty in the estimates of the various groundwater budget components but also likely includes a small reduction in natural groundwater discharge captured by pumping. Lowland groundwater is predominantly recharged by infiltration of surface water (116,000 acre-ft/yr) through streams, floodwater, and irrigation, with a lesser amount as groundwater inflow from uplands and minimal recharge beneath Malheur and Harney Lakes. Recharge from streams and floodwater (natural and irrigation) was estimated using a balance of measured and estimated surface-water inflow to and outflow from lowland areas including streamflow, springflow, and ET where a portion of surface-water inflow to lowland areas is comprised of upland discharge to streams and springs. Groundwater ET (119,000 acre-ft/yr) is the predominant natural discharge mechanism in lowland areas and was estimated as the mean from two remote-sensing based approaches incorporating groundwater ET measurements from other similar basins and 23 years (1987–2015) of Landsat imagery. Discharge of lowland groundwater into Malheur and Harney Lakes is about 700 acre-ft/yr and is represented in groundwater ET estimates. The remaining natural groundwater discharge from lowland areas issues from Sodhouse Spring (8,900 acre-ft/yr) and as groundwater flow to the Malheur River Basin through Virginia Valley (3,100 acre-ft/yr). The relatively large amount of groundwater discharged to springs in Warm Springs Valley (25,000 acre-ft/yr) is accounted for in groundwater ET estimates. Natural groundwater discharge in lowland areas of the Harney Basin has remained relatively constant during the last 80 years based on comparisons with estimates north of Malheur Lake and west of Harney Lake published in the 1930s.

---

[1]U.S. Geological Survey

[2]Oregon Water Resources Department

Annual net amount of groundwater pumped (pumpage) from the Harney Basin during 2017–18 averaged 144,000 acre-ft. The net value is the difference between pumpage (about 152,000 acre-ft/yr) and reinfiltration of groundwater pumped for irrigation and non-irrigation purposes (about 8,000 acre-ft/yr). Net pumpage was estimated in concurrent studies that compiled groundwater-use data and coupled reported groundwater pumpage data from wells with remote-sensing-based ET estimates from groundwater-irrigated fields. Total pumpage for irrigation has increased from about 54,000 acre-ft/yr during 1991–92 to 145,000 acre-ft/yr during 2017–18. Presently, pumpage is greatest in the lowland region north of Malheur Lake (81,000 acre-ft/yr), with lesser amounts to the north and northwest of Harney Lake (41,000 acre-ft/yr) and to the south and east of Malheur Lake (22,000 acre-ft/yr).

During this study, mean annual lowland groundwater discharge (including pumpage) exceeded mean annual recharge, indicating that the lowland hydrologic budget is out of balance. Net groundwater pumpage during 2017–18 is similar to groundwater discharge from all other sources in the lowlands and is four times the imbalance between non-pumping lowland recharge and discharge (34,000 acre-ft/yr). Declining groundwater levels at depth across many parts of the Harney Basin lowlands indicate that pumpage is depleting aquifer storage and is likely capturing a small amount of natural groundwater discharge to springs and ET in some lowland areas. If pumping continues, aquifer storage depletion will continue until the capture rate of natural discharge to springs and ET is equal to the pumping rate. If groundwater development occurs in upland areas and reduces either the streamflow or groundwater inflow to lowland areas, the deficit in the lowland water budget will increase.

Introduction

Increasing groundwater development for crop irrigation in the Harney Basin since the early 1990s has resulted in substantial groundwater-level declines beneath lowland areas. By 2015, annual permitted groundwater use in the Harney Basin totaled 287,000 acre-feet (acre-ft; Oregon Water Resources Department, 2015). Recognizing that declining groundwater levels might indicate groundwater over-appropriation, the Oregon Water Resources Department (OWRD) adopted Administrative Rule 690-512-0020 in April 2016, which put a moratorium on permits for additional groundwater development until an improved understanding of the groundwater-flow system is available (Oregon Water Resources Department, 2016).

Prior to this study, knowledge of the Harney Basin groundwater-flow system was limited to specific parts of the basin. Hydraulic connections across the basin and the extent to which existing groundwater development might affect nearby groundwater and surface-water resources were poorly understood. With increasing resource demand across the basin, the limited hydrologic understanding proved inadequate to accurately evaluate the sustainability of permitted groundwater uses and potential for additional groundwater development. In 2016, OWRD and U.S. Geological Survey (USGS) entered into a cooperative agreement to conduct a comprehensive study of the Harney Basin groundwater-flow system. The phased objectives of this study are to develop a conceptual and quantitative understanding of the Harney Basin groundwater-flow system (phase 1) and develop a numerical hydrologic model to test and refine the conceptualized groundwater system and accurately simulate its response to historical pumping, current conditions, and future groundwater development scenarios (phase 2). This report is one part of phase 1, and it describes the hydrologic budget for the Harney Basin groundwater system.

Purpose and Scope

This report provides a basin-wide hydrologic budget for the Harney Basin groundwater system. The hydrologic budget includes estimates of all groundwater recharge and groundwater discharge components in upland and lowland areas and for each of the major stream-drainage basins, providing an understanding of the fate of groundwater from entry to exit. The report integrates information from previous studies with data collected and generated during the current study. This report presents two groundwater budgets for the Harney Basin: one for upland areas and one for lowland areas. The development of two separate budgets avoids the issue of double counting water that infiltrates, discharges, and reinfiltrates in a different part of the basin. A full basin-wide account of all budget components is particularly useful for numerical simulation of all hydrologic physical processes in the groundwater system; however, basin-wide budget estimates are not useful for groundwater use, development, or management purposes because the sum of all recharge (or discharge) components necessarily double counts water that flows into, out of, and back into the system. The upland groundwater budget provides practical information about inflow and outflow components relevant to hydrologic study of upland areas at local and watershed scales. The lowland groundwater budget describes the inflow and outflow components of the groundwater system where nearly all groundwater development and use has occurred. The lowland groundwater budget can help water-resource managers and water users evaluate the outcome of groundwater-management decisions.

Groundwater recharge and discharge were estimated for the period during 1982–2016 (hereinafter referred to as "the study period") from precipitation, streamflow, evapotranspiration (ET), springflow, and groundwater pumpage data with various periods of availability. Some of the periods referred to in this report include 1991–2018 for pumpage (groundwater pumped from wells), 1903–2017 for springflow, 1900–2016 for long-term precipitation, 1981–2010 for 30-year mean precipitation, and 1987–2015 for natural ET estimates.

Groundwater recharge estimates include infiltration of precipitation and snowmelt through soils in upland mountain areas, infiltration of streams, floodwater, and lake water in lowland areas, and infiltration of irrigation and non-irrigation pumpage. Groundwater-discharge estimates include groundwater discharge by ET from natural vegetation in lowland areas, groundwater discharge to springs, streams, and lakes, groundwater outflow to the Malheur River Basin, and pumpage for irrigation and other uses. Groundwater-recharge estimates are constrained by multiple components of groundwater discharge, including discharge to springs, streams, and pumpage for irrigation. Therefore, groundwater-discharge components are presented first, followed by groundwater-recharge components.

The information contained herein builds upon and complements four other reports describing the Harney Basin hydrologic system. The physical hydrology and geochemistry of the groundwater-flow system and summary of the budget presented in this report are provided in Gingerich and others (2022), the geology of the Harney Basin is described in Boschmann (2021), irrigation pumpage is provided in Beamer and Hoskinson (2021), and non-irrigation pumpage is summarized in Grondin (2021).

Study Area

The Harney Basin is a closed surface-water basin that encompasses about 5,240 square miles (mi^2) in southeastern Oregon (fig. 1). The basin covers most of Harney County and includes small parts of Grant, Lake, and Crook Counties. For discussion and analysis purposes in this report, the Harney Basin was divided into three regions (northern, southern, and western), each dominated by one of the three major streams and including tributary and similar watersheds (fig. 1). Regions are based on topography in the uplands where only minor groundwater interactions between regions are likely, allowing for evaluation of water resources independently. In the lowlands, regions are based on presumed groundwater-flow paths during 2018 hydrologic conditions (Gingerich and others, 2022). Pumping-induced changes in hydrologic

conditions could cause changes in the region boundaries in the lowlands, but they are considered steady for the purposes of water-budget accounting in this report. The Harney Basin represents the surface-water drainage area of three adjacent terminal lakes, Malheur Lake, Harney Lake, and Mud Lake, which are fed primarily by the watersheds of the Silvies River (most of the northern region), the Donner und Blitzen River (most of the southern region), and Silver Creek (most of the western region). The Silvies River flows southward from the Blue Mountains, the Donner und Blitzen River flows northward from Steens Mountain, and Silver Creek flows southeastward from the Blue Mountains onto the Harney Basin lowlands. For this report, the Harney Basin lowlands (hereinafter referred to as "lowlands" or "lowland areas") refers to the general extent of Quaternary alluvial, lacustrine, and aeolian deposits (about 1,070 mi^2) within the center of the basin including the floodplains of Silver Creek, the Silvies River, and the Donner und Blitzen River and their tributaries (fig. 1). The lowlands generally correspond to the area where groundwater ET occurs (see section "Groundwater Evapotranspiration Area"). The Harney Basin uplands (hereinafter referred to as "uplands" or "upland areas") represent all areas within the Harney Basin that are not within the lowland delineation. While the Harney Basin is a closed surface-water basin, a small fraction of groundwater leaves the study area, primarily through Virginia Valley and into the Malheur River Basin.

Land cover in the Harney Basin is predominately sagebrush steppe, which covers much of the central and southern portion of the basin. Large areas of greasewood (*Sarcobatus vermiculatus*) and saltgrass (*Distichlis spicata*) surround the many playas in the lowest elevations of the basin. The sagebrush-steppe community transitions to ponderosa pine (*Pinus ponderosa*) forests and mountain meadows in the Blue Mountain uplands northward and transitions to alpine grasslands and meadows on Steens Mountain southward. Nearly 70 percent of the land in the Harney Basin is publicly owned and managed by various Federal and State agencies, including the Bureau of Land Management (BLM), U.S. Forest Service (USFS), the U.S. Fish and Wildlife Service (USFWS), and Oregon Department of State Lands.

The USFWS manages the 293-mi^2 Malheur National Wildlife Refuge (MNWR), which includes Malheur Lake, Harney Lake, and adjacent marshlands (fig. 1). Privately owned land is concentrated in the lowlands of the basin and is largely devoted to grazing and irrigated agriculture (primarily hay production). More than half of the approximately 7,500 basin residents live in the cities of Burns and Hines with the remainder settled in small communities and on ranches across the basin.
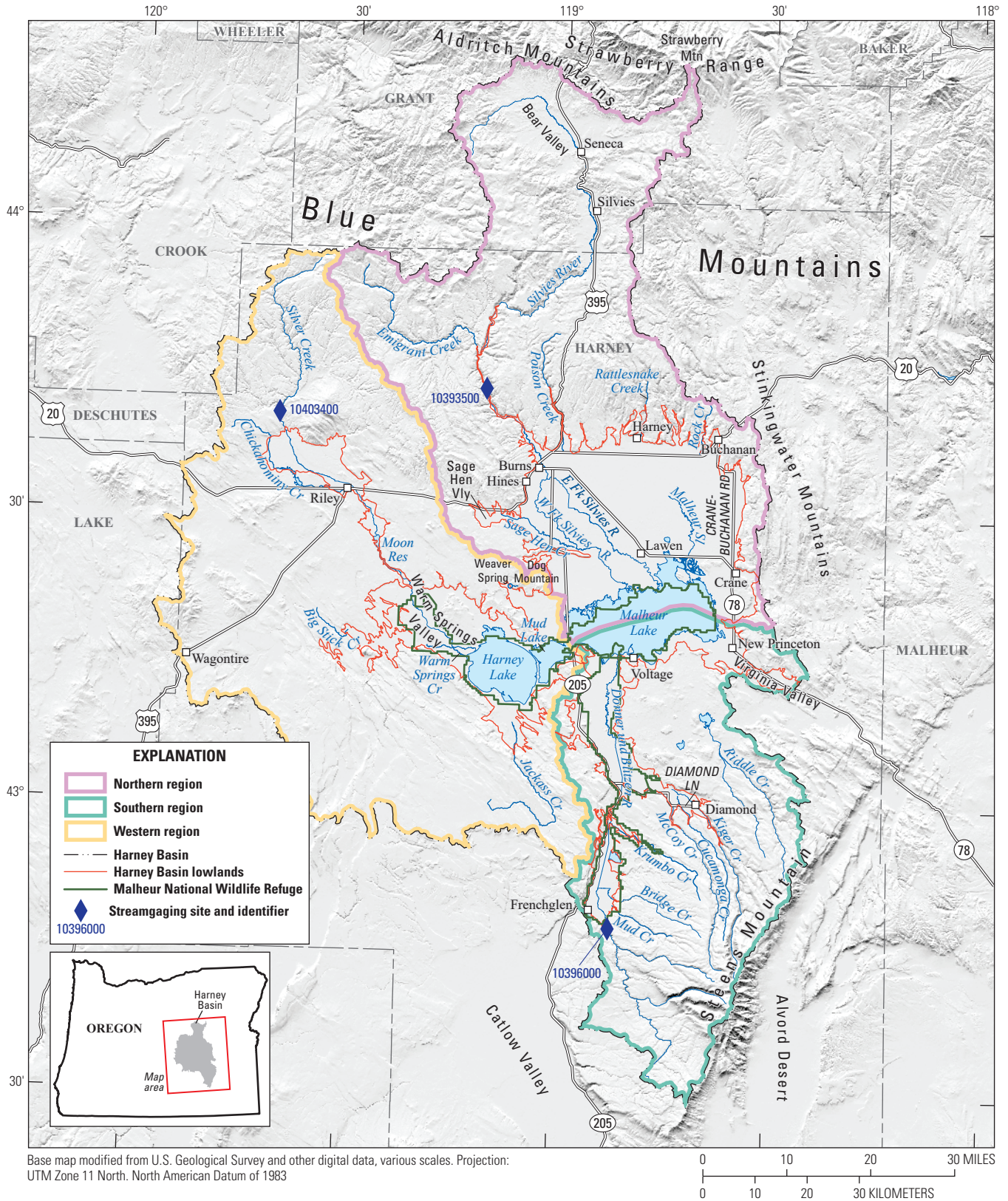
Figure 1.   Location of the Harney Basin, southeastern Oregon, and its major geographic and cultural features. Northern, southern, and western regions are included for discussion and analysis purposes.

Previous Investigations

Russell (1903) published the first investigations of groundwater in the Harney Basin, briefly mentioning a few springs and wells in a general report on southeastern Oregon hydrogeology. Waring (1908, 1909) completed the earliest comprehensive study of Harney Basin hydrology, including discussions about soils, geology, vegetation, and surface and groundwater resources. Piper and others (1939) conducted a 3-year investigation of the basin's water resources, which greatly expanded and revised Waring's preliminary investigations. These studies first recognized that (1) surface water from the Silvies River alluvial fan provides most of the recharge to the groundwater system beneath the lowlands north of Malheur Lake, (2) ET by phreatophytic vegetation, or deep-rooted plants that consume groundwater, is the primary mechanism for groundwater discharge in the lowlands north of Malheur Lake, (3) the shallow and deep groundwater systems beneath the northern lowlands have different responses to pumping and recharge, and (4) prior to any substantial groundwater development, groundwater levels in deep alluvial sediments beneath northern lowland areas rose in response to the weight of springtime floodwater, but this response did not reflect direct infiltration of that water to the deeper sediments. Piper and others (1939) made the first estimates of recharge to parts of the basin lowlands using estimates of groundwater storage, groundwater discharge, and a balance of streamflow and ET across lowland areas. Mean groundwater-recharge estimates to lowland areas ranged from 86,000 to about 170,000 acre-ft/yr. Robison (1968) estimated 260,000 acre-ft/yr of recharge from precipitation, ranging from 60,000 acre-ft/yr along the Silver Creek drainage and other areas draining to Harney Lake to 100,000 acre-ft/yr in both the Silvies and Donner und Blitzen River drainages. A study of Malheur Lake by Hubbard (1975) concluded that groundwater seepage into and out of the lake was negligible (less than 1 percent of the lake budget). Leonard (1970) and Aquaveo, LLC (2012), updated groundwater-level maps for the basin. Aquaveo, LLC (2012), made a preliminary basin-wide recharge estimate of 360,000 acre-ft/yr based on a deep-percolation model (Bauer and Vaccarro, 1987) and recommended a program of groundwater-use reporting and development of a groundwater-flow model of the basin.

Physical Setting

The Harney Basin is a broad depression located at the intersection of the Oregon High Lava Plains, the Blue Mountains, and the Basin and Range physiographic provinces (Dicken, 1950; Walker, 1977; Eaton, 1982). The basin lies at a relatively high altitude with valley floor elevations above 4,000 feet, benchland elevations averaging 4,500 feet, and adjacent mountain elevations up to 9,700 feet (Oregon Water Resources Board, 1967).

Climate

The climate of the Harney Basin is semi-arid and characteristic of a high desert region with mild summers and cool winters. Precipitation is highest in the uplands (fig. 2) and occurs primarily between November and May. The 30-yr (1981–2010) monthly mean temperature varied little by location and elevation, ranging from 27 °F in December to 67 °F in July at the Malheur Refuge Headquarters near Malheur Lake and from 25 °F in December to 65 °F in July at the Fish Creek Snow Telemetry (SNOTEL) station on Steens Mountain (Western Regional Climate Center, 2019; National Water and Climate Center, 2019). Total annual precipitation varies markedly across the basin with elevation; for example, 30-yr mean (1981–2010) precipitation was 10 in at Malheur Refuge Headquarters (4,110-ft elevation) and 44 in at the Fish Creek SNOTEL site (7,660-ft elevation; Western Regional Climate Center, 2019; National Water and Climate Center, 2019; fig. 2; table 1).

Comparisons between study-period (1982–2016) and longer-term (1900–2016) annual precipitation highlight the temporal and spatial variability within the Harney Basin. To facilitate these comparisons, relations between measured precipitation at five sites (representative of the range of conditions, geographic location, and measurement years in the Harney Basin) and estimates from the PRISM (Parameter-elevation Relationships on Independent Slopes Model; PRISM climate group, 2019) climate model for those locations extending back to 1900 were used to extrapolate the short-term measurements (fig. 3) (see app. 1 for more information about PRISM). In the northern uplands at the Seneca site (fig. 2; table 1), mean precipitation during the study period was 7 percent higher than the 116-year mean. Study-period mean precipitation at sites in the central lowlands (Burns Federal Building) and on the lowlands of the western basin (Northern Great Basin Experimental Range) was within 1 percent of the 116-year mean. Near the center of the Harney Basin just west of Harney Lake (Double O Ranch, also referred to as OO Ranch), precipitation over the previous century exhibited greater decadal-scale variability than other sites with few wet or dry periods lasting more than a decade. Study-period mean precipitation at the Double O Ranch site was equal to the 116-year mean. On Steens Mountain to the south, study-period mean precipitation at Fish Creek, the highest elevation site, was 9 percent below the 116-yr mean (fig. 3). The 1980s and 1990s generally were wetter than the 2000s. Excluding the Fish Creek site, the 1980s and 1990s were some of the wettest periods during the 116-yr record (fig. 3)

Table 1. Precipitation data at long-term measurement sites near the Harney Basin, southeastern Oregon.

[**Precipitation site**: Long-term measurement site from the National Weather Service (COOP) and Natural Resources Conservation Service (SNOTEL). **Elevation**: In feet above North American Vertical Datum of 1988. Latitude and longitude referenced to the North American Datum of 1983. **30-year mean precipitation**: Based on calendar year and from Natural Resources Conservation Service National Water and Climate Center. **Abbreviations**: COOP, Cooperative Observer Network; SNOTEL, Snowpack Telemetry Network; NWS, National Weather Service; NRCS, Natural Resources Conservation Service; km, kilometers; —, not estimated.]

Precipitation site	Type	Agency	Agency identifier	Elevation (feet)	Latitude (decimal degrees)	Longitude (decimal degrees)	Period of record	Site years	Measurement period precipitation (inches)	30-year mean precipitation (inches)	
										1961–90	1981–2010
Andrews 2 S	COOP	NWS	350188	4,104	42.4333	-118.6167	1915-42	24	7.09	—	—
Andrews Weston Mine	COOP	NWS	350189	4,779	42.5500	-118.5500	¹1969-93	21	17.68	—	—
Bear Valley	COOP	NWS	350574	5,000	44.2333	-119.1167	1909-30	9	14.64	—	—
Blitzen	COOP	NWS	350808	4300	42.6333	-119.0667	1915-33	10	9.20	—	—
Blue Mountain Spring	SNOTEL	NRCS	357	5,870	44.2500	-118.5200	1978-2019	40	34.09	—	33.80
Buena Vista Station	COOP	NWS	351124	4,140	43.0667	-118.8667	¹1958-91	31	8.96	9.24	10.62
Burns Federal Building	COOP	NWS	24134	4,160	43.5833	-119.0500	¹1939-79	41	11.61	—	—
Burns Junction	COOP	NWS	351174	4,140	42.7833	-117.8500	¹1973-95	20	8.76	—	—
Burns Municipal Airport	COOP	NWS	351175	4,140	43.5833	-118.9500	1981-2015	31	10.89	9.96	10.92
Dayville	COOP	NWS	352168	2,362	44.4667	-119.5333	1900-78	35	12.10	—	—
Diamond 4 WNW	COOP	NWS	352305	4,160	43.0333	-118.7500	1912-14, ¹1943-56	18	9.86	—	—
Drewsey	COOP	NWS	352415	3,515	43.8081	-118.3776	¹1970-2014	32	10.55	—	11.25
Fields	COOP	NWS	352876	4,227	42.2643	-118.6759	¹1973-2015	8	6.39	—	9.05
Fish Creek	SNOTEL	NRCS	477	7,660	42.7100	-118.6300	1978-2018	39	44.24	—	44.80
Harney Branch Experimental Station	COOP	NWS	353659	4,140	43.5833	-118.9333	1924-51	28	8.83	—	—
John Day	COOP	NWS	354291	3,063	44.4233	-118.9594	¹1903-2019	53	12.93	13.33	13.17
Long Creek	COOP	NWS	355020	3,740	44.7135	-119.1018	¹1908-2019	26	14.84	15.11	17.94
Malheur Refuge Headquarters	COOP	NWS	355162	4,110	43.2833	-118.8333	¹1959-2012	19	10.23	9.93	9.97
Double O Ranch (or "OO Ranch")	COOP	NWS	356302	4,140	43.2833	-119.3167	¹1952-2003	29	8.92	10.24	9.76
P Ranch Refuge	COOP	NWS	356853	4,210	42.8080	-118.8778	¹1897-2011	32	11.28	11.76	11.80
Prairie City	COOP	NWS	356845	3,544	44.4581	-118.7054	1911-51	25	15.14	—	—

Table 1. Precipitation data at long-term measurement sites near the Harney Basin, southeastern Oregon.—Continued

[**Precipitation site**: Long-term measurement site from the National Weather Service (COOP) and Natural Resources Conservation Service (SNOTEL). **Elevation**: In feet above North American Vertical Datum of 1988. Latitude and longitude referenced to the North American Datum of 1983. **30-year mean precipitation**: Based on calendar year and from Natural Resources Conservation Service National Water and Climate Center. **Abbreviations**: COOP, Cooperative Observer Network; SNOTEL, Snowpack Telemetry Network; NWS, National Weather Service; NRCS, Natural Resources Conservation Service; km, kilometers; —, not estimated.]

Precipitation site	Type	Agency	Agency identifier	Elevation (feet)	Latitude (decimal degrees)	Longitude (decimal degrees)	Period of record	Site years	Measurement period precipitation (inches)	30-year mean precipitation (inches)	
										1961–90	1981–2010
Riley 10 WSW	COOP	NWS	004128	4,583	43.4711	-119.6917	2003-19	15	10.30	—	11.43
Rock Springs	SNOTEL	NRCS	721	5,290	43.9800	-118.8500	1980–2018	37	18.05	—	18.10
Seneca	COOP	NWS	357675	4,660	44.1383	-118.9750	[1]1908–2018	48	12.82	13.15	13.84
Silvies	SNOTEL	NRCS	759	6,990	42.7500	-118.6900	1979–2018	38	30.51	—	—
Snow Mountain	SNOTEL	NRCS	767	6,230	43.9500	-119.5400	1978–2018	39	27.55	—	27.80
Northern Great Basin Experimental Range	COOP	NWS	358029	4,660	43.4833	-119.6833	[1]1940–77	45	10.95	10.95	11.66
Starr Ridge	SNOTEL	NRCS	789	5,250	44.2600	-119.0200	1980-2019	38	20.75	—	20.80
Sunrise Valley	COOP	NWS	358245	3,714	43.1000	-118.1667	1913-36	18	9.15	—	—
Suntex	COOP	NWS	358250	4,336	43.6000	-119.6333	[1]1967–88	19	9.40	8.94	—
Wagontire	COOP	NWS	358948	4,726	43.2500	-119.8833	[1]1960-86	21	10.74	10.26	—
Whitehorse Ranch	COOP	NWS	359290	4,380	42.3370	-118.2346	[1]1965-2006	13	8.30	8.48	—
Voltage 2 NW Sod House2	COOP	NWS	355162	4,110	43.2833	-118.8333	1959-2005	—	—	—	—

[1]Intermittent measurement years

[2]Site used for pan evaporation measurements only. Site is the same as the Malheur Refuge Headquarters, but pan evaporation data is associated with the Voltage 2 NW site name.
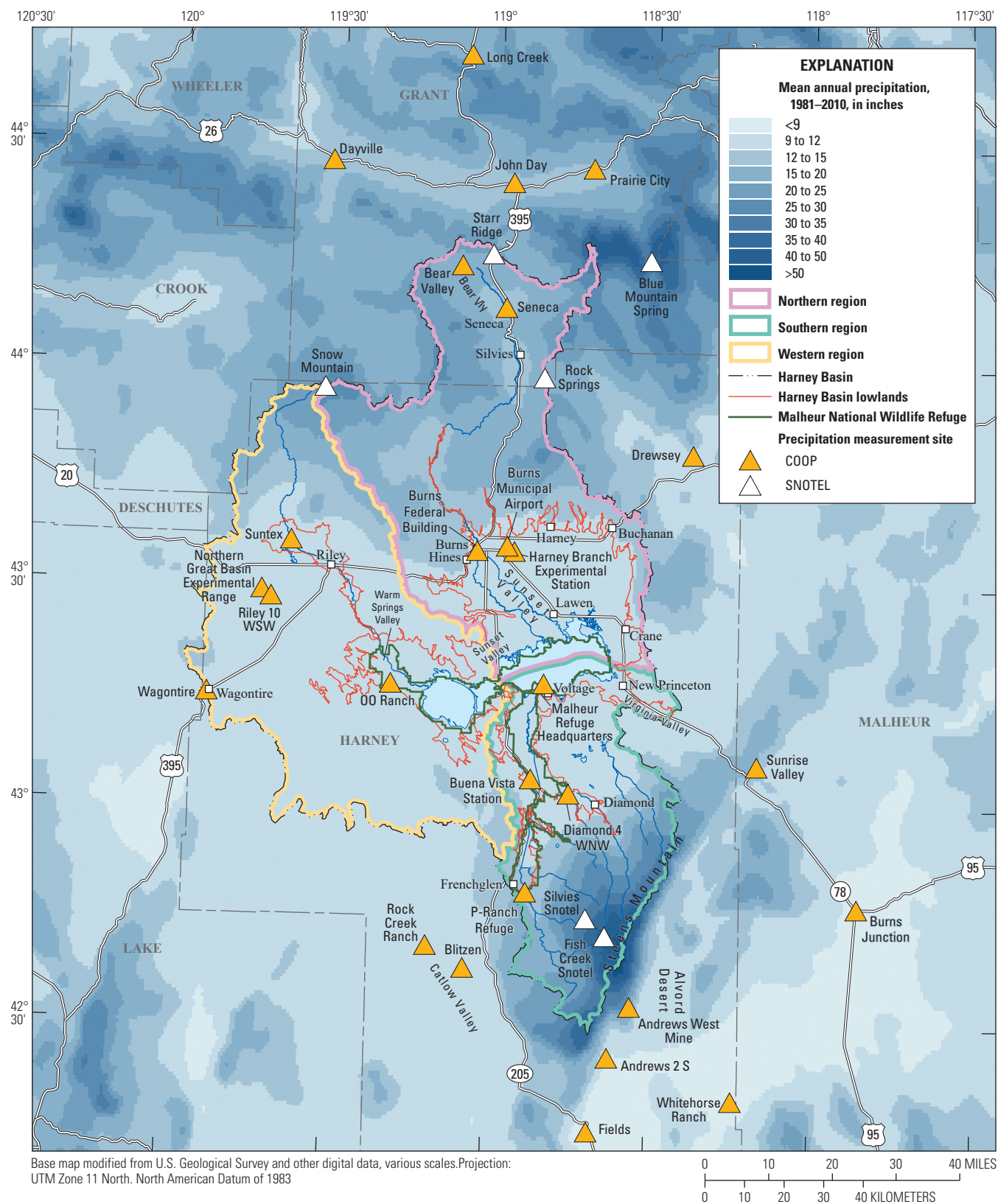
Figure 2.   Mean annual precipitation for 1981-2010 from PRISM climate model and locations of selected precipitation sites near Harney Basin, southeastern Oregon. PRISM, Parameter-elevation Relationships on Independent Slopes Model; COOP, National Weather Service Cooperative Observer Program; SNOTEL, National Resources Conservation Service Snow Telemetry.
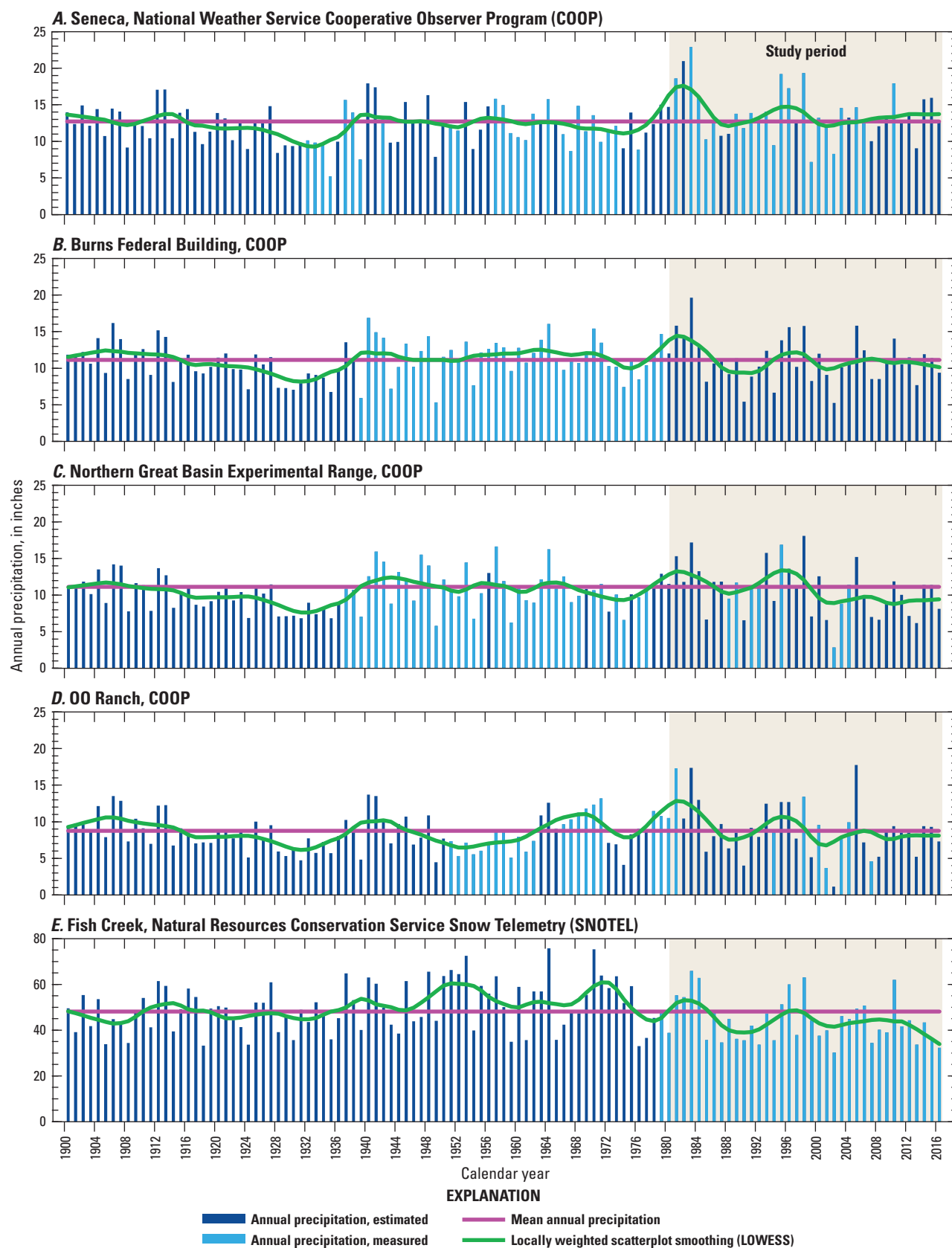
Figure 3.   Measured and estimated annual precipitation at selected sites, Harney Basin, southeastern Oregon, 1900–2016.

Surface Water

Three major streams drain the Harney Basin: Silvies River, Donner und Blitzen River, and Silver Creek (fig. 1). Headwaters of the Silvies River and Silver Creek are in the Blue Mountains in northern and western regions of the Harney Basin and the Donner und Blitzen River headwaters are on Steens Mountain in the southern region of the Harney Basin. Upon leaving the upland areas, the three streams flow across the Harney Basin lowlands and discharge into Malheur Lake (Silvies and Donner und Blitzen Rivers) or Harney Lake (Silver Creek). The Silvies River and Silver Creek are generally gaining in the uplands, where most reaches flow year-round, and generally losing in the lowlands, where their water infiltrates and recharges the shallow groundwater system. Streamflow within and among the three major streams varies widely, with the highest flows occurring during spring-time runoff and lowest flows during late summer and early autumn. Generally, streamflow in the three major streams exhibits a sharp rise during springtime and a broad decline during late-spring to mid-summer in response to snowmelt. During the low-flow period in most years, large portions of Silver Creek and Silvies River go dry between the uplands and the lakes. Most of the total annual streamflow in the Silvies River and Silver Creek is from direct runoff of precipitation and snowmelt, but during the low-flow period from July through October, streamflow is mostly from the discharge of groundwater to the main stem and tributaries in the uplands. In contrast, springs and base flow provide a larger portion of the total annual streamflow in the Donner und Blitzen River and it discharges perennially to Malheur Lake without any reaches going dry.

The northern region uplands of the Harney Basin (fig. 1) are drained by the Silvies River, which enters the Harney Basin lowlands just north of Burns. As it enters the lowlands, the Silvies River branches into braided distributaries and sloughs that ultimately converge into the East and West Fork Silvies Rivers. During springtime high flow in most years, the river spreads far beyond its distributary channels in the Harney Basin lowlands and inundates crop land and natural wet meadow and marsh areas before delivering water to Malheur Lake. Most floodwater is consumed by ET (see section "Groundwater Discharge through Evapotranspiration") and a smaller portion either percolates downward and recharges the groundwater system (see section "Groundwater Recharge") or returns to the main channels through overland flow or shallow subsurface flow. By July of most years, streamflow in the Silvies River does not reach Malheur Lake due to diminished flow from the uplands, diversion for irrigation, ET by riparian and marsh vegetation, and recharge to shallow groundwater. Flow from the Silvies River into Malheur Lake typically does not resume until the following year's springtime freshet. The northern region also includes the watersheds of many smaller creeks issuing from the uplands to the north and east of the Harney Basin lowlands north of Malheur Lake, the largest among these include Rattlesnake Creek, Rock Creek, Sagehen

Creek, and Poison Creek. Upon reaching the lowlands, these smaller creeks are either diverted for irrigation or branch into braided sloughs. Streamflow from these small streams is completely lost to ET, as recharge to shallow groundwater, or diverted for irrigation prior to reaching Malheur Lake.

In the southern region, the Donner und Blitzen River accumulates water from most of the streams that drain the northwestern side of Steens Mountain. The river transitions from the uplands to the lowlands near the town of Frenchglen, Oregon. About half of the river's annual discharge into Malheur Lake originates in the watershed of the main stem upstream of Frenchglen. The other half of the river's annual discharge into Malheur Lake originates in watersheds drained by Kiger, McCoy, Bridge, Mud, Krumbo, and Cucamonga Creeks (fig. 1), and from spring discharge and diffuse groundwater inflow to the main stem between Frenchglen and Diamond Lane. In the lowlands, most reaches of the Donner und Blitzen River and its tributaries are gaining flow from groundwater upstream of Diamond Lane and losing flow to groundwater downstream of Diamond Lane (fig. 1; Gingerich and others, 2022). Like the Silvies River to the north, the Donner und Blitzen River and its tributaries also spread beyond their channels during springtime runoff; however, unlike the Silvies River, the Donner und Blitzen River perennially flows into Malheur Lake. Downstream of Frenchglen, the channel of the Donner und Blitzen River is heavily modified, and the routing of its water is managed by USFWS through a series of canals, headgates, and laterals to distribute water to the wet meadows and marshes of the MNWR. Additional wet meadow and marsh areas are irrigated by surface-water diversions managed by private ranchers and farmers within the river valley.

The western region (fig. 1) predominantly is drained by Silver Creek, which issues from the Blue Mountains in the northwest part of the basin. Silver Creek discharges onto the Harney Basin lowlands about 10 miles northwest of Riley. Chickahominy Creek, which is intermittent, is the only notable tributary to Silver Creek in the lowlands. Silver Creek fills Moon Reservoir (about 10 miles southeast of Riley) with spring snowmelt during normal precipitation years. The channel of Silver Creek south of Moon Reservoir meanders across a low-gradient plain and joins Harney Lake near Double O Road. During late-summer and early-autumn of most years, Silver Creek flows intermittently downstream of Riley owing to irrigation diversions, infiltration to groundwater, reduced flow from the uplands, and riparian ET. Warm Springs Creek, with headwaters in Warm Springs Valley (fig. 1), also discharges into Harney Lake and nearly all its flow originates from high-volume springs. In the absence of measurements, anecdotal evidence and a time series of satellite imagery indicate Warm Springs Creek perennially flows into Harney Lake during most years. Big Stick and Jackass Creeks, south and west (respectively) of Warm Springs Valley and Harney Lake, are intermittent along much of their course and rarely reach the valley lowlands (Piper and others, 1939).

Malheur, Harney, and Mud Lakes occupy the center of the Harney Basin and serve as the terminus of the surface-water flow system (fig. 1). During wet years, Malheur Lake spills into Mud Lake, which in turn spills into Harney Lake. Harney Lake is the basin sump with a lake-bed elevation roughly 10 ft below the lakebed of Malheur Lake (Philips and Van Denburgh, 1971). Malheur Lake and the contiguous wet-lands surrounding it are one of the largest freshwater marshes in the United States (Hubbard, 1975) and are fed primarily by discharge from the Silvies and Donner und Blitzen Rivers. During extremely wet years, Ninemile Slough also discharges into Malheur Lake through Malheur Slough from the north (Hubbard, 1989). Harney Lake is considerably more saline than Malheur Lake (Philips and Van Denburgh, 1971; Rinella and Schuler, 1992) and is fed primarily by Silver Creek and Warm Springs Creek to the west but receives overflow from Mud Lake during extremely wet years.

Malheur, Mud, and Harney Lakes collectively are drained through evaporation and go dry during extreme droughts (Piper and others, 1939; Phillips and Van Denburgh, 1971; and Hubbard, 1975). During wet years, the MNWR regulates flow from Malheur Lake westward into Mud Lake through a narrow control channel called The Narrows. During extremely wet years, Mud Lake can overflow westward into Harney Lake at Sand Gap, a natural gap in sand dunes that fills and scours intermittently when overflow occurs or when modified for irrigation diversions. During 1984–86, following nearly a decade of above-average precipitation, the three lakes merged forming a continuous lake with an areal extent of more than 160,000 acres, the largest extent in the previous century (Hubbard, 1989; Hostetler and Bartlein, 1991).

Water exchange between the central lakes and the groundwater system is minimal during dry to average water years (Hubbard, 1975), but some investigators have speculated that groundwater discharges to the lakes during extremely wet years like those observed during the mid-1980s (Hamilton and others, 1986; Hubbard, 1989). Because surface-water budget estimates during the mid-1980s were unable to fully account for lake inflow, groundwater discharge was assumed to con-tribute to the observed lake extent. Hubbard (1989) noted that discrepancies in the mid-1980s surface-water budgets could be attributed to unmeasured streams and unmeasured base flow between streamgaged sites and the flooded lake. Although seepage from the groundwater system to the lakes through lakebed sediments is limited by thick, low-permeability clay and peat-rich lakebed sediments that underlie the lakes (Piper and others, 1939; Hubbard, 1975), low-volume springs dis-charging within the lake beds are visible in aerial images taken during low lake levels.

Groundwater

The Harney Basin contains a single, predominantly closed, groundwater-flow system, and has little exchange with surrounding groundwater basins. Generally, groundwater flows from the uplands toward Harney and Malheur Lakes and is controlled by the distribution of precipitation and the geology and hydrostratigraphy underlying the basin. The areas receiving the most precipitation, and hence the largest sources of groundwater recharge, are the Blue Mountain uplands in the north and Steens Mountain in the south (fig. 1). The Blue Mountain uplands largely are comprised of low-permeability sedimentary, volcanic, and metamorphic rocks that promote runoff of rainfall and snowmelt and limit the depth of recharge penetration and length of groundwater flow paths. However, in the western part the Blue Mountains north and west of Riley, Dry Mountain lavas and High Lava Plains basalt likely have high-permeability zones that promote greater recharge and longer groundwater-flow paths. Steens Mountain is underlain by a thick sequence of moderately permeable northwestward-dipping basaltic lava flows that allow for greater recharge through infiltration of rainfall and snowmelt, but a large portion of recharged groundwater on Steens Mountain is intercepted by the streams and springs that occupy deeply incised valleys, many of which were carved by glaciers during the Pleistocene between 2.5 million and 12,000 years ago. Although the hydrogeology is different between the northern and southern uplands, most of the upland recharge reemerges as mountain streamflow upstream of the upland/lowland boundary. Hydraulic gradients indicate that groundwater also might flow from the west into west-central Harney Basin, but adjoining western areas are substantially drier than the Harney Basin, therefore groundwater inflow from the west likely is a minor component of the groundwater budget and was not considered further in this study (Gingerich and others, 2022).

The Harney Basin lowlands are underlain by up to several hundred feet of unconsolidated sedimentary deposits, which are in turn underlain by a thick sequence of complexly interfingering volcanic and sedimentary deposits, includ-ing lava flows, air-fall and ash-flow tuffs, and volcanically derived sedimentary rocks. Generally, the permeability of the lowland deposits is low; however, deposits having higher permeability are present locally, including the outer margins of the Harney Basin lowlands such as the Weaver Spring/Dog Mountain area, Virginia Valley, and beneath the Silver Creek/Chickahominy Creek floodplain north of U.S. Highway 20. Infiltration of streamflow into the basin-fill deposits is the principal source of groundwater recharge to the lowland groundwater system (fig. 1), although some groundwater does flow directly from the upland areas into the deposits underlying the lowlands. Within the lowlands, most natural groundwater discharge is to springs or through ET, but a small amount bypasses the lakes and exits the basin through Virginia Valley toward the Malheur River Basin. A substantial amount of discharge also occurs through groundwater pumping for irrigation and other uses.

Groundwater pumping for irrigation in the Harney Basin lowlands can cause moderate to extensive depressions in groundwater levels (or drawdown) depending on the permeability of underlying deposits. Areas in the Harney Basin lowlands with substantial groundwater-level depressions are the Weaver Spring/Dog Mountain area, near Crane, and the northeastern floodplains between Burns and Buchanan along U.S. Highway 20 (fig. 1); declines of 1.5–7 ft/yr were observed in these three areas during 2010–19 (Gingerich and others, 2022). In contrast, more modest groundwater-level declines were observed in Virginia Valley along the southeastern edge of the Harney Basin (up to 10 ft during 2010–19) and in the upper Silver Creek floodplain near Riley (less than 10 ft since 1980) (Gingerich and others, 2022). Smaller, localized groundwater-level depressions have formed around other individual wells or groups of wells throughout the lowlands (for more detail see Gingerich and others, 2022). Groundwater levels in most shallow wells (less than 100-ft deep) in the Harney Basin lowlands have exhibited gradual declines of less than a few feet since the early 1990s (similar to well HARN0052234 in fig. 4) compared to steeper declines (tens of feet) in deep wells near pumping areas (similar to wells HARN0052235 and HARN0052631 in fig. 4; Gingerich and others, 2022).

Differences in groundwater levels between shallow and deep parts of the groundwater system are largely controlled by the vertical permeability of the deposits. The vertical permeability of deposits underlying lowland areas is variable, but generally low. The vertical permeability of the thick sequences of clay and silt lake deposits near the basin center preclude substantial vertical movement of groundwater in this area (Gingerich and others, 2022). Low-permeability deposits between Younger and Older basin fill or proximal to permeable deposits underlying lowland areas can mask pumping-induced drawdown at depth by attenuating the pumping signal and giving the appearance of separate groundwater systems. This effect is evident in the groundwater levels at adjoining well pair HARN0052234 and HARN0052235 (fig. 4), where deep groundwater levels fluctuate by more than 40 ft in response to pumping at depth, and shallow groundwater levels remain relatively unchanged. In areas such as the Weaver Spring/Dog Mountain area, higher vertical permeability within proximal vent deposits provides better communication between shallow and deeper parts of the system. For example, nearly coincident groundwater-level fluctuations at deep (HARN0052631) and shallow (HARN0052630) wells indicate little vertical attenuation of deep pumping signals (fig. 4). The curious reader is referred to Gingerich and others (2022) and Boschmann (2021) for greater detail on the hydrogeology and geology of the Harney Basin.

Water-Resource Development in the Harney Basin Lowlands

Surface-water and groundwater development in the Harney Basin have affected the natural groundwater-flow system differently across the basin. Several gaged streams in the Harney Basin are diverted upstream for consumptive uses and storage. The largest upstream diversions are from the Silvies River upstream of the Silvies River near Burns (USGS /OWRD streamgage 10393500) near the towns of Silvies and Seneca (fig. 1), where about 27 ft^3/s is diverted, mostly during April–June (Oregon Water Resources Department, 2018; Cooper, 2002). Although diversions upstream of the Silvies River streamgage have affected measured streamflow, the overall impact of diversions on annual streamflow measurements and base-flow estimates are largely unknown. Diversions from Silver Creek (about 0.5 ft^3/s) and Donner und Blitzen River (about 0.9 ft^3/s) occur upstream of Silver Creek near Nicoll Creek and Donner und Blitzen River near Frenchglen streamgages (OWRD and USGS streamgages 10403400 and 10396000, respectively; fig. 1) and are substantially lower than on the Silvies River. The smaller diversions upstream of Silver Creek and Donner und Blitzen River streamgages likely have a much smaller impact, if any, on annual streamflow measurements and base-flow estimates. Despite these surface-water diversions, upland recharge, which is predominantly from infiltration of precipitation and snowmelt, likely has been minimally impacted by water-resource development (on average).

In contrast, surface-water diversions and groundwater extraction in the lowlands has likely modified groundwater recharge patterns and reduced groundwater storage and discharge in many parts of the lowland groundwater system. The areal extent of surface-water irrigated agricultural fields in the northern and western region lowlands today likely exceeds the area that naturally flooded prior to development and the current volume of surface water consumed through ET from flood-irrigated agriculture likely exceeds the annual volume naturally consumed before development. On the MNWR (fig. 1) in the southern region lowlands, a system of water-management structures developed for farming in the early 1900s is used to divert streamflow to manage migratory bird habitat (Mayer and others, 2007). Marshes and meadows are flood irrigated, and irrigation water not consumed by ET returns to the stream or seeps into the groundwater system. The effects of surface-water redistribution over the last 150 years on recharge magnitude in the Harney Basin lowlands is unclear. Greater ET losses today might be equally offset by an increase in recharge from percolation beneath the larger extent of flood-irrigated areas (fig. 5). In addition to surface-water development, groundwater development likely has led to increased recharge in some areas of the Harney Basin lowlands, owing to the conversion of semi-arid shrubland into irrigated agriculture and subsequent percolation of irrigation water below the root zone in these areas.
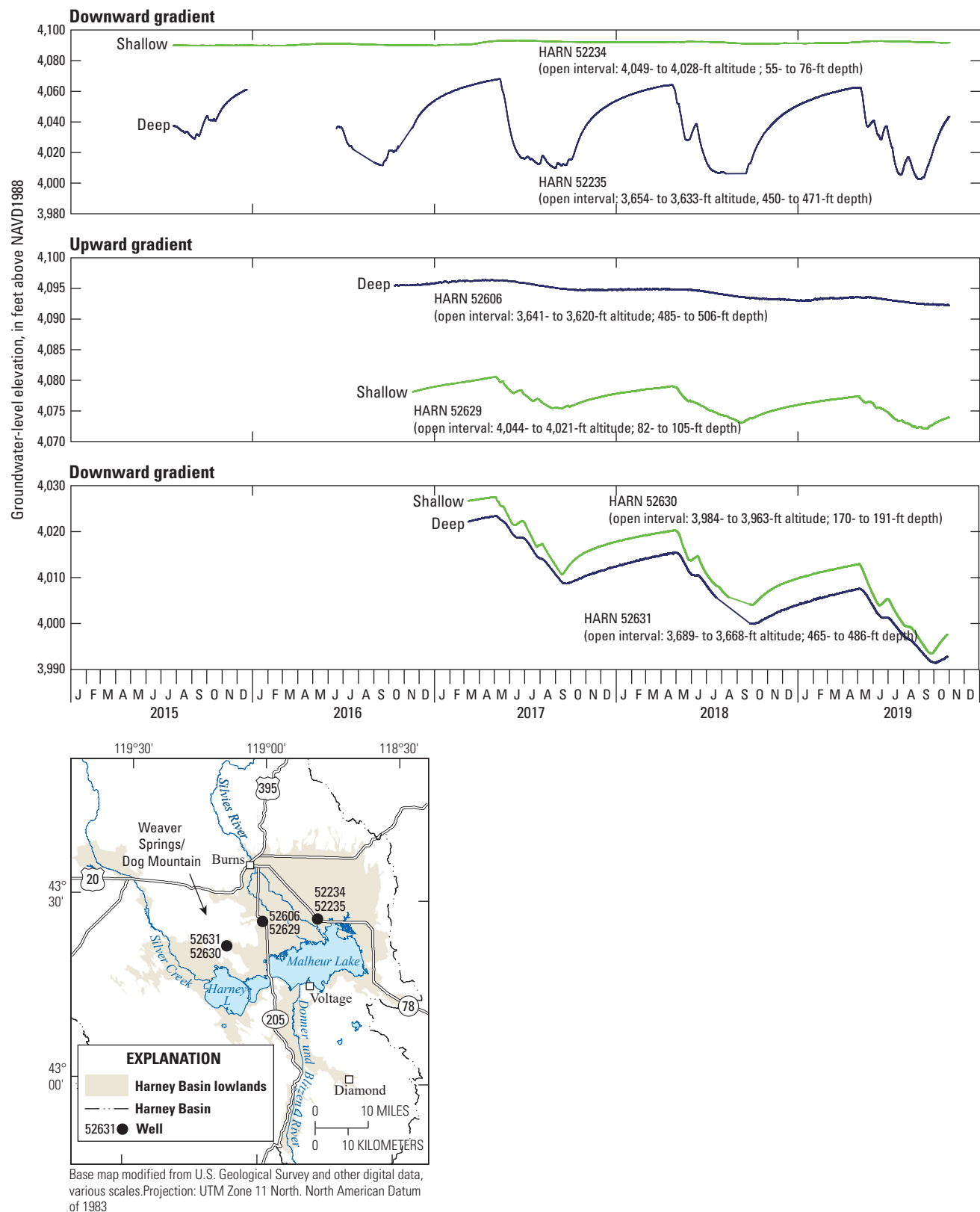
Figure 4.   Groundwater levels at selected wells showing vertical gradients in the Harney Basin, southeastern Oregon.

Predevelopment

Post-development

EXPLANATION

→ **Recharge (inflow)**

→ **Discharge (outflow)**

Note: ET = evapotranspiration
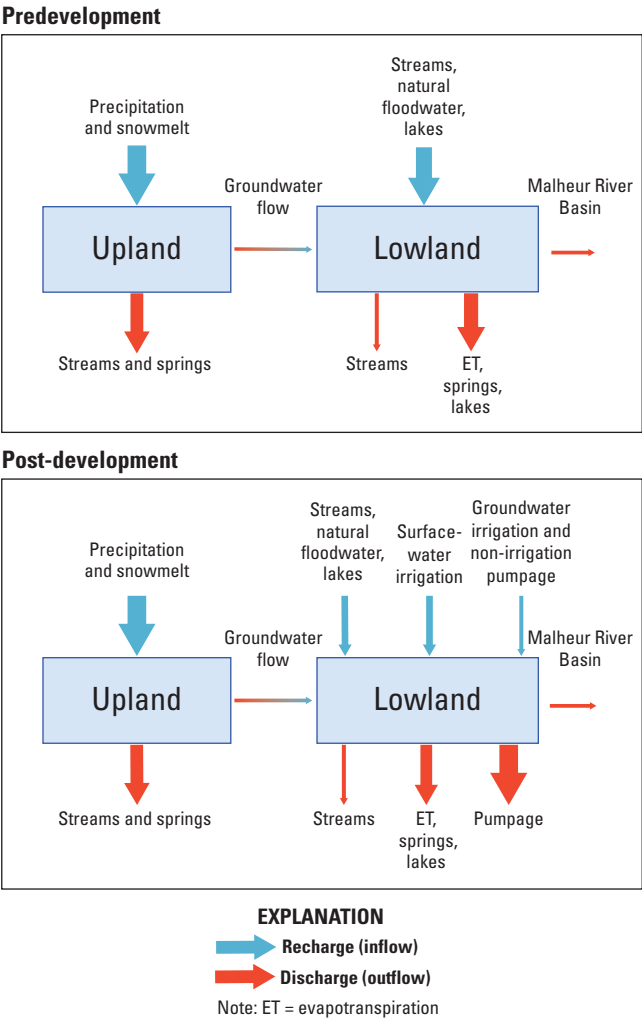
Figure 5. Simplified predevelopment and post-development groundwater recharge and discharge components of the Harney Basin hydrologic budget, southeastern Oregon.

Prior to development, ET was the primary mechanism for groundwater discharge in the Harney Basin lowlands with a smaller amount of discharge as groundwater flow that moved through Virginia Valley into the Malheur River Basin to the east (fig. 1). Groundwater ET, or ET_g, occurs in areas dominated by phreatophytes, which are deep-rooted plants that obtain a portion of their water supply from shallow groundwater or from the capillary fringe above the water table. Increased pumpage has greatly increased groundwater discharge from the Harney Basin lowlands, but there is little evidence that pumpage has appreciably affected the natural discharge of groundwater by phreatophytes (ET_g). Most groundwater-irrigated fields are outside or near the periphery of phreatophyte-dominated areas because soils in these areas typically are poorly drained and saline, and unsuitable for

irrigated agriculture (Cannon, 1960; Soil Survey Staff, 2018). Within phreatophyte-dominated areas, water-table drawdown from pumpage is limited to a few localized areas such as near the Weaver Spring/Dog Mountain area (fig. 4) and in Virginia Valley (fig. 1) where shallow sediments are more permeable. Field and satellite observations in the Harney Basin lowlands by Albano and others (2020) highlighted a few areas where phreatophyte communities exhibited signs of water stress, but these areas are adjacent to surface-water flooded areas (natural and irrigated), indicating the observed stress is more likely related to the availability of surface-water recharge rather than changes in groundwater use. Studies in basins with similar climate and vegetation indicate phreatophytic shrubs such as greasewood can adapt to a gradual decline in groundwater levels if the depth to water remains within an adequate range for species survival (typically less than 30 ft) (Meinzer, 1927; Robinson, 1958; Glancy and Rush, 1968; Devitt and Bird, 2016).

Description of Groundwater Hydrologic Budget Components

The hydrologic budget of a groundwater system provides an accounting of groundwater inflows (recharge) and outflows (discharge) and constrains the occurrence and movement of groundwater within the system. Understanding the groundwater-flow system requires full accounting of groundwater and relevant surface-water hydrologic components. Groundwater-budget components are quantified separately for upland and lowland areas, and a net groundwater budget for both areas is presented (fig. 5). A basin-wide budget that sums all recharge and discharge components misrepresents the amount of water actually circulating in the Harney Basin because it double-counts water that recharges and discharges in the uplands, flows down a stream channel, and reinfiltrates back into the groundwater system in the lowlands.

Prior to the onset of groundwater development in the Harney Basin in the late 19th century, the long-term mean annual groundwater recharge and discharge were about equal, so the groundwater hydrologic budget was balanced. Components of the groundwater budget can be represented quantitatively as:

$$Discharge \ = \ Recharge \ \pm Change \ in \ Storage \qquad (1)$$

where

Discharge	is the total groundwater discharge in the Harney Basin,
Recharge	is the total groundwater recharge in the Harney Basin, and
Change in Storage	is the total change in groundwater storage per time in the Harney Basin.

A series of above-average precipitation years would result in an increase in groundwater storage, with groundwater recharge exceeding discharge as the aquifer system fills. Conversely, a series of below-average precipitation years would result in discharge exceeding recharge and groundwater storage would decrease until a new equilibrium is reached. Changes in groundwater storage manifest as a rise or decline in the water-table elevation or potentiometric head. If long-term mean recharge equals mean discharge, then equation (1) requires that the long-term mean change in storage is zero. So, while groundwater levels may respond to yearly departures from mean recharge, they will oscillate around long-term mean values.

Like Masbruch and others (2011), the detailed groundwater budgets for the Harney Basin and the Harney Basin lowlands during the study period are represented quantitatively in the following equations (as volume per unit time):

$$\text{Harney Basin:}$$
$$Q_{ppt}^{in} + Q_{sw}^{in} + Q_{irr}^{in} \ = \ ET_g + Q_{sw}^{out} + Q_p^{out} + Q_{go}^{out} + \Delta S_{gw}. \tag{2}$$

$$\text{Harney Basin lowlands:}$$
$$Q_{gi}^{in} + Q_{sw}^{in} + Q_{irr}^{in} \ = \ ET_g + Q_{sw}^{out} + Q_p^{out} + Q_{go}^{out} + \Delta S_{gw} \tag{3}$$

where

Q_{ppt}^{in} is groundwater recharge from infiltration of precipitation and snowmelt through soils and permeable bedrock (occurs in upland areas only),

Q_{sw}^{in} is groundwater recharge from infiltration of surface water (streams, floodwater, and lakes; commonly referred to as mountain-front recharge),

Q_{irr}^{in} is groundwater recharge from infiltration of irrigation water (surface water and groundwater) and pumpage for non-irrigation use,

ET_g is groundwater discharge through ET by plants that access groundwater and (or) bare soil,

Q_{sw}^{out} is groundwater discharge to surface water (springs, streams, and lakes),

Q_p^{out} is groundwater discharge through pumpage,

Q_{go}^{out} is groundwater discharge through groundwater outflow from the Harney Basin to the Malheur River Basin,

ΔS_{gw} is change in groundwater storage, and

Q_{gi}^{in} is lowland groundwater recharge resulting from groundwater flow from uplands to lowlands (commonly referred to as mountain-block recharge).

The movement of groundwater in the Harney Basin and its relation to specific groundwater-budget components can be illustrated by considering the fate of upland precipitation and snowmelt, which is the primary source of all groundwater in the basin (figs. 5, 6; see section "Groundwater"). Upland precipitation and snowmelt that is not consumed by ET or direct runoff to streams infiltrates the soil and percolates through the rocks and sedimentary deposits underlying upland areas toward the water table (Q_{ppt}^{in}). Part of this upland recharge discharges while still within the uplands to mountain springs or as base flow to mountain streams (Q_{sw}^{out}), and a smaller amount of this upland groundwater is consumed through ET (ET_g). Another fraction of this upland recharge moves directly through the subsurface from the uplands into the unconsolidated deposits underlying the adjacent Harney Basin lowlands (Q_{gi}^{in}) (commonly referred to as "mountain-block recharge"). Streamflow exiting the uplands conveys a mixture of groundwater discharged as base flow and direct runoff of precipitation and snowmelt, and a portion of this water recharges deposits underlying the Harney Basin lowlands (Q_{sw}^{in}; fig. 6; commonly referred to as "mountain-front recharge"). Lowland recharge from infiltration of streamflow and floodwater occurs predominantly through unconsolidated deposits beneath stream channels and floodplains. Recharge from streamflow and floodwater generally decreases with distance from the upland-lowland boundary as downward percolation is limited by unconsolidated basin-fill deposits that generally become finer toward the basin center. Another portion of streamflow is diverted for irrigation and a portion of the irrigation water percolates below the root zone and recharges the lowland deposits (Q_{irr}^{in}). A minor portion of streamflow that reaches Malheur and Harney Lakes recharges the underlying lowland deposits through lake-bed sediments when the hydraulic gradient is away from the lake toward the water table (such as in areas where groundwater levels are depressed by pumping or when lake levels are high). Lowland precipitation does not contribute to recharge because ET exceeds precipitation in most lowland areas. Most lowland groundwater ultimately discharges in the lowlands as ET (ET_g) or through pumpage (Q_p^{out}; fig. 6); a smaller proportion discharges to springs and seeps (which ultimately evaporates; Q_{sw}^{out}) or leaves the Harney Basin as groundwater outflow (Q_{go}^{out}) to the Malheur River Basin. A minor amount of groundwater discharges to Malheur and Harney Lakes through seepage and springs (Q_{sw}^{out}) when the hydraulic gradient is toward the lake (such as in areas unaffected by pumping or when lake levels are low). Although most pumpage is consumed as crop ET, a small portion returns to the groundwater system as recharge (Q_{irr}^{in}) from percolation below the root zone of groundwater-irrigated fields and from non-irrigation groundwater use such as beneath septic tanks and domestic and commercial lawns and gardens.
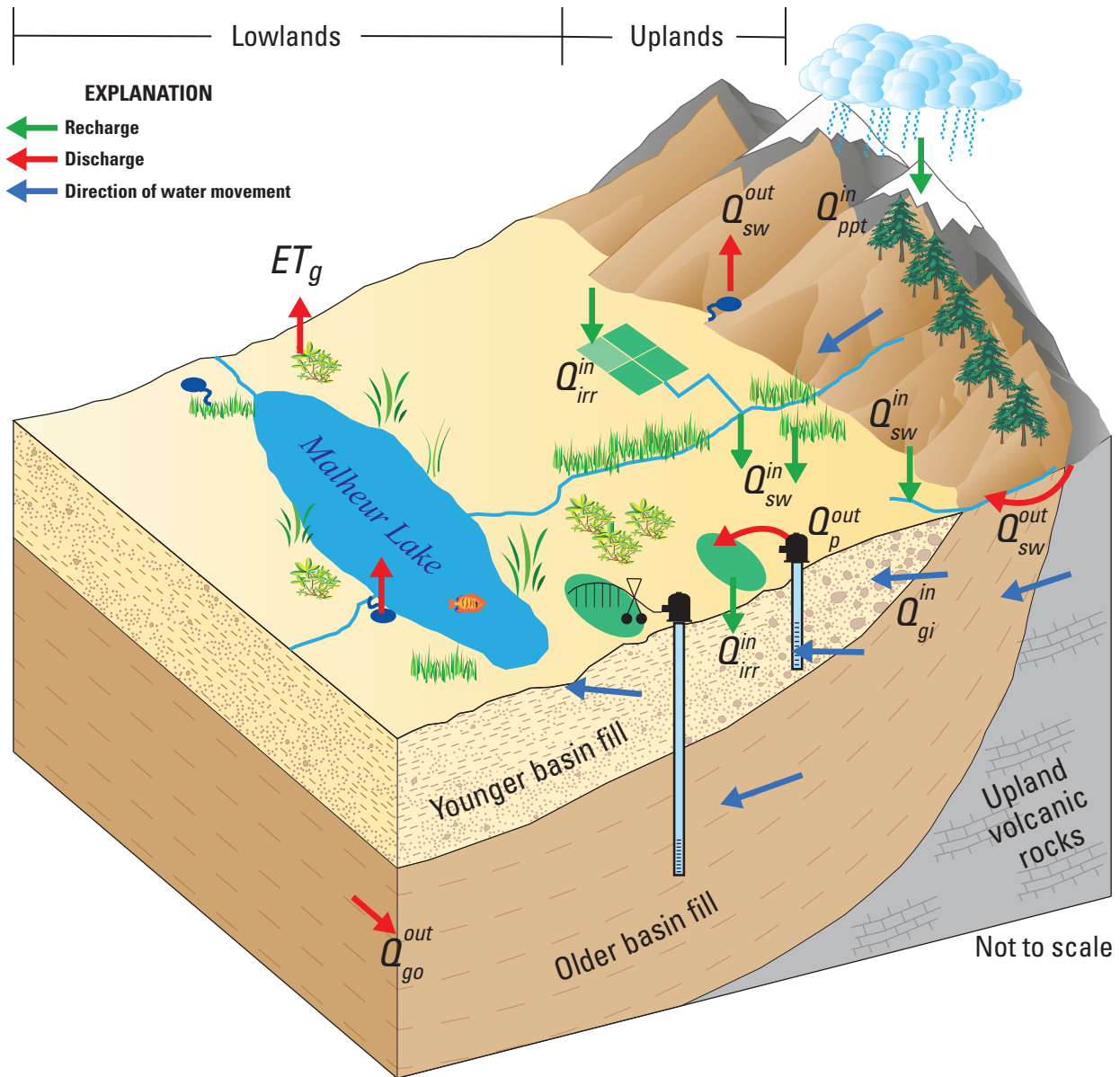
Figure 6.   Groundwater recharge and discharge, Harney Basin, southeastern Oregon. Modified from Masbruch and others (2011). Recharge and discharge components are from equations 2-3 and include: Q_{ppt}^{in}, upland recharge from precipitation and snowmelt; Q_{gi}^{in}, groundwater inflow from uplands to lowlands; Q_{sw}^{in}, lowland recharge from surface water; Q_{irr}^{in}, lowland recharge from irrigation water and other non-irrigation water use; ET_g, groundwater discharge through evapotranspiration; Q_{sw}^{out}, groundwater discharge to surface water; Q_p^{out}, groundwater discharge through pumpage; and Q_{go}^{out}, groundwater outflow to the Malheur River Basin.

Accurate estimation of the lowland groundwater budget (eq. 5) requires full accounting of all upland and lowland groundwater budget components. Full accounting of upland components is necessary because upland groundwater recharge that does not discharge in the uplands becomes lowland recharge (Q_{gi}^{in}). Overestimation of upland groundwater recharge or underestimation of upland groundwater discharge will result in overestimation of lowland recharge as groundwater flow from upland areas. Likewise, underestimation of upland recharge or overestimation of upland groundwater discharge will result in underestimation of lowland recharge. Full accounting of lowland groundwater budget components is necessary so that water-resource managers and water users can adequately evaluate and manage groundwater resources for current and future use.

The following sections describe groundwater discharge and recharge components of the Harney Basin groundwater budget in detail. Methods used to estimate each groundwater budget component included in equations 2 and 3 and the magnitude and variability of resulting estimates are presented. Discharge components are presented first, followed by recharge components because discharges such as upland base flow were used to constrain recharge from precipitation and snowmelt. Components are presented and results are summarized and discussed by upland and lowland areas and by region within the Harney Basin.

Groundwater Discharge

Groundwater discharges naturally in upland and lowland areas and by pumping for agricultural and other uses. Most natural upland discharge is to streams or springs, but a portion of upland groundwater flows through the subsurface to lowland areas. Natural lowland discharge is predominantly to ET, springs, and groundwater flow to the Malheur River Basin, with a lesser portion to the lakes. Water discharged from the aquifer system as pumpage occurs primarily in lowland areas. Estimation methods and results for each groundwater discharge component are discussed in the following subsections. Groundwater discharge through ET is presented first because many other discharge components are accounted for in ET_g estimates.

Groundwater Discharge through Evapotranspiration

Groundwater ET in the Harney Basin lowlands was estimated as a function of land-cover characteristics within mapped areas where ET_g occurs naturally as bare-soil evaporation and (or) transpiration of groundwater by phreatophytes. The volume and rate of ET_g vary with vegetation type and density, depth to groundwater, soil characteristics, and microclimate (Laczniak and others, 1999, 2008; Moreo and others, 2007; Allander and others, 2009). The following subsections

describe the types of plants that use groundwater in the Harney Basin lowlands and the methods used to distinguish and group groundwater ET areas (GETAs), followed by methods used to estimate and distribute ET_g across the Harney Basin lowlands and results from the ET_g analysis.

Groundwater Use by Plants in the Harney Basin

Natural discharge of groundwater in the Harney Basin predominantly occurs through ET by phreatophytes. The dominant phreatophytic shrub in the Harney Basin lowlands is greasewood (*Sarcobatus vermiculatus* [Hooker] Torrey). Greasewood has been documented to access groundwater as deep as 62 ft below land surface (bls; Robinson, 1958; Glancy and Rush, 1968). Rabbitbrush is widely distributed across the Harney Basin lowlands, but occurs in both phreatophytic form, rubber rabbitbrush (*Ericameria nauseosa* [Pall. Ex Pursh]), and nonphreatophytic form, green rabbitbrush (*Chrysothamnus vicidiflorus* [Hook.] Nutt). Rubber rabbitbrush roots have been documented at depths of 10–16 ft bls (Donovan and others, 1996; Stromberg, 2013). Green rabbitbrush, the nonphreatophytic form, is more plentiful and often mistaken for rubber rabbitbrush. Big sagebrush (*Artemisia tridentata* Nuttail) is abundant across lower salinity soils in the Harney Basin lowlands, but likely only uses groundwater intermittently where it is collocated with greasewood or where silt- or clay-rich soils promote a thick capillary fringe above the water table (see app. 2). Big sagebrush taproots can extend up to about 13 ft bls and penetrate the top of the capillary zone above the water table (Mozingo, 1987). The understory in phreatophyte-dominated areas consists of phreatophytic perennial grasses such as saltgrass (*Distichlis spicata* [L.] Greene) and basin wildrye (*Elymus condensatus* Presl.). Saltgrass and basin wildrye have been documented in areas where the water-table depths extend to about 13 ft bls (Blaney and others, 1933; Robinson, 1958).

Groundwater also is utilized by plants in dry meadows, wet meadows, open marsh, and riparian areas along stream channels in the Harney Basin lowlands. Vegetation in open marsh includes various cattail (*Typha* spp.) and sedges (*Scirpus* spp.), whereas dry and wet meadows are composed of saltgrass, basin wildrye, rushes (*Juncus* spp.), catchfly (*Silene* spp.), and sedges (*Carex* spp.) among other species (Daniel Craver, USFWS, written commun., 2017). Willow (*Salix* spp.) is the common phreatophyte occupying riparian areas along stream channels.

Adjacent to ET_g areas where depth-to-water is greater, plants are predominantly xerophytes (plants that need very little water) that obtain water from soil moisture replenished by precipitation. The most common xerophytic shrubs on the valley lowlands include green rabbitbrush, shadscale (*Atriplex confertifolia* [Torr. & Frém.] S. Watson), and big sagebrush where the water table and capillary fringe are well below plant roots. Common grasses include two introduced species: crested wheatgrass (*Agropyron cristatum* [L] Gaertn) and cheat grass (*Bromus tectorum* L.).

Groundwater Evapotranspiration Area

The Harney Basin GETA boundary represents an 860 mi^2 (550,000 acre) area of the Harney Basin lowlands (about 80 percent) where phreatophytes grow and groundwater actively discharges through ET (fig. 7). Within the GETA boundary is a mixture of bare soil and playas (4 percent), open water (3 percent), phreatophytes and xerophytes (67 percent), and irrigated agriculture (26 percent). The GETA boundary represents the transition from a topographically higher, upslope region that is characterized by xerophytic shrubs and grasses with an unsaturated zone typically more than 20 ft bls, to a downslope region of mixed xerophytic and phreatophytic shrubs and an unsaturated zone that generally is less than about 20-ft thick.

The Harney Basin GETA was mapped (see Garcia and others, 2022) following methods used in studies elsewhere in the Great Basin (Nichols, 2000; Smith and others, 2007; Allander and others, 2009; Garcia and others, 2015; Berger and others, 2016). The GETA was delineated at a scale of about 1:24,000 by refining phreatophyte boundaries from existing vegetation maps including Oregon Gap Analysis Program (GAP; Kagan and Caicco, 1992) and MNWR maps (Daniel Craver, USFWS, written commun., November 2016). Previous mapping was validated and modified, if necessary, using (1) vegetation point data either collected in this study, by USFWS (Daniel Craver, USFWS, written commun., November, 2016) or by BLM (Jimmy Kagan, Oregon Biodiversity Information Center, written commun., May, 2018), (2) high-resolution imagery from 2016 National Agricultural Imagery Program (NAIP; U.S. Department of Agriculture, 2016) and 2017 Oregon Statewide Imagery Program (OSIP, 2017) to distinguish the boundary between greasewood-dominated communities and other phreatophytes, (3) a 10-m digital elevation model to limit the discharge area to relatively flat plains where plants could not be distinguished via imagery, and (4) groundwater-level data to ensure that depth to groundwater did not exceed typical phreatophytic-shrub rooting depths of roughly 20–30 ft bls. GETA maps were verified using spot checks of stable isotope compositions of plant water to confirm direct groundwater uptake (app. 2).

Evapotranspiration Units Within the Groundwater Evapotranspiration Area

Recent studies in the Great Basin (Smith and others, 2007; Allander and others, 2009; Garcia and others, 2015; Berger and others, 2016) have applied remote-sensing techniques and field mapping within groundwater discharge areas to identify and group areas having similar ET rates based on (1) vegetation type and density and (2) soil type and wetness. These groups are referred to as "ET units." Eleven ET units were identified from field and imagery observations of land cover and include bare soil or playa, marsh, dry meadow, wet meadow, open water, riparian, mixed shrubland, phreatophyte shrubland, sagebrush shrubland, xerophyte shrubland, and xerophyte grassland (table 2). Irrigated areas were not assigned to an ET unit because ET from these areas was calculated using a different method (see section "Groundwater Discharge through Pumpage").

The GETA was divided into the 11 identified ET units by classifying remotely sensed spectral reflectance and image texture characteristics that identify similarities and patterns in observed vegetation and soil conditions through supervised learning. Supervised learning uses a set of observations at specific locations to train an algorithm to make a prediction at all locations. The supervised classification model used in this study relied on multi-band Landsat and NAIP imagery, Landsat-derived vegetation and water indices (see apps. 1 and 3 for more information about these indices), and more than 1,400 field- and image-based observations of land cover to divide the GETA into the 11 ET units. A map of the 11 ET units was constructed using the trained algorithm (fig. 7). Refer to appendix 3 for details on the process of ET-unit delineation. For ET_g estimation, mixed shrubland and phreatophyte shrubland ET units were combined into a single unit (phreatophyte shrubland), and xerophyte shrubland and xerophyte grassland were combined into a single unit (xerophyte shrubland and grassland).

Methods for Groundwater Evapotranspiration Estimation in the Groundwater Evaportranspiration Area

Groundwater discharge through ET for each ET unit in the Harney Basin GETA was estimated volumetrically as the product of estimated ET_g rates and representative areas across which ET_g is occurring. Because no published measurements of ET_g rates from natural vegetation exist for the Harney Basin, rates were extrapolated from published measurements at sites in the Great Basin having similar soil, vegetation, and meteorological conditions as the Harney Basin GETA. Rates of ET_g were extrapolated using two methods: a method modified from Laczniak and others (2008) and the method of Beamer and others (2013). Hereinafter, the method modified from Laczniak and others (2008) is referred to as the "physics-based method" and the method of Beamer and others (2013) is referred to as the "empirical method."

Physics-based and empirical methods use remote sensing to spatially distribute estimates of ET across the GETA. Using the physics-based method (modified for this study), mean ET rates are estimated within the Harney Basin ET units by scaling published site-ET measurements with the enhanced vegetation index (EVI) from Landsat imagery in the Harney Basin. The empirical method uses an empirical equation developed between published ET measurements and EVI to estimate ET rates in the Harney Basin GETA. The ET estimates from both methods are converted to ET_g rates by considering ET source water in each ET unit, and ET_g volume is computed by multiplying ET_g rates from the different methods by representative areas. These methods are discussed in more detail in the following subsections and in appendix 3.
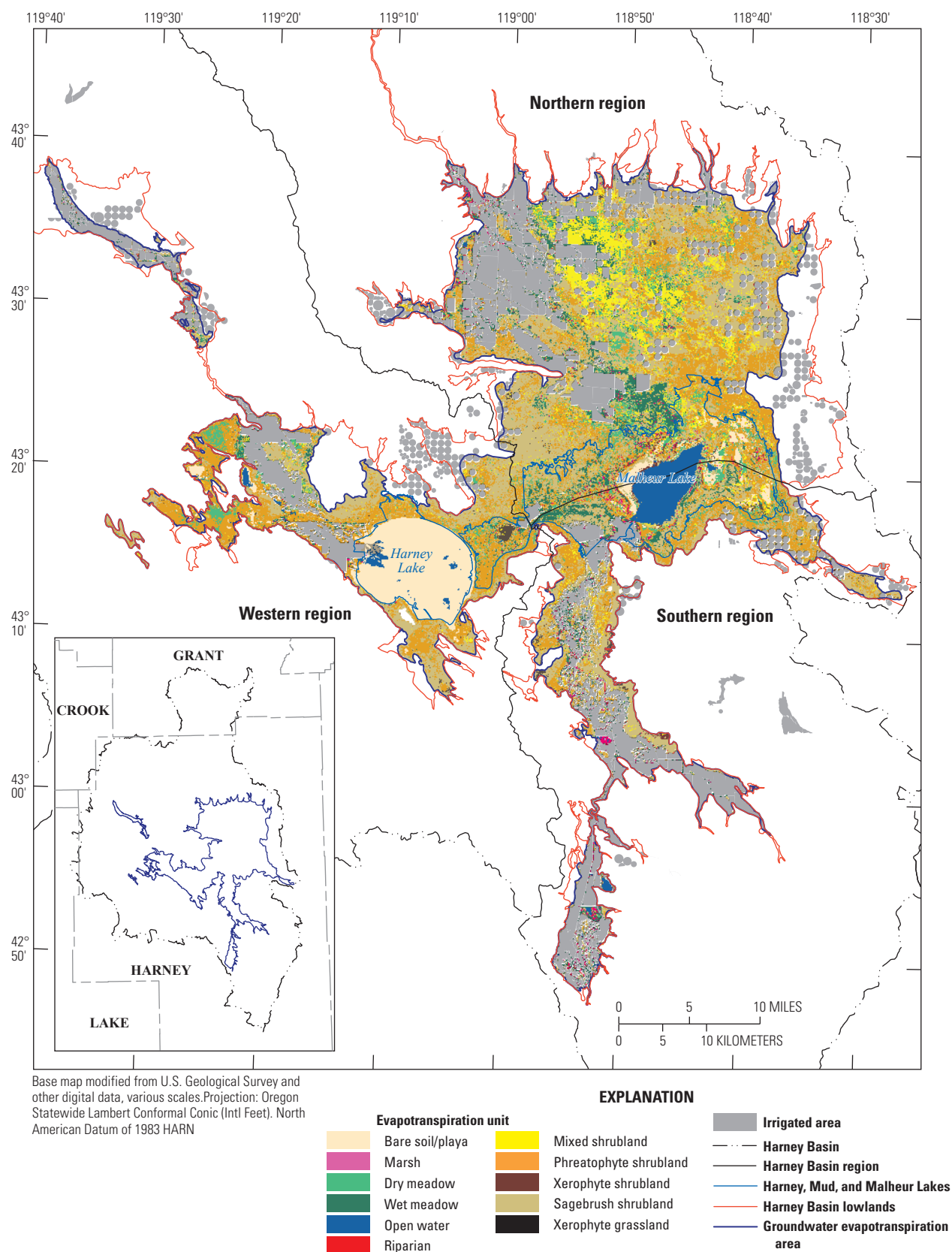
Figure 7. Delineated groundwater evapotranspiration area, evapotranspiration units, and maximum extent of irrigated areas, Harney Basin, southeastern Oregon, 1991–2018.

Table 2.   Evapotranspiration (ET) units identified, delineated, and mapped in the groundwater ET area, Harney Basin, southeastern Oregon.

[**Abbreviations**: ET, evapotranspiration; ft, feet; GETA, groundwater evapotranspiration area]

ET unit	ET unit number	Description
Bare soil-playa	1	Area dominated by bare soil or playa. Playa areas are intermittently to fully inundated with surface water depending on the water year. This area includes Harney Lake, which was fully inundated from 1983 to 2000 and intermittently dry since.
Marsh	2	Area dominated by submerged and emergent aquatic vegetation along shallow parts of open water bodies. Area is perennially flooded and vegetation uses groundwater and surface water.
Dry meadow	3	Area dominated by sparse to dense perennial grasses with lesser amounts of shrubs. Grasses are commonly comprised of saltgrass and basin wildrye where depth to groundwater is deeper and sedges and other grasses where water tables are shallower. Soils are moist to dry. Area is occasionally flooded. Groundwater is below land surface.
Wet meadow	4	Area dominated by moderately dense to dense wetland vegetation, primarily rushes, sedges, catchfly, and other grasses. Area is ephemerally flooded with groundwater near land surface.
Open water	5	Area of open water, including lakes, reservoirs, and ponds. Reservoir water bodies vary in size seasonally. Unit represents an unlimited source of water available for evaporation.
Riparian	6	Area dominated by willows and other riparian vegetation. Can include moderately dense phreatophytic shrubs and saltgrass. Depth to groundwater can range from land surface to more than 10 ft below land surface. Vegetation uses groundwater and surface water. This unit primarily occupies the area along perennial stream corridors.
Mixed shrubland	7	Area dominated by big sagebrush and green rabbitbrush with lesser amounts of greasewood, rubber rabbitbrush, basin wildrye, and saltgrass. Vegetation cover ranges from less than 5 to less than 20 percent. Depth to groundwater can vary from about 10 to more than 20 ft below land surface.
Phreatophyte shrubland	8	Area dominated by phreatophytic shrubs including greasewood and rubber rabbitbrush with lesser amounts of big sagebrush and green rabbitbrush. Areas occasionally contain sparse to moderately dense cover of basin wildrye and saltgrass. Shrub combinations vary from site to site but are typically dominated by greasewood. Vegetation cover ranges from less than 5 to 40 percent. Depth to groundwater can vary from less than 5 to more than 20 ft below land surface.
Xerophyte shrubland	9	Minor area dominated by xerophytic shrubs such as green rabbitbrush with lesser amounts of big sagebrush. This unit typically occurs near disturbed areas or near the GETA boundary where depth to groundwater typically is near or greater than 20 ft below land surface.
Sagebrush shrubland	10	Area dominated by big sagebrush with lesser amounts of cheatgrass and other perennial xerophytic grasses. Depth to groundwater ranges from less than 10 to more than 20 ft below land surface.
Xerophyte grassland	11	Minor area dominated by xerophytic perennial grasses such as wheatgrass. This unit typically occurs near disturbed areas or near the GETA boundary where depth to groundwater exceeds 20 ft below land surface.

Net Evapotranspiration and Normalized Net Evapotranspiration Rates

The source of ET in the Harney Basin GETA and at semi-arid measurement sites utilized in this study (app. 3) includes precipitation, groundwater, and in some cases surface water. In natural non-irrigated environments, estimates of annual ET in excess of precipitation, or ET_{net}, represent either ET_g, surface-water ET (ET_{sw}), or a combination of the two, assuming antecedent soil moisture from the previous water year(s) minimally contributes to ET. The following equations describe sources of ET and define ET_{net} in the Harney Basin GETA:

$$ET = P + ET_g + ET_{sw}, \tag{4}$$

$$ET_{net} = ET - P, \text{ and} \tag{5}$$

$$ET_{net} = ET_g + ET_{sw}, \tag{6}$$

where
ET	is total evapotranspiration,
ET_{net}	is net evapotranspiration,
P	is precipitation,
ET_g	is evapotranspiration of groundwater, and
ET_{sw}	is evapotranspiration of surface-water inflow.

Relations between site ET measurements and EVI in physics-based and empirical methods use estimates of ET_{net}, normalized using precipitation and atmospheric ET demand (quantified with grass-reference ET or ET_o; Allen and others, 2005). Normalized ET_{net} (ET^*), is specific to vegetated and bare soil or playa areas, but independent of precipitation and ET_o, allowing for transferability of ET_{net} from basin to basin. The following equation by Beamer and others (2013) is used for both methods and defines ET^* based on ET_{net}, precipitation, and ET_o:

$$ET^* = \frac{(ET_{net})}{(ET_o - P)} \tag{7}$$

where
ET^*	is normalized net evapotranspiration (unitless),
ET_{net}	is annual net evapotranspiration (ft/yr),
P	is annual precipitation at the ET measurement site (ft/yr), and
ET_o	is annual grass-reference evapotranspiration at the ET measurement site (ft/yr).

Physics-Based Method

The physics-based method was applied using the following multi-step process, which is described in greater detail in this section:

(1) Select published ET data from measurement sites located in other basins that are representative of the Harney Basin GETA,

(2) Adjust site ET for energy balance closure and compute ET^* at each site, and

(3) Compute mean ET^* for ET units in the Harney Basin by scaling site ET^* with EVI.

Measured ET from 21 sites in north-central Nevada and southern Oregon were selected based on similar land-cover characteristics and regional climate (see app. 3 for more information about selection criteria and comparisons). Evapotranspiration from the selected sites generally is sourced from precipitation and either groundwater or surface-water inflow. Site locations, elevation, period of record used, vegetation type, and measurement sources are shown in table 3. Evapotranspiration measurements were adjusted for full energy balance closure using the Bowen Ratio method (Twine and others, 2000; Foken and others, 2012), site-specific ET_o was computed using the Penman-Monteith equation (Allen and others, 2005), and site-specific ET^* was computed using equation 7 (see app. 3 for more information about data adjustments and computations).

Spatially weighted mean ET^* for the Harney Basin ET units was determined by linearly scaling the range of site ET^* values that represent each ET unit using the EVI. The scaling procedure assigns the highest EVI value computed in the ET unit and region (northern, southern, and western regions) to the highest ET^* value of the range and the lowest EVI value in the ET unit and region to the lowest ET^* value of the range using the following equation:

$$\overline{ET^*} = ET_{min}^* + \frac{\overline{EVI}\left(ET_{max}^* - ET_{min}^*\right)}{\left(EVI_{max} - EVI_{min}\right)} \tag{8}$$

where
$\overline{ET^*}$	is the spatial mean ET* within an ET unit and region,
$ET^*_{min/max}$	is minimum or maximum ET* assigned within an ET unit for all regions,
$\overline{EVI}$	is the spatial mean EVI within an ET unit and region, and
$EVI_{min/max}$	is minimum or maximum EVI within an ET unit for all regions.

Table 3. Evapotranspiration (ET) sites, location, vegetation type, and annual rates of ET, precipitation, net ET (ETnet), normalized ETnet, and other variables used in the physics-based approach for groundwater ET estimation, Harney Basin, southeastern Oregon.

[Latitude and longitude in North American Datum of 1983. **Elevation** in feet above North American Vertical Datum of 1988. **Measurement period:** Dates shown as month/day/year. ET_o, Short grass reference evapotranspiration computed using the Penman-Monteith equation. ET_c: Annual evapotranspiration estimated using the eddy-covariance method and adjusted for full energy-balance closure. **PPT:** Precipitation. ET_{net}: ET_c minus PPT and is about equal to groundwater ET at all sites but KB-BUL, KB-MIX, and DV-PL2. **ET*:** Normalized ET_{net} computed as the ratio of ET_{net} and ET_o minus precipitation. **Source:** 1, Moreo and others (2007); 2, Allander and others (2009); 3, Stamard and others (2013); 4, Garcia and others (2015); 5, Berger and others (2016). **Abbreviations:** ET, evapotranspiration; ft, feet; ft/yr, feet per year; ft bls, feet below land surface; NA, not available; —, not estimated; USGS, U.S. Geological Survey]

Site	Vegetation type	Representative ET unit	USGS site number	Latitude (decimal degrees)	Longitude (decimal degrees)	Elevation (ft)	Depth to groundwater (ft bls)	Measurement period	ET_o (ft/yr)	ET_c (ft/yr)	PPT (ft/yr)	ET_{net} (ft/yr)	ET* (unitless)	Source
DV-DV	Greasewood, big saltbush	Shrubland	39455117573605	39.762511	-117.960100	3,431	17	10/1/2009 - 9/30/2010	4.39	1.51	0.51	1.00	0.26	4
								10/1/2010 - 9/30/2011	4.42	1.56	0.72	0.84	0.23	
DV-SV	Greasewood	Shrubland	39434118040205	39.730106	-118.067264	3,387	15–18	10/1/2009 - 9/30/2010	4.29	0.69	0.46	0.23	0.06	4
								10/1/2010 - 9/30/2011	4.35	0.93	0.61	0.32	0.09	
SNV-1	Greasewood	Shrubland	39082511403430 1	39.140153	-114.061989	5,110	17	10/1/2005 - 9/30/2006	4.77	0.93	0.50	0.43	0.10	1
								10/1/2006 - 9/30/2007	4.78	0.79	0.35	0.44	0.10	
SPV-1	Greasewood, rabbitbrush	Shrubland	38463911428040 1	38.777550	-114.467789	5,790	10	10/1/2005 - 9/30/2006	4.34	1.03	0.69	0.34	0.09	1
								10/1/2006 - 9/30/2007	4.54	0.74	0.48	0.26	0.06	
SPV-2	Greasewood, rabbitbrush	Shrubland	38470911427560 1	38.785864	-114.465656	5,795	7	10/1/2005 - 9/30/2006	4.33	0.94	0.74	0.20	0.06	1
								10/1/2006 - 9/30/2007	4.49	0.72	0.51	0.21	0.05	
SPV-3	Meadow grass	Meadow	38561214251601	38.936672	-114.421233	5,785	4	10/1/2005 - 9/30/2006	4.21	2.24	0.65	1.59	0.45	1
								10/1/2006 - 9/30/2007	4.38	2.13	0.52	1.61	0.42	
WRV-1	Greasewood	Shrubland	38244911503030 1	38.413572	-115.050944	5,230	32	10/1/2005 - 9/30/2006	4.52	1.06	0.72	0.34	0.09	1
								10/1/2007 - 9/30/2007	4.68	0.92	0.73	0.19	0.05	
WRV-2	Greasewood	Shrubland	38382615061001	38.640525	-115.102631	5,320	24	10/1/2005 - 9/30/2006	4.82	1.21	0.92	0.29	0.07	1
								10/1/2007 - 9/30/2007	5.04	0.85	0.63	0.22	0.05	
KV-1	Greasewood, rabbitbrush, sagebrush	Shrubland	39321416212402	39.537100	-116.357600	6,099	9	08/25/2011–08/24/2012	4.45	0.70	0.50	0.20	0.05	5
KV-2	Greasewood, rabbitbrush, saltgrass, sagebrush	Shrubland	39371116124501	39.619700	-116.213400	6,052	2	8/28/2010 - 8/27/2011	3.78	1.50	0.78	0.72	0.24	5
								8/28/2011 - 8/27/2012	4.11	1.05	0.49	0.56	0.15	
KV-3	Greasewood, rabbitbrush, wildrye, saltgrass	Shrubland	39355311625240 1	39.598100	-116.424200	6,131	4	8/5/2010 - 8/4/2011	3.65	1.76	0.90	0.86	0.31	5
								8/5/2011 - 8/4/2012	4.15	1.28	0.42	0.86	0.23	
KV-4	Meadow grass	Meadow	39355116094802	39.598700	-116.164200	6,013	4	11/03/2011–11/02/2012	4.21	1.86	0.65	1.21	0.34	5
GRE	Greasewood	Shrubland	38542611844080 1	38.907083	-118.735667	4,087	NA	3/9/2005 - 3/8/2006	4.80	0.79	0.38	0.41	0.09	2
GRE2	Greasewood	Shrubland	38511411844341 01	38.853861	-118.742889	4,015	NA	10/1/2006 - 9/30/2007	4.92	0.91	0.16	0.75	0.16	2
SAL	Saltgrass	Meadow	38515411844300 1	38.864944	-118.741639	4,008	NA	3/9/2005 - 3/8/2006	4.71	1.24	0.38	0.86	0.20	2
SAL2	Saltgrass	Meadow	38520311845060 1	38.867389	-118.751806	4,015	NA	10/1/2006 - 9/30/2007	5.17	2.40	0.16	2.24	0.45	2

Table 3. Evapotranspiration (ET) sites, location, vegetation type, and annual rates of ET, precipitation, net ET (ETnet), normalized ETnet, and other variables used in the physics-based approach for groundwater ET estimation, Harney Basin, southeastern Oregon.—Continued

[**Latitude and longitude** in North American Datum of 1983. **Elevation** in feet above North American Vertical Datum of 1988. **Measurement period**: Dates shown as month/day/year. ET_o: Short grass reference evapotranspiration computed using the Penman-Monteith equation. ET_c: Annual evapotranspiration estimated using the eddy-covariance method and adjusted for full energy-balance closure. **PPT**: Precipitation. ET_{net}: ET_c minus PPT and is about equal to groundwater ET at all sites but KB-BUL, KB-MIX, and DV-PL2. ET^*: Normalized ET_{net} computed as the ratio of ET_{net} and ET_o minus precipitation. **Source**: 1, Moreo and others (2007); 2, Allander and others (2009); 3, Stannard and others (2013); 4, Garcia and others (2015); 5, Berger and others (2016). **Abbreviations**: ET, evapotranspiration; ft, feet; ft/yr, feet per year; ft bls, feet below land surface; NA, not available; —, not estimated USGS, U.S. Geological Survey]

Site	Vegetation type	Representative ET unit	USGS site number	Latitude (decimal degrees)	Longitude (decimal degrees)	Elevation (ft)	Depth to groundwater (ft bls)	Measurement period	ET_o (ft/yr)	ET_c (ft/yr)	PPT (ft/yr)	ET_{net} (ft/yr)	ET^* (unitless)	Source
RAB	Rabbitbrush	Shrubland	385330118461601	38.891750	-118.771083	4,068	NA	3/9/2005 - 3/8/2006	4.81	0.96	0.38	0.58	0.13	2
KB-Bul	Bulrush	Marsh	NA	42.513578	-122.034692	4,140	standing water	10/1/2008 - 9/30/2009	3.04	3.30	1.16	2.14	1.14	3
								10/1/2009 - 9/30/2010	2.95	2.78	0.95	1.83	0.92	
KB-Mix	Bulrush, cattail, wocus	Marsh	NA	42.476889	-122.068347	4,141	standing water	10/1/2008 - 9/30/2009	3.19	3.01	1.16	1.85	0.91	3
								10/1/2009 - 9/30/2010	3.00	2.66	0.95	1.71	0.83	
DV-PL1	Playa[1]	Playa	394508118025505	39.752167	-118.048508	3,386	4	10/1/2009 - 9/30/2010	—	0.52	0.44	0.08	—	4
								10/1/2010 - 9/30/2011	—	0.62	0.56	0.06	—	
DV-PL2	Playa[1]	Playa	394559118013705	39.766444	-118.026831	3,383	3	10/1/2009 - 9/30/2010	—	0.46	0.42	0.04	—	4
								10/1/2010 - 9/30/2011	—	0.55	0.53	0.02	—	

[1]ET values were cited directly from the literature and were not adjusted for full energy balance closure.

Table 4.   Representative normalized net evapotranspiration values used to scale net evapotranspiration to the Harney Basin evapotranspiration units with the physics-based method, southeastern Oregon.

[Harney Basin ET units and ET unit values from table 2. **Description**: Describes ET* estimate and representative ET unit from table 2. **Abbreviations**: ET, evapotranspiration; *ET**, normalized net evapotranspiration]

Harney Basin ET unit		*ET** (unitless)			
		Minimum		**Maximum**	
Name	**ET unit number**	**Value**	**Description**	**Value**	**Description**
Marsh, riparian	2, 6	0.37	Mean of meadow ET unit values	1.41	Maximum of marsh ET unit values
Dry meadow	3	0.20	Minimum of meadow ET unit values	0.37	Mean of meadow ET unit values
Wet meadow	4	0.37	Mean of meadow ET unit values	0.45	Maximum of meadow ET unit values
Phreatophyte and mixed shrubland	7, 8	0.05	Minimum of shrubland ET unit values	0.31	Maximum of shrubland ET unit values
Sagebrush shrubland	10	0	ET sourced from precipitation only	0.37	Mean of meadow ET unit values
Xerophyte shrubland and grassland	9, 11	0	ET sourced from precipitation only	0	ET sourced from precipitation only

Values of $\overline{ET^*}$ were calculated for 46 summer EVI images for 23 years (1987–2015). The *ET** ranges applied in equation 8 for each vegetated Harney Basin ET unit (table 2) were based on sites located in similar representative ET units (table 4).

ET_{net} was calculated for each of the 46 EVI images (1987–2015) covering the Harney Basin GETA by rearranging equation (5) using the approach of Beamer and others (2013):

$$ET_{net} = (ET_o - P)ET^* \qquad (9)$$

where

ET_{net}	is estimated annual net evapotranspiration,
ET_o	is annual grass reference evapotranspiration from GridMET,
P	is annual precipitation from GridMET, and
ET^*	is normalized ET_{net}.

Spatially weighted mean ET_{net} rates for the Harney Basin ET units were calculated from mean *ET** and mean GridMET estimates of ET_o and P, spatially weighted by ET unit within each region for each year analyzed. Mean ET_{net} rates were averaged for years with multiple summer EVI images to obtain an annual ET_{net} rate for each ET unit, resulting in 23 years of spatially distributed ET_{net} rates by ET unit and region.

Mean annual (1987–2015) ET_{net} rates were computed by ET unit and analysis regions within the Harney Basin GETA. A long-term mean estimate of ET_{net} is considered more representative than annual estimates because annual estimates often reflect temporal and spatial variability in the imagery and in
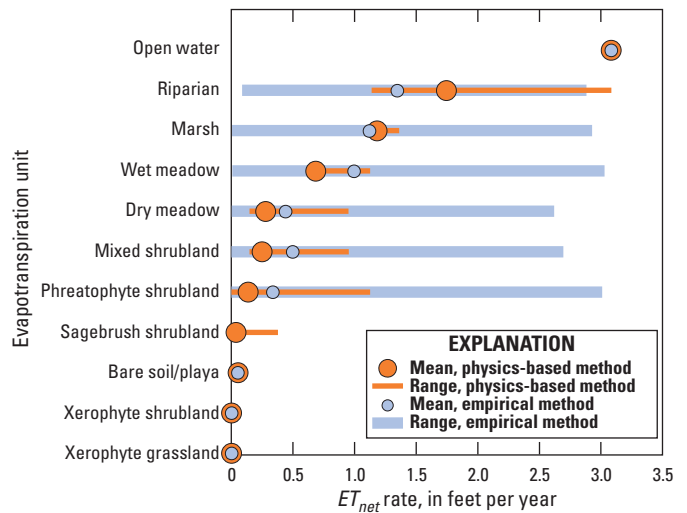
Figure 8.   Mean annual net evapotranspiration (ET) rates by ET unit, Harney Basin, southeastern Oregon. Net ET (ET_{net}) rates are the difference between total ET and precipitation. For lowland areas where groundwater supplies ET, ET_{net} is positive (ET exceeds precipitation at these locations).

surface-water contributions to ET rather than variability in regional groundwater discharge. Groundwater discharge by ET is generally constant with time because it is controlled by the mostly constant long-term water-table elevation and unchanging hydraulic properties of the groundwater system (Jackson and Fenelon, 2018). Ranges in calculated ET_{net} rates by ET unit are shown in figure 8.

Empirical Method

The empirical method of Beamer and others (2013) uses an empirical equation to estimate ET^* directly from EVI values. The empirical equation is a second-order polynomial that relates ET^* estimates from 26 sites in central and southern Nevada to concurrent site-area weighted means of midsummer Landsat EVI values computed from 30-m resolution Landsat imagery (eq. 10):

$$ET^* = -1.592\,(EVI)^2 + 2.904(EVI) - 0.196 \quad (10)$$

where
- ET^* is normalized net evapotranspiration and
- EVI is enhanced vegetation index.

Spatial distributions of annual ET^* and ET_{net} and mean annual ET_{net} were computed on a cell-by-cell basis within the GETA using the empirical method. Using equation 10, the spatial distribution of ET^* in the Harney Basin GETA was

calculated over 46 30-m EVI images from the Harney Basin spanning 1987–2015. The annual ET_{net} rate was calculated from ET^* using equation 9 for each 30-m cell in each of the 46 EVI images (1987–2015) covering the Harney Basin GETA. For years having multiple EVI images, the mean ET_{net} rate was calculated to obtain an annual ET_{net} rate for each 30-m cell, resulting in 23 years of spatially distributed ET_{net} rates. For each ET unit, the mean annual ET_{net} rate was calculated as the mean of the 23 years of ET_{net} rates. The mean annual ET_{net} rate was calculated for the entire Harney Basin GETA and for each of the geographic analysis regions.

Estimates in the sagebrush shrubland and xerophyte shrubland and grassland ET units were excluded because the empirical method only is applicable in areas where plants are actively discharging groundwater. Although some misclassifications exist within delineated ET units (app. 3; table 3.1), the sagebrush shrubland ET unit largely is comprised of xerophytes, which use little to no groundwater.

Table 5. Evapotranspiration (ET) unit area and mean annual groundwater ET rates and volumes from physics-based and empirical groundwater ET estimation methods, Harney Basin, southeastern Oregon, water years 1987–2015.

[Acreage rounded to the nearest 10 acres. Mean annual groundwater evapotranspiration volume rounded to three significant figures for values less than 100,000 and 4 significant figures for values greater or equal to 100,000. **Abbreviations**: acre-ft, acre-feet; ET, evapotranspiration; ft/yr, feet per year; —, not estimated]

ET unit	ET unit number	Acres	Physics-based method Rate (ft /yr)	Physics-based method Volume (acre-ft)	Empirical method Rate (ft /yr)	Empirical method Volume (acre-ft)	Mean Volume (acre-ft)
Bare soil-playa	1	36,240	0.05	1,810	0.05	1,810	1,810
Marsh	2	3,870	0.87	3,380	0.54	2,160	2,770
Dry meadow	3	22,970	0.68	15,700	0.44	10,100	12,900
Wet meadow	4	26,550	0.68	18,100	0.41	11,300	14,700
Open water (groundwater)	5	1,750	3.08	5,400	3.08	5,400	5,400
Open water (surface water)	5	11,090	0	0	0	0	0
Riparian	6	1,290	0.95	1,230	0.69	870	1,050
Phreatophyte and mixed shrubland	7,8	146,520	0.26	37,600	0.37	57,100	47,400
Sagebrush shrubland	10	151,080	0.14	21,800	—	—	21,800
Xerophyte shrubland and grassland	9,11	4,780	0	0	—	—	0
Areas irrigated with lowland spring discharge		9,260	—	—	—	—	[1]11,500
Total		[3]415,400		[4]116,500		[2,4]122,000	119,300

[1]Value determined from Mapping EvapoTranspiration using high Resolution and Internalized Calibration (METRIC; Allen and others, 2007) estimates of irrigation water use (see section "Irrigation Pumpage").

[2]Value includes sagebrush shrubland estimate from the physics-based approach.

[3]Excludes areas irrigated with pumped groundwater, surface water, or upland spring discharge. Total groundwater ET area, inclusive of irrigated areas, is 550,000 acres.

[4]Value includes mean estimate for areas irrigated with lowland spring discharge

Table 6.   Regional estimates of mean annual groundwater and surface-water evapotranspiration (ET) volume from non-irrigated areas and ET-unit area, Harney Basin, southeastern Oregon, water years 1987–2015.

[Regions are shown on figure 1. Acreage rounded to the nearest 10 acres. Surface-water evapotranspiration volumes shown in parentheses. Volumes rounded to two significant figures. **Abbreviations**: ET, evapotranspiration]

ET unit	ET unit number	Mean annual groundwater (and surface-water) evapotranspiration					
		Northern region		Southern region		Western region	
		Acres	Volume (acre-feet)	Acres	Volume (acre-feet)	Acres	Volume (acre-feet)
Bare soil-playa	1	3,620	180	2,210	110	34,410	1,520
Marsh	2	1,750	1,200 (1,200)	1,890	1,410 (1,410)	230	171 (171)
Dry meadow	3	14,330	8,340	3,410	1,680	5,230	2,870
Wet meadow	4	16,430	9,570 (8,700)	7,550	3,710 (4,190)	2,570	1,430 (1,340)
Open water	5	3,390	0 (10,400)	7,700	0 (23,700)	1,750	5,400 0
Riparian	6	470	357 (357)	630	534 (534)	200	162 (162)
Phreatophyte and mixed shrubland	7, 8	85,060	30,100	24,230	7,310	37,230	10,000
Sagebrush shrubland	10	86,220	14,700	34,520	5,090	30,350	2,050
Xerophyte shrubland and grassland	9, 11	1,700	0	1,980	0	1,100	0
Areas irrigated with spring discharge						9,260	11,500
Total		212,970	64,400 (21,000)	84,120	19,800 (30,000)	118,330	35,100 (1,670)

Groundwater Evapotranspiration Rates for Evapotranspiration Units with No Surface Water

Because dry meadow, phreatophyte shrubland, and sagebrush shrubland ET units evapotranspire precipitation and groundwater during average water years, ET_g rates are assumed equal to ET_{net} (eq. 6). The dryland ET units that exist where seasonal or routine flooding do not occur collectively cover 325,000 acres (tables 5–6), or about 60 percent of the GETA. Xerophyte shrubland and grassland were assigned ET_g rates of zero since precipitation is the only moisture source available to these ET units.

Groundwater Evapotranspiration Rates for Wet Meadow, Riparian, and Marsh Evapotranspiration Units

Wet meadow, riparian, and marsh ET units evapotranspire precipitation, groundwater, and surface-water inflow; therefore, ET_{net} is a combination of ET_g and ET_{sw} (eq. 6), and an estimate of ET_{sw} is needed to estimate ET_g in these ET units. Vegetated ET units with seasonal surface-water inflow collectively cover about 32,000 acres, or 6 percent of the GETA (table 5). Wet meadow and marsh ET units lie within river

floodplains and border Malheur Lake where flooding and inundation occur seasonally; riparian areas lie along stream channels where groundwater is close to the land surface (table 2).

The spatial extent of surface-water flooding and depth of inundation vary considerably from year to year and within a season depending on winter precipitation volume and timing of snowmelt. For example, the maximum extent of surface-water flooding during average (2005) and wet water years (2011; 30 percent above average) is estimated to increase from 1 to 20 percent of the GETA during March 15–July 15 based on the normalized difference moisture index computed from Landsat imagery (fig. 9; app. 1; Gao, 1996; Wilson and others, 2002). The average floodwater extent observed in 2005 occurs seasonally, whereas the extent in 2011 occurs episodically. Episodic flood events in the Harney Basin during 1982–2016 have a roughly 6-yr recurrence interval based on comparison of precipitation datasets (fig. 3) and Landsat imagery (data not shown). Evaluation of seasonal and episodic flood inundation depths and persistence were beyond the scope of this study, but the years evaluated (2005, 2011) provide a reasonable bound to consider longer-term contributions of floodwater to ET_{net}.

A. 2005

EXPLANATION

Maximum normalized difference moisture index, March 15– July 15

- 0.4 to 0.5
- 0.5 to 0.6
- 0.6 to 0.7
- 0.7 to 0.8
- 0.8 to 1

— - — **Harney Basin**

——— **Harney Basin lowlands**

——— **Groundwater evapotranspiration area**

Base map modified from U.S. Geological Survey and other digital data, various scales.Projection: UTM Zone 11 North. North American Datum of 1983

B. 2011
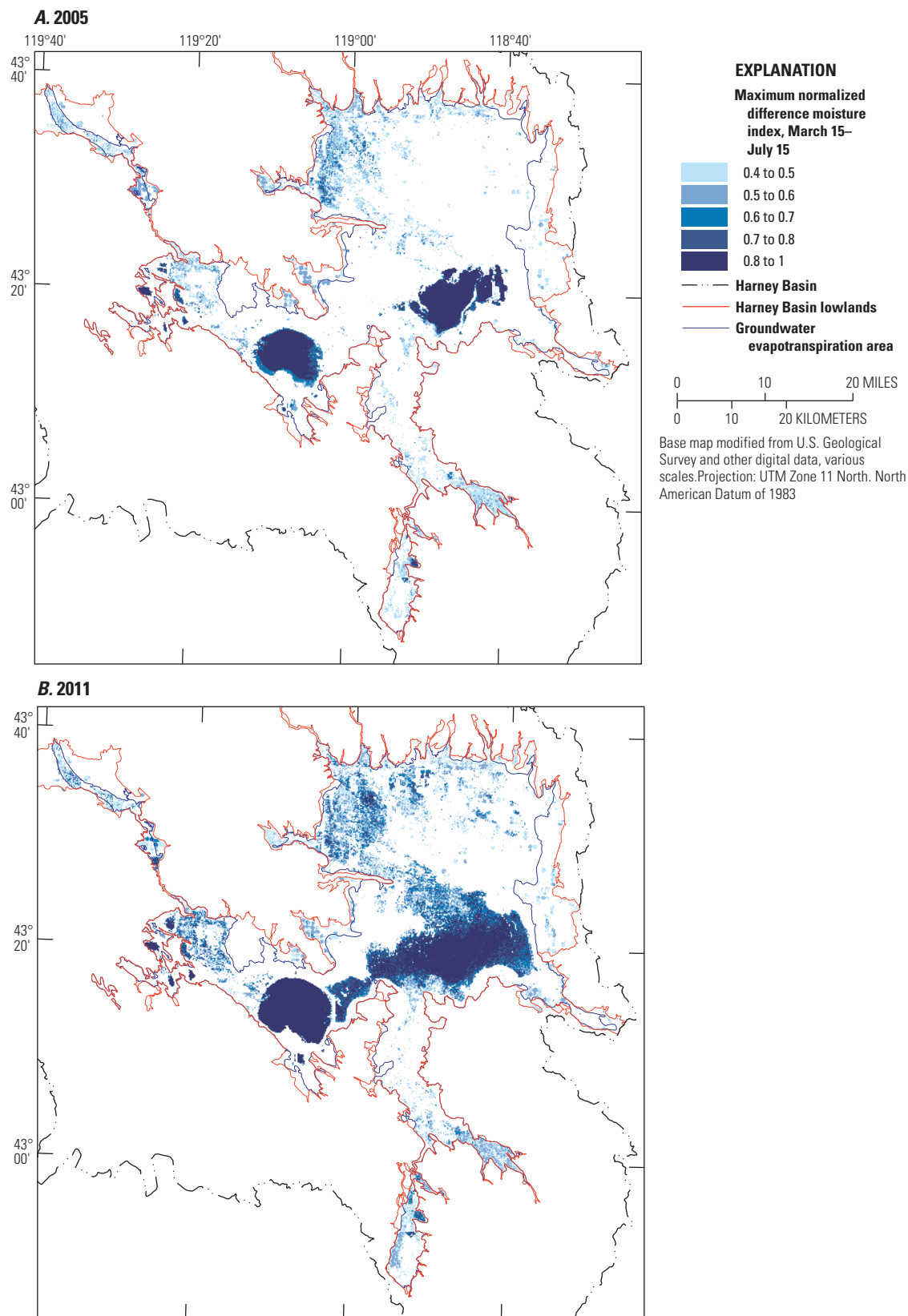
Figure 9. Maximum extent of surface-water flooding on the Harney Basin lowlands, southeastern Oregon, during March 15–July 15, 2005 (*A*) and 2011 (*B*). Maximum normalized-difference moisture index values of 0.4 or more are assumed to indicate flooded or snow-covered areas.

The ET_g rate in wet meadow ET units was considered the same as the ET_g rate in dry meadow ET units (table 6). The equivalence of ET_g rates in wet and dry meadows is supported by generally similar depth to groundwater and soil hydraulic properties among the two ET units. Because wet meadows commonly are adjacent to, but at a slightly lower elevation than, dry meadows, they receive additional water (with respect to dry meadows) through seasonal flooding from nearby streams.

The ET_{net} source in marsh and riparian areas, which collectively represent about 1 percent of the GETA area (table 5), was equally partitioned between groundwater and surface water (table 6). Marsh and riparian ET units were delineated along both perennial and ephemeral surface-water features and the partitioning of ET_{net} between ET_g and ET_{sw} likely varies spatially within the ET units. Although ET_g and ET_{sw} contributions are uncertain, ET_g in marsh and riparian ET units collectively represents only 3 percent of the lowland ET_g, and adjustments to the partitioning between ET_g and ET_{sw} would minimally affect lowland estimates.

Groundwater Evapotranspiration Rates for Open Water and Bare Soil-Playa Evapotranspiration Units

Open-water ET units represent either stream- or spring-supplied water bodies; therefore, ET_{net} rates were equal to either ET_{sw} or ET_g (table 6). Open-water ET units cover nearly 13,000 acres, or 2 percent of the GETA (table 5). Stream-supplied water bodies cover about 11,100 acres, mostly Malheur Lake, and spring-supplied water bodies cover 1,750 acres, mostly along the periphery of Harney Lake and to the west in Warm Springs Valley (fig. 7). Open-water ET rates were based on evaporation estimates from Malheur Lake. Hostetler and Bartlein (1990) estimated a 6.5-yr mean open-water evaporation rate of 37 in/yr (3.08 ft/yr) using an eddy-diffusion model calibrated to lake levels at Malheur Lake. The open-water ET rate of 3.08 ft/yr is slightly lower than shallow lake estimates from Linsley and others (1982; 40 in/yr or 3.3 ft/yr) and Farnsworth and others (1982; 45 in/yr or 3.8 ft/yr), and the 1959-2005 pan evaporation estimate (45.4 in/yr or 3.8 ft/yr; Western Regional Climate Center, 2020) from the Voltage 2 NW Sod House pan evaporation site (table 1) located just south of Malheur Lake. The range in open-water ET estimates is about equal to mean annual GridMET precipitation over open water bodies in the Harney Basin (8 in or 0.68 ft); therefore, the open-water ET rate of 3.08 ft/yr was assumed to account for precipitation inputs and considered equal to ET_{net} during 1987–2015. The open-water ET_{net} rate of 3.08 ft/yr is like the maximum ET_{net} rate estimated for vegetated ET units using physics-based and empirical methods (fig. 8). For open-water bodies fed entirely by groundwater, the ET_g rate is equal to ET_{net}.

The minimum extent of Malheur Lake in 2015 was categorized within the open-water ET unit (figs. 1, 7). Vegetated areas within the seasonal and interannual footprint of Malheur Lake were included as vegetated ET units rather than open water to allow for ET_g estimation during dry years. During wet periods when the larger Malheur Lake extent inundated vegetated ET units with open water, ET_{net} and ET_g estimates generated with physics-based and empirical methods declined toward zero as standing water reduced EVI to negative values.

Bare soil-playa ET units evaporate precipitation and groundwater. The bare soil-playa ET unit covers nearly 24,000 acres and represents about 6 percent of the unirrigated GETA. Groundwater ET rates for the bare soil-playa ET unit are based on playa ET_g measurements from north-central Nevada (Garcia and others, 2015). A mean annual bare soil-playa ET_g of 0.05 ft (0.6 in) was used in this study and was not adjusted for differences in evaporative demand or precipitation.

The extent of Harney Lake was predominantly categorized as a playa ET unit, with a small fraction distinguished as open water where perennial springs discharge onto the lakebed surface. Although periodically inundated with streamflow from Silver Creek (or Malheur Lake, via Mud Lake, during the mid-1980s), Harney Lake represents a seepage face where groundwater discharges through bare-soil evaporation.

Results and Discussion for Groundwater Evapotranspiration in the Groundwater Evapotranspiration Area

Mean Annual Groundwater Evapotranspiration Rates

Mean-annual ET_g rates varied by ET unit and estimation method with the highest rates attributed to open water, marsh, and riparian areas and the lowest rates attributed to bare soil-playa areas (table 5). Marsh and riparian ET_g rates estimated with the physics-based method averaged 0.87 ft/yr, whereas those from the empirical method averaged about 0.54 ft/yr. Rates of ET_g calculated for dry and wet meadow ET units were lower than estimates from marsh and riparian units for each respective estimation method and averaged 0.68 ft/yr for the physics-based method and 0.43 ft/yr for the empirical method. The ET_{net} estimates used to compute ET_g from marsh, riparian, and wet meadow ET units (fig. 8) are near the range of estimates for similar vegetation in previous studies where ET_{net} was fully attributed to either groundwater or surface water (1.2–2.1 ft/yr; table 3).

Mean ET_g rates for phreatophyte shrubland ET units ranged from 0.26 ft/yr for the physics-based method to 0.37 ft/yr for the empirical method and were within the range of ET_{net} estimates in previous studies in shrubland areas where ET_{net} was equal to ET_g (table 3). The open-water evaporation rate of 3.08 ft/yr was used for groundwater-fed open water bodies (spring pools) and was adopted from evaporation estimates from Malheur Lake (Hostetler and Bartlein, 1990).

Mean Annual Groundwater Evapotranspiration Volume

The estimated mean annual volume of ET_g from natural, non-irrigated areas across the Harney Basin GETA totaled 119,000 acre-ft and was calculated by averaging estimates from empirical and physics-based methods for each ET unit and summing ET-unit estimates in the Harney Basin GETA (table 5). The ET_g volume from the phreatophyte shrubland ET unit was estimated at 47,400 acre-ft and represents the largest proportion from the various ET units. Sagebrush shrubland was the next largest contributor to ET_g with an estimated volume of 21,800 acre-ft. Dryland ET units including bare soil-playa, phreatophyte shrubland, sagebrush shrubland, and dry meadow areas accounted for 70 percent of the ET_g volume whereas wetter ET units including marsh, wet meadow, riparian, spring pools, and areas irrigated with spring discharge in Warm Springs Valley contributed to 30 percent of the ET_g volume (table 5). Groundwater ET estimates from areas irrigated with spring discharge were estimated using a separate approach (see section "Irrigation Pumpage" for more detail) but are included here for completeness as spring discharge would otherwise be consumed by ET.

Groundwater ET estimates summarized in table 6 represent mean annual conditions within the Harney Basin GETA during 1987–2015 and are assumed to represent estimates during the 1982–2016 study period. Groundwater ET volumes from natural areas varied among the three regions (fig. 1) and were related to varying acreage of different ET units within each region (table 6). The ET_g volume was about 20,000 acre-ft over about 84,000 acres in the southern region, 64,000 acre-ft over about 213,000 acres in the northern region, and 35,000 acre-ft over about 118,000 acres in the western region, which included 11,500 acre-ft of spring discharge to irrigate about 9,300 acres. Within the three regions, phreatophyte and sagebrush shrubland ET units represented 57–80 percent of ET-unit acreage and comprised 34–70 percent of ET_g. The remaining contributions to ET_g were from riparian, marsh, and open-water ET units, and spring-irrigated crops.

Uncertainties in Groundwater Discharge through Evapotranspiration

Groundwater ET estimates made in this study are likely within 20 percent of actual totals for ET units. Assumptions affecting the accuracy of mean annual discharge estimates are: (1) ranges in ET_g rates assigned to ET units (fig. 8) adequately represent the range for that unit, (2) estimates of ET from surface-water flooding accurately represent the mean-annual volume, (3) regional groundwater is evaporated and transpired from surfaces delineated as discharge areas, and (4) vegetation was classified correctly and assigned to the proper ET unit. Despite differences in approaches, mean-annual ET_g estimates

from the physics-based method and empirical method are within 10 percent of one another, which provides an additional level of confidence in the results. Comparisons between basin- and regional-scale groundwater-ET estimates and groundwater-recharge estimates provide additional insight into estimate uncertainty.

ET-rate accuracy (assumption 1) is linked to the accuracy of published measurements and scaling approaches used to estimate ET in this study. Accuracy associated with published measurements is expected to be as good as 10 percent (Meyers and Baldocchi, 2015). Because ET was computed from precipitation and ET_o-adjusted measurements made in other basins, confidence in rates and the degree to which they represent mean annual values and the mean value over an entire ET unit would be improved with spatially distributed measurements made within the Harney Basin. An additional assumed uncertainty of 10 percent is attributed to scaling rates from other basins to the Harney Basin using vegetation indices. The empirical equation developed by Beamer and others (2013) (and used herein) predicted site measurements to within a mean of 20 percent, but the accuracy range was generally 0–60 percent. The largest inaccuracies reported by Beamer and others (2013) occurred in sparsely vegetated areas where soil-background noise and annual grasses such as cheatgrass can confound EVI (see app. 1 for more information about the effects of background noise on EVI). In this study, ET estimates from empirical and physics-based methods were averaged over 23 years, which likely reduced the effects of EVI fluctuations from background noise.

The absolute magnitude of ET from surface-water flooding (assumption 3) is uncertain as estimates are based on limited data. During dry years with minimal flooding beyond irrigated areas, higher ET rates in wet meadow, riparian, and marsh areas, with respect to dry meadow areas, are likely supported by antecedent soil moisture replenished during previous flood years. Where groundwater is shallow (within 10 ft of land surface) beneath wet meadow, riparian, and marsh areas, floodwater might recharge groundwater during wet years and groundwater, in turn, might support higher ET rates in those areas during dry years (compared to dry meadows). If floodwater in wet meadow areas is actively recharging the groundwater system during wet years, then the mean-annual ET_{sw} estimate of 18,000 acre-ft likely represents an upper bound. In contrast, mean-annual ET_{sw} estimates from naturally flooded areas could be biased low as shrubland areas are episodically flooded during wet years like 2011 (fig. 9B). Greater ET_{sw} from episodically flooded shrubland areas would have little effect on ET_g in those areas because ET_g rates were constrained each year by the physics-based approach. Despite these caveats, ET_{sw} estimates likely are well within an estimate uncertainty of 20 percent for the full GETA.

Groundwater ET rates in sagebrush-dominated shrubland averaging 0.14 ft/yr could be biased high if plants are not using groundwater (assumption 3). Sagebrush-water isotope compositions presented in appendix 2 indicate direct root-water uptake of groundwater at two of six areas sampled (fig. 2.2). At most plant-water sampling areas, sagebrush appeared to be using evaporated soil water that could represent a mixture of evaporated, upward moving groundwater and evaporated precipitation. Sagebrush shrubland represents the second largest ET unit within the GETA and validation of the ET-unit classification indicates more than 10 percent of both phreatophytic shrubland and dry meadow observations were misclassified as sagebrush shrubland (app. 3; table 3.1). Groundwater ET rates of 0.14 ft/yr are common for sparsely distributed phreatophytes; therefore, the mean rate for the sagebrush shrubland ET unit could, in part, reflect higher ET_g rates from misclassified phreatophytic vegetation. Despite uncertainties in source water or vegetation classification, uncertainty in ET_g volume for the sagebrush shrubland ET unit is well within a 20-percent estimate uncertainty.

Groundwater Discharge to Springs

Groundwater discharges to springs throughout the study area (fig. 10). The National Hydrography Dataset (NHD; U.S. Geological Survey, 2016) contains nearly 2,600 springs in the Harney Basin, which likely represents a minimum number since springs in forested areas and within deep canyons are difficult to identify. Most springs discharge in the uplands (97 percent of NHD springs; fig 10) at small volumes reflecting discharge of local, recently recharged groundwater, whereas spring discharge in the lowlands occurs in few locations at considerably larger volumes reflecting regional discharge of older groundwater (Gingerich and others, 2022). Discharge from springs provides a year-round source of water to lowland spring-fed streams and ponds during most years. Discharge from some upland springs coalesces into spring brooks that merge with streams flowing toward the lowlands; this discharge is part of stream base flow and is included in streamflow measurements. Upland springs also discharge to meadows, wetlands, and spring brooks of limited length where the discharge is completely consumed by ET. All springflow discharged in the Harney Basin lowlands leaves the system as ET from either non-irrigated areas or irrigated areas following springflow routing. Springflow that is consumed by ET in non-irrigated lowland areas or areas irrigated by springflow in the western region lowlands are included in ET_g estimates within the GETA (see section "Groundwater Discharge through Evapotranspiration" and tables 5, 6). Measured spring discharge in upland areas that merges with streams downgradient of measurement streamgages is explicitly accounted for in discharge totals.

Springflow measurements were compiled for 30 springs from measurements documented in previous studies (fig. 10) and from measurements made by OWRD in July 2017 at springs in Warm Springs Valley (table 7). Springs with at least one discharge measurement represent 1 percent of mapped springs in the Harney Basin, but likely constitute most of the spring discharge owing to selective measurement of large-volume springs. Discharge from unmeasured springs was bounded using spring discharge measurements from all measured springs in southeastern Oregon stored in the USGS National Water Information System (NWIS) database (U.S. Geological Survey, 2021). Discharge measurements (110) were obtained for 75 springs in the region bounded between 42° and 44.5° north latitude and -117.5° and -120° west longitude. The discharge measurements were made during 1907–2020, with 70 measurements made during 2017–20. Discharge measurements ranged from 0 to 10,840 acre-ft/yr. More than one-third of the springs (26) were reported as not having any discharge when visited. The median discharge for all visited springs was 0.2 acre-ft/yr with an interquartile range of 4 acre-ft/yr; among springs that were not dry, the median discharge was 2.1 acre-ft/yr with an interquartile range of 7.9 acre-ft/yr. Spring-discharge measurements are limited; therefore, estimates presented herein are based on the assumptions that the mean of irregularly sampled measurements represents the long-term mean and that springflow has not changed greatly since the early 1900s.

Discharge from Upland Springs

The NHD contains 2,474 mapped springs that discharge from upland areas of the Harney Basin. Of these, 12 have documented discharge measurements (table 7). Measured discharge from upland springs totaled 14,200 acre-ft/yr and is 30 percent of the total measured spring discharge in the Harney Basin. Discharge from unmeasured upland springs was estimated to range from 500 to 9,800 acre-ft/yr based on the spring discharge from measured springs elsewhere in southeastern Oregon. The smaller estimate is calculated from the median discharge from all springs and the larger estimate is calculated from the 75th percentile of discharge from all springs.
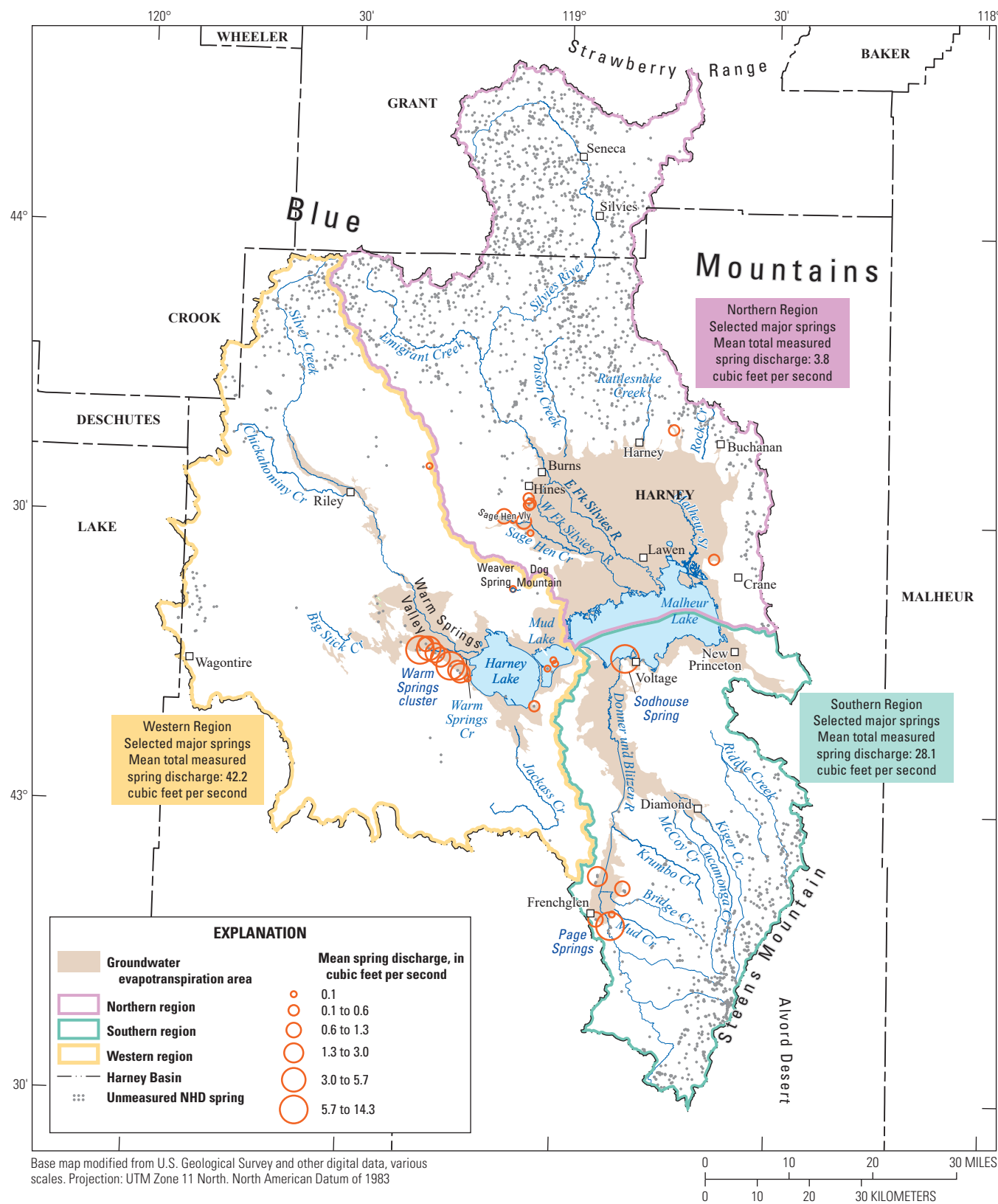
Figure 10. Locations and mean discharge rates of selected major springs, summed by region, and unmeasured springs from the National Hydrography Dataset (NHD), Harney Basin, southeastern Oregon, 1903–2017.

Table 7. Mean groundwater discharge to selected springs (1903–2017), Harney Basin, southeastern Oregon.

[**Discharge, July 2017**: Single measurements made by OWRD in July 2017. **Mean discharge**: Over period of record. **Range of measurement dates**: Unless otherwise noted, measurements collected 1902–32 from Piper and others (1939); 1939–40, 1984, 2017 from Oregon Water Resources Department (2020); 1968 from Leonard (1970); 1972–73 from Hubbard (1975); 1997–2016 by Timothy Mayer, U.S. Fish and Wildlife Service, written commun., 2017. **Latitude and Longitude:** Referenced to North American Datum of 1983. **Elevation:** in feet above North American Vertical Datum of 1988. Geographic position: position of water-bearing units from which discharge occurs. **Abbreviations:** ft³/s, cubic feet per second; L, lowland; meas., measurements; N, no; number; OWRD, Oregon Water Resources Department; U, upland; USGS, U.S. Geological Survey; Y, yes; —, not measured]

Local spring name or state spring number	Discharge, July 2017 (ft³/s)	Mean discharge (ft³/s)	No. of meas.	Measured discharge range (ft³/s)	Range of measurement dates	OWRD spring number	USGS site number	Latitude (decimal degrees)	Longitude (decimal degrees)	Elevation (feet)	Geographic position/ discharge routed to stream, canal, or irrigated area
Northern region											
Goodman Spring	—	0.36	5	0.06–0.67	1930–31, 1968	SPRG0018713	433827118173801	43.528502	-119.081420	4,140	L/N
Cow Creek Spring	—	0.50	2	0.50–0.50	1930–31	SPRG0018717	433949118442401	43.663522	-118.739953	4,207	U/Y
Mill Pond Spring	—	0.57	4	0.02–1.11	1930–31, 1968	SPRG0018720	433224119045401	43.540296	-119.082092	4,147	U/Y
SPRG0018721	—	0.26	6	0.01–0.67	1930–31, 1968	SPRG0018721	433153119045001	43.530860	-119.077340	4,138	L/N
SPRG0018724	—	0.76	4	0.56–0.96	1930–31, 1968	SPRG0018724	433029119082301	43.508056	-119.139722	4,156	U/Y
SPRG0018725	—	0.11	2	0.01–0.17	1930–31	SPRG0018725	433008119070601	43.502222	-119.118333	4,139	U/Y
Roadland Spring	—	0.84	4	0.65–1.08	1930–31, 1968	SPRG0018726	433000119053001	43.500000	-119.092593	4,138	U/Y
SPRG0018728	—	0.11	2	0.11–0.11	1930–31	SPRG0018728	432849119043301	43.480278	-119.075833	4,131	L/N
Crane Hot Spring	[1]0.00	0.27	9	0.0–0.40	1903, 1907, 1930–31, 1968, 1984, 2017	SPRG0018279	432630118382601	43.441000	-118.639000	4,122	L/N
Western region											
Elliot Spring	—	0.002	1	0.002	[2]1980	SPRG0022260	433530119191301	43.591667	-119.320278	5,114	U/N
Weaver Spring	—	0.03	3	0.02–0.04	1907, 1930–31	SPRG0018730	432258119065201	43.382778	-119.114444	4,153	U/Y
Double O Cold Spring	—	0.85	2	0.70–1.00	1907, 1931	SPRG0018731	431649119190800	43.283850	-119.317240	4,126	L/Y
Double O Barnyard Spring	3.70	5.74	12	3.00–9,20	1916-19, 1931, 2017	SPRG0018733	431635119183601	43.276100	-119.310200	4,124	L/Y

Table 7. Mean groundwater discharge to selected springs (1903–2017), Harney Basin, southeastern Oregon.—Continued

[**Discharge, July 2017**: Single measurements made by OWRD in July 2017. **Mean discharge:** Over period of record. **Range of measurement dates:** Unless otherwise noted, measurements collected 1902–32 from Piper and others (1939); 1939–40, 1984, 2017 from Oregon Water Resources Department (2020); 1968 from Leonard (1970); 1972–73 from Hubbard (1975); 1997–2016 by Timothy Mayer, U.S. Fish and Wildlife Service, written commun., 2017. **Latitude** and **Longitude:** Referenced to North American Datum of 1983. Elevation: in feet above North American Vertical Datum of 1988. Geographic position: position of water-bearing units from which discharge occurs. **Abbreviations:** ft³/s, cubic feet per second; L, lowland; meas., measurements; N, no, number; OWRD, Oregon Water Resources Department; U, upland; USGS, U.S. Geological Survey; Y, yes; —, not measured]

Local spring name or state spring number	Discharge, July 2017 (ft³/s)	Mean discharge (ft³/s)	No. of meas.	Range of measurement dates	OWRD spring number	USGS site number	Latitude (decimal degrees)	Longitude (decimal degrees)	Elevation (feet)	Geographic position/ discharge routed to stream, canal, or irrigated area
					Western region—continued					
Basque (East Double O) Spring	1.80	2.40	9	1907, 1916–17, 1931–32, 2017	SPRG0018734	431607119174201	43.268960	-119.294920	4,124	L/Y
Johnson Spring	1.60	1.71	7	1907, 1916–17, 1931, 2017	SPRG0018737	431542119165401	43.261600	-119.281700	4,122	L/Y
Hughet Spring	13.00	12.59	9	1916–17, 1931–32, 2017	SPRG0018738	431453119153101	43.247370	-119.258200	4,116	L/Y
Upper Sizemore Spring	1.40	2.15	7	1916–17, 1931–32, 2017	SPRG0018739	431423119142501	43.239730	-119.240120	4,123	L/Y
Lower Sizemore Spring	1.70	1.72	7	1916-17, 1931, 2017	SPRG0018740	431406119140201	43.235060	-119.233860	4,126	L/Y
Hibbard Spring	9.20	14.29	15	1907, 1913, 1916–19, 1921, 1932, 2017	SPRG0023236	431623119195001	43.273350	-119.330690	4,127	L/N
Soldier Spring	—	0.06	1	1931	SPRG0018814	431333119125901	43.225950	-119.216130	4,105	L/N
Unnamed Hot Spring	—	0.48	4	1902, 1907, 1930–31	SPRG0018745	431052119032701	43.181100	-119.057000	4,110	L/N
SPRG0018746	—	0.06	1	1931	SPRG0018746	431541119005201	43.261389	-119.014444	4,100	L/N
SPRG0018747	—	0.02	1	1931	SPRG0018747	431520119003601	43.255556	-119.010000	4,098	L/N
Lynch Spring	—	0.06	1	1931	SPRG0018748	431448119014001	43.246630	-119.027775	4,098	L/N

Table 7. Mean groundwater discharge to selected springs (1903–2017), Harney Basin, southeastern Oregon.—Continued

[**Discharge, July 2017**: Single measurements made by OWRD in July 2017. **Mean discharge**: Over period of record. **Range of measurement dates**: Unless otherwise noted, measurements collected 1902–32 from Piper and others (1939); 1939–40, 1984, 2017 from Oregon Water Resources Department (2020); 1968 from Leonard (1970); 1972–73 from Hubbard (1975); 1997–2016 by Timothy Mayer, U.S. Fish and Wildlife Service, written commun., 2017. **Latitude** and **Longitude**: Referenced to North American Datum of 1983. Elevation: in feet above North American Vertical Datum of 1988. Geographic position: position of water-bearing units from which discharge occurs. **Abbreviations**: ft³/s, cubic feet per second; L, lowland; meas., measurements; N, no, number; OWRD, Oregon Water Resources Department; U, upland; USGS, U.S. Geological Survey; Y, yes; —, not measured]

Local spring name or state spring number	Discharge, July 2017 (ft³/s)	Mean discharge (ft³/s)	No. of meas.	Measured discharge range (ft³/s)	Range of measurement dates	OWRD spring number	USGS site number	Latitude (decimal degrees)	Longitude (decimal degrees)	Elevation (feet)	Geographic position/discharge routed to stream, canal, or irrigated area
					Southern region						
Fivemile (Hog House) Spring	—	3.00	2	2.00–4.00	1907, 1932	SPRG0018751	425321118535501	42.889167	-118.898611	4,165	U/Y
Knox Spring	—	1.25	2	1.00–1.50	1911, 1932	SPRG0018752	425210118502201	42.869444	-118.839444	4,282	U/Y
Warm Spring near Frenchglen	—	0.93	7	0.19–2.50	1907, 1916, 1932, 2003	SPRG0018753	424854118540201	42.815000	-118.900556	4,201	U/Y
SPRG0018754	—	0.13	2	0.04–0.22	1907, 1932	SPRG0018754	424927118514601	42.824167	-118.862778	4,201	U/Y
Page Springs	—	11.52	34	2.40–21.50	1997–98, 2003, 2005, 2007, 2009, 2011–16	SPRG0000055	424814118515801	42.803778	-118.866000	4,241	U/Y
Sodhouse Spring	—	12.27	20	4.50–19.0	1907, 1930–31, 1939–40, 1972–1973, [3]1978–80	SPRG0018735	431559118504001	43.266377	-118.845150	4,100	L/Y

[1]Spring is no longer flowing

[2]Townley (1980)

[3]U.S. Geological Survey (2021)

Discharge from Lowland Springs

The NHD contains 79 mapped springs in lowland areas of the Harney Basin and 18 have documented discharge measurements (table 7). Measured discharge from lowland springs totaled about 34,000 acre-ft/yr (46.9 ft^3/s), which is 70 percent of the total measured spring discharge in the Harney Basin. Most of the measured lowland discharge occurs in Warm Springs Valley and from Sodhouse Spring. Discharge from unmeasured lowland springs was estimated to range from 12 to 240 acre-ft/yr based on the median and 75th percentile of spring discharge rates, respectively, from measured springs elsewhere in southeastern Oregon. Estimated discharge from unmeasured lowland springs is considerably less than the uncertainty in the combined measured discharge of lowland springs (15 percent; Oregon Water Resources Department, 2020) and is not considered hereinafter.

Spring Discharge by Region

Spring discharge varies regionally from a maximum of about 24,600 acre-ft/yr (34 ft^3/s) in the western region to a minimum of about 2,500 acre-ft/yr (3.5 ft^3/s) in the northern region (fig. 10). The upper range of unmeasured spring discharge discussed earlier was used to calculate total spring discharge by region and is used to provide an upper limit on the estimated discharge from springs for these areas.

In the northern region, spring discharge primarily occurs in the uplands (94 percent) and measured spring discharge accounts for 28 percent of the total estimated spring discharge in this region. Nearly 20 percent of mean measured discharge in the northern region issued from a few small lowland springs located south of Hines near Sage Hen Valley and 7 percent of mean measured discharge issued from Crane Hot Spring located in the lowlands west of Crane, but 2017 measurements indicate Crane Hot Spring is no longer discharging at land surface. Measurements and field observations made during this study indicate that discharge from individual springs in the northern region typically is low (<0.1–0.8 ft^3/s) and discharge from most of the unmeasured upland springs visited in the northern region during this study flows into wetlands, meadows, and riparian corridors of limited length rather than coalescing or flowing into a perennial stream. However, some larger spring complexes do occur in the northern uplands and are important sources of base flow to major upland streams, such as those in the headwaters of Emigrant Creek (fig. 1).

In the western region, spring discharge primarily occurs in the lowlands (96 percent), and measured spring discharge during 2017 accounts for 96 percent of the total estimated spring discharge in this region. Upland springs in the western region are similar to those noted in the northern region owing to their shared topographic and geologic setting: most springs are low-volume and their discharge issues to wetlands, meadows, and spring brooks of limited length, but there are important complexes that provide base flow to upper reaches and tributaries of Silver Creek. Unlike the northern region

of Harney Basin, however, the western region has the largest concentration of lowland spring discharge in the Warm Springs Valley. This area of regional groundwater discharge is comprised of numerous major springs or spring complexes that emerge along a prominent fault southwest of Harney Lake (fig. 10). Discharge to springs in Warm Springs Valley measured in 2017 totaled 23,500 acre-ft/yr (32 ft^3/s) and accounted for about 95 percent of measured spring discharge in the western region and 50 percent of the basin-wide measured spring discharge (table 7). Piper and others (1939) noted that temporal fluctuations in discharge among the five largest springs in Warm Springs Valley ranged from about 40 to 100 percent and likely resulted from changes in spring pool stage from intermittent irrigation diversions and multi-year fluctuations in precipitation. Much of the discharge from springs in Warm Springs Valley is used to irrigate hay and grasses and the remainder supplies water to native wetlands and marshes. Discharge from these springs that is not transpired by plants either ends up in one of the many playas in this region, the largest of which is Harney Lake, or reinfiltrates and is discharged downgradient.

In the southern region, spring discharge primarily occurs in the uplands (63 percent), and measured spring discharge, mostly along the upland-lowland boundary, accounts for 90 percent of the total estimated spring discharge in this region. Mapped upland springs in the southern region are concentrated in the upper slopes of Steens Mountain and within stream canyons. A line of relatively high-discharge springs occurs near the upland-lowland boundary near Frenchglen and includes Page Springs, Knox Spring, Fivemile Spring, and Warm Spring. The southern region contains one major spring in the lowlands: Sodhouse Spring which discharges near Malheur Lake. Page Springs and Sodhouse Spring are the largest springs in the region and account for 74 percent of the total spring discharge and 82 percent of the measured spring discharge in this region (table 7). Both springs exhibit substantial variability in discharge. Discharge at Page Springs averaged 8,300 acre-ft/yr (11.5 ft^3/s) during 1997–2016 and ranged from 1,700 to 15,600 acre-ft/yr (2.4 to 21.5 ft^3/s). Discharge at Sodhouse Spring averaged 8,900 acre-ft/yr (12 ft^3/s) during 1907–80 and varied from 3,300 to 13,800 acre-ft/yr (4.5 to 19 ft^3/s). The large variability in discharge at Sodhouse Spring could indicate it lies a short distance from its recharge source, is largely influenced by water-table fluctuations caused by variable stage in the nearby Donner und Blitzen River, responds to multi-year precipitation patterns, and (or) discharges from a highly-transmissive portion of the groundwater system (Gingerich and others, 2022). Stable isotope measurements reported by Gingerich and others (2022) indicate that the source of water supplying Sodhouse Spring is likely recharged from the Donner und Blitzen River. Similar variability in discharge at Page Springs, which is geographically positioned at the base of Steens Mountain southeast of Frenchglen, likely indicates it responds to multi-year precipitation patterns and discharges from a highly transmissive portion of the groundwater system.

Fate and Accounting of Spring Discharge in the Groundwater Budget

Like most water in the Harney Basin, spring discharge ultimately leaves the hydrologic system as ET. However, accounting for spring discharge in the groundwater budget is more complex than most other budget components because the ET of spring water can occur directly from spring-fed vegetation or from playas and ponds, or the ET of spring water can occur after spring discharge has joined a flowing stream and comingled with base flow, rainfall runoff, and snowmelt. The fate of streamflow–including its spring-discharge component–is fully accounted for in the next section of the report, but can include (1) infiltration to and discharge from the groundwater system either as ET, pumpage, or new spring discharge, (2) diversion for irrigation, and (3) discharge to playas and lakes. Considering the fate of spring discharge is necessary to avoid double counting it in the groundwater budget.

Discharge from most upland springs generally is accounted for in other budget estimates. The discharge from upland springs that joins flowing streams is accounted for in base-flow estimates of those streams (see section "Groundwater Discharge to Streams [Base Flow]"). Conversely, discharge from upland springs that issues into wet meadows, marshes, and spring brooks of limited length is accounted for in the upland ET estimates (see section "Groundwater Recharge from Infiltration of Precipitation and Snowmelt"). The discharge from most measured upland springs is explicitly accounted for in the groundwater budget because the springs discharge water downstream of the streamgage at which base flow is estimated; such as Page Springs, Knox Spring, Warm Springs, and Fivemile Spring in the southern region. Spring discharge that joins the stream downstream of streamgages is ultimately treated as part of base flow in its dissipation from the system.

Discharge from most lowlands springs is accounted for in ET_g estimates as discussed in the section "Groundwater Discharge through Evapotranspiration." This includes the large volume of discharge in Warm Springs Valley, which is accounted for as ET from irrigated and non-irrigated vegetation and (or) ET from open water. The discharge from Sodhouse Spring is the only lowland spring discharge explicitly accounted for in the groundwater budget because it issues at the edge of Malheur Lake and its water largely flows into the lake where it eventually evaporates.

Uncertainty in Spring Discharge Estimates

The uncertainty of the assumption that spring-discharge estimates based on the mean of measurements made over the last century are representative of study-period (1982–2016) conditions is largely unknown and likely depends on climate variability and proximity to areas of groundwater development. Springs near the southern lowland boundary are upgradient from groundwater development and therefore are affected by climate only, whereas those near Sage Hen Valley and the Weaver Spring/Dog Mountain area are adjacent to groundwater-irrigated areas (fig. 10). In Warm Spring Valley (south of the Weaver Spring/Dog Mountain pumping area) July 2017 springflow measurements totaling 23,500 acre-ft/yr (32.4 ft^3/s; table 7) are within 11 percent of the 1931 estimate reported by Piper and others (1939) (26,500 acre-ft/yr), within 20 percent of the 1907–2017 mean, and within the range of early 1900s measurements at 6 of the 7 springs measured. Considering the variability noted by Piper and others (1939) and springflow measurement accuracy of about 15 percent (Oregon Water Resources Department, 2020), differences between 2017 and early 1900s springflow in Warm Springs Valley likely reflect climate variability and (or) management of irrigation diversions rather than nearby groundwater development.

Springflow measurements in Warm Springs Valley represent about 60 percent of western-region ET_g estimates (table 6) and are within 10 percent of adjacent ET_g estimates in and around Warm Springs Valley (about 21,600 acre-ft/yr). Differences between springflow and adjacent ET_g estimates are within estimate uncertainty, but could also result from climate variability (July 2017 compared to average conditions during 1987–2016), the effects of intermittent diversions noted by Piper and others (1939), or downgradient ET of excess springflow, beyond the area evaluated.

Groundwater Discharge to Streams (Base Flow)

Natural groundwater discharge to streams or base flow is the primary groundwater discharge mechanism in upland areas and occurs in limited areas in the Harney Basin lowlands (fig. 6). Base flow is the primary source of water in streams of the Harney Basin in late summer and autumn, when runoff from rain and snowmelt is minimal. Stream gains from and losses to the groundwater system across specified stream reaches (seepage) can be measured directly by taking concurrent measurements upstream and downstream during periods of low flow. Seepage measurements made during the study showed gaining perennial stream reaches in the lower parts of the uplands and in limited areas in the lowlands near the mountain front; however, across most of the lowland area, streams predominately lose water to the groundwater system (app. 6). No seepage measurements were made in streams high in the uplands, which generally are gaining reaches. Discrete seepage measurements are time consuming and representative of the measurement period only. Pairs of gaging stations along a stream reach can be used to obtain a longer time series of groundwater seepage; however, this technique is limited in two respects: (1) few streamgages are operated in the Harney Basin and (2) direct partitioning of streamflow into base flow and runoff can only be done during periods when there is no runoff from precipitation or snowmelt–roughly August through October in the Harney Basin. For these reasons, mean annual estimates of base flow in the Harney Basin were made using

three other techniques: hydrograph separation techniques, low-flow streamflow measurements, and for ungaged streams, scaling estimated streamflow using nearby streamgaged streams. Estimates of mean annual base flow using any one of the three estimation techniques also require estimates of mean annual streamflow. These methods and results are described in the following subsections.

Mean Annual Streamflow Estimates

Streams drain the uplands of the Harney Basin through many watersheds distributed across the northern, southern, and western regions (fig. 11; table 8). Far fewer streams on the Harney Basin lowlands ultimately discharge into Malheur and Harney Lakes. About half the major watersheds draining upland and lowland areas in the Harney Basin have continuous streamflow measurements (streamgages) for some period over the previous century (fig. 11). In the Harney Basin, only the streamgage at the Donner und Blitzen River near Frenchglen has an uninterrupted record of streamflow during the study period of 1982–2016. The Silvies River near Burns streamgage has a nearly continuous record for the period, missing only water years 2007–08. At most other streams, however, only short periods or assorted single years of record are available, and many of these streamgages predate the study period. Evaluating regional base flow using streamgage data with short or differing periods of record can introduce uncertainty. For example, the period of record at one stream might reflect a wet period while the period of record at another might be representative of a dry period. At these two hypothetical sites, base-flow estimates likely would be biased high during wet periods and low during dry periods when compared to long-term mean streamflow. Record-extension procedures were applied to short-term records where possible to evaluate more representative longer-term average conditions and streamflow was estimated in ungaged areas.

Water year (1982–2016) mean streamflow estimates within the Harney Basin are a composite of measured streamflow and extended streamflow records from short-term streamgages in gaged watersheds and estimated values in ungaged watersheds and other upland areas. Short-term or discontinuous records in gaged watersheds were extended to the period 1982–2016 using the Kendal-Thiel Robust Line (KTRL) method (Helsel and others, 2020) and ordinary-least squares (OLS) linear regression. Streamflow from ungaged watersheds was estimated using a streamflow-precipitation model developed from gaged watersheds. The techniques used to extend and estimate annual streamflow for the Harney Basin are described in appendix 4.

Mean annual streamflow draining upland areas during 1982–2016 totaled 287 ft³/s in the northern region, 319 ft³/s in the southern region, and 102 ft³/s in the western region. Streamflow varied across watersheds depending on elevation (which is highly correlated with precipitation) and

watershed size (app. 4; fig. 11; table 4.3). The largest mean annual streamflow at a streamgage was measured at the Silvies River near Burns streamgage (10392500; fig. 11; 195 ft³/s), which drains the Blue Mountains within the basin and more than 60 percent of the northern region upland area (fig. 11). Nearly 60 percent of the Silvies River flow measured at the Burns streamgage originates downstream of the Silvies River near Silvies streamgage (10392500). The second largest mean streamflow was at the Donner und Blitzen River near Frenchglen streamgage (131 ft³/s), which drains Steens Mountain but represents about 20 percent of the southern region upland area.

Streamflow from gaged (short and long-term) streams measured over the last century comprises about 75 percent of the estimated 1982–2016 mean annual streamflow generated in the Harney Basin uplands. Upland streams measured continuously for some period during 1982–2016 contributed to about 50 percent of total upland streamflow in the southern region, 65 percent of total upland streamflow in the western region, and about 70 percent of total upland streamflow in the northern region.

Mean annual lowland streamflow was estimated at historically measured streamgages near Malheur Lake, including the East and West Fork Silvies Rivers in the northern region and the Donner und Blitzen River near Voltage in the southern region. Lowland Silvies River estimates during 1982–2016 are based on extended record from the 1970s, whereas lowland Donner und Blitzen River estimates represent a composite of measured and extended records. Streamflow on the Silvies River decreased from 195 ft³/s at the Silvies River near Burns streamgage to a combined flow of 31 ft³/s at the East and West Forks of the Silvies River streamgages, indicating that a substantial amount of streamflow was diverted for irrigation and recharged the lowland groundwater system. Streamflow in the Donner und Blitzen River decreased from 131 ft³/s near Frenchglen to 124 ft³/s near Voltage. This apparently modest loss obscures the fact that additional streamflow (up to 118 ft³/s; table 4.3) entered the Donner und Blitzen River between the Frenchglen streamgage and Diamond Lane as tributary inflow from Mud Creek, Bridge Creek, Krumbo Creek, McCoy Creek, Cucamonga Creek, and Kiger Creek (fig. 11; table 4.3). An unknown amount of springflow routed through canals and groundwater seepage also discharges to this reach of the river. These gains are completely offset by diversions for irrigation on MNWR and losses that occur downstream of Diamond Lane and result in the apparently modest loss noted between the streamgages at Frenchglen and Voltage.

In addition to these measured and estimated streamflow discharges to Malheur Lake, additional unmeasured flow in lowland areas that reaches Malheur and Harney Lakes includes intermittent streamflow to Malheur Lake through Malheur Slough during very wet years and discharge to Harney Lake through Silver Creek during above-average precipitation years.

Methods for Estimating Groundwater Discharge to Streams

Continuous streamflow data can be particularly useful for estimating base flow. Base flow is supplemented by runoff from precipitation or snowmelt, resulting in peaks on streamflow hydrographs. The process of dividing these peaks into base flow and runoff is called hydrograph separation (Neff and others, 2005). Many regional studies have used some form of graphical streamflow hydrograph separation to estimate the spatial distribution of base flow (for example, Arnold and Allen, 1999; Lee and Risley, 2002; Wolock, 2003a, b).

Annual low flows at some streamgages also can provide reasonable estimates of the base-flow component of streamflow. In Oregon, natural streamflow during summer and early autumn (that is, after snow has melted) is often entirely base flow during periods of low precipitation. Previous groundwater studies of the Upper Deschutes Basin in central Oregon and the Upper Klamath Basin in southern Oregon used late season streamflow as a method to evaluate base flow (Gannett and others 2001; 2007). The accuracy of any one base-flow estimation method is difficult to assess and Halford and Mayer (2000) recommend using multiple methods.

Base-flow estimates from chemical hydrograph separation methods provide improvements over graphical separation methods (Burns, 2002), but chemical data such as specific conductance, chloride, or stable isotopes of water are rarely available at gaging stations. Stewart and others (2007) reported that BFI and other methods that only consider watershed drainage area and daily streamflow can differ from more accurate chemical separation methods by up to 200 percent.

Base flow was estimated using the mean of estimates from base-flow index (BFI) graphical hydrograph-separation and mean-annual low-flow methods at 11 streamgages in the Harney Basin that had at least a full water year of continuous streamflow data during the previous century. Base-flow estimates from chemical hydrograph separation with specific conductance were used to validate base-flow estimates computed as the mean of BFI and low-flow estimates at the Donner und Blitzen River near Frenchglen streamgage (1975–2018) and at the Silver Creek below Nicoll Creek streamgage (2016–20). The BFI and low-flow methods are advantageous because they require only streamflow data to compute base-flow estimates whereas chemical hydrograph separation also requires complementary water-chemistry data. Based on comparisons with results from the chemical separation method at two sites, the mean of BFI and low-flow estimates was found to reasonably compensate for biases inherent in the two methods. For example, the BFI method can overestimate base flow during periods of snowmelt (Miller and others, 2015), which occur in the Harney Basin during springtime and early-to-mid summer months. The low-flow method generally provides accurate estimates of base flow in late summer and autumn, but likely underpredicts total annual base-flow volumes because it does not account for potential changes in groundwater discharge throughout the year. Therefore, BFI base-flow values reported herein are considered upper-bound estimates of base flow

and low-flow base-flow values are considered lower-bound estimates. Chemical hydrograph separation methods are considered the most accurate because water chemistry data such as specific conductance distinguishes snowmelt runoff from groundwater components of streamflow. The following subsections describe the methods used to estimate base flow at continuous streamgages, validation of base-flow estimates with results from chemical hydrograph separation analyses, and the method used to scale base flow from streamgaged watersheds to all other upland areas.

Base-Flow-Index Method

The BFI graphical hydrograph separation method (Wahl and Wahl, 1995) was used to estimate base flow from daily streamflow records at streamgaged watersheds using the USGS groundwater toolbox implementation of the BFI standard method (Barlow and others, 2015). At all sites, the N value was set to 5 days and the turning point test factor was set to 0.9 (Institute of Hydrology, 1980a, b). The periods over which base flow was estimated using the BFI method were limited to water years with complete daily streamflow records. BFI results were summarized by month for comparison with low-flow estimates (for example, at the Donner und Blitzen River near Frenchglen; fig. 12) and over the full measurement period to compute mean annual BFI base flow (table 9).

Low-Flow Method

The low-flow method estimates base flow as the lowest monthly mean discharge measured at a streamgage (Gannett and others 2001, 2007). Monthly mean discharge was computed from daily discharge for each month of each year, and monthly means were then summarized over the period of record to obtain mean discharge rates for each month of the calendar year at a streamgage. The month with the lowest mean flow for all years analyzed was identified and monthly mean flow for the identified month was used each year to represent low flow (for example, the Donner und Blitzen River near Frenchglen streamgage; fig. 12). Annual low-flow estimates were interpolated between years to estimate monthly low flow and compared with BFI values. Annual low-flow estimates were summarized over the full measurement period to compute low flow during 1982–2016 (table 9). At most sites, the month with the lowest mean flow was during summer or autumn—most commonly in July, August, or September.

Late-summer diversions upstream of the streamgages at Silvies River near Burns and Silver Creek below Nicoll Creek likely reduced late-season streamflow measurements and estimates. Based on mean annual estimates by OWRD's water availability reporting system, diversions remove more than 40 percent of July–September streamflow upstream of the Silvies River streamgage and more than 10 percent of streamflow upstream of the Silver Creek streamgage (Cooper, 2002; Oregon Water Resources Department, 2018). Diversions upstream of the Donner und Blitzen River near Frenchglen are negligible during summer and autumn.
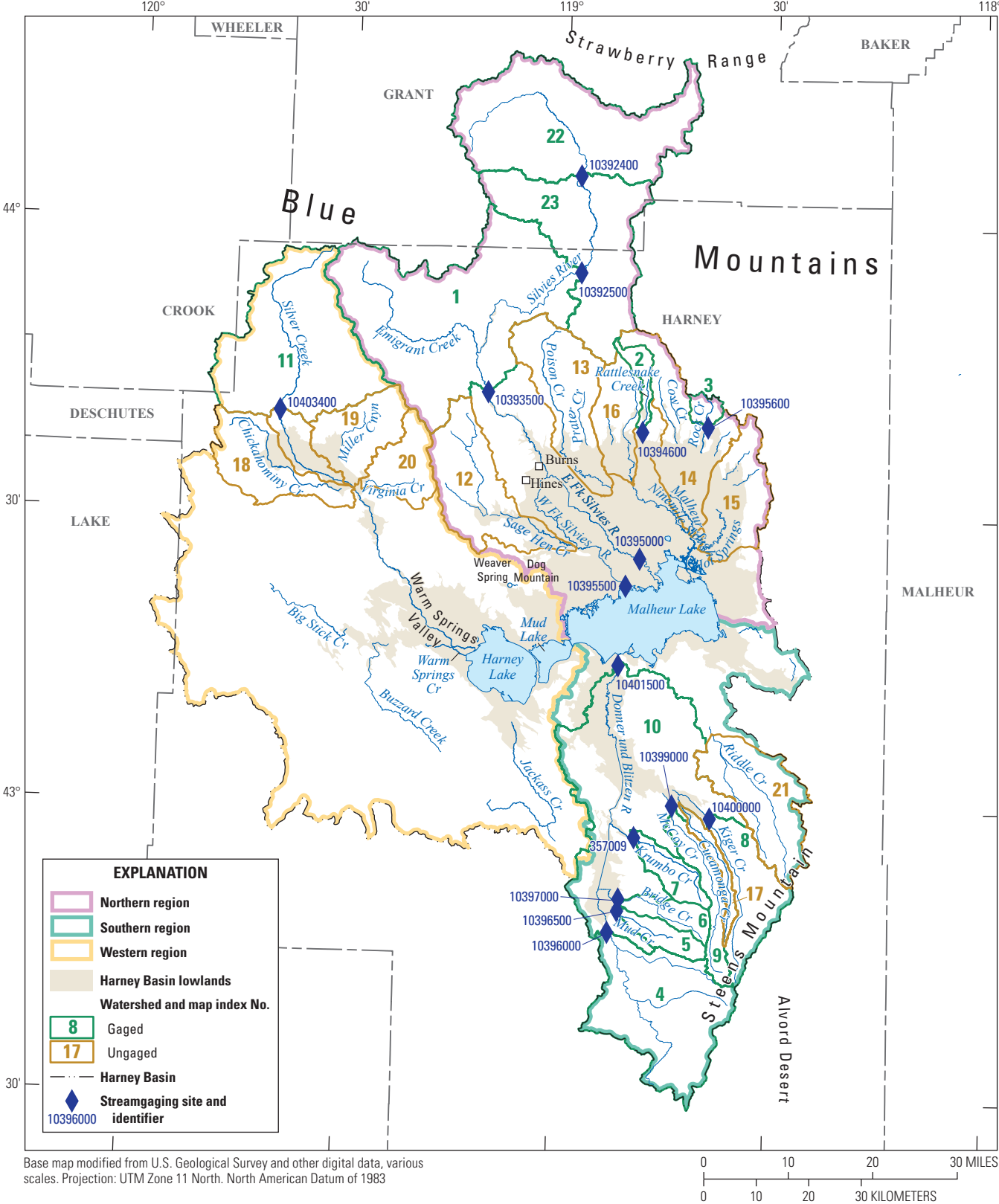
Figure 11. Stream locations, hydrologic regions, and selected areas summarized in table 8, including streamgages and streamgaged and ungaged watersheds, Harney Basin, southeastern Oregon.

Table 8. Site information and summary of measured and estimated streamflow data from streams in the Harney Basin, southeastern Oregon.

[**Map index number:** Locations of streamgaged and ungaged watersheds are shown on fig. 11. **Measured mean water-year flow rate:** Mean of values presented for long- and short-term streamgage records. **Latitude and longitude** in reference to the North American Datum of 1983. **Elevation:** In feet above North American Vertical Datum of 1988. **Abbreviations:** ft, feet; ft³/s, cubic feet per second; mi², square miles; OWRD, Oregon Water Resources Department; USGS, U.S. Geological Survey; OWRD, Oregon Water Resources Department; —, not available]

Site name	USGS/ OWRD site number	Other site number	Map index number	Contributing drainage area (mi²)	Latitude (decimal degrees)	Longitude (decimal degrees)	Elevation (ft)	Water years with complete streamflow records (or estimation years)	Measured mean water-year flow rate (ft³/s)
				Gaged watersheds					
Silvies River near Burns, OR[1]	10393500	—	1	934	43.716	-119.177	4,195	1904–05, 1910–12, 1918–20, 1923–2006, 2009–18	173.5
Rattlesnake Creek near Harney, OR	10394600	—	2	18	43.651	-118.812	4,195	No full water years	—
East Fork Silvies River near Lawen, OR	10395000	—	—	—[2]	43.426	-118.802	4,104	1973–77	9.6
West Fork Silvies River near Lawen, OR	10395500	—	—	—[2]	43.383	-118.834	4,104	1973–77	11.2
Rock Creek near Burns, OR	10395600	—	3	12	43.660	-118.661	4,214	1964, 1966, 1969, 1972–74, 1976	5.6
Donner und Blitzen River near Frenchglen, OR	10396000	[3]357010	4	206	42.791	-118.868	4,254	1912, 1913, 1915, 1916, 1918–21, 1939–2018	124.8
Mud Creek near Diamond, OR[7]	10396500	—	5	30	42.831	-118.851	4,200	1912–16	5.6
Bridge Creek near Frenchglen, OR	10397000	[3]357004	6	30	42.844	-118.850	4,185	1913–16, 1939–70, 2005–17	14.0
Krumbo Creek below Krumbo Reservoir[4]	—	[3]357009	7	35	42.955	-118.814	4,181	2004–17	[4]3.5
Kiger Creek near Diamond, OR	10399000	—	8	75	42.989	-118.638	4,311	No full water years	—
McCoy Creek near Diamond, OR	10400000	[3]357007	9	45	43.009	-118.721	4,180	1918, 1919, 1921	22.6
Donner und Blitzen River near Voltage, OR	10401500	[3]357005	10	760	43.253	-118.857	4,097	1939–43, 1973–77, 2003–11, 2013–17	104.6
Silver Creek below Nicoll Creek near Riley, OR	10403400	—	11	265	43.672	-119.671	4,387	2011–18	48.3

Table 8. Site information and summary of measured and estimated streamflow data from streams in the Harney Basin, southeastern Oregon.—Continued

[Map index number: Locations of streamgaged and ungaged watersheds are shown on fig. 11. Measured mean water-year flow rate: Mean of values presented for long- and short-term streamgage records. Latitude and longitude in reference to the North American Datum of 1983. Elevation: In feet above North American Vertical Datum of 1988. Abbreviations: ft, feet; ft³/s, cubic feet per second; mi², square miles; OWRD, Oregon Water Resources Department; USGS, U.S. Geological Survey; OWRD, Oregon Water Resources Department—, not available]

Site name	USGS/OWRD site number	Other site number	Map index number	Contributing drainage area (mi²)	Latitude (decimal degrees)	Longitude (decimal degrees)	Elevation (ft)	Water years with complete streamflow records (or estimation years)	Measured mean water-year flow rate (ft³/s)
					Gaged watersheds—Continued				
Silvies River below Soda Spring near Seneca, OR	10392400	—	22	294	44.088	-118.972	4,644	2016–18	50.7
Silvies River near Silvies, OR	10392500	—	23	511	43.923	-118.958	4,530	2016–18	70.2
					Ungaged watersheds				
Sagehen Creek at Silvies River	—	531200202	12	133	43.448	-118.959	4,113	—	—
Poison Creek Slough at Ninemile Slough	—	531200106	13	125	43.553	-118.884	4,137	—	—
Malheur Slough above Ninemile Slough	—	531200107	14	131	43.476	-118.692	4,115	—	—
Hot Springs Slough at Malheur Slough	—	531200102	15	92	43.451	-118.673	4,114	—	—
Soldier Creek at Poison Creek Slough	—	531200105	16	64	43.557	-118.829	4,120	—	—
Cucamonga Creek at Kiger Creek	—	531200303	17	23	43.016	-118.706	4,168	—	—
Chickahominy Creek at Silver Creek	—	531200402	18	95	43.538	-119.485	4,210	—	—
Miller Canyon at Silver Creek	—	531200404	19	79	43.547	-119.480	4,215	—	—
Virginia Creek at Silver Creek	—	531200403	20	57	43.540	-119.469	4,217	—	—
Riddle Creek[6]	—	—	21	121	—	—	—	—	—

[1]Gage regulated to account for substantial diversions upstream.

[2]Contributing drainage area not reported.

[3]U.S. Fish and Wildlife Service (Mayer and others, 2007)

[4]Flow likely influenced by the operation of Krumbo Reservoir, located upstream of streamgage–Value might not be representative of actual streamflow during measurement period.

[5]Watersheds from Oregon Water Resources Department (Cooper, 2002)

[6]Ungaged area surrounding Riddle Creek, northeast of the Kiger Creek watershed

[7]Continuous data time step varied from daily to weekly flow during late summer and autumn.
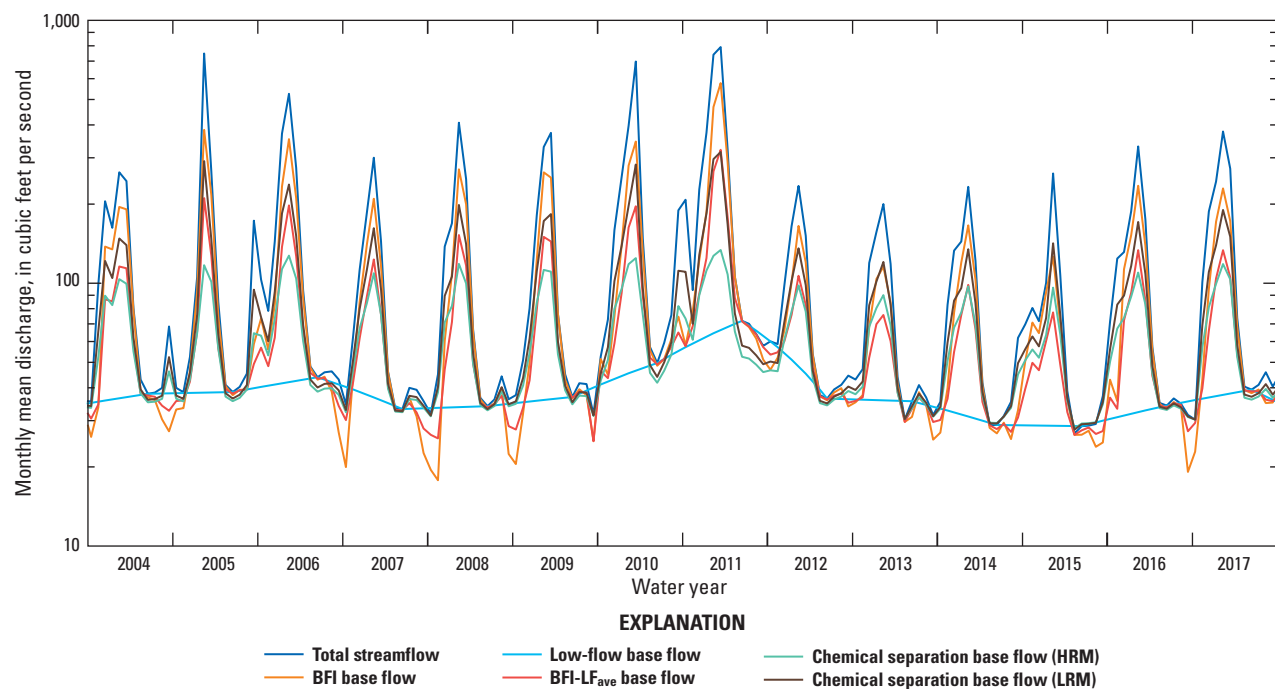
Figure 12. Comparison of monthly mean base-flow estimates and total streamflow for the Donner und Blitzen River near Frenchglen, OR, streamgage (10396000), water years 2004–18. BFI, base-flow index; BFI-LF$_{ave}$, mean of monthly BFI and low-flow estimates; HRM, high runoff model; LRM, low runoff model. Y-axis is displayed on a logarithmic scale.

Table 9.   Estimated base-flow summaries for streamgaged watersheds (fig. 11; table 8) over the measurement record, 1904–2018, Harney Basin, southeastern Oregon.

[**Map index number**: Locations of streamgaged and ungaged watersheds are shown on figure 11. **Base-flow scale factor**: Computed as the ratio of the "mean water year BFI-LF$_{ave}$ base flow" and "mean Streamflow during period" used in the base-flow analysis. **Abbreviations**: Aug., August; BFI, base flow Index, standard; BFI-LF$_{ave}$, mean of BFI base flow and Lowest mean monthly flow; ft^3/s, cubic feet per second; Nov., November; Sept., September; USGS, U.S. Geological Survey; OWRD, Oregon Water Resources Department; — , not applicable.]

Site name	USGS/OWRD site number (other site number)	Map index number	Month of lowest mean monthly flow	Lowest mean monthly flow (ft^3/s)	Mean water year BFI base flow (ft^3/s)	Mean water year BFI-LF$_{ave}$ base flow (ft^3/s)	Mean Streamflow during period (ft^3/s)	Base-flow scale factor
Silvies River near Burns, OR[1]	10393500	1	Sept.	13.7	111.5	62.2	173.5	0.36
East Fork Silvies River near Lawen, OR	10395000	—	Sept.	0.0	8.9	[2]0.0 – 4.5	9.6	[3]0.23
West Fork Silvies River near Lawen, OR	10395500	—	July	0.0	9.4	[2]0.0 – 4.7	11.2	[3]0.21
Rock Creek near Burns, OR	10395600	3	July	0.0	3.4	[2]0.0 – 1.6	5.6	[3]0.15
Donner und Blitzen River near Frenchglen, OR	10396000 [4](357010)	4	Sept.	41.4	86.0	63.5	124.8	0.51
Bridge Creek near Frenchglen, OR	10397000 [4](357004)	6	Nov.	12.0	12.8	12.2	14.0	0.87
Mccoy Creek near Diamond, OR	10400000 [4](357007)	9	Sept.	4.7	14.6	9.7	22.6	0.43
Donner und Blitzen River near Voltage, OR	10401500 [4](357005)	10	Sept.	36.9	72.4	53.5	104.6	0.51
Silver Creek below Nicoll Creek near Riley, OR	10403400	11	Aug.	1.9	28.0	19.7	48.3	0.41
Silvies River below Soda Spring near Seneca, OR	10392400	22	Aug.	0.1	29.9	15.0	50.7	0.30
Silvies River near Silvies, OR	10392500	23	Sept.	0.0	43.8	21.9	70.2	0.31

[1]Streamgage regulated to account for substantial diversions upstream.

[2]At sites where lowest mean monthly flow is equal to 0.0, a range bracketing the likely base flow value was used. The upper end of this range is considered an upper limit and probably overpredicts the mean water year base flow.

[3]Mean of the range computed from mean water year BFI-LFave base flow.

[4]U.S. Fish and Wildlife Service (Mayer and others, 2007)

Chemical Hydrograph Separation Method

Chemical hydrograph separation using specific conductance (SC) was used to estimate upland base-flow contributions to Silver Creek and the Donner und Blitzen River. The technique works well in systems where the SC of the base-flow and runoff components of streamflow differ sufficiently to construct a two-end-member mixing model (Pinder and Jones, 1969; Dinçer and others, 1970). Conservation of the chemical species gives the two end-member mixing model:

$$SC_s \times Q_s = SC_{bf} \times Q_{bf} + SC_{ro} \times Q_{ro} \qquad (11)$$

where
  SC_s is the SC of the stream,
  SC_{bf} is the SC of the base-flow component,
  SC_{ro} is the SC of the runoff component,
  Q_s is the daily mean discharge of the stream,
  Q_{bf} is the daily mean discharge of the base-flow
      component of streamflow, and
  Q_{ro} is the daily mean discharge of the runoff
      component of streamflow.

The daily mean discharge is the sum of the base-flow and runoff contributions (conservation of mass of streamflow; eq. 12).

$$Q_s = Q_{bf} + Q_{ro} \qquad (12)$$

Replacing Q_{ro} in equation 11 with $Q_s - Q_{bf}$, the equation can be rearranged to solve for Q_{bf} (eq. 13).

$$Q_{bf} = Q_s \times \left[\frac{(SC_s - SC_{ro})}{(SC_{bf} - SC_{ro})} \right] \qquad (13)$$

A chemical separation using equation 13 can be accomplished at sites where SC_s and Q_s are measured and SC_{ro} and SC_{bf} can be estimated, which leaves Q_{bf} as the only unknown term in the equation. Daily flow, Q_s, is obtained from the streamgage. Daily SC_s was estimated from discrete measurements using regression analysis (Miller and others, 2015). Estimates of SC_{bf} were based on the SC record during periods of extended base flow and estimates of SC_{ro} were based on the SC record during time of peak runoff. Stream SC during peak runoff periods is dominated by, but not wholly runoff, therefore SC_{ro} estimates are less than the stream value during peak flows, but greater than rain or snow (typically <20 µS/cm; Williams and Melack, 1991) owing to the addition of solutes picked up in the soil.

Continuous SC was not available at any streamgages in the Harney Basin, so the daily SC was estimated from discrete SC measurements and daily discharge using a simplified relation developed for each streamgage separately following the techniques of Miller and others (2015). An OLS regression was developed between the natural logarithm of discrete SC and the natural logarithm of daily mean discharge. Daily

SC (SC_{est}) was estimated using the slope and intercept of the regression and retransformed from logarithmic values using the bias correction factor of Ferguson (1986). Regression residuals were evaluated for normality, homoscedasticity, and structure that could invalidate the relation.

The SC_{est} regression for the Donner und Blitzen River was developed from 107 discrete SC measurements made during 1975–2018 over a range of flow conditions (fig. 13A). The SC and discharge measurements were made at the Donner und Blitzen River near Frenchglen streamgage. The r^2 of the regression was 0.54. Removing one large outlier improved the r^2 to 0.66 with little effect on the slope and intercept. Residuals were normally distributed and homoscedastic with respect to discharge. The regression systematically overpredicted SC at values less than 50 µS/cm by a median of 15 µS/cm and underpredicted SC at values greater than 90 µS/cm by a median of 6 µS/cm (fig. 13A). The SC_{est} regression for Silver Creek, was developed from 10 discrete SC measurements made during 2016–20 over a range of flow conditions (fig. 13B). The SC measurements were made at the McCanlies Rd bridge (USGS station ID 434205119381400) about 3 miles upstream from the Silver Creek below Nicoll Creek streamgage (10403400; fig. 11; table 9); only one small tributary (Rough Creek) contributes to Silver Creek between the two sites. The r^2 of the regression was 0.64. To the extent they can be meaningfully evaluated with the small number of samples, residuals were normally distributed and homoscedastic with respect to discharge.

For the Donner und Blitzen River, SC_{bf} was set to 96 µS/cm (table 10), which is the mean plus 1 standard deviation of the measured SC values during low-flow months (August–October). The mean value during low-flow months was not used directly because the snowpack on Steens Mountain might not fully melt off each year, therefore the summer low-flow period can include a small amount of runoff. Measurements of SC_{ro} were not directly made in the watershed; therefore, chemical hydrograph separations were computed using two values for SC_{ro}: (1) 41 µS/cm, the minimum of the observed values from the snowmelt period (April–June) and (2) 20 µS/cm, the maximum SC of precipitation reported by Williams and Melack (1991).

For Silver Creek, SC_{bf} was set to 235 µS/cm, which is the maximum of the observed values during low-flow months ($n=4$). The mean value was not used due to the small number of samples. The maximum value during low-flow months is considered a reasonable estimate of base-flow contribution because the snowpack fully melts off each year in the Silver Creek Basin. Similar to the Donner und Blitzen River, chemical hydrograph separations were computed using two values for SC_{ro}: (1) 89 µS/cm, the minimum of the observed values from the snowmelt period (April – June) and (2) 45 µS/cm, which is one-half the observed minimum value during the snowmelt period. Higher values of SC_{ro} in Silver Creek (compared to the Donner und Blitzen River) reflect carbonate-bearing pre-Tertiary rocks, sediment, and soil in the watershed that contribute solutes to the runoff prior to entering the stream system.

A. Donner und Blitzen River
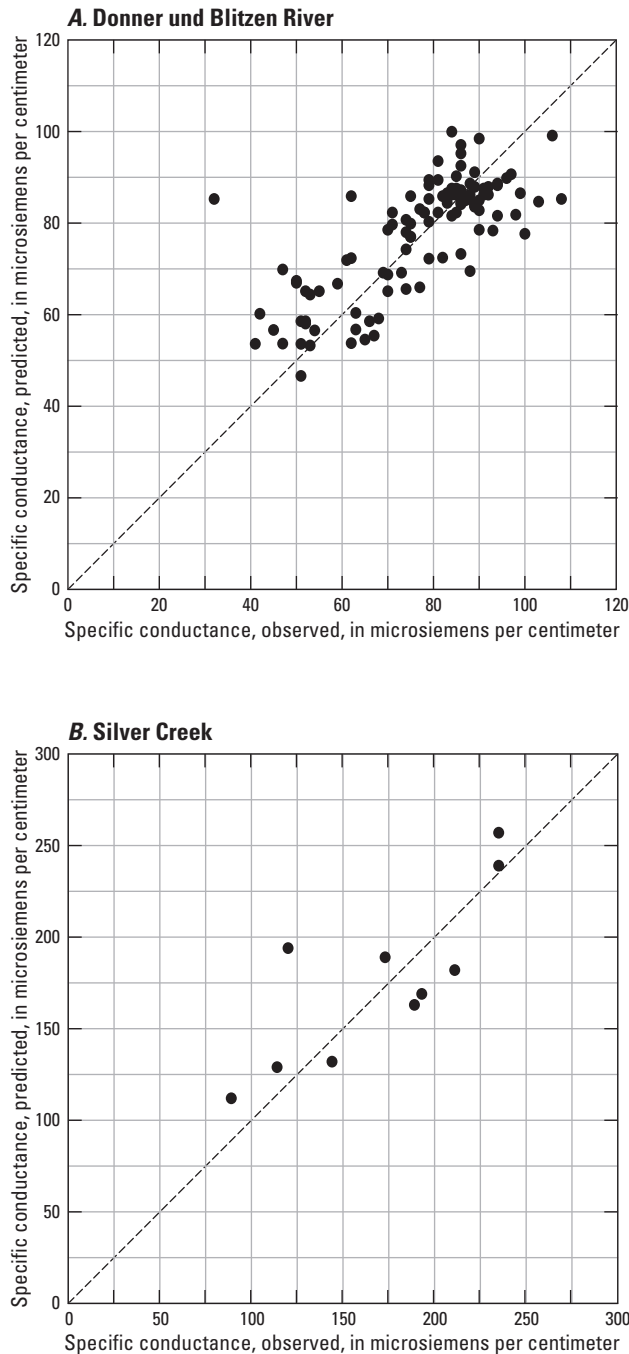
B. Silver Creek

Figure 13. Relation between observed and predicted values of specific conductance as a function of streamflow for (*A*) the Donner und Blitzen River and (*B*) Silver Creek.

Base Flow Validation and Trends

The mean of the BFI and low-flow estimates (BFI-LF$_{ave}$) agreed better with chemical base-flow estimates than did either the BFI or low-flow values separately (fig. 14). Comparisons between monthly means of BFI-LF$_{ave}$ and chemical separation data were reasonable during all times of the year (fig. 12). During late-summer months (when the proportion of base flow to total streamflow is high and the proportion of runoff to total streamflow is low) BFI, low-flow, and chemical separation methods yielded similar results. During autumn, winter, and springtime (when the proportion of base flow to total streamflow is low and the proportion of runoff to total streamflow is high), BFI estimates were generally higher than chemical-separation estimates while low-flow estimates were generally lower than chemical separation estimates (fig. 12).

Scaled Base Flow

Measurement-period base-flow estimates were scaled to 1982–2016 to ensure that estimates used were representative of similar long-term average conditions. The ratio of base flow and total streamflow during the measurement period was considered representative of the long-term mean, despite using short-term records at some sites. Although the amount of base flow in a stream might fluctuate during wet and dry years, linear total streamflow–base flow relations at multiple streamgages indicate the mean proportion of base flow to total streamflow (or scale factor) remains relatively constant (fig. 15).

Base-flow scale factors were computed at gaged sites using BFI-LF$_{ave}$ estimates and mean annual measurement-period streamflow and varied by region (table 9). In the southern region, base flow accounted for about 60 percent of total discharge from upland streams, indicating that most annual streamflow is comprised of base flow. In the northern and western regions, base flow accounted for only about 30 and 41 percent of total flow, respectively. These observations are consistent with overall streamflow patterns in these systems: Silvies River and Silver Creek exhibit more variability with larger differences between high and low flow relative to the Donner und Blitzen River. Observed streamflow and base-flow patterns also support interpretations of the hydrogeology in the regions, with the Blue Mountains (northern and western region) having lower overall permeability compared to Steens Mountain (southern region; Gingerich and others, 2022).

Base-flow scale factors were used to scale base-flow estimates to 1982–2016 using composite measured and extended streamflow records (app. 4; table 4.3). Base flow in ungaged watersheds and those with less than 1 year of continuous streamflow data was estimated as the product of extended streamflow records (app. 4; table 4.3) and the base-flow scale factor (table 9) from comparable gaged streams (table 11).

Results for Groundwater Discharge to Streams

About 225,000 acre-ft/yr (309 ft^3/s; table 11) of groundwater discharges to streams in upland areas as base flow in the Harney Basin (fig. 10). The upland region with the largest base flow is the southern region (125,000 acre-ft/yr; 172 ft^3/s), followed by the northern region (75,000 acre-ft/yr; 103 ft^3/s), and then the western region (25,000 acre-ft/yr; 34 ft^3/s). Base flow from ungaged watersheds and other upland areas is about 25 percent of total upland base flow (table 11).
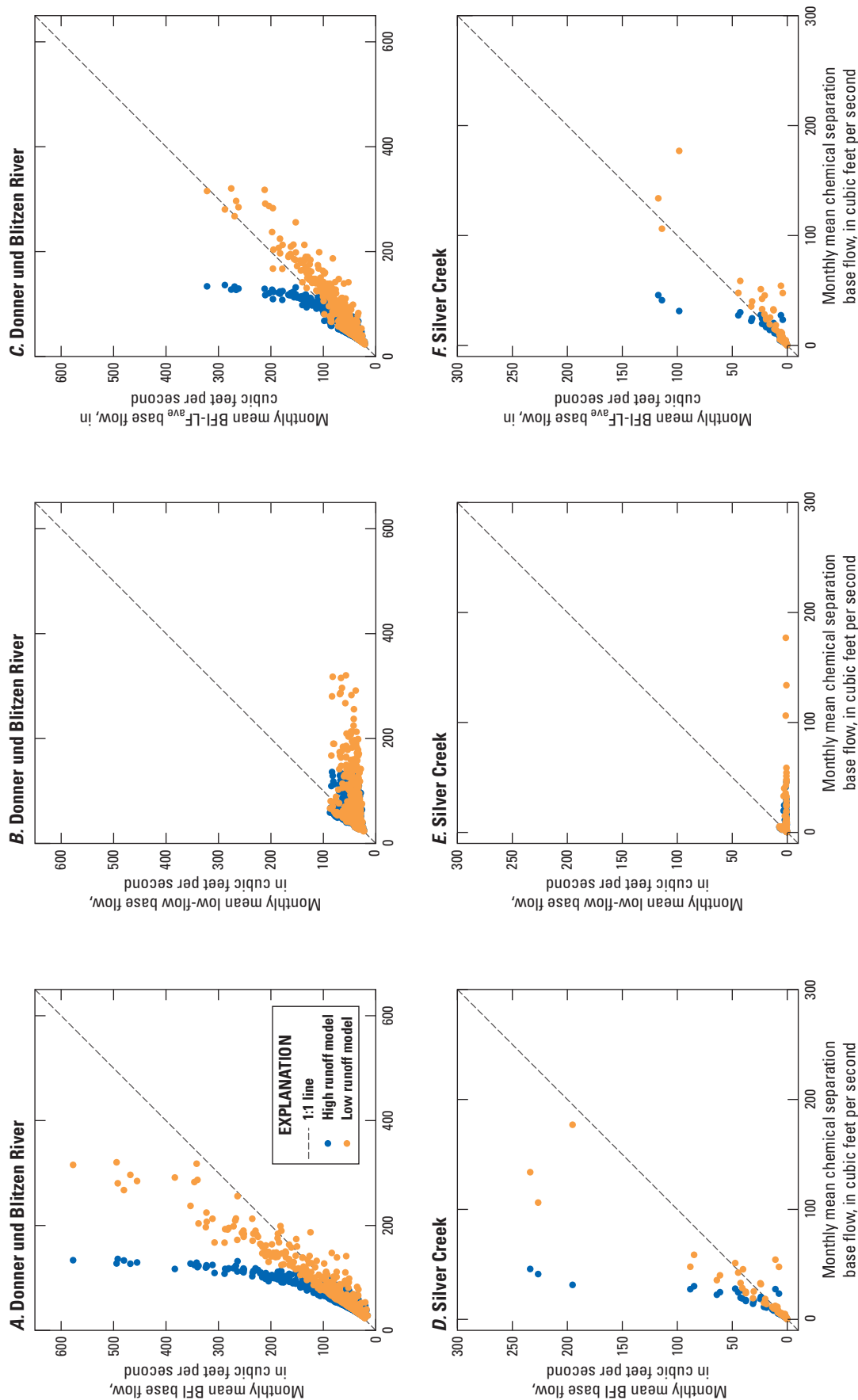
Figure 14. Comparison of base-flow estimates from chemical hydrograph separation (high and low runoff models) and (*A,D*) base-flow index (BFI), (*B,E*) low-flow, and (*C,F*) mean of BFI and low-flow (BFI-LF$_{ave}$) methods at Donner und Blitzen River near Frenchglen (*A-C*), October 1980–September 2018 and Silver Creek below Nicoll Creek (*D-F*), August 2011–August 2018. Good agreement is indicated by datapoints that lie on or near the dashed line.
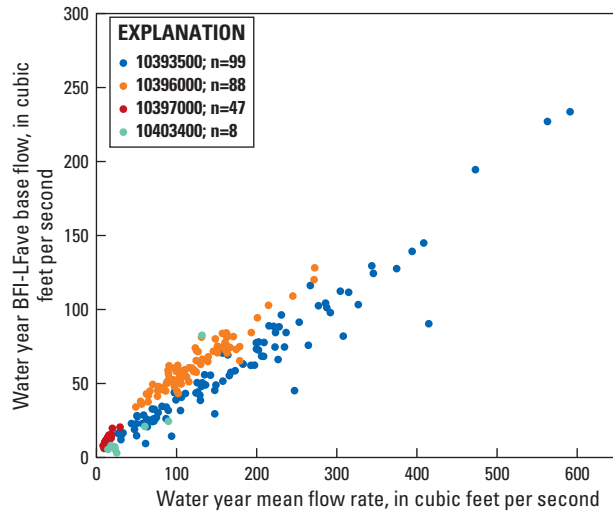
Figure 15. Linear relation between total water-year streamflow and water-year base flow (BFI-LF$_{ave}$ [mean of base-flow index and low-flow estimation methods]) at Silvies River near Burns (10393500), Donner und Blitzen River near Frenchglen (10396000), Bridge Creek near Frenchglen (10397000), and Silver Creek below Nicoll Creek (10403400) streamgages, Harney Basin, southeastern Oregon. Sites are shown in figure 11 and included in table 8. Symbol "n" represents the number of water years at each site.

Hydrographs comparing annual total streamflow, annual mean estimated base-flow (BFI-LF$_{ave}$) and runoff (total streamflow minus mean base flow) components, and annual precipitation for the Donner und Blitzen River near Frenchglen (fig. 16), the Silvies River near Burns (fig. 17), and Silver Creek near Riley (fig. 18) demonstrate annual changes in base-flow magnitude in the northern, southern, and western region uplands of the Harney Basin. Annual fluctuations in flow components frequently reflect responses to precipitation.

The highest annual base flows in the Silvies River near Burns and the Donner und Blitzen River near Frenchglen were estimated during wetter periods (1983–84, 1996–99, and 2011), whereas the lowest annual base flows were estimated during drier periods (1991–93, 2001–03, and 2013–15) (figs. 16–17), corresponding to years of below average precipitation (fig. 3). The measured streamflow record in the western region is relatively short and recent but also demonstrates changes in annual base flow with precipitation (figs. 3, 18).

About 51,000 acre-ft/yr (70 ft^3/s) of base flow was estimated in lowland areas from three watersheds (fig. 11; table 11), but most of this flow likely originates from upland areas. The highest single-river base flow estimated on the lowlands is at the Donner und Blitzen River near Voltage streamgage (about 46,000 acre-ft/yr [64 ft^3/s]; fig. 11; table 11). Base flow at the Voltage streamgage is predominately base flow from upland areas but includes some groundwater discharge from the Harney Basin lowlands. Water-table contours on the lowlands point upstream between Diamond Lane and Frenchglen (fig. 1), indicating that the Donner und Blitzen River likely is gaining flow in this area; however, the amount has not been quantified (Gingerich and others, 2022). The remaining 5,000 acre-ft/yr (7 ft^3/s) of lowland base flow was estimated in the northern region at gages on East and West Fork Silvies Rivers (fig. 11). Water-table contours point downstream along these streams, indicating they are above the water table and hence losing reaches (Gingerich and others, 2022), and base-flow estimates at these gages reflect upland water rather than groundwater discharge in the lowlands.

The proportion of base flow to total streamflow in gaged, upland streams also varied by region (table 9). In the southern region, base flow accounted for about 60 percent of total discharge from upland streams, indicating that most annual streamflow is comprised of base flow. In the northern and western regions, base flow accounted for only about 30 and 41 percent of total flow, respectively.

Table 10. Summary of data used for chemical hydrograph separations, Harney Basin, southeastern Oregon.

[Specific conductance values are in units of microsiemens per centimeter. **Abbreviations**: SC$_{bf}$, specific conductance of base flow; Sc$_{ro}$, specific conductance of runoff]

Site name	Streamflow site number	Specific conductance site number	SC$_{bf}$	SC$_{ro}$	
				(minimum)	(maximum)
Donner und Blitzen River near Frenchglen, OR	10396000	10396000	96	20	41
Silver Creek below Nicoll Creek near Riley, OR	[1]10403400	434205119381400	235	45	89

[1]Oregon Water Resources Department streamgage number
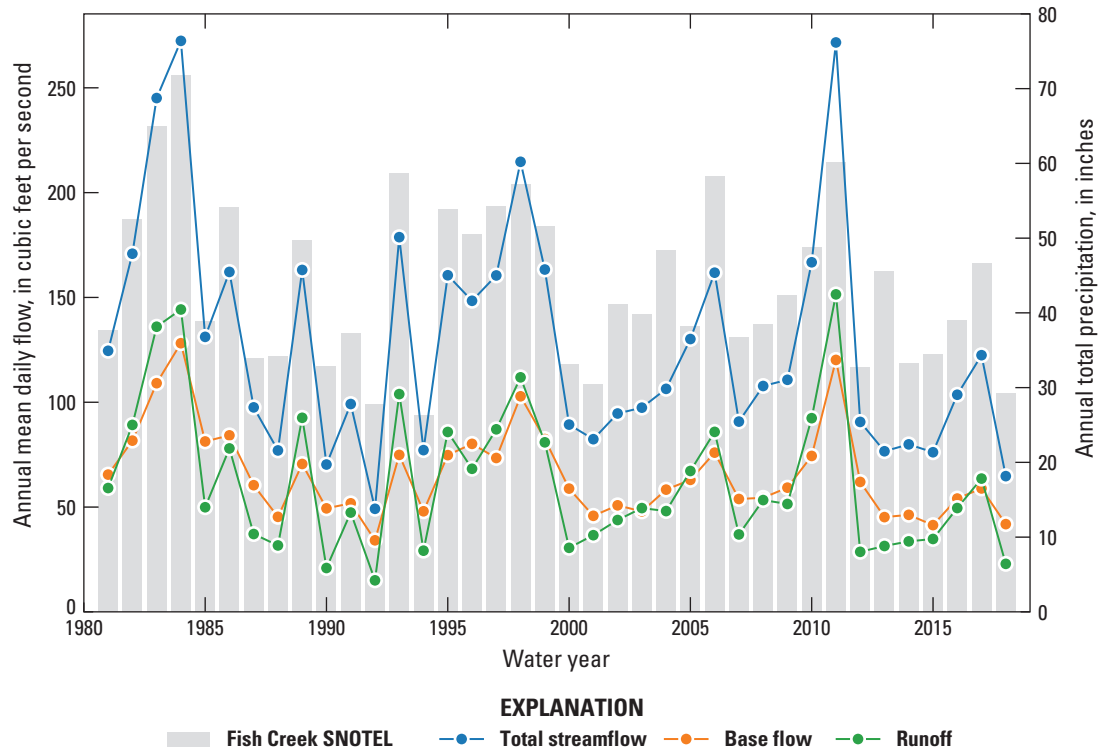
Figure 16. Comparison of annual runoff and base-flow components of total streamflow at the Donner und Blitzen River near Frenchglen, OR, streamgage (10396000). Base flow is the mean of base-flow index and low-flow estimates and runoff is annual total streamflow minus base flow. Annual precipitation from the nearby Fish Creek Natural Resources Conservation Service Snow Telemetry (SNOTEL) site (fig. 2) is shown for comparison.
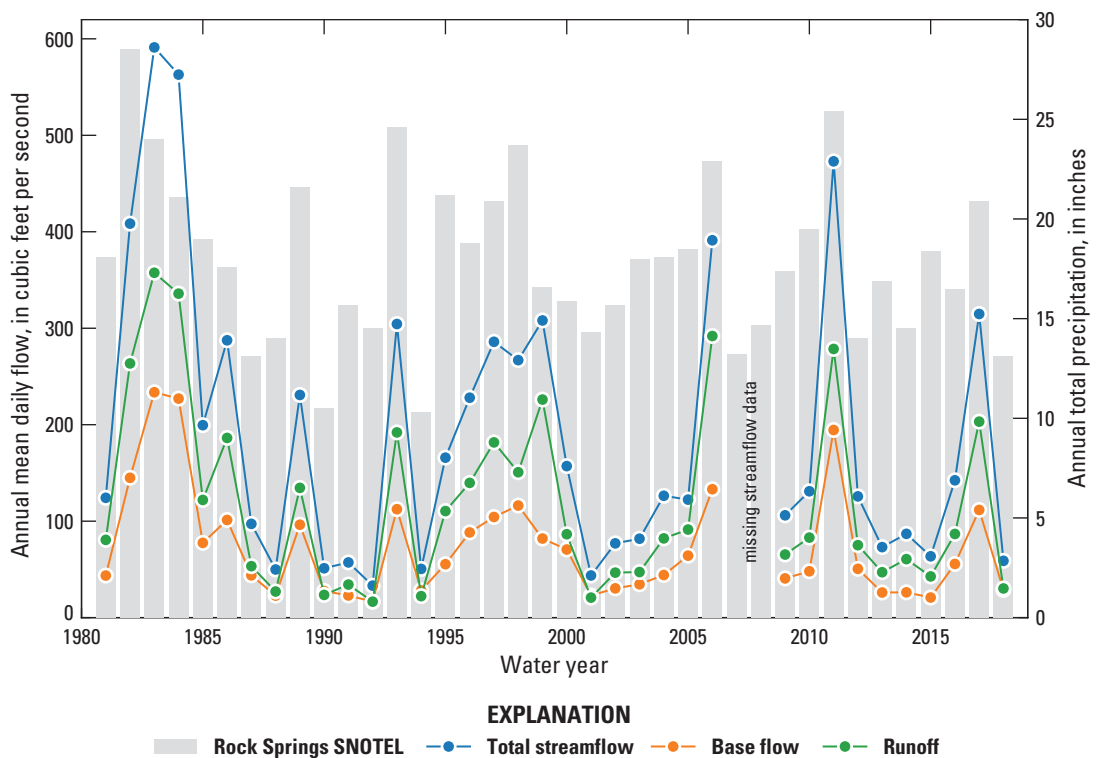
Figure 17. Comparison of annual runoff and base-flow components of total streamflow at the Silvies River near Burns, OR, streamgage (10393500). Base flow is the mean of base-flow index and low-flow estimates and runoff is annual total streamflow minus base flow. Annual precipitation from the nearby Rock Springs Natural Resources Conservation Service Snow Telemetry SNOTEL site (fig. 2) is shown for comparison.

Table 11.   Estimated base-flow summaries from streamgaged and ungaged watersheds in the Harney Basin, southeastern Oregon, scaled to 1982–2016.

[Scale factors for sites listed in table 9 were averaged and applied to the site of interest. **Map index number**: Locations of streamgaged and ungaged watersheds are shown on figure 11. **Estimated base flow scaled to 1982–2016**: Calculated as the product of the mean water-year flow rate 1982–2016 (table 4.3) and the selected base-flow scale factor (table 9). **Reference site used to scale base flow**: Sites used to scale base flow to 1982–2016. Values of "SI" indicate that only the scale factor for the site of interest was used to scale base flow. **Abbreviations:** USGS, U.S. Geological Survey; OWRD, Oregon Water Resources Department; SI, site of interest; ft³/s, cubic feet per second; —, not applicable; NA, not available]

Site name	USGS/OWRD site number (other site number)	Map index number	Region	Stream category	Estimated base flow scaled to 1982–2016 (ft³/s)	Reference site used to scale base flow
Watersheds with more than one complete water year of streamgage records							
Silvies River near Burns, OR[1]	10393500	1	Northern	Upland	70.0	SI
East Fork Silvies River near Lawen, OR	10395000	—	Northern	Lowland	3.3	SI
West Fork Silvies River near Lawen, OR	10395500	—	Northern	Lowland	3.6	SI
Rock Creek near Burns, OR	10395600	3	Northern	Upland	1.2	SI
Donner und Blitzen River near Frenchglen, OR	10396000 [2](357010)	4	Southern	Upland	66.6	SI
Mud Creek near Diamond, OR	10396500	5	Southern	Upland	3.3	10396000, 10397000, 10400000
Bridge Creek near Frenchglen, OR	10397000 [2](357004)	6	Southern	Upland	12.9	SI
Mccoy Creek near Diamond, OR	10400000 [2](357007)	9	Southern	Upland	10.7	SI
Donner und Blitzen River near Voltage, OR	10401500	10	Southern	Lowland	63.5	SI
Silver Creek below Nicoll Creek near Riley, OR	10403400	11	Western	Upland	20.4	SI
Watersheds with less than one complete water year of streamgage records							
Rattlesnake Creek near Harney, OR	10394600	2	Northern	Upland	1.9	10393500, 10403400
Krumbo Creek, below Krumbo Reservoir[1,3]	[2](357009)	7	Southern	Upland	6.9	10396000, 10397000, 10400000
Kiger Creek near Diamond, OR	10399000	8	Southern	Upland	37.1	10396000, 10397000, 10400000
Ungaged watersheds							
Sagehen Creek at Silvies River	[4](31200202)	12	Northern	Upland	4.7	10393500, 10403400
Poison Creek Slough at Ninemile Slough	[4](31200106)	13	Northern	Upland	8.0	10393500, 10403400
Malheur Slough above Ninemile Slough	[4](31200107)	14	Northern	Upland	4.7	10393500, 10403400
Hot Springs Slough at Malheur Slough	[4](31200102)	15	Northern	Upland	2.6	10393500, 10403400

Table 11.   Estimated base-flow summaries from streamgaged and ungaged watersheds in the Harney Basin, southeastern Oregon, scaled to 1982–2016.—Continued

[Scale factors for sites listed in table 9 were averaged and applied to the site of interest. **Map index number**: Locations of streamgaged and ungaged watersheds are shown on figure 11. **Estimated base flow scaled to 1982–2016**: Calculated as the product of the mean water-year flow rate 1982–2016 (table 4.3) and the selected base-flow scale factor (table 9). **Reference site used to scale base flow**: Sites used to scale base flow to 1982–2016. Values of "SI" indicate that only the scale factor for the site of interest was used to scale base flow. **Abbreviations:** USGS, U.S. Geological Survey; OWRD, Oregon Water Resources Department SI, site of interest; ft³/s, cubic feet per second; —, not applicable; NA, not available]

Site name	USGS/OWRD site number (other site number)	Map index number	Region	Stream category	Estimated base flow scaled to 1982–2016 (ft³/s)	Reference site used to scale base flow
Ungaged watersheds—Continued						
Soldier Creek at Poison Creek Slough	[4](31200105)	16	Northern	Upland	3.3	10393500, 10403400
Cucamonga Creek at Kiger Creek	[4](31200303)	17	Southern	Upland	4.5	10396000, 10397000, 10400000
Chickahominy Creek at Silver Creek	[4](31200402)	18	Western	Upland	0.7	10393500, 10403400
Miller Canyon Creek at Silver Creek	[4](31200404)	19	Western	Upland	2.9	10393500, 10403400
Virginia Creek at Silver Creek	[4](31200403)	20	Western	Upland	1.8	10393500, 10403400
Riddle Creek area[5]	NA	21	Southern	Upland	18.8	10396000, 10397000, 10400000
Other upland areas[6]						
Northern region	—	—	Northern	Upland	6.7	10393500, 10403400
Southern region	—	—	Southern	Upland	11.1	10396000, 10397000, 10400000
Western region	—	—	Western	Upland	8.3	10393500, 10403400

[1]Streamgage regulated to account for substantial diversions upstream.

[2]U.S. Fish and Wildlife Service (Mayer and others, 2007)

[3]Estimate based on 1982–2016 streamflow estimated with the streamflow-precipitation model (flow-PPT; table 4.3).

[4]Oregon Water Resources Department (Cooper, 2002)

[5]Ungaged area surrounding Riddle Creek, NE of the Kiger Creek watershed

[6]Upland areas without delineated watersheds
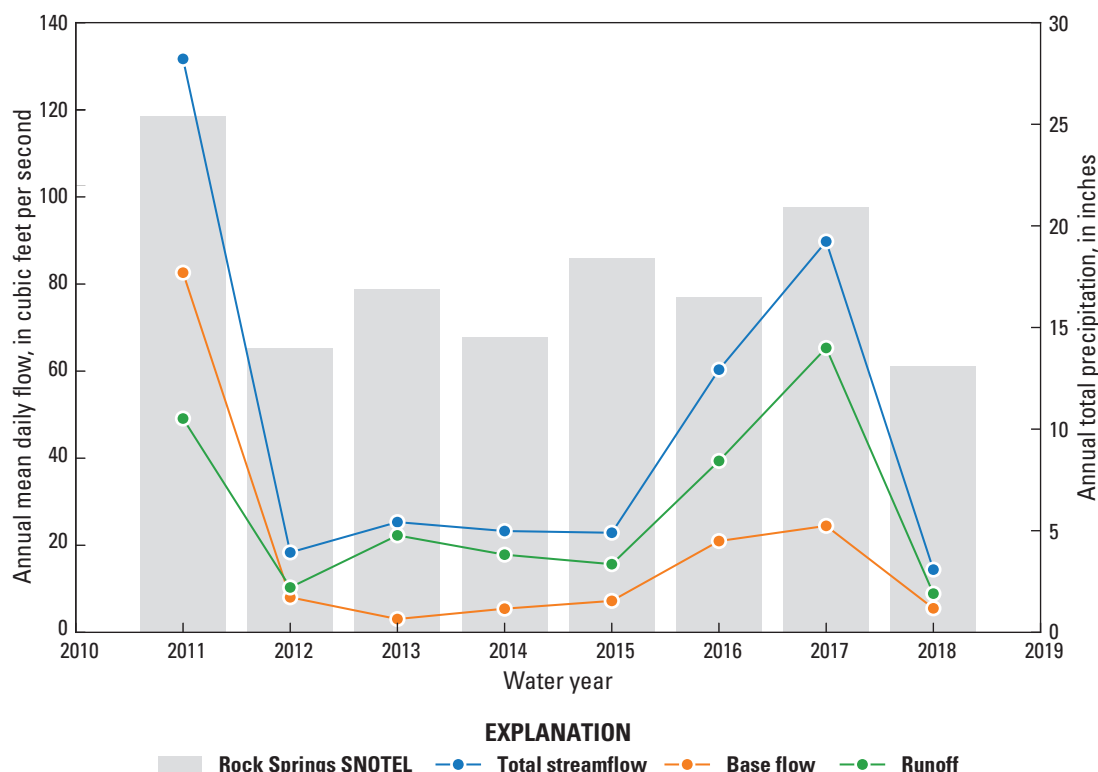
Figure 18. Comparison of annual runoff and base-flow components of total streamflow at the Silver Creek below Nicoll Creek near Riley, OR, streamgage (10403400). Base flow is the mean of base-flow index and low-flow estimates and runoff is annual total streamflow minus base flow. Annual precipitation from the nearby Rock Springs Natural Resources Conservation Service Snow Telemetry SNOTEL site (fig. 2) is shown for comparison.

Estimates of groundwater discharge to streams are most reliable in gaged watersheds with long-term records. Summer irrigation diversions on Silver Creek and the Silvies River likely led to underestimation of late-season flow (affecting the low-flow estimate of base flow), but this likely represents a small portion of annual base flow. Base-flow estimates are least reliable in ungaged watersheds and other upland areas that are based on the streamflow-precipitation model and base-flow scale factors in gaged watersheds. For example, in the southern part of the western region uplands, streamflow measurements are unavailable to validate the magnitude of base-flow estimates, but the presence of water in multiple stream reaches during the summer and early autumn low-flow period is supported by high resolution satellite imagery. Despite any uncertainties in long-term mean groundwater discharge estimates, the presence of discharge at the listed locations is well established, and the general distribution and magnitude of groundwater discharge to streams in the Harney Basin is well understood.

Groundwater Discharge to Malheur and Harney Lakes

Natural groundwater discharge to Malheur and Harney Lakes was estimated as the diffuse subsurface flow from the groundwater system through lake sediments and was a minor component of the total groundwater discharge in the Harney Basin. The groundwater flow to Malheur and Harney Lakes was computed using the hydraulic gradient determined from mapped groundwater and lake levels (fig. 19; Gingerich and others, 2022) and estimates of near-lake sediment transmissivity (table 12).

Groundwater discharges to the lakes through seeps and springs along the lake peripheries, but direct measurements of seep and spring discharge are not available. However, seep and spring discharge from the groundwater-flow system is controlled by hydraulic gradients and subsurface hydraulic properties. Therefore, estimates of seep and spring discharge can be made using some simplifying assumptions about the sediment geometry through which groundwater flows and Darcy's Law:

$$Q = T(dh/dl)w \qquad (14)$$

where

Q	is discharge $[L^3T^{-1}]$,
T	is aquifer transmissivity $[L^2T^{-1}]$ (aquifer hydraulic conductivity multiplied by aquifer thickness),
dh/dl	is hydraulic gradient $[LL^{-1}]$, and
w	is width of flow region $[L]$.
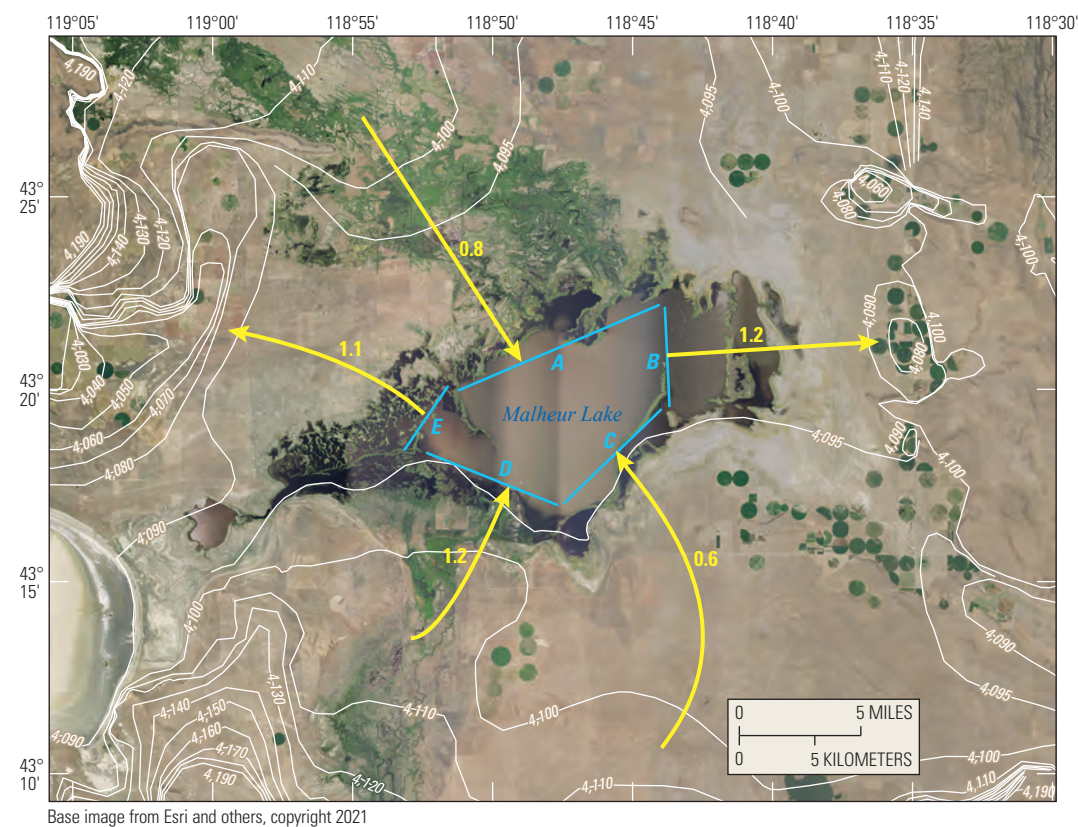
Figure 19. Groundwater-level contours and estimated hydraulic gradients used to estimate groundwater flow to (A) Harney Lake and (B) Malheur Lake through multiple shoreline segments around the lakes, Harney Basin, southeastern Oregon. Groundwater-level contours are from Gingerich and others (2022).

Table 12.   Estimation of groundwater flow toward Malheur and Harney Lakes, Harney Basin, southeastern Oregon.

[Zone locations are shown on figure 19. Gradients and estimated groundwater flow toward the lakes are positive and away from lakes are negative.
Abbreviations: acre-ft/yr, acre feet per year; ft/mi, feet per mile; ft²/day, square feet per day; ft³/day, cubic feet per day]

Lake	Zone	Upgradient head (feet)	Downgradient head (feet)	Distance (mile)	Gradient (ft/mi)	Zone width (mile)	Transmissivity (ft²/day)	Estimated groundwater flow	
								(ft³/day)	(acre-ft/yr)
Malheur	A	4,104	4,094	12.0	0.8	9.0	700	5,250	44
	B	4,094	4,084	8.6	-1.2	4.0	700	-3,325	-28
	C	4,104	4,094	15.9	0.6	5.6	700	2,450	21
	D	4,104	4,094	8.3	1.2	5.7	700	4,725	40
	E	4,094	4,084	9.0	-1.1	3.0	700	-2,275	-19
								Total in	105
								Total out	-47
Harney	A	4,086	4,076	2.1	-4.8	6.0	700	-19,250	-161
	B	4,096	4,086	3.6	2.8	6.5	700	12,600	106
	C	4,096	4,086	1.0	8.9	7.1	700	43,750	367
	D	4,096	4,086	2.1	4.8	6.0	700	19,250	161
								Total in	634
								Total out	-161

Groundwater discharge to Malheur and Harney Lakes was estimated using equation 14 for approximate zones surrounding each lake and mapped groundwater levels and hydraulic property estimates from Gingerich and others (2022). Hydraulic-gradient estimates between groundwater and lake level were made across several zones bounding each lake by measuring the approximate distance from the edge of each lake outward and perpendicular to the groundwater-level contour 10 feet higher than the lake-surface elevation in each direction (fig. 19). For Malheur Lake, hydraulic gradients were measured across five zones from a lake elevation of 4,094 ft to approximate head contours of 4,104 ft (zones A, C, and D) or 4,084 (zones B and E) (fig. 19B; table 12). For Harney Lake, hydraulic gradients were measured across four zones from a lake elevation of 4,086 ft to approximate head contours of 4,096 (zones B, C, and D) or 4,076 ft (zone A) (fig. 19A). The median transmissivity of the Younger basin fill hydrostratigraphic unit is about 700 ft²/d (n = 43; interquartile range: 210–3,500 ft²/d; Gingerich and others, 2022). This transmissivity estimate, from wells throughout the Harney Basin lowlands, is likely higher than the expected value for the fine-grained sediments near the lakes where measurements aren't available. Playa lake-bed transmissivity reported for a similar hydrologic setting in Dixie Valley, Nevada, ranges from 0.1 to 270 ft²/d (Garcia and others, 2015).

Hydraulic gradients surrounding Harney Lake indicate groundwater flows toward the lake from the west, south, and east (zones B–D) and away from the lake to the north (fig. 19A). Gradients toward the lake range from 2.8 to 8.9 ft/mi and the gradient away from the lake is 4.8 ft/mi. The westward gradient toward Harney Lake (zone D) likely manifests as spring discharge from the numerous springs in Warm Springs Valley (fig. 19), whereas gradients from the south (zone C) and east (zone B) might discharge as seeps or diffuse discharge directly into Harney Lake sediments. The northward gradient from Harney Lake (zone A) indicates groundwater flows toward the Weaver Spring/Dog Mountain area (fig. 1) where groundwater levels have declined by more than 50 ft owing to groundwater pumpage for irrigation.

Near Malheur Lake, approximate hydraulic gradients are toward the lake at rates of 0.6–1.2 ft/mi from the south and southwest (zones C and D, respectively) and a rate of 0.8 ft/mi from the northwest (zone A; fig. 19B). Toward the west and east (zones E and B), hydraulic gradients are away from the lake and are just over 1 ft/mi. These gradients are considered approximate because groundwater flow isn't strictly perpendicular to the lake shoreline, especially near zones A and E. Nevertheless, these approximations help bound the estimate of groundwater flow into or out of the lake.

Hydraulic gradients measured in shallow wells near Malheur Lake during 1972–73 showed similar results south and west of the lake despite differences in lake area and lake elevation between the early 1970s and this study (Hubbard, 1975). In the 1970s, the gradient was away from the lake at zone E (2.1 ft/mi) and toward the lake at zone D (0.5–2.1 ft/mi) (fig. 19B; table 12). Hubbard (1975) did not report gradients to the northwest (zone A) or east (zone B) of Malheur Lake. The one unresolved difference is for the gradient northeast of Malheur Lake where Hubbard (1975) reported a gradient away from the lake. Although no recent shallow

groundwater-level data are available in this region to confirm if this gradient is currently present, pumping for irrigation in the lowlands bordering the west side of the Stinkingwater Mountains has reduced groundwater levels below the elevation of Malheur Lake (Gingerich and others, 2022), so flow in that direction is physically plausible.

Using hydraulic gradient and transmissivity approximations, estimates of groundwater flow into and out of Malheur Lake (table 12) are about 100 acre-ft/yr toward the lake from the north and south and about 50 acre-ft/yr away from the lake toward areas of groundwater decline east and west of the lake, yielding a net groundwater discharge of about 50 acre-ft/yr into Malheur Lake for a lake-stage elevation of about 4,094 ft. At Harney Lake, the estimates indicate about 630 acre-ft/yr flows toward the lake from the east, south, and west sides and about 160 acre-ft/yr flows northward away from the lake toward the area of groundwater decline in the Weaver Spring/Dog Mountain area, yielding a net groundwater discharge of 470 acre-ft/yr into Harney Lake for a lake-stage elevation of about 4,084 ft.

The largest uncertainty in the estimates of groundwater flow to the lakes stems from the transmissivity used to calculate the flow. The transmissivity estimate used in table 12 represents the median value for wells completed in Younger basin fill throughout the Harney Basin lowlands (Grondin and others, 2021) and likely is substantially higher than the transmissivity of fine grained silts and clays that comprise lake-bed sediments. Transmissivity could be orders of magnitude lower based on measurements at and model simulations for similar playa lakes in Nevada (Garcia and others, 2015; Jackson and others, 2018). Secondary uncertainties in groundwater-flow estimates include hydraulic gradient measurements and approximating the lake boundaries as linear features. Despite these uncertainties, estimates of groundwater consumed by ET from bare soil-playa ET units within and surrounding the lakes (fig. 7) substantiate the flow estimates into the lake. The ET_g estimates are about 730 acre-ft/yr from Harney Lake for the area within the zones depicted in figure 19 (about 14,7000 acres) and about 150 acre-ft/yr from bare soil surrounding Malheur Lake. Groundwater-flow estimates to the lakes are accounted for by ET_g estimates and therefore are not included in total discharge estimates.

Lake-flow estimates into the groundwater system are included in groundwater recharge totals and likely reflect pumping-induced recharge of lake water rather than natural conditions. Under natural non-pumping conditions, hydraulic gradient magnitudes east and northwest of Malheur Lake and north of Harney Lake likely would be substantially lower than estimated in this study (table 12), but the direction is unknown. Regardless of steeper pumping-induced gradients, low transmissivities surrounding the lakes minimize exchanges between the lakes and groundwater system.

Groundwater Outflow to the Malheur River Basin

Groundwater flows from the Harney Basin into the Malheur River Basin through Virginia Valley, which is underlain by a paleochannel that was filled by the highly permeable Voltage basalt and permeable Younger basin fill. Groundwater discharge from the Harney Basin through Virginia Valley was minor based on calculations of the Darcy flux (eq. 14) through an area just outside the Harney Basin where groundwater flow is likely constrained in a valley less than a mile wide where Voltage basalt outcrops at the surface. The hydraulic gradient between the groundwater level in Harney Basin well HARN0001517 and the surface elevation of the South Fork Reservoir in the Malheur River Basin is about 0.0028 ft/ft ([4,035–3,940 ft] / 34,320 ft; fig. 20). A layer of Voltage basalt (median transmissivity of 28,000 ft^2/d, n=23; interquartile range: 7,600–54,000 ft^2/d; Gingerich and others, 2022), 0.9-mi wide (4,752 ft) is assumed to transmit groundwater flow from the Harney to the Malheur River Basin. The resulting estimate of subsurface groundwater flow from the Harney to the Malheur River Basin is about 3,100 acre-ft/yr. Assuming a different paleochannel geometry and (or) a higher or lower transmissivity would proportionally change the volume of groundwater outflow. However, the flow likely would not be substantially larger due to constraints imposed by the geometry of Virginia Valley and the lack of major springs or large amounts of base flow in the upper South Fork Malheur River. Additionally, this discharge likely includes some groundwater flow from the northern flank of Steens Mountain, an area where the surface-water boundary of the Harney Basin might not correspond with the groundwater-flow boundary.

Groundwater Discharge through Pumpage

Groundwater pumpage for water use includes irrigated agriculture, livestock, municipal and community supply, rural domestic supply, and commercial-industrial, and accounts for a large portion of groundwater discharge from the Harney Basin. Since the early 1990s, pumpage for livestock, municipal, domestic supply has changed little, but pumpage for irrigated agriculture has increased substantially. Most groundwater is pumped from or adjacent to the Harney Basin lowlands. Although most groundwater pumpage is considered lost from the hydrologic system, a small portion reinfiltrates and recharges the groundwater-flow system beneath irrigated fields and from non-irrigation groundwater use such as beneath septic tanks and domestic and commercial lawns and gardens (see section "Groundwater Recharge from Irrigation").
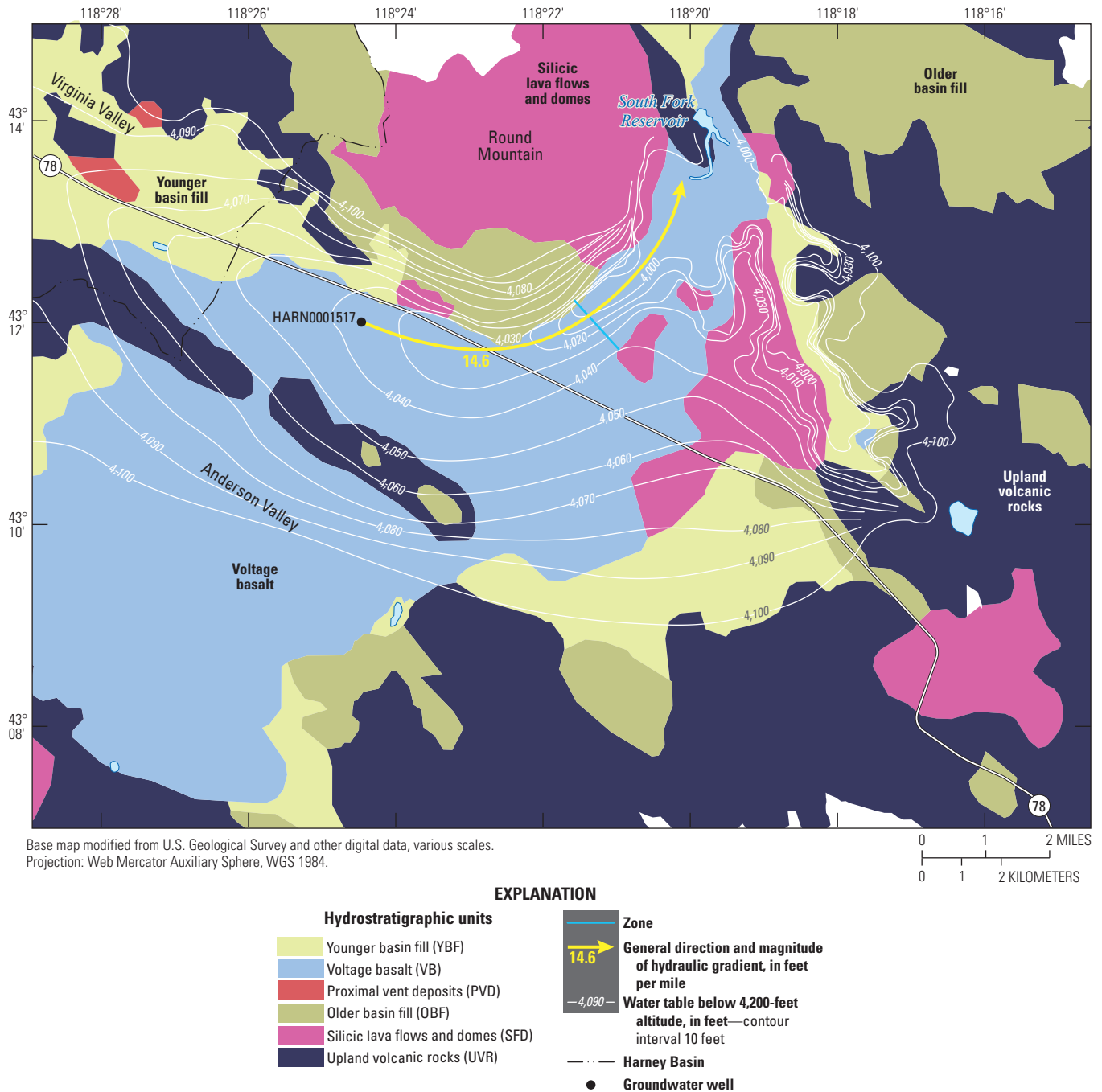
Figure 20. Groundwater-level contours and estimated hydraulic gradient used to estimate groundwater flow from the Harney Basin to the Malheur River Basin, Oregon. Contours, hydrostratigraphic units, and associated hydraulic properties are from Gingerich and others (2022).

Irrigation Pumpage

Estimates of irrigation pumpage and applied surface-water irrigation during 1991–2018 published by Beamer and Hoskinson (2021) are used in this study. Beamer and Hoskinson (2021) coupled modeled-ET estimates derived from remotely sensed satellite imagery with irrigation-efficiency estimates determined from available groundwater-pumpage data in the Harney Basin. The source of water used to irrigate each field was obtained from OWRD water-rights information. Reported pumpage volumes from OWRD's Water Use Reporting database and literature-reported irrigation efficiencies were used to estimate pumpage from the ET estimates. The growing season for irrigated areas generally represents May–September. Methods and results from Beamer and Hoskinson (2021) for analyses of ET and groundwater pumpage in irrigated areas are summarized in the following subsections.

Evapotranspiration from Irrigated Areas

Total ET and ET of irrigation water (total ET minus precipitation, or ET_{irr}) were estimated with a surface-energy-balance approach using the Mapping EvapoTranspiration at high Resolution with Internalized Calibration (METRIC) model (Allen and others, 2007), Landsat imagery, and GridMET precipitation and alfalfa (*Medicago sativa*) reference ET (ET_r). GridMET ET_r was corrected for bias in irrigated areas (Abatzoglou, 2013) prior to using in the METRIC model. The amount of irrigation water consumptively used by plants, ET_{irr}, is sourced from groundwater, surface water, or a combination of both. METRIC ET and ET_{irr} were computed monthly and seasonally over 14 growing seasons (May–September) during 1991–2019. A time series beginning in 1991 was selected to capture the increase in groundwater irrigation that began in the early 1990s. The years analyzed include 1991, 1992, 1994, 2000, 2001, 2005, 2009, 2011, and 2014–19. METRIC ET data from 2017 to 19 was compared with measured eddy-covariance ET data from an alfalfa-field site near Crane in the Harney Basin, and the comparison was used to scale METRIC estimates to measured values.

Seasonal ET_{irr} volumes were computed as the product of seasonal ET_{irr} rates and the area of irrigated fields and distinguished by irrigation source water. Rates of ET_{irr} were estimated subtracting monthly precipitation from monthly ET for each mapped field. Field boundaries are based on the common land unit (CLU) polygons (Farm Service Agency, 2008) and were refined using NAIP imagery, mapped water rights places of use (POU), and Landsat May-September maximum normalized difference vegetation index (NDVI), where a threshold of 0.4 was used to classify fields as irrigated or non-irrigated (Beamer and Hoskinson, 2021).

The seasonal ET_{irr} estimates assume antecedent soil moisture, resulting from precipitation since the prior growing season, has been fully depleted by May 1st and that growing-season ET is comprised of irrigation applied and precipitation that fell during the growing season only. Comparisons of cumulative spatially weighted mean monthly ET and precipitation rates for each irrigation source water support this assumption and indicate that antecedent soil moisture resulting from winter precipitation is fully depleted by April, at which time cumulative monthly ET exceeds precipitation (fig. 21). During the growing season, the ET water source is almost exclusively irrigation as cumulative ET increases while cumulative precipitation plateaus, reflecting the nominal amount of precipitation that falls in the Harney Basin during the summer and early autumn.

The source of irrigation water was identified for each irrigated field for each of the 13 analysis years based on OWRD water-rights information. Fields were categorized by their source of irrigation water as (1) groundwater only, (2) surface water only, or (3) groundwater and surface water. The irrigated area within the MNWR (assigned a constant 46,300 acres for the period) primarily was irrigated with surface water (Daniel Craver, U.S. Fish and Wildlife Service, written commun., 2017).

Irrigated land in the Harney Basin lowlands increased from roughly 128,000 acres in 1991 to nearly 190,000 acres in 2018 (figs. 22C-D), and groundwater-irrigated fields comprised about 70 percent of the change in irrigated acreage (or 43,500 acres; fig. 23). Fields irrigated exclusively with groundwater increased from 20,200 acres in 1991 to 57,900 acres in 2018, and fields irrigated with groundwater and surface water increased from 10,400 acres in 1991 to 16,200 acres in 2018 (fig. 23). Surface water has been fully appropriated since the mid-1900s and the year-to-year variability in the acreage irrigated with surface water depends on the availability of surface water to meet existing demand, and not the development of newly irrigated fields (fig. 22). For example, the annual streamflow at the Silvies River near Burns and Donner und Blitzen River near Frenchglen streamgages was about 40 percent lower during 1991–92 relative to 2017–18, and the total acreage irrigated by surface water was about 15 percent lower during 1991–92 relative to 2017–18.

The spatially weighted mean seasonal (May–September) ET_{irr} rates for the Harney Basin are 1.43 ft/yr for fields irrigated with surface water only, 1.49 ft/yr for fields irrigated with surface water and groundwater, and 1.51 ft/yr for fields irrigated with groundwater only (table 13). Rates varied from a low of nearly 0 near the edges of irrigated fields to a high of about 2 ft/yr in fields completely covered by irrigation systems or flood-irrigated wetlands adjacent to the Donner und Blitzen River and Warm Springs Valley.

The ET_{irr} volume varied by irrigation source water during 1991–2018, following interannual changes in irrigated acreage and area-weighted ET (fig. 24). For groundwater-irrigated fields, ET_{irr} volume increased from a mean of 31,000 acre-ft/yr in the early 1990s to a mean of 87,000 acre-ft/yr during 2017–18. The ET_{irr} volume from surface-water irrigated fields varied throughout the period owing to year-to-year variability in surface-water availability.
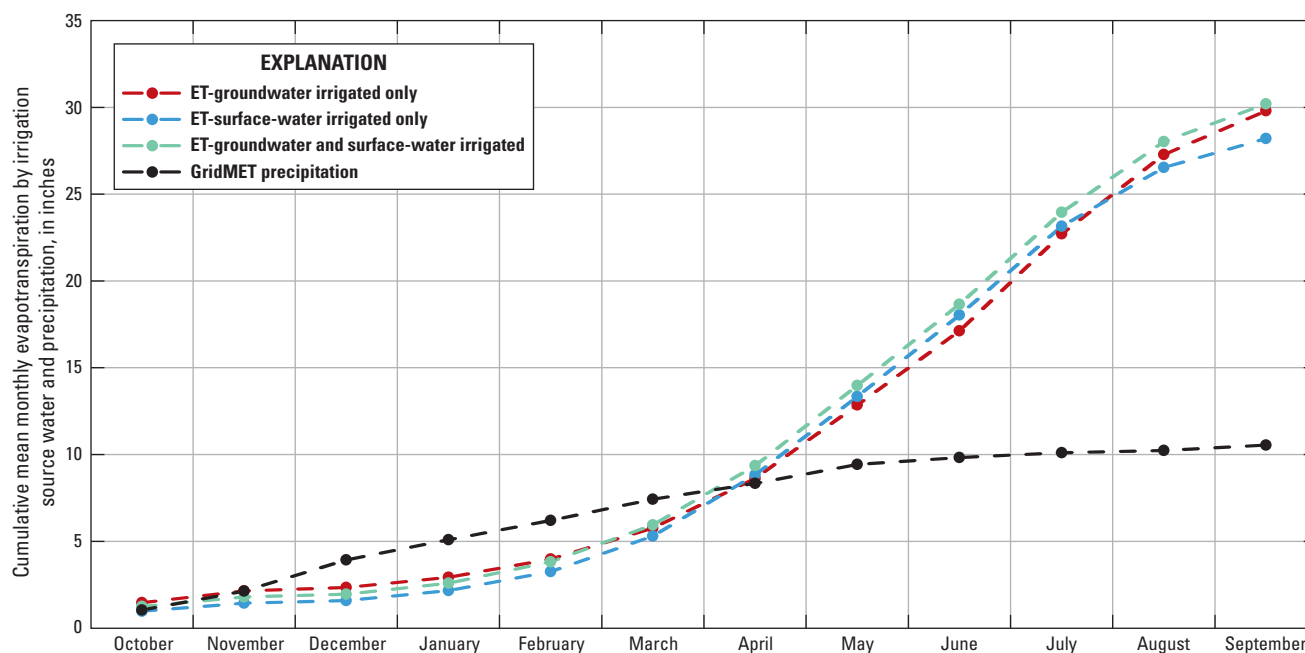
Figure 21. Comparison of cumulative mean monthly evapotranspiration rates by irrigation source water and precipitation for water years 2014–18, Harney Basin, southeastern Oregon. Mean monthly evapotranspiration was spatially weighted by irrigation source within a water year and then temporally weighted across water years 2014–18.
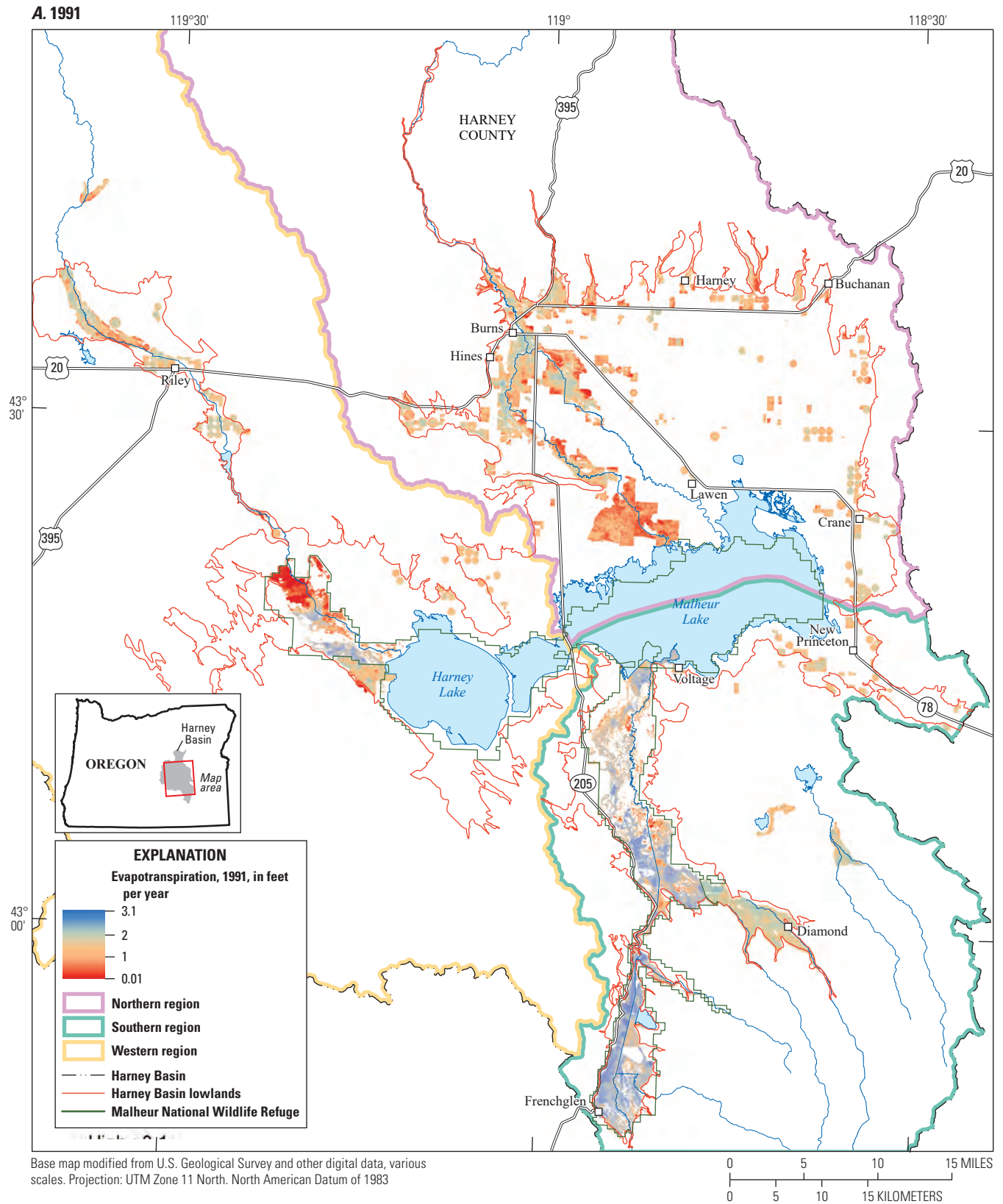
Figure 22.   Maximum extent of irrigated areas and evapotranspiration of irrigation water (ET_{irr}) from May to September 1991 (*A*) and 2018 (*B*) and irrigated fields by irrigation source type in 1991 (*C*) and 2018 (*D*), Harney Basin, southeastern Oregon.

B. 2018

EXPLANATION

Evapotranspiration, 2018, in feet per year

3.1
2
1
0.01

Northern region

Southern region

Western region

Harney Basin

Harney Basin lowlands

Malheur National Wildlife Refuge

Base map modified from U.S. Geological Survey and other digital data, various scales. Projection: UTM Zone 11 North. North American Datum of 1983

0   5   10   15 MILES

0   5   10   15 KILOMETERS

Figure 22.—Continued

C. 1991

EXPLANATION
Irrigation source, 1991
- Groundwater irrigated
- Surface-water irrigated
- Groundwater and surface-water irrigated
- Northern region
- Southern region
- Western region
- Harney Basin
- Harney Basin lowlands
- Malheur National Wildlife Refuge

Base map modified from U.S. Geological Survey and other digital data, various scales. Projection: UTM Zone 11 North. North American Datum of 1983

0   5   10   15 MILES
0   5   10   15 KILOMETERS

Figure 22.—Continued

D. 2018

EXPLANATION

Irrigation source, 2018

- Groundwater irrigated
- Surface-water irrigated
- Groundwater and surface-water irrigated
- **Northern region**
- **Southern region**
- **Western region**
- **Harney Basin**
- **Harney Basin lowlands**
- **Malheur National Wildlife Refuge**

Base map modified from U.S. Geological Survey and other digital data, various scales. Projection: UTM Zone 11 North. North American Datum of 1983

Figure 22.—Continued
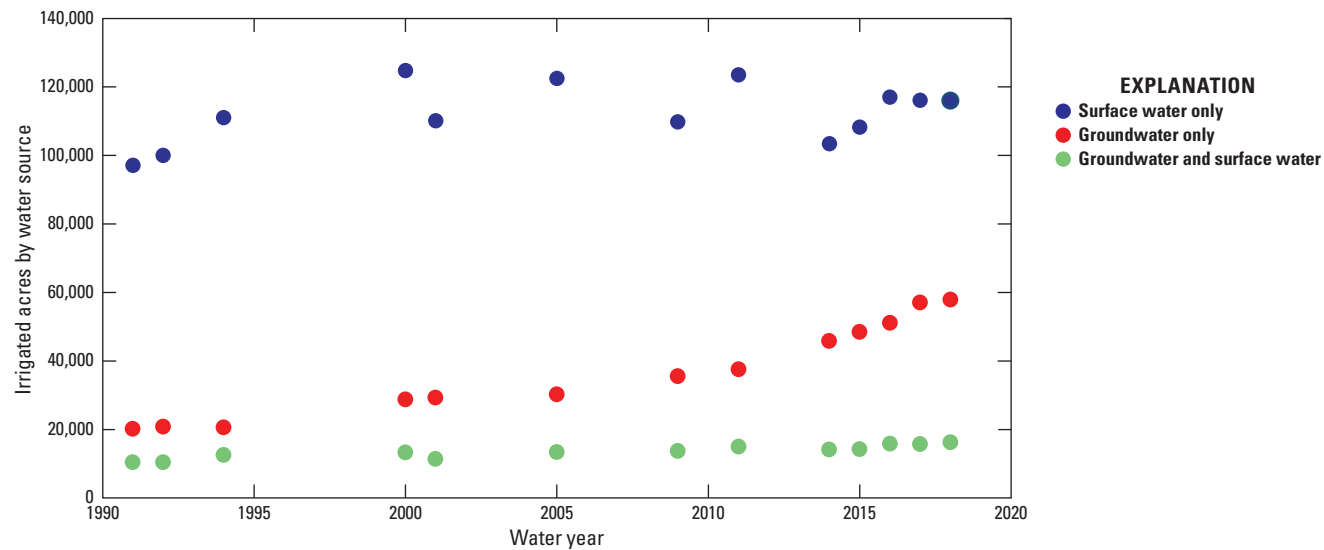
Figure 23.   Irrigated acreage by water source for years with METRIC data, Harney Basin, southeastern Oregon. METRIC, Mapping Evapotranspiration using high Resolution and Internalized Calibration.

Table 13.   Mean seasonal May–September evapotranspiration rates of irrigation water and pumpage rates by irrigation source and region, 1991–2018, Harney Basin, southeastern Oregon.

[Regions are shown on figure 1. **Mean seasonal evapotranspiration rate of irrigation water**: Total evapotranspiration minus precipitation. Mean values represent both spatial and temporal ranges. Pumpage rate for fields irrigated with groundwater and surface water represents groundwater pumpage only]

Irrigation source	Mean seasonal evapotranspiration rate of irrigation water (feet/year)			
	Northern region	Southern region	Western region	Harney Basin
Groundwater only	1.48	1.51	1.57	1.51
Groundwater and surface water	1.44	1.60	1.66	1.49
Surface water only	1.27	1.64	1.29	1.43
	Mean seasonal pumpage rate (feet/year)			
Groundwater only	2.12	2.15	2.24	2.16
Groundwater and surface water	1.20	1.34	1.38	1.24
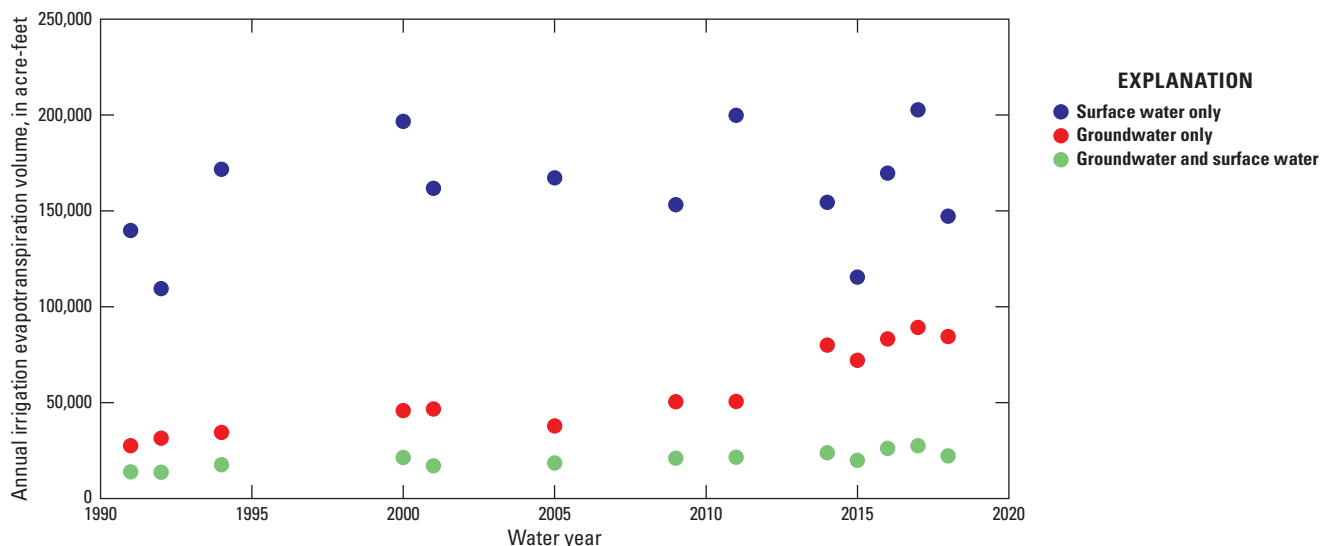
Figure 24. Annual irrigation evapotranspiration volume by irrigation source water for years with METRIC data, Harney Basin, southeastern Oregon, water years 1991–2018. Missing years were excluded because of excess cloud cover. METRIC, Mapping Evapotranspiration using high Resolution and Internalized Calibration.

Table 14. Summary of irrigation systems corresponding to irrigated areas and irrigation source water in 2016, Harney Basin, southeastern Oregon.

Irrigation source water	Irrigated acres	Irrigation system (percent)		
		Center pivot	Hand-move and wheel-line sprinkler	Flood
Surface water only	51,100	90	8	2
Groundwater and surface water	15,900	36	11	53
Groundwater only	70,500	1	0	99
Total[1]	137,500	38	4	57

[1]Corresponds with total irrigated acres and percentage of each irrigation system across all irrigated acres.

The mean annual volume of ET_{irr} from recent years (2014–18) was about 260,000 acre-ft, with 82,000 acre-ft from groundwater-irrigated fields, 24,000 acre-ft from fields irrigated with surface water only and groundwater, and 158,000 acre-ft from surface-water-irrigated fields. About 42 percent or 67,000 acres of surface-water irrigated fields were within the MNWR.

Groundwater Pumpage and Irrigation Efficiency

Annual groundwater pumpage for irrigation in the Harney Basin was estimated using ET_{irr} volume from fields irrigated with groundwater or a combination of groundwater and surface water and irrigation efficiencies. Irrigation efficiency is the ratio of crop water use and total applied water based on the irrigation method. Irrigated fields were categorized into three irrigation system types—flood, hand-move and wheel line sprinkler, and center pivot (table 14). An irrigation efficiency of 50 percent was assigned for surface-water flood-irrigated

fields in the Harney Basin based on literature-reported values ranging from 35–60 percent (Washington State Department of Ecology, 2005).

The irrigation efficiency for groundwater-irrigated fields averaged about 70 percent and was estimated as the ratio of seasonal ET_{irr} from fields and pumpage volumes for 59 well pairs during 2014–16 (fig. 25). Wind-drift efficiency losses of 20 percent were assigned based on a study in southern Washington in which the fraction of applied water that reached the soil surface from MESA (mid-elevation sprinkler application) center-pivot irrigation systems, like most center pivots in the Harney Basin, was 0.8 (Sarwar and others, 2019). The remaining 10 percent of efficiency losses were equally partitioned between runoff and percolation below the root zone. For a setting in Nebraska with center pivot irrigation systems and silt loam soil like those in the Harney Basin, percolation below the root zone accounted for 5–6 percent of the total applied water (Irmak, 2017).
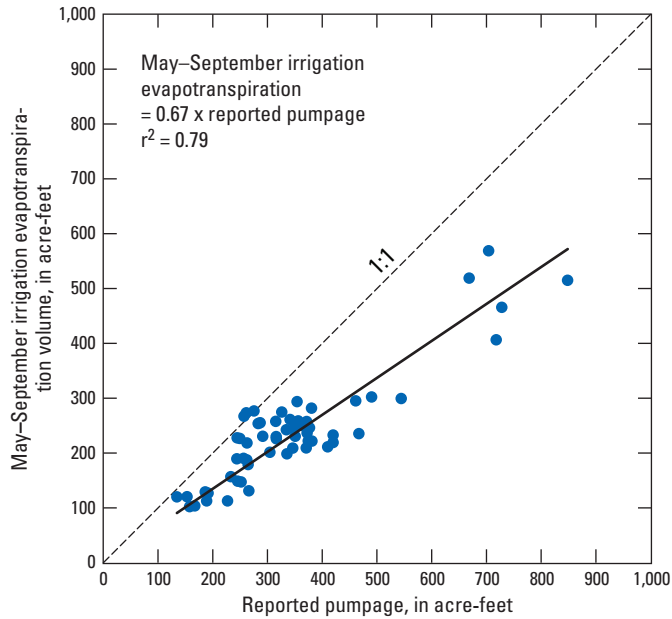
Figure 25.   Relation between seasonal evapotranspiration of irrigation water (ET_{irr}) from groundwater-irrigated areas and reported annual pumpage used to estimate irrigation efficiency, 2014–16. Parameter r^2 is the coefficient of determination from the ordinary least-squares relation.

Total groundwater pumpage was estimated from fields irrigated with groundwater only and those irrigated with groundwater and surface water. Irrigation source water volumes were equally divided on fields irrigated with surface water and groundwater based on previous studies (Conlon and others, 2005; Gannett and others, 2007; Adam Sullivan, Nevada Department of Water Resources, written commun, 2019); these fields were assigned an efficiency of 60 percent, which is the mean of the surface-water-irrigation efficiency (50 percent) and groundwater-irrigation efficiency (70 percent). Estimates of total groundwater pumpage for each year were made using equation 15:

$$\text{Total groundwater pumpage} = \frac{ET_{irr-GW}}{0.7} + \frac{(ET_{irr-GWSW}) \times 0.5}{0.6} \quad (15)$$

where

ET_{irr-GW} is the volume of irrigation ET for fields irrigated with groundwater only and

$ET_{irr-GWSW}$ is the volume of irrigation ET for fields irrigated with both surface water and groundwater.

Total groundwater pumpage for irrigation in the Harney Basin increased substantially during 1991–2018, and most of the increase occurred on fields irrigated with groundwater only (fig. 26) and reflects the increase in new agricultural land

that occurred during this period. Total groundwater pumpage increased from a mean of 54,000 acre-ft/yr during 1991–92 to a mean of 145,000 acre-ft/yr during 2017–18, nearly three times the 1991–92 rate (fig. 26; table 15). The largest rate of change occurred during 2011–14. Total pumpage in recent years (2014–18) has ranged from about 120,000 to 150,000 acre-ft/yr.
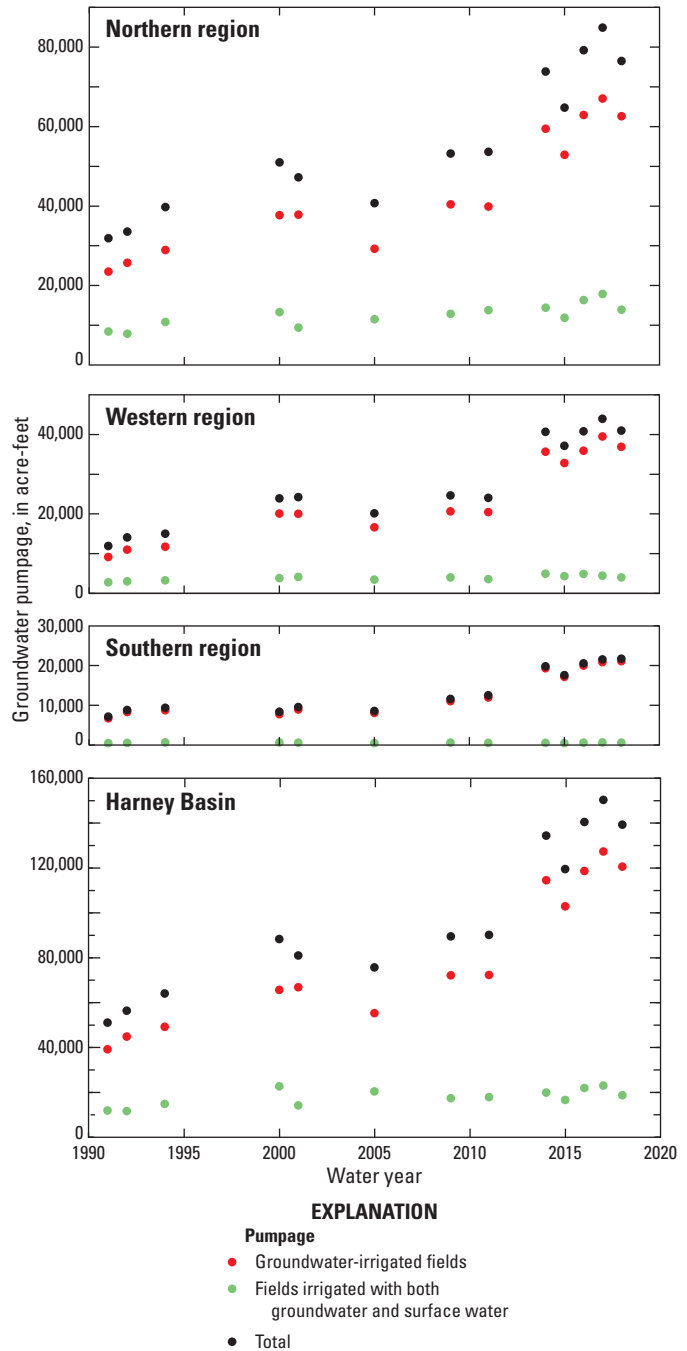
Figure 26.   Estimated annual groundwater pumpage for irrigation by region, Harney Basin, southeastern Oregon, 1991–2018.

Table 15. Total estimated annual groundwater pumpage by region in the Harney Basin, southeastern Oregon, for select years during 1991–2018 and the 2017–18 mean.

[Regions are shown on figure 1. Groundwater pumpage is rounded to the nearest 100 acre-feet]

Year	Groundwater pumpage (acre-feet)			
	Northern region	Southern region	Western region	Total
1991	31,900	7,100	11,900	50,900
1992	33,500	8,800	14,100	56,400
1994	39,700	9,400	15,000	64,100
2000	51,000	8,400	23,900	83,300
2001	47,200	9,600	24,200	81,000
2005	40,700	8,500	20,100	69,300
2009	53,200	11,600	24,700	89,500
2011	53,600	12,500	24,100	90,200
2014	73,800	19,800	40,600	134,200
2015	64,700	17,600	37,100	119,400
2016	79,200	20,500	40,800	140,500
2017	84,900	21,500	43,900	150,300
2018	76,500	21,700	41,000	139,200
2017–18 mean	80,700	21,600	42,500	144,800

Estimates of groundwater pumpage are highest in the northern region and lowest in the southern region (table 15). The 2-yr mean during the most recent period (2017–18) was computed to represent the current groundwater pumpage estimate. The 2-yr mean annual pumpage estimate for each region is 80,700 acre-ft in the northern region (2.5 times the 1991–92 estimate), 21,600 acre-ft in the southern region (nearly 3 times the 1991–92 estimate), and 42,500 acre-ft in the western region (more than 3 times the 1991–92 estimate). The 2-year mean groundwater pumpage estimate for irrigation in the Harney Basin is 145,000 acre-ft.

Uncertainties in Irrigation Pumpage

Pumpage estimates from irrigated areas likely are accurate to within 20 percent. Uncertainties result from estimates and assumptions of ET, ET_{irr}, and irrigation efficiency. Final ET and ET_{irr} estimates for irrigated areas by Beamer and Hoskinson (2021) have an estimated accuracy of 10–20 percent and compare well with independent estimates of crop ET for the Harney Basin that have been used over recent decades (Cuenca and others, 1992). Spatially averaged growing-season ET and ET_{irr} rates for groundwater-irrigated fields, which are predominantly alfalfa, fall within the range of alfalfa ET rates and net irrigation requirements, respectively, from Cuenca and others (1992), but rates for surface-water irrigated fields, which are predominantly pasture grass, are about 30 percent less than pasture-grass estimates by Cuenca and others (1992). Lower growing-season rates from surface-water irrigated fields, with respect to previous estimates, were expected owing to the limited surface-water supply after July in most years. The growing-season ET_{irr} from

groundwater-irrigated fields represents the lower bound of crop water use because it assumes all precipitation is used for ET (100 percent effective); if some precipitation runs off the field, then ET of applied groundwater must be larger to satisfy the measured METRIC ET. Estimates of irrigation efficiency made in this study are assumed accurate to within 10 percent and estimated values fall within the range of literature values for the common irrigation systems (table 14) in the basin. Estimated efficiencies based on the 23 wells in the basin were assumed to adequately characterize the irrigation systems and physical properties across all groundwater-irrigated fields in the basin. Likewise, literature-based efficiency estimates for surface-water flood-irrigated fields were assumed to represent mean conditions in surface-water irrigated fields in the Harney Basin.

Non-Irrigation Pumpage

Non-irrigation groundwater pumpage estimates from Grondin (2021) are used in this study and include (1) public municipal supply systems for the towns of Burns, Hines, and Seneca, (2) private and public small community water systems, (3) private rural domestic household systems, (4) private and public livestock watering systems, and (5) commercial and industrial water systems. Estimated pumpage for non-irrigation uses totaled about 6,900 acre-ft/yr, with about 6,000 acre-ft/yr consumed and about 900 acre-ft/yr reinfiltrating and recharging the groundwater system (table 16). Results from Grondin (2021) are summarized below by water use type and generally represent water use during 1999–2018.

Table 16.   Estimated annual groundwater pumped, returned, and consumed for non-irrigation uses in the Harney Basin, southeastern Oregon.

[Regions are shown on figure 1. Values rounded to the nearest integer and then by up to three significant figures]

Region	Number of wells used	Groundwater volume (acre-feet)		
		Pumped	Returned	Consumed
Public municipal supply[1]				
Northern region	10	2,200	0	2,200
Southern region	0	0	0	0
Western region	0	0	0	0
Harney Basin	10	2,200	0	2,200
Community systems[2]				
Northern region	14	58	42	16
Southern region	9	12	10	1
Western region	6	10	9	1
Harney Basin	29	80	62	19
Rural domestic[3]				
Northern region	872	947	545	402
Southern region	121	131	76	56
Western region	110	119	69	51
Harney Basin	1,100	1,200	690	508
Livestock[4]				
Northern region	339	814	0	814
Southern region	138	331	0	331
Western region	113	271	0	271
Harney Basin	590	1,420	0	1,420
Commercial-industrial				
Northern region	5	2,040	148	1,890
Southern region	0	0	0	0
Western region	0	0	0	0
Harney Basin	5	2,040	148	1,890
Totals				
Northern region	1,240	6,060	735	5,320
Southern region	268	474	86	388
Western region	229	401	78	323
Harney Basin	[5]1,740	6,940	900	[5]6,040

[1]Mean of groundwater pumped by Burns, Hines, and Seneca in 2000 and 2010 reported to Oregon Water Resources Department (OWRD).

[2]Derived from 1) household connections reported to Oregon Health Authority and household use calculated from municipal groundwater pumped in 2000 and 2010 reported to OWRD or 2) published per-person use estimates for each facility type multiplied by the estimated population served within a year. See Grondin (2021) for more information.

[3]Derived from total rural domestic wells with water well reports (well-logs) filed at OWRD and household use calculated from municipal groundwater pumped in 2000 and 2010 reported to OWRD.

[4]Derived from U.S. Department of Agriculture (2018, 2019a, b) and Lovelace (2009, table 1).

[5]Any numerical inconsistencies due solely to rounding.
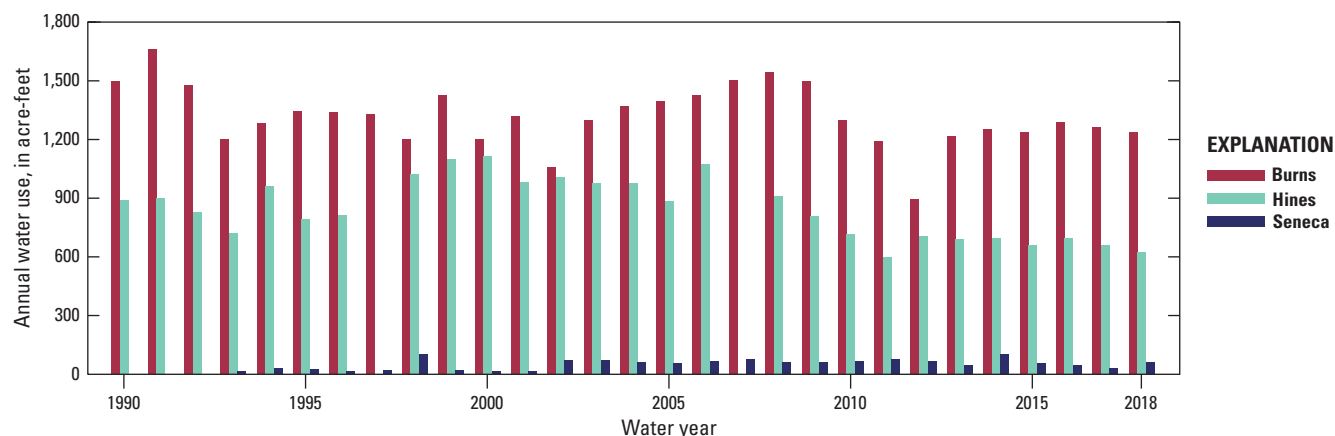
Figure 27.   Annual groundwater pumped for the three municipal systems within the Harney Basin, southeastern Oregon, water years 1990–2018.

Groundwater pumpage for public municipal supply systems reported to OWRD (Oregon Water Resources Department, 2019b, c, d) ranged from 2,000 to 2,500 acre-ft/yr during 1993–2018 (fig. 27). The mean per capita use was 415 gallons per day (gal/d) and the mean household use was 969 gal/d per household, or 1.09 acre-ft/yr (Grondin, 2021). Pumpage for public municipal supply systems is assumed to be entirely consumed. Wastewater in Burns and Hines is discharged to closed evaporation ponds and prior to 2020, wastewater in Seneca evaporated from leaky disposal ponds located within 500 ft of Silvies River.

Twenty-five small community water systems in the Harney Basin, registered with the Oregon Health Authority (Oregon Health Authority, 2019a, b), supply schools, motels, restaurants, stores, campgrounds, field stations, one rest stop, an airport, and an unincorporated neighborhood with 30 household connections. Total groundwater pumped was estimated at about 80 acre-ft/yr and nearly 80 percent of the pumped water was estimated to return to the groundwater system via septic systems and infiltration below small lawns (table 16; Grondin, 2021).

Water well drillers have filed roughly 1,100 water well reports (Oregon Water Resources Department, 2019e) for rural domestic wells in the Harney Basin (fig. 28). The groundwater pumped by rural domestic wells was estimated at about 1,200 acre-ft/yr with about 510 acre-ft/yr consumed and 690 acre-ft/yr returned to groundwater via septic systems.

An estimated 105,000 cattle and nearly 2,400 sheep are raised in Harney County (U.S. Department of Agriculture, 2018, 2019a, b). The estimated maximum groundwater pumped for livestock is about 1,400 acre-ft/yr for the Harney Basin or 2.4 acre-ft/yr for each livestock well in the basin. All the groundwater pumped for livestock is assumed to be consumed. Additional details regarding non-irrigation water use in the Harney Basin can be found in Grondin (2021).

Three facilities categorized as commercial, industrial, or geothermal are supplied by groundwater in the northern region lowlands. One facility's water right includes irrigation use, but this use was excluded from non-irrigation pumpage estimates. The estimated maximum groundwater discharge for commercial-industrial use is about 2,040 acre-ft/yr (since 1999) for the Harney Basin with about 148 acre-ft/yr returned to groundwater through an injection well and about 1,890 acre-ft/yr consumed.

Summary of Groundwater Discharge

During 1982–2016, mean annual natural discharge was about 239,000 acre-ft in upland areas and 131,000 acre-ft/yr in lowland areas. Pumpage for irrigation and non-irrigation uses increased from less than 54,000 acre-ft/yr (1991–92) to about 145,000 acre-ft/yr (2017–18; tables 15–17). Much of the upland groundwater discharge is conveyed by perennial and intermittent streams to the Harney Basin lowlands where it reinfiltrates and recharges the basin-fill deposits (figs. 5–6). This secondary recharge of upland groundwater reemerges as groundwater discharge through ET and springs in the GETA. More than 90 percent of natural groundwater discharge in lowland areas is through ET (119,000 acre-ft/yr), and the remaining lowland discharge occurs through springs unaccounted for in ET estimates (7 percent or 8,900 acre-ft/yr) or as groundwater flow to the Malheur River Basin (2 percent or 3,100 acre-ft/yr). Groundwater pumpage in lowland areas exceeds natural discharge by more than 15 percent (table 17).

Natural groundwater discharge in upland areas follows elevation-based precipitation distributions (fig. 2) with the greatest discharge in the southern region (about 137,000 acre-ft/yr) followed by the northern region (77,000 acre-ft/yr) and western region (25,000 acre-ft/yr). Upland discharge estimates in ungaged areas were mostly attributed to base flow, but a portion of this discharge also might be springflow where stream channels are poorly defined (fig. 11). Most of the upland discharge in ungaged areas likely evaporates before reaching lowland areas, especially in the southwest portion of the western region and the eastern portion of the northern region.

Natural groundwater discharge in lowland areas roughly corresponds with the GETA extent with the greatest discharge in the northern region (64,000 acre-ft/yr) followed by the western region (35,000 acre-ft/yr) and southern region (32,000 acre-ft/yr) (tables 6, 17), but the mechanism by which discharge occurs varies regionally. In northern and western regions ET_g fully accounts for natural discharge, but northern region ET_g is predominantly through root-water uptake from the water table or capillary fringe whereas western region ET_g is largely ET of springflow. In the southern region, ET_g accounts for about two-thirds of natural discharge through root uptake from the water table or capillary fringe and the other one-third of discharge occurs as springflow or groundwater flow to the Malheur River Basin. Natural groundwater discharge in the southern region could be larger than estimated because base-flow gains are likely between Frenchglen and Diamond Lane (see subsection "Results for Groundwater Discharge to Streams"). However, base-flow gains likely are equally offset by streamflow losses downstream between Diamond Lane and the Donner und Blitzen River near Voltage streamgage; therefore, net base flow in the southern region lowlands is likely negligible.

About 95 percent of groundwater pumpage in the Harney Basin is used for irrigation (table 17) and all but 0.1 percent occurs either within the lowland boundary or within 2 miles of the lowland boundary. The magnitude of groundwater pumpage and relative comparison with natural lowland groundwater discharge varies regionally. Pumpage in the northern region totaled 87,000 acre-ft/yr during 2017–18, representing nearly 60 percent of total pumpage from the Harney Basin. Northern region pumpage exceeds natural lowland discharge in the region by nearly 40 percent. In the western region, pumpage totaled 43,000 acre-ft/yr, nearly 30 percent of the basin total, and exceeds natural lowland discharge in the region by more than 20 percent. Pumpage in the southern region totaled 22,000 acre-ft/yr, 14 percent of the basin total, and is within about 30 percent of natural lowland discharge in the southern region.

Natural groundwater discharge estimates from the Harney Basin lowlands in the northern and western regions are similar to historical estimates from Piper and others (1939) made nearly a century ago. They estimated about 26,500 acre-ft/yr of spring discharge from Warm Springs Valley in the western region, which is like spring-discharge estimates made in this study (table 7). In the northern region lowlands, Piper and others (1939) estimated 57,000 acre-ft/yr of ET_g distributed as about 40,000 acre-ft/yr along the Silvies River floodplain between Burns and Malheur Lake and 17,000 acre-ft/yr along the northeast plain extending eastward toward Buchanan (fig. 1). Despite nearly a century of agricultural land use, ET_g estimates from the northern region valley lowlands made in this study are within 12 percent of historical estimates. Similar ET_g estimates in the northern region indicate that ET_g has not yet been notably altered by groundwater development.

Base map modified from U.S. Geological Survey and other digital data, various scales.
Projection: UTM Zone 11 North. North American Datum of 1983
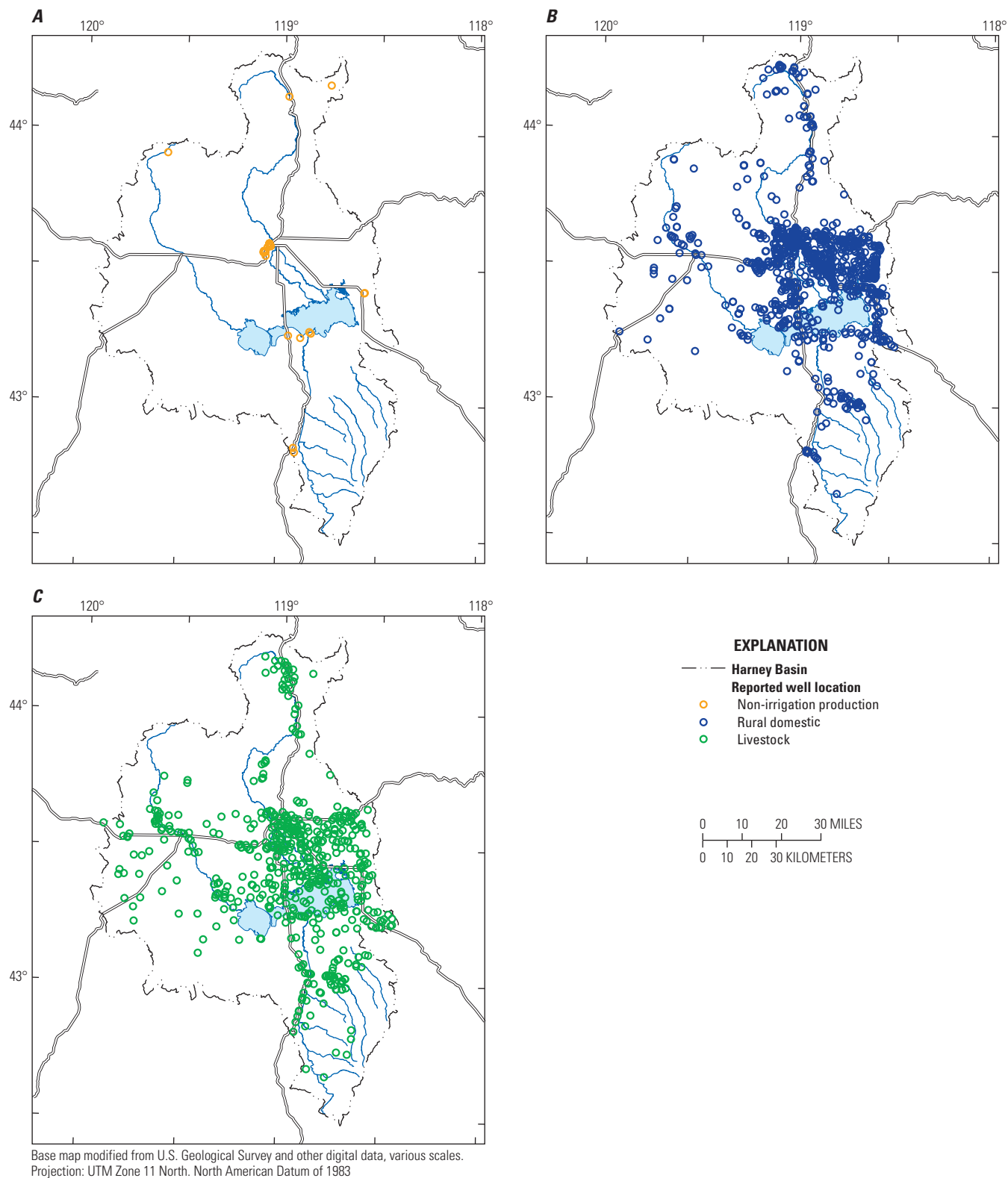
Figure 28.   Distribution of (*A*) municipal, community, commercial-industrial wells, (*B*) rural domestic wells, and (C) livestock wells with water-well reports filed with the Oregon Water Resources Department (Oregon Water Resources Department, 2019a, e), Harney Basin, southeastern Oregon.

Table 17.   Estimated mean annual groundwater discharge by region, Harney Basin, southeastern Oregon, 1982–2016.

[**Geographic position**: Position of water-bearing units where recharge and discharge occur. **Mean annual discharge by region**: Values represent the mean of input ranges. Discharge estimates are rounded to two significant figures for values below 100,000 and three significant figures for values above 100,000. Discharge totals are summarized by column and row and therefore might differ. Regions are shown on figure 1. Values presented in parentheses are accounted for in ET$_g$ estimate totals. **Abbreviations**: ET$_g$, groundwater evapotranspiration; MRB, Malheur River Basin; NA, not applicable]

Geographic position	Component	Mean annual discharge by region (acre-feet)			
		Northern	Southern	Western	Harney Basin
Upland	Base flow	75,000	125,000	25,000	225,000
	Springs[1]	2,000	12,000	22	14,000
	Total	77,000	137,000	25,000	239,000
Lowland	Springs	(530)	[4]8,900	[5](25,000)	8,900
	ET$_g$ (natural)[2]	64,000	20,000	35,000	119,000
	Diffuse flux to lakes[3]	(45)	(60)	(630)	(730)
	Groundwater flow–MRB	NA	3,100	NA	3,100
	Total non-pumpage	64,000	32,000	35,000	131,000
	Irrigation pumpage[6,7]	81,000	22,000	[8]42,000	145,000
	Non-irrigation pumpage[7]	6,100	470	400	7,000
	Total pumpage	87,000	22,000	[8]43,000	152,000
	Lowland total	151,000	54,000	78,000	283,000

[1]Estimates represent discharges unaccounted for in base-flow estimates and include current and historical spring discharge measurements (table 7).

[2]ET_g from non-irrigated areas and spring-irrigated agriculture. Includes ET_g of spring discharge.

[3]Sum of groundwater fluxes toward Malheur and Harney Lakes. Estimates accounted for in ET_g (natural) estimates.

[4]Mean of measurements made during 1907–80 (table 7).[5]Summation of current and historical measurements from table 7.

[6]2017–18 mean groundwater pumpage (table 15)

[7]All but 0.1 percent of pumpage occurs either within the lowland boundary or within 2 miles of the lowland boundary.[8]Summation discrepancies solely from rounding of component estimates in table 15.

Groundwater Recharge

Precipitation falling within the Harney Basin is the primary source of groundwater recharge. Most precipitation falls as winter snowfall on the mountain ranges, with lesser amounts falling as snow and rain across the entire basin. The principal recharge areas in the Harney Basin are the uplands of the Blue Mountains and Steens Mountain and the floodplains of the Silvies River, Donner und Blitzen River, Silver Creek, and the smaller streams entering the Harney Basin lowlands (figs. 1–2). Upland recharge occurs through infiltration of precipitation and snowmelt, and lowland recharge occurs through groundwater inflow from upland areas, infiltration of surface water beneath stream channels and areas flooded with snowmelt runoff, and through infiltration of irrigation water on irrigated fields and from surface diversions and non-irrigation pumpage (fig. 6). Infiltration of precipitation in lowland areas generally is consumed by ET before reaching the water table because ET exceeds precipitation in most lowland areas (see section "Groundwater Discharge through Evapotranspiration"); hence, precipitation in the lowlands does not contribute to lowland recharge. Groundwater recharge estimation methods and results are described in the following subsections.

Groundwater Recharge from Infiltration of Precipitation and Snowmelt

Recharge from infiltration of precipitation through soils was estimated using the Soil-Water Balance (SWB) model (Westenbroek, 2010). Although the SWB model extended across the Harney Basin, recharge estimates were restricted to upland areas where precipitation and snowmelt generally exceed ET. Most lowland areas correspond with the GETA where ET generally exceeds precipitation and is sourced from a combination of precipitation, groundwater, and (or) surface water. Recharge mechanisms in the Harney Basin lowlands such as infiltration of surface water and irrigation water were not explicitly considered in the Harney SWB model and were estimated independently. The SWB model estimates recharge

as precipitation minus interception, runoff, ET, and soil-water storage. Recharge estimated with the SWB model ultimately discharges to upland streams as base flow, to upland springs that merge with streams, and as groundwater flow to lowland areas. Small recharge volumes that discharge to upland ET_g or to upland springs that ultimately dissipate as ET were not estimated with SWB because the model is calibrated to total ET (from precipitation and snowmelt, and groundwater and surface water, if any). An overview of the construction and calibration of the SWB model for the Harney Basin uplands is provided in the next few subsections. Additional details of the model are provided in appendix 7.

Soil-Water-Balance Model Description, Assumptions, and Inputs

The SWB model simulates recharge to groundwater as the daily difference between water sources (precipitation and snowmelt) and sinks (interception of precipitation by plants before reaching the soil, runoff of water on the soil surface, ET of soil water, and soil-water storage) (Westenbroek and others, 2010). Recharge occurs when water sources exceed all sinks and soil-water storage has reached holding capacity. The SWB model has been used to estimate spatially and temporally variable recharge for diverse regional systems across the United States, including a number of semi-arid and volcanic regions such as the glacial aquifer system east of the Rocky Mountains (Trost and others, 2018), the Williston River and Powder River Basins in Montana, Wyoming, North Dakota, and South Dakota (Aurand, 2013), the upper Chehalis River Basin in southwest Washington (Gendaszek and Welch, 2018), the Island of Maui, Hawai'i (Johnson and others, 2018), and the State of Maine (Nielsen and Westenbroek, 2019).

A SWB model (Westenbroek and others, 2010; version 1.2, October 2019) was developed for the Harney Basin study area to estimate the spatial distribution of upland recharge. The model area was divided into 1-square-kilometer (0.62-mi) grid cells consisting of 299 rows and 251 columns, and the model domain includes active grid cells that extend at least 15 miles beyond the Harney Basin to minimize boundary effects. Grid spacing was selected to balance the grid cell size of the input datasets and computational requirements. The model domain included the Harney Basin lowlands but results from this area were not used. Model input included spatially distributed and tabular datasets that are described in detail in appendix 7.

The model simulated a period of nearly 36 years (January 1981–September 2016) that included a 9-month initialization period (January 1981–September 1981), a 15-yr calibration period (water years 2001–16), and an 18-yr validation period (water years 1982–2000). A 21-month model initialization period (January 1999–September 2000) was completed prior to calibration to stabilize soil-moisture and snow-cover conditions that were initialized at 100 percent cover. An 18-year validation period (water years 1982–2000)

that excluded the model calibration period was evaluated thereafter. Mean-annual recharge was estimated during water years 1982–2016.

Calculation of water-budget components by SWB for each model cell is summarized here and described in detail by Westenbroek and others (2010). Daily precipitation, minimum air temperature, and maximum air temperature were specified for each model cell. Air temperature is used to distinguish precipitation as rainfall or snowfall and control snowmelt (Dripps and Bradbury, 2007). Rainfall and snowfall that does not reach the ground is modeled as interception. The interception process for most land-use types was disabled in the model, and interception was accounted for in the ET process as ET observations used to calibrate the model include evaporation of intercepted water (see section "Model Calibration" below). However, in the high elevations of Steens Mountain where mean-annual precipitation exceeds 20 inches, the interception process in the model was used to simulate and account for sublimation (evaporation of snow) losses that are not modeled by SWB. SWB calculates runoff using the NRCS curve number rainfall-runoff relation (Cronshey and others, 1986), and this water is assumed to travel directly to streams (that is, does not accumulate and infiltrate downslope). Potential ET for each cell was calculated using the Hargreaves-Samani method (Hargreaves and Samani, 1985). Soil-moisture accumulation and depletion were tracked with the accumulated potential water loss term (Thornwaite and Mather, 1957) and excess soil moisture became recharge when precipitation exceeded potential ET and soil moisture exceeded the maximum water-holding capacity.

Model Calibration

Upland recharge from precipitation and snowmelt was estimated by automatically calibrating the Harney Basin SWB model simulations to estimated annual runoff, ET, and base-flow estimates with Parameter ESTimation (PEST) software (Doherty, 2010) and manually adjusting parameters thereafter, and manually calibrating model simulations to measured monthly snow-water equivalent (SWE) at two SNOTEL sites. Estimates and measurements used for model calibration are hereinafter referred to as observations in the context of SWB model calibration.

Observations and Parameter Estimation

Simulated values were compared with observations of runoff, base flow, ET, and SWE to ensure that simulated water-budget components were reasonable, thereby allowing for reasonable simulated values of upland recharge for the Harney Basin. Annual runoff observations were computed as the difference between annual streamflow measurements and annual base-flow estimates (figs. 16–18). Observations of annual watershed-scale water-year runoff, base flow, and ET were compared with SWB-simulated values in the northern, southern, and western regions of the Harney Basin. Runoff and

base-flow observations from seven upland gaged watersheds were compiled during 1982–2016 (watersheds 1, 4, 6, 11, 22, and 23; fig. 11; tables 8–9). Annual ET observations were computed during 2001–16 for the same upland watersheds (and watershed 5; fig. 11; table 9) using 1-km (0.62-mi) gridded operational Simplified Surface Energy Balance (SSEBop) ET datasets (Senay and others, 2013) calibrated to site-based ET measurements made in Oregon and Idaho for similar land-cover types (app. 7; table 7.4). Monthly SWE data were compiled during water years 2011–16 for Rock Springs SNOTEL site in the Silvies River watershed and Fish Creek SNOTEL site in the Donner und Blitzen River watershed to evaluate the volume and timing of SWB-simulated snowpack and snowmelt (fig. 7.3). The snowmelt index used in this study was reduced from the Dripps and Bradbury default-value of 0.059 inches (1.5 mm) to 0.026 inches (0.65 mm) to improve model simulation of snow-water equivalent and snowmelt for the Harney Basin (see app. 7 for more information).

Supervised calibration using PEST was used to fit simulated and observed runoff and ET, and simulated recharge was compared with base-flow observations to ensure that recharge was equal to or exceeded base-flow observations so that groundwater flow from uplands to lowlands was possible. This calibration approach has been applied in SWB models in other basins (Aurand, 2013; Nielsen and others, 2019). Parameters were manually adjusted to match simulated to observed SWE time series and improve comparisons between mean-annual (1982–2016) simulated recharge and estimated natural groundwater discharge.

Weights were assigned to observations and a weighted objective function (the squared sum of residuals between model outputs and observations, each multiplied by their weight) was calculated during calibration. Generally, annual observations of runoff were weighted highest (most important to the objective function) followed by ET, and then base-flow observations, which were weighted lowest (least important to the objective function). For additional details about observation datasets, observation weights, and parameter estimation used in SWB model calibration see appendix 7 and Corson-Dosch and Garcia (2022).

Model Fit—Comparison of Simulated Values to Annual Observations

Model fit was evaluated with scatter plots of observed and simulated values and residuals (observed minus simulated values) for recharge (and base flow), runoff, and ET. Calibration to annual runoff and ET observations and base-flow comparisons were evaluated with scatter plots of simulated and measured values and summary statistics including the Nash-Sutcliffe model efficiency coefficient (NSE; Nash and Sutcliffe, 1970), absolute mean error, RMS error, mean residual error, and mean relative error. Agreement between

SWE values was evaluated with hydrographs comparing simulated and measured daily SWE and monthly runoff from associated watersheds and is discussed in appendix 7. Values are expressed as a depth of water uniformly distributed across the area of interest (for example, calibration watersheds, regions, or upland areas) or as a rate per unit area.

Automated calibration processes compared 242 weighted observations of runoff (61), ET (120), and base flow (61). The model generally matched annual observed runoff and ET estimates over the full simulation period (fig. 29) and had an NSE coefficient of 0.86. The NSE coefficient is a normalized statistic that indicates how well the plot of observed against simulated values fit the 1:1 line in a scatter plot, where a coefficient of 1 indicates perfect calibration (Nash and Sutcliffe, 1970; Nielsen and Westenbroek, 2019; Trost and others, 2018).

Annual simulated runoff compared favorably to observed estimates overall in all regions (RMS error = 1.27 in, mean relative error of 9 percent, 99 observations; figs. 30B, E; table 18), but residuals are somewhat skewed. The model tends to underestimate runoff in areas where observed runoff exceeds about 4–5 in/yr (positive residuals in fig. 30E) and overestimates runoff in areas where observed runoff is less than about 2 in/yr (negative residuals in fig. 30E). Underestimation in watersheds with large runoff might reflect SWB's simplified representation of the complex physics controlling snowpack accumulation and melt, which ultimately affects partitioning of water into the runoff part of the water budget when runoff is high (see app. 7 for more information). Overall, simulated runoff was reasonably estimated during the calibration period (mean relative error of 0 percent). During the validation period, however, simulated runoff generally was lower than observed (mean relative error of -17 percent; table 18) and mostly was attributed to southern region estimates. Differences between simulated and observed runoff during the two time periods likely result from differences in precipitation magnitude (validation period wetter than calibration period; fig. 3) and GridMET precipitation accuracy. Rainfall-runoff curve numbers calibrated to the drier calibration period likely restricted runoff and enhanced recharge runoff during the wetter validation period. Additionally, the slight underestimation of GridMET precipitation in northern and western regions, relative to measurements at higher precipitation (typically upland) sites (app. 1; fig. 1.1), was greater during calibration (4 percent) than validation periods (2 percent), and likely resulted in underestimation of runoff during calibration periods. Over the full simulation period, runoff underestimation during the calibration period was balanced by overestimation during the validation period in northern and western regions. In the southern region, runoff was underestimated over the full simulation period (mean relative error of -14 percent).
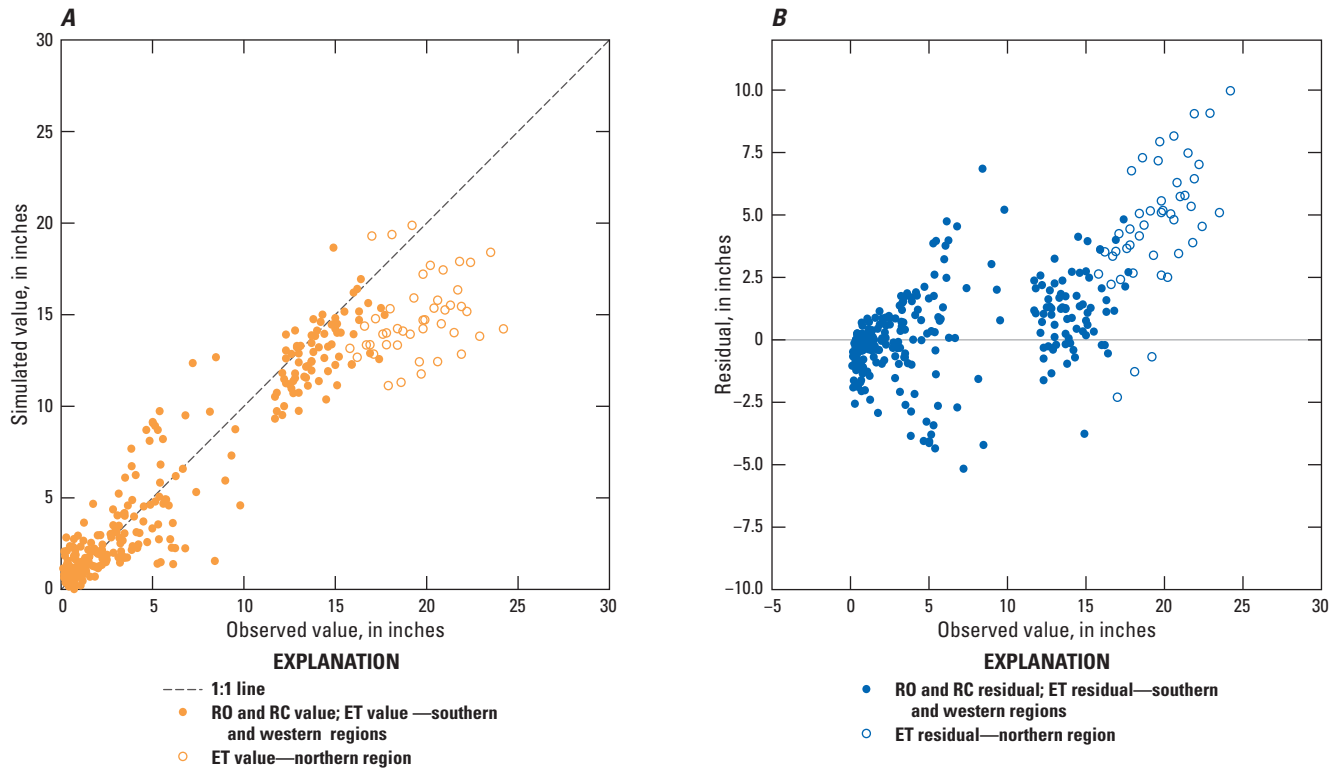
Figure 29. Scatter plots showing how well simulated values from the Soil-Water-Balance model match observed values during 2001–16, Harney Basin, southeastern Oregon. Observed and simulated values of runoff (RO) and recharge (RC) are compared by plotting (*A*) observed compared to simulated values and (*B*) residuals compared to observed values.

Table 18. Model evaluation statistics between estimated runoff, evapotranspiration, and base-flow observations and complimentary runoff, evapotranspiration, and recharge values simulated with the Harney Basin Soil-Water-Balance model for eight calibration and verification basins during calibration (2001–16) and validation periods (1982–2000).

[Regions are shown on figure 1. **Evaluation period**: The full model simulation (1982–2016), calibration, or validation period. **Abbreviation:** ET, evapotranspiration.]

Region	Data	Evaluation period	Number of observations	Absolute mean error (in/yr)	Root-mean square error (in/yr)	Mean residual error (in/yr)	Mean relative error (percent)
All	Runoff and ET	Full	219	1.92	2.78	-1.46	-15
	Baseflow/recharge	Full	98	1.38	2.04	0.38	13
	Runoff	Full	99	0.91	1.27	-0.21	-9
	Runoff	Calibration	61	0.91	1.32	0.00	0
	Runoff	Validation	38	0.90	1.17	-0.56	-17
	ET	Calibration	120	2.76	3.58	-2.48	-15
Northern	Runoff	Full	34	0.71	0.93	0.04	2
	ET	Calibration	45	4.90	5.33	-4.71	-24
	Base flow/recharge	Full	33	0.31	0.41	-0.02	-2
Southern	Runoff	Full	59	1.06	1.99	-0.38	-14
	ET	Calibration	60	1.37	1.74	-1.12	-8
	Base flow/recharge	Full	59	2.04	2.59	0.66	16
Western	Runoff	Full	6	0.54	0.65	-0.02	-2
	ET	Calibration	21	1.86	2.23	-1.23	-8
	Base flow/recharge	Full	6	0.75	0.91	-0.12	-11

In all regions the model somewhat underestimated SSEBop-ET observations, but in the northern region underestimation was more substantial as is shown by the prevalence of positive residuals (figs. 30*C*, *F*), a mean relative error of -24 percent, and an RMS error of 5.3 in. (table 18). Simulated ET in southern and western regions was closest to observed values (mean relative error of -8 percent and RMSE = 1.74 and 2.23 in., respectively). Although northern and western regions share some similar ET characteristics and land cover (evergreen forest, western juniper, and low sagebrush, app. 7; fig. 7.1), the northern region uplands contain sizable grassland and shrubland areas that might not have been adequately characterized by ET observations.

Simulated recharge generally exceeded observed upland base flow (fig. 30*A*), meaning a portion of the upland recharge remains in the ground and is available to recharge the basin fill underlying the Harney Basin lowlands. Base-flow observations were minimally weighted during calibration and were primarily included for comparison with simulated values. Simulated recharge consistently exceeded observed base flow at two of the three southern region calibration watersheds but was underestimated by about half (3 in/yr) at the Bridge Creek near Frenchglen watershed. The ratio of estimated base-flow contributions to total flow (0.88) at Bridge Creek greatly exceeded the estimates at the Donner und Blitzen River near Frenchglen (0.51) (fig. 11; table 9). Differences in base-flow proportions among the southern region calibration watersheds highlight variability in hydraulic properties within similar mapped hydrostratigraphic units in the southern region that were not simulated by SWB. Despite differences in simulated recharge among watersheds in the southern region, the general trend of greater simulated recharge than estimated base flow in upland watersheds indicates that groundwater recharged in the uplands flows through the subsurface into the basin fill beneath the Harney Basin lowlands. However, underestimation of runoff and ET in southern region watersheds likely indicates recharge volume is overestimated.

Differences between simulated recharge and estimated base-flow observations were lower in northern and western regions than in the southern region. In the northern region simulated recharge generally matched high and low base-flow observations in the Silvies River near Burns calibration watershed (RMS error = 0.41, mean relative error = -2 percent; table 18). In the western region, high base-flow observations in the Silver Creek below Nicoll Creek near Riley calibration watershed were underestimated and low base-flow observations were overestimated. Over the six calibration years, observed values exceeded simulated values by a mean of 11 percent (RMS error = 0.91, mean relative error = -11 percent) and error was biased toward higher flows, but during the full simulation period simulated recharge exceeded base flow by 24 percent. Comparable estimates of recharge and base flow in the Silvies River near Burns calibration watershed in the northern region indicates that most if not all upland

recharge that occurs in this watershed is discharged as base flow in upland areas and little if any upland recharge within this watershed discharges as subsurface flow to downgradient basin fill. In the western region, some discharge to basin fill occurs, but the proportion of total recharge is smaller than in the southern region.

Results for Groundwater Recharge from Infiltration of Precipitation and Snowmelt

Mean annual upland groundwater recharge simulated with the SWB model during 1982–2016 is 288,000 acre-ft and represents about 8 percent of the approximately 3.4 million acre-ft of mean annual precipitation in the uplands (table 19). Simulated recharge from precipitation through soils was limited to upland areas only because lowland areas predominantly are groundwater discharge areas. Expressed as a depth of water uniformly distributed across upland areas, mean annual recharge is about 1.3 inches. Of the remaining mean annual precipitation that falls in the Harney Basin uplands, 79 percent (2.7 million acre-ft) returns to the atmosphere through ET, about 9 percent (about 290,000 acre-ft) runs off as overland flow to streams, and about 4 percent (127,000 acre-ft) is lost during winter to snow sublimation (unaccounted for in simulated ET losses), or is blown out of the Harney Basin (table 19).

Annual mean upland recharge rates varied with annual precipitation and ranged from less than 1 in/yr to 4 in/yr (fig. 31). Recharge was highest during years with large amounts of precipitation and snowmelt (1982–84, 1995–98) and lowest during years with small amounts of precipitation and snowmelt (1987– 94, 2012–16). Simulated recharge and runoff were similar in magnitude and temporal response to precipitation variability during most years (fig. 31).

Spatially, the 1982–2016 mean-annual recharge rate ranged from less than 1 in/yr to nearly 25 in/yr across a broad range of coupled climate, land-cover, and soil conditions (fig. 32). The lowest rates were simulated at low elevations where precipitation is lowest, vegetation is comprised primarily of low sagebrush, big sagebrush, and western juniper, and soils are mapped as low-permeability hydrologic soil group D (figs. 32, 7.1). Low recharge rates of less than 1 in/yr also were simulated at high elevations in northern and western regions where most precipitation is consumed by evaporation and sublimation from the forest canopy (interception), ET from trees and shrubs in the evergreen forests, or in precipitation-limited upland areas. The highest recharge rates were simulated in the southern region near the crest of Steens Mountain where annual precipitation commonly exceeds 40 in/yr (fig. 2) and soils are most permeable (hydrologic soil groups B and C) and in northern and western regions at higher elevations composed of western juniper and more permeable hydrologic soil group C soils.

Table 19.   Simulated mean annual water-budget components by region from the Harney Basin Soil-Water-Balance model, southeastern Oregon.

[**Upland recharge area by region**: Model areas between the Harney Basin boundary and the Harney Basin lowlands shown on figure 1. **Percentage within calibration watersheds**: Represents the percentage of watershed surface area to upland recharge area. Only calibration watersheds with both ET and streamflow observations included in reported percentage. Mean annual estimates in acre-feet per year by region. **Abbreviations**: ET, evapotranspiration; —, not applicable]

Upland recharge area by region	Percentage within calibration watersheds	Component	Quantity		Fraction of precipitation
			Inches	Acre-feet	
Northern[1]	64	Precipitation	17	1,254,150	—
		Runoff	1.5	111,920	0.09
		ET[1]	14	1,055,290	0.84
		Recharge	**1.1**	**85,803**	**0.07**
Southern	22	Precipitation	19	965,001	—
		Sublimation/wind[2] losses	2.5	127,010	0.13
		Runoff	1.5	77,343	0.08
		ET	12	600,649	0.62
		Recharge	**3.1**	**157,095**	**0.16**
Western	13	Precipitation	12	1,188,150	—
		Runoff	1.1	104,280	0.09
		ET	11	1,036,550	0.87
		Recharge	**0.5**	**44,648**	**0.04**
All regions	33	Precipitation	15	3,407,301	—
		Sublimation/wind losses	1	127,010	0.04
		Runoff	1	293,543	0.09
		ET	12	2,692,489	0.79
		Recharge	**1.3**	**287,545**	**0.08**

[1]Runoff and potential recharge likely overestimated owing to underestimation of ET as indicated by mean relative error between simulated and observed ET (table 18).

[2]Component included because simulated ET in alpine areas of the southern region does not adequately account for sublimation\wind losses owing to a lack of alpine ET observations used for calibration. ET observations in northern and western regions were assumed to account for sublimation losses (see app. 7 for more information).
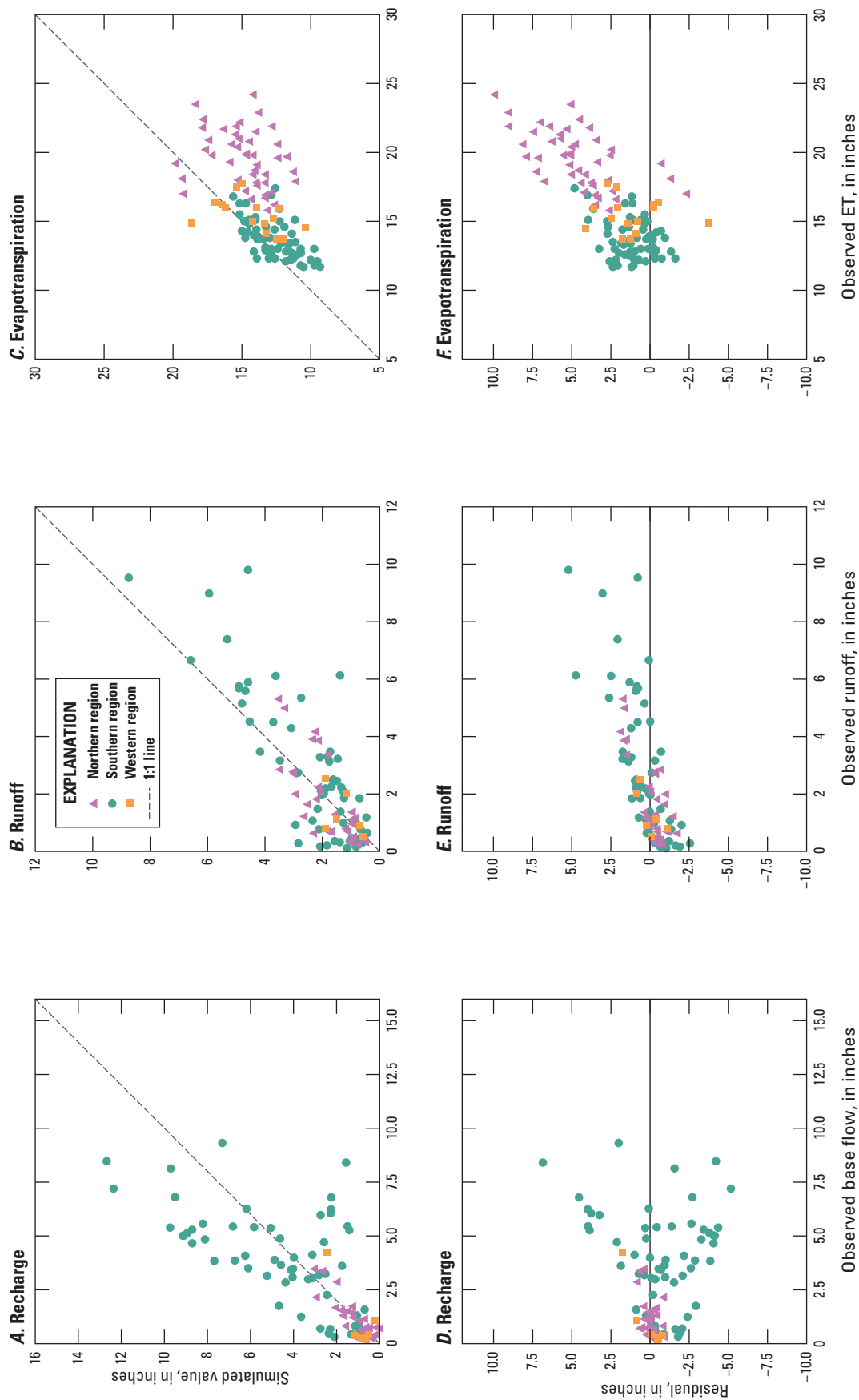
Figure 30. Scatter plots showing how well simulated values from the Soil-Water-Balance model match observed values during 2001–16, Harney Basin, southeastern Oregon. Values are compared by plotting (*A*) observed base flow and simulated recharge, (*B*) observed and simulated runoff, and (*C*) observed and simulated evapotranspiration (ET) for eight watersheds during the calibration period (2001–16), and plots of residuals compared to observed (*D*) base flow, (*E*) runoff, and (*F*) evapotranspiration (ET). Values are distinguished by region to highlight regional model performance in simulating observed values for each component.
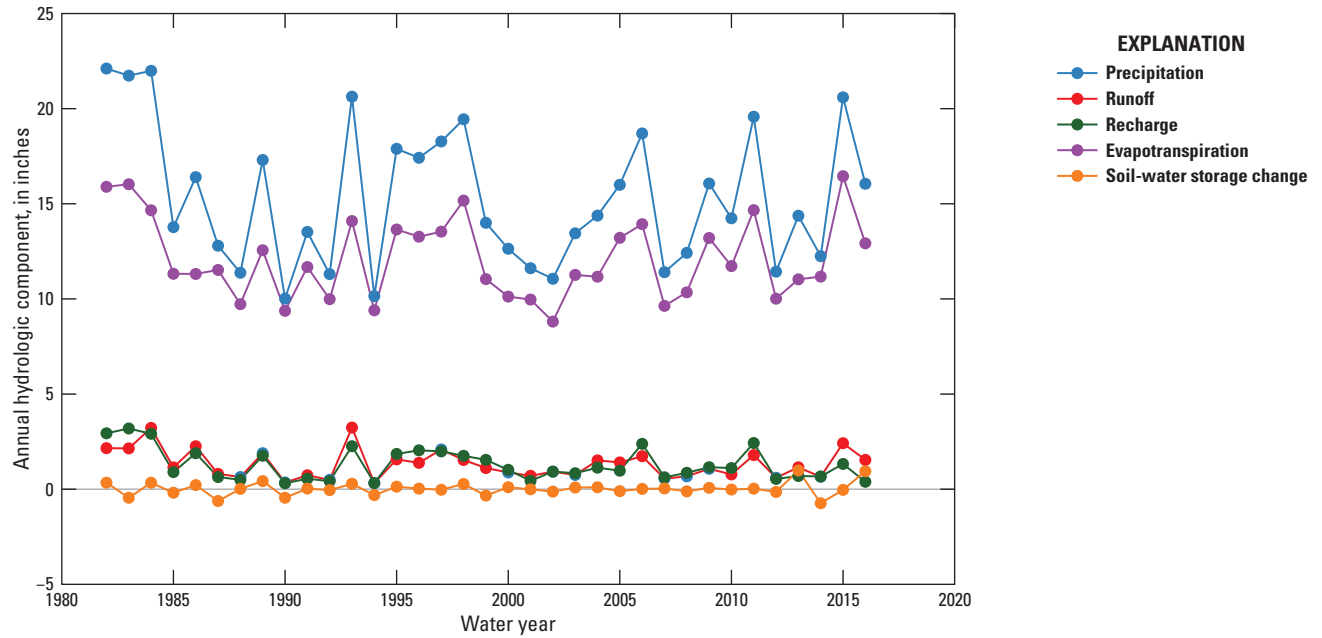
Figure 31. Annual precipitation from GridMET and groundwater recharge from infiltration of precipitation and snowmelt, evapotranspiration, runoff, and soil-water storage change simulated with the Harney Basin Soil-Water-Balance (SWB) model, 1982–2016
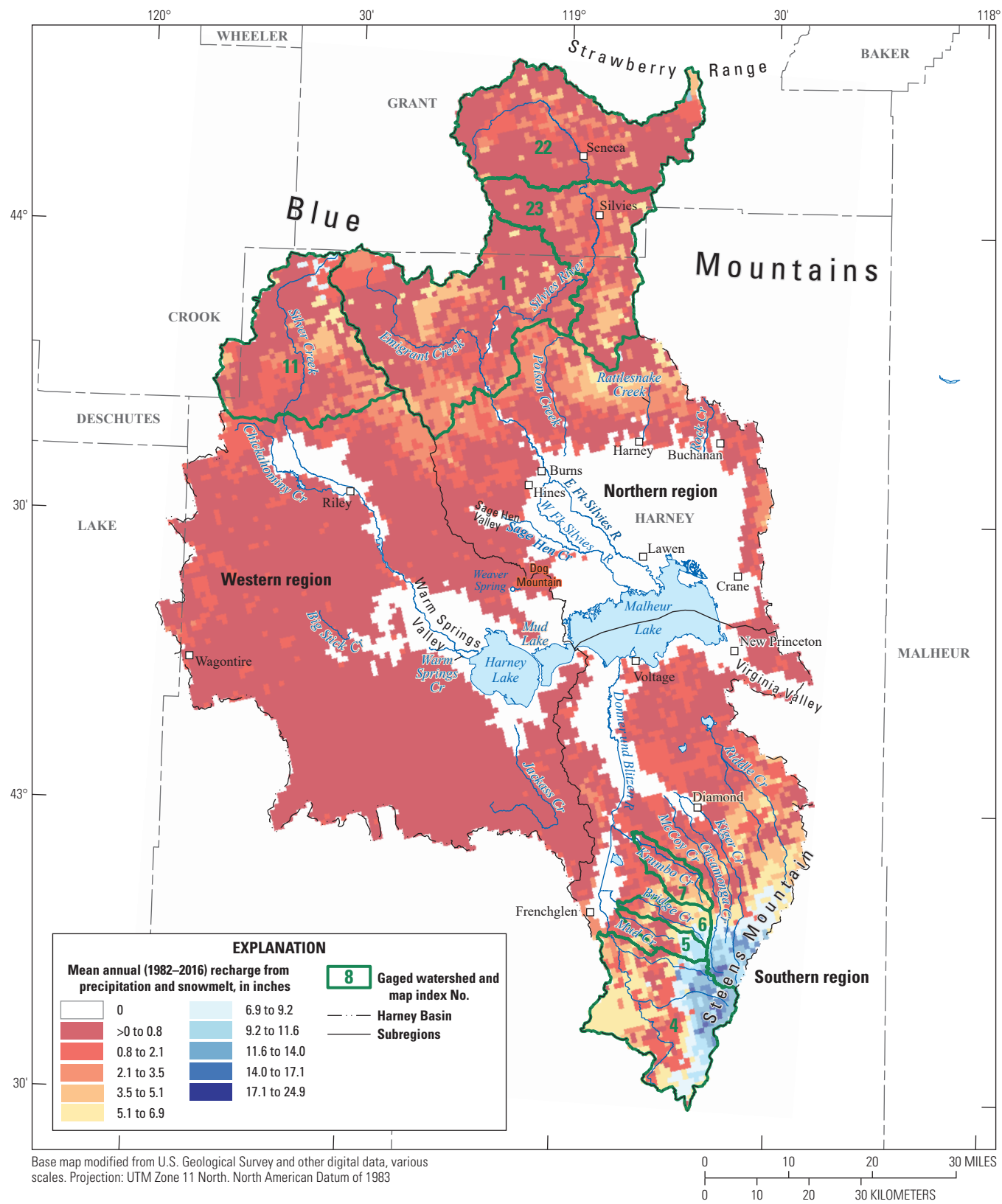
Figure 32. Distribution of mean annual groundwater recharge from infiltration of precipitation and snowmelt, 1982–2016, simulated with the Harney Basin Soil-Water-Balance model.

The calibrated SWB model demonstrated changes in annual recharge through time in the northern, southern, and western regions of the Harney Basin that resulted from precipitation variability (fig. 33). Annual recharge rates in all three regions generally decreased from the early 1980s to early 1990s corresponding to declining precipitation rates. During the early 1980s, annual precipitation was well above mean annual rates over the previous century, especially in the northern region where precipitation was nearly 100 percent above the 116-yr mean (figs. 2, 3). Precipitation in the mid-to-late 1990s also was well above the long-term mean, resulting in another multi-year period of elevated recharge in all regions (figs. 3, 33). During the late 1990s until 2016, recharge has corresponded with precipitation patterns with little to no trend.

The mean annual recharge during 1982–2016 was about 45,000 acre-ft in the western region, 86,000 acre-ft in the northern region, and 157,000 acre-ft in the southern region (table 19). The mean recharge as a fraction of precipitation in the southern region (0.16) was more than twice the fraction in the northern region (0.07) and four times the fraction in the western region (0.04; fig. 34; table 19). The proportion of precipitation converted to ET, runoff, and recharge was similar in the northern and western regions owing to similar land cover and hydrologic soil groups, with most precipitation consumed by ET (mean fraction of 0.86) and similar proportions of precipitation converted to recharge and runoff (fig. 31; table 19). In the southern region, the recharge fraction was twice the runoff fraction and the proportion of precipitation converted to ET was 20 percent below estimates in the northern and western regions.

Mean annual recharge estimates within calibration watersheds are the most reliable and cover about 60 percent of the upland recharge area. Based on mean relative errors between simulated and observed ET and runoff, estimate uncertainty within calibration watersheds is likely within 20 percent (table 18). Estimates outside the calibration watersheds and where land cover is underrepresented in observation datasets (app. 7; fig. 32; table 7.1) are less reliable. The data release (Corson-Dosch and Garcia, 2022) contains all files necessary to run the Harney Basin Soil-Water-Balance (SWB) model described in this report. The model archive also contains model outputs, including the 1982–2016 water-year recharge grids, the mean annual recharge grid, and Python post-processing scripts used to develop water year grids and extract data to compare with observations.
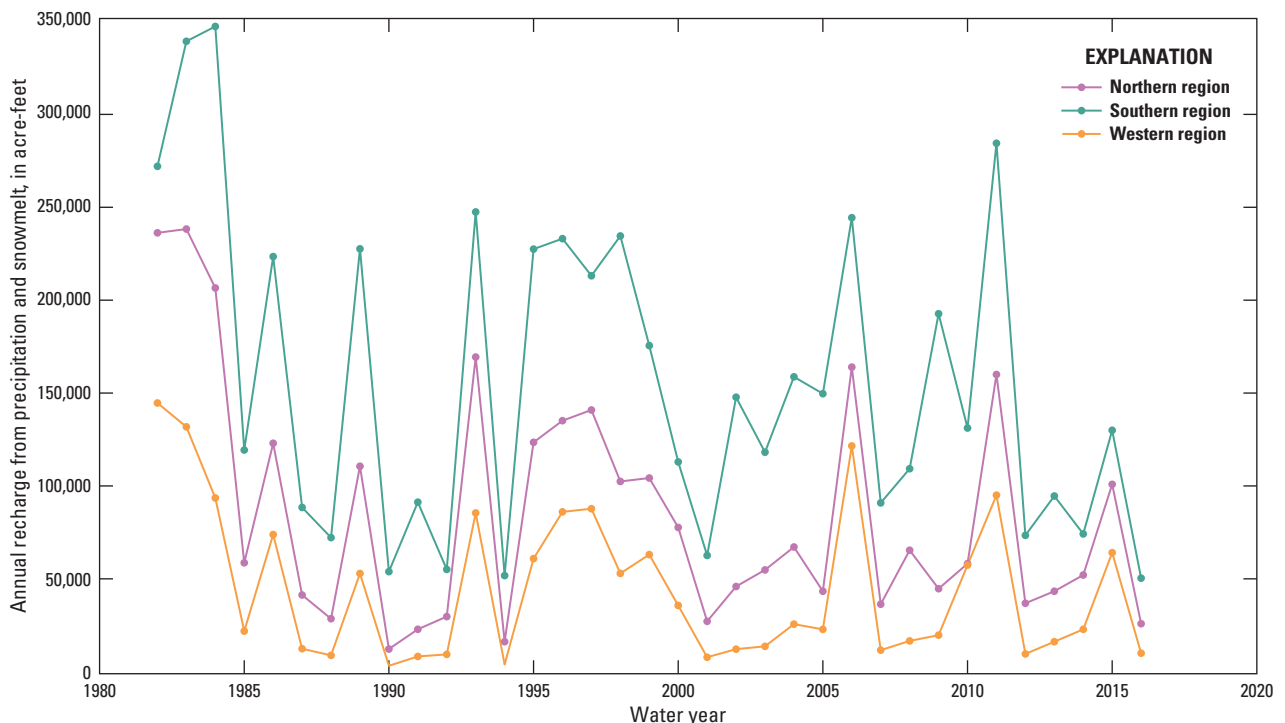
Figure 33. Annual regional groundwater recharge from infiltration of precipitation and snowmelt simulated with the Harney Basin Soil-Water-Balance model, 1982–2016.
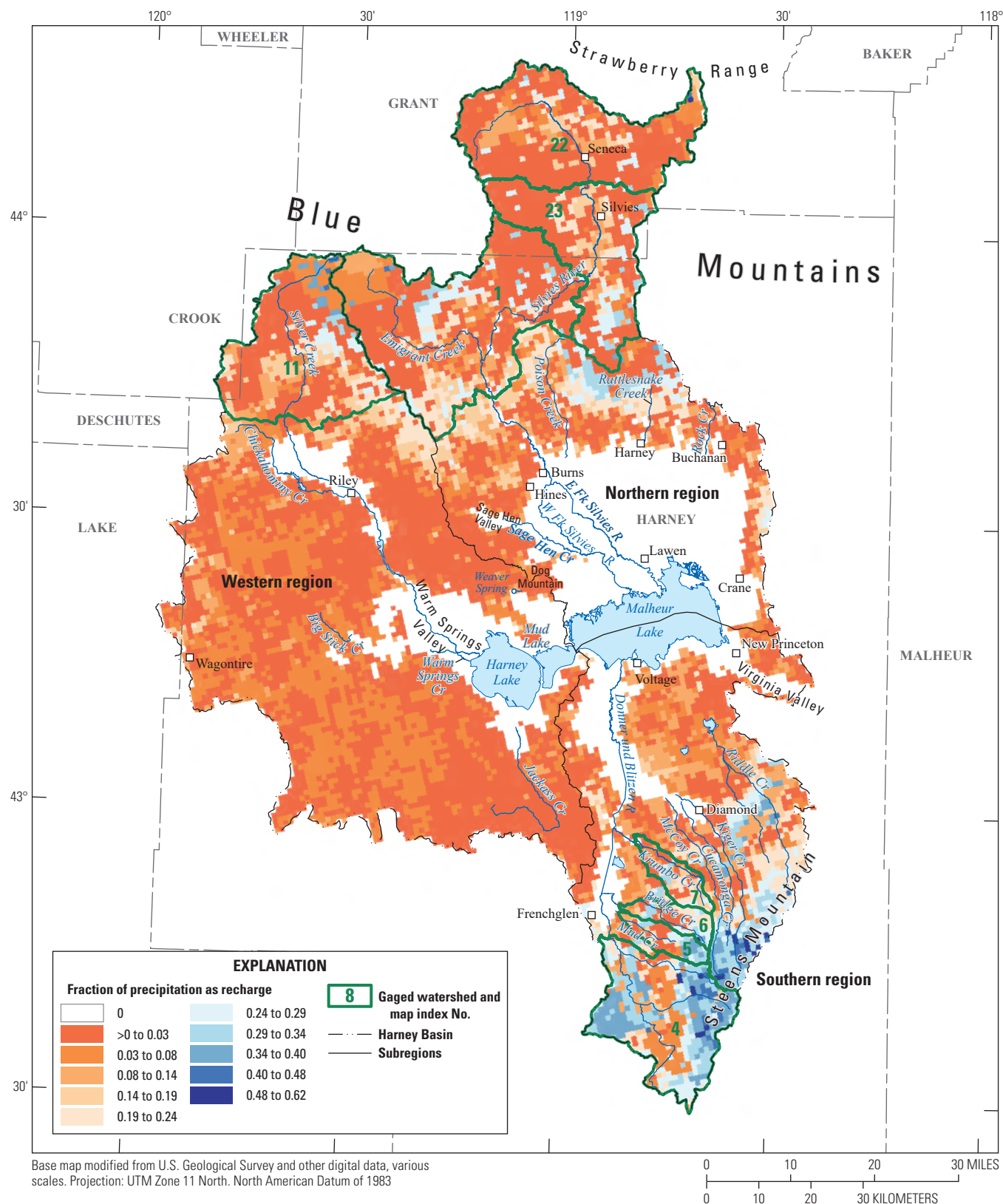
Figure 34.   Distribution of mean annual groundwater recharge from infiltration of precipitation and snowmelt, as a fraction of mean annual precipitation, simulated with the Harney Basin Soil-Water-Balance model.

Groundwater Recharge as Groundwater Inflow from Uplands to Lowlands

During 1982–2016, lowland recharge by groundwater inflow from uplands totaled about 48,000 acre-ft/yr and was estimated by subtracting upland base flow and spring discharge from upland recharge estimates. Groundwater inflow from uplands was 9,000 acre-ft/yr in the northern region, 20,000 acre-ft/yr in the southern region, and 20,000 acre-ft/yr in the western region (see section "Summary of Groundwater Recharge" for more information).

Groundwater Recharge from Streams and Floodwater

The major streams draining the uplands and conveying surface water across the Harney Basin lowlands include the Silvies River, Donner und Blitzen River, and Silver Creek. Seepage measurements made during this study on the Silvies River, Poison Creek, Rattlesnake Creek, and Silver Creek during late summer and early autumn low-flow periods provided evidence of groundwater recharge through channel losses in the Harney Basin lowlands (app. 6). Although measured during late summer to ensure base-flow conditions, the within-channel losses persist year-round from these streams. In addition to in-channel losses, during the springtime and early summer in many years these streams flood well beyond their meandering channels, filling topographic lows and creating ephemeral ponds and wetlands of varying sizes across the Harney Basin lowlands. In the months following springtime runoff, most floodwater is consumed by ET but a small portion percolates downward and recharges the groundwater system. Recharge from streams and floodwater also occurs along narrow stream corridors in upland valleys such as the Silvies Valley between the Silvies River at Silvies and Silvies River at Seneca streamgages, but this recharge is localized and is either consumed by ET or returns to the gaining stream during the same year. The net recharge from streams and floodwater in upland areas, if any, is accounted for in recharge estimates from infiltration of precipitation and snowmelt because the SWB model is calibrated to total ET (from precipitation, groundwater, and floodwater) and total runoff and base flow in all upland areas. Therefore, localized upland recharge from streams and floodwater was not considered further in this study.

Recharge from streams and floodwater was calculated in lowland areas as the difference between surface-water inflow to the Harney Basin lowlands and surface-water outflow

from the Harney Basin lowlands (eq. 16). Recharge estimates computed with equation 16 represent recharge from streams, natural floodwater, and surface-water irrigated areas:

$$Q_{sw}^{in} = SW_{sf}^{in} + SW_{sp}^{in} - SW_{sf}^{out} - ET_{fl}^{out} - E_{fl}^{out} - ET_{swirr}^{out} - E_{pond}^{out} \quad (16)$$

where

Q_{sw}^{in} is recharge from infiltration from streams and floodwater,

SW_{sf}^{in} is streamflow from the uplands entering the Harney Basin lowlands,

SW_{sp}^{in} is discharge from springs at the upland-lowland margins that is unaccounted for in streamflow estimates (SW_{sf}^{in}),

SW_{sf}^{out} is streamflow to Malheur and Harney Lakes,

ET_{fl}^{out} is ET of seasonal floodwater in non-irrigated areas,

E_{fl}^{out}. is open-water evaporation of seasonal and episodic floodwater in non-irrigated areas,

ET_{swirr}^{out} is ET of surface-water irrigation, and

E_{pond}^{out} is open-water evaporation from ephemeral ponds and reservoirs (excludes Malheur and Harney Lakes).

Surface-water inflow to the Harney Basin lowlands is comprised of gaged or estimated streamflow from upland areas and discharge from springs at the upland-lowld boundary that merge with a stream channel downstream of the gaged location or are diverted for irrigation. Surface-water outflow from the Harney Basin lowlands is comprised of streamflow to Malheur and Harney Lakes where it mostly evaporates, ET of surface water from annual flooding in non-irrigated areas, evaporation of seasonal and episodic floodwater in non-irrigated areas, ET from surface-water irrigated areas, and evaporation from ephemeral ponds and reservoirs filled by surface water (excluding Malheur and Harney Lakes).

Streamflow and Springflow

Mean water-year (1982–2016) streamflow estimates within the Harney Basin are a composite of measured and extended values for gaged watersheds and estimated values for ungaged watersheds (table 4.3). Descriptions of record-extension and streamflow-estimation procedures are provided in appendix 4. Springflow at the upland-lowland margin, unaccounted for in streamflow estimates, is based on published data and measurements made in this study.

Regional streamflow and springflow draining from upland onto lowland areas was about 54,000 acre-ft/yr (75 ft³/s) in the western region, 173,000 acre-ft/yr (239 ft³/s) in the northern region, and 204,000 acre-ft/yr (282 ft³/s) in the southern region (table 20). Measured and extended streamflow from gaged watersheds near the lowland boundary is assumed to fully reach lowland areas. For ungaged watersheds where streamflow is often ephemeral, only half of the estimated streamflow was assumed to reach the lowlands and half was assumed consumed by ET in upland areas. Streamflow from Virginia Creek and Chickahominy Creek watersheds (ungaged) in the western region and from all other upland areas without delineated watersheds (table 4.3) was assumed to reach the lowlands episodically during wet years (about once every 6 years during the 35-year record); during average-to-dry years upland streamflow in these areas was assumed fully consumed by ET before reaching the lowlands because stream channels connecting upland and lowland areas were generally poorly defined. Episodic flow from these areas is supported by episodic flooding that inundates much of the Harney Basin lowlands based on satellite imagery (fig. 9B; see section "Open-water Evaporation of Floodwater from Non-Irrigated Areas"). Episodic streamflow for Virginia Creek and Chickahominy Creek watersheds, and all other upland areas (without delineated watersheds, table 4.3), was estimated as the product of mean annual streamflow during the study (table 4.2) and a 6-year recurrence interval (0.17).

Mean streamflow into Malheur Lake estimated from short-term streamgages ranged from a combined flow of about 23,000 acre-ft/yr (32 ft³/s; table 20) from the East and West Fork Silvies Rivers draining the northern region to 90,000 acre-ft/yr (124 ft³/s) from the Donner und Blitzen River near Voltage draining the southern region. Estimates from the East and West Fork Silvies Rivers during 1982–2016 are based on extended record from the 1970s whereas the estimates for the Donner und Blitzen River near Voltage during 1982–2016 are a composite of measured and extended records.

Malheur and Harney Lakes receive periodic flow from two channels that have no gaging records near the lakes: Silver Creek and Ninemile Slough through Malheur Slough. Evaluation of satellite imagery through Google Earth Engine time lapse (Gorelick and others, 2017) indicates Silver Creek likely reached Harney Lake 30 percent of the years during 1984–2016 and flow from Ninemile Slough through Malheur Slough likely reached Malheur Lake in 1984, 2006, and 2011 (9 percent of the years). For comparison, time-lapse imagery indicates the Silvies River likely discharged into Malheur Lake perennially about 70 percent of the years during 1984–2016. Estimates of discharge to Malheur and Harney

Lakes from these ungaged channels were based on the estimated mean annual fraction of streamflow at the Silvies River near Burns that reached Malheur Lake through the East and West Fork Silvies Rivers (0.16) and the frequency with which those channels flow into the lakes based on the time-lapse imagery (eq. 17):

$$Q_{est}^i \ = \ 0.16 \times Q_{mf}^i \times \frac{p_i}{70} \qquad (17)$$

where

i	is Silver Creek or Ninemile/Malheur Slough,
Q_{est}^i	is estimated discharge into the terminal lake by channel i,
Q_{mf}^i	is discharge onto the Harney Basin lowlands contributing to channel i, and
p_i	is percent of the period of record that channel i discharges to its terminal lake.

Using equation 17, the mean discharge from Silver Creek into Harney Lake was about 3,900 acre-ft/yr (5.4 ft³/s; table 20), and the mean discharge from Ninemile Slough into Malheur Lake (through Malheur Slough) was about 400 acre-ft/yr (0.6 ft³/s; table 20).

Evapotranspiration of Seasonal Floodwater from Non-Irrigated Areas

The spatial extent of seasonal surface-water flooding and depth of inundation on the Harney Valley lowlands varies considerably from year to year and within a season depending on winter precipitation volume and timing of snowmelt. Seasonally flooded areas of the Harney Basin lowlands include wet meadows, stream-channel riparian areas, marshes, and ephemeral ponds formed by floodwater in topographic lows (and distant from springs; fig. 7). Estimates of ET for seasonally flooded areas, ET_{fl}^{out}, were determined using the physics-based and empirical approaches and aggregated by ET unit (table 6) for areas upstream of gaged outflow locations in northern and southern regions (fig. 35) and for all seasonally flooded areas in the western region. Seasonally flooded areas downstream of gaged outflow locations in the northern and western regions were likely flooded by lake water that was accounted for in stream outflow estimates (table 20). Mean ET_{fl}^{out} totaled about 13,000 acre-ft/yr (table 6) and varied from about 1,800 acre-ft/yr in the western region to 3,600 acre-ft/yr in the southern region and 8,100 acre-ft/yr in the northern region.

Table 20. Mean annual surface-water inflow and outflow and estimated recharge from infiltration of streamflow and floodwater in northern, southern, and western regions of the Harney Basin lowlands, southeastern Oregon, 1982–2016.

[Regions are shown on figure 1. Mean annual streamflow estimates for individual streams are from table 4.3. **Abbreviations**: Ck, creek; ET, evapotranspiration; Lk, lake; nr, near; R., river; Sl, slough; Sp, spring; Spgs, springs; —, not applicable]

Type	Component	Northern region Component description	Northern region Mean annual discharge (acre-feet)	Southern region Component description	Southern region Mean annual discharge (acre-feet)	Western region Component description	Western region Mean annual discharge (acre-feet)
Inflow	Measured and estimated streamflow (gaged watersheds)	Silvies R. nr Burns, Rock Ck, Rattlesnake Ck	146,400	Donner und Blitzen R. nr Frenchglen, Bridge Ck, Mud Ck, Krumbo Ck[10], Kiger Ck, McCoy Ck	175,100	Silver Ck blw Nicoll Ck	47,600
	Estimated streamflow (ungaged watersheds)[1]	Sagehen Ck, Poison Ck, Soldier Ck, Malheur Sl, Hot Spgs Sl	22,300	Cucamonga Ck, Riddle Ck	14,100	Miller Canyon	2,780
	Estimated streamflow (other upland areas)[2]	—	2,180	—	2,260	Chickahominy Ck, Virginia Ck, other upland areas	3,510
	Springs[3]	Cow Ck Sp, Mill Pond Sp, SPRG0018724-25, Roadland Sp	2,010	Fivemile Sp, Knox Sp, Page Sp, Warm Sp nr Frenchglen, SPRG0018754	12,200	—	—
	Total		**172,900**		**203,660**		**53,900**
Outflow	Measured and estimated streamflow (gaged watersheds)	East and West Forks Silvies R.	22,700	Donner und Blitzen R. nr. Sodhouse	89,900	—	—
	Estimated streamflow (ungaged watersheds)	Ninemile Sl (through Malheur Sl)	400	—	—	Silver Ck at Harney Lk	3,900
	Surface-water ET[4]	Irrigated areas[5]	71,700	Irrigated areas[5]	77,900	Irrigated areas[5]	21,400
		Naturally flooded areas[6]	8,060	Naturally flooded areas[6]	3,630	Naturally flooded areas[6]	1,780
		Open-water evaporation of floodwater[7]	6,340	Open-water evaporation of floodwater[7]	[9]1,990	Open-water evaporation of floodwater[7]	1,230
		Ponds and reservoirs[8]	--	Ponds and reservoirs[8]	3,390	Ponds and reservoirs[8]	600
	Total		**109,200**		**176,800**		**28,900**
Inflow - Outflow	**Recharge**		**63,700**		**[11]126,900**		**25,000**

[1]Half of estimated streamflow is assumed to reach lowland areas and half is assumed lost to ET in upland areas.

[2]Episodic streamflow estimated as the product of mean annual streamflow and a 6-year recurrence interval.

[3]Springs merge with downgradient stream channels or flow directly to flood-irrigated fields.

[4]Surface-water ET is total ET minus precipitation, where surface water and precipitation are the only water sources.

[5]Irrigated areas include those irrigated with surface water and with both surface water and groundwater, where half of the ET from areas irrigated with both sources was assumed to be from surface water. Open water evaporation is included in estimates.

[6]Naturally flooded areas include those flooded by streamflow. Areas exclude those flooded with lake water (downstream of gaged outflow locations) and irrigated areas.

[7]Estimated using a rate of 0.36 ft/yr (April/May fraction of annual open water evaporation based on 1959–2005 pan evaporation at the Voltage 2 NW Sod House station; table 1), the maximum floodwater extent during 2011 (fig. 9), and a recurrence interval of 6 years. Excludes irrigated areas and flooded areas downstream of outflow locations.

[8]Pond and reservoir ET: Estimated as the product of cumulative surface area and a net evaporation rate of 3.08 feet per year.

[9]Floodwater extent likely confounded by vegetation.

[10]Contribution of flow from Krumbo Creek represents that which enters the valley lowlands downstream of the reservoir.

[11]Recharge from channel losses in southern region is assumed balanced by base flow between Frenchglen and Diamond Lane (fig. 1).
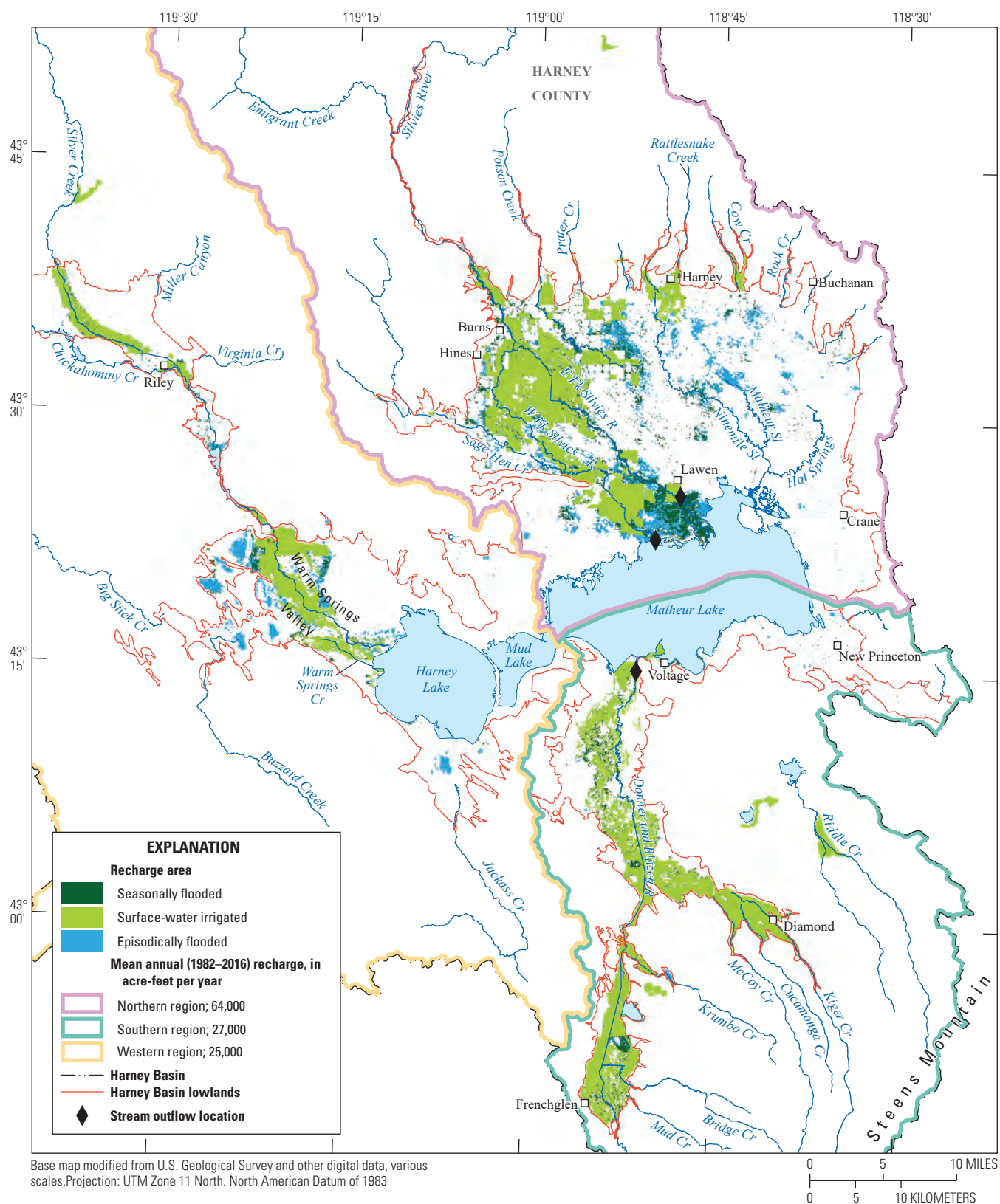
Figure 35. Locations of groundwater recharge from streams, seasonal and episodic floodwater, and surface-water irrigation, Harney Basin, southeastern Oregon.

Open-Water Evaporation of Floodwater from Non-Irrigated Areas

Standing floodwater during springtime snowmelt accumulates seasonally in wet meadow, marsh, and riparian areas (fig. 7). Floodwater also accumulates episodically (roughly once every 6 years) across a larger extent of the Harney Basin lowlands as evidenced in satellite imagery (fig. 9B). Although episodic floodwater can remain on the landscape from a few days to longer than 2 months, floodwater was assumed to remain on the land surface as standing water and evaporate for an average period of 1-month during April or May before being fully evaporated or infiltrated. The volume of standing floodwater consumed through evaporation was estimated by multiplying an open-water evaporation rate of 0.36 ft/mo by seasonally flooded areas on an annual basis, and by episodically flooded areas (maximum floodwater extent during 2011; fig. 9B) at a recurrence interval of once every 6 years (which translates to a mean evaporation rate of 0.06 ft/yr during 1982–2016 for episodically flooded areas). The evaporation rate of 0.36 ft/mo was estimated as the product of annual open-water evaporation (3.08 ft/yr or 37 in/yr; Hostetler and Bartlein, 1990; see subsection "Groundwater Evapotranspiration Rates for Open Water and Bare Soil-Playa Evapotranspiration Units" for discussion about this rate) and the ratio of monthly pan evaporation during April–May to annual pan evaporation at the Voltage 2 NW Sod House evaporation station (1959–2005; table 1; Western Regional Climate Center, 2020). Mean E_{fl}^{out} totaled about 6,300 acre-ft/yr in the northern region, 2,000 acre-ft/yr in the southern region, and 1,200 acre-ft/yr in the western region (table 20).

Evapotranspiration of Surface-Water Irrigation

Surface-water irrigated fields include those irrigated exclusively with surface water and those irrigated with surface water and groundwater. Refer to the "Irrigation Pumpage" subsection of the "Groundwater Discharge" section for additional details on fields irrigated with surface water and groundwater. Annual estimates of ET_{swirr}^{out} are available for 13 years (fig. 24); values for the remaining 23 years during 1982–2016 were estimated from the relation between 13 years of ET_{irr}^{out} and observed streamflow at the Silvies and Donner und Blitzen Rivers.

Annual volumetric estimates of ET_{swirr}^{out} in northern and western regions are highly correlated with annual streamflow at the Silvies River near Burns streamgage (Pearson's r of 0.91 and 0.82, respectively; table 21). Ordinary least-squares regression was used to relate ET_{swirr}^{out} estimates and annual streamflow in northern and western regions and extrapolate ET_{swirr}^{out} for years without data during 1982–2016. Mean (1982–2016) ET_{swirr}^{out} estimates of about 72,000 acre-ft/yr in the northern region and 21,000 acre-ft/yr in the western region

(table 20) were used in equation 16 to compute recharge from surface water. In the southern region of the Harney Basin, however, ET_{swirr}^{out} is poorly correlated with annual discharge at the Donner und Blitzen River near Frenchglen (Pearson's r of 0.13) and interannual variability in streamflow has little effect on annual ET. Therefore, mean METRIC ET_{swirr}^{out} over the 11 years evaluated (78,000 acre-ft/yr) was assumed representative of 1982–2016 conditions and used in equation 17.

Correlations between regional ET from surface-water irrigated areas and streamflow provide insight into water sources contributing to ET. Strong positive correlations in northern and western regions indicate that ET is predominantly supported by the annual surface-water supply and reliance on residual water sources such as antecedent soil moisture from previous years or shallow groundwater is minimal. ET reliance on same-year surface-water availability indicates that excess irrigation water during wet years does not replenish the root-zone soil-water reservoir for use in subsequent years; rather, it either (1) flows through surface runoff and is consumed downgradient by ET during the same year or (2) percolates downward below the root zone within the same year and eventually recharges the shallow water table. The fate of irrigation that ultimately recharges the water table is either to return to the stream as base flow where the field is adjacent to a gaining stream reach or continue along the regional groundwater flow path if the stream reach is losing or if the irrigated field is distant from the stream. The poor correlation between ET and streamflow in the southern region likely indicates that during dry years, plants utilize either antecedent soil moisture that is replenished during wetter years or shallow groundwater, which might be recharged during wet years.

Evapotranspiration from Ponds and Reservoirs

Mean annual volumetric evaporation loss from ephemeral surface-water ponds and reservoirs (ET_{pond}^{out}) was estimated as the product of open-water area and an open-water evaporation rate of 3.08 ft/yr (see subsection "Groundwater Evapotranspiration Rates for Open Water and Bare Soil-Playa Evapotranspiration Units" for details about this rate). Only ephemeral ponds and reservoirs beyond surface-water flooded, irrigated, or spring-fed areas were included in the analysis and open-water extents. Ponds and reservoirs in the southern region include open water distinguished in the GETA (table 6) but excluding Malheur Lake, and a few open-water bodies east of the lowland boundary (fig. 35). The extent of ephemeral reservoirs in the western region was limited to the average extent of Moon Reservoir. Pond and reservoir permanence were determined from Google Earth Engine time-lapse imagery during 1984–2016 (Gorelick and others, 2017). Estimated ET_{pond}^{out} was 600 acre-ft/yr in the western region and 3,400 acre-ft/yr in the southern region. Ephemeral ponds or reservoirs were not observed in the northern region.

Table 21.   Variables describing relations between annual METRIC evapotranspiration from surface-water irrigated areas and the logarithm of annual streamflow, Harney Basin, southeastern Oregon.

[Regions are shown on figure 1. **Regression statistics**: Based on annual ET in acre-feet per year and the logarithm of annual mean water-year streamflow in cubic feet per second. **Abbreviations**: ET, evapotranspiration —, not estimated]

Site name	Region	Regression statistics			
		Pearson's r	Slope	Intercept	Coefficient of determination
Silvies River near Burns, OR	Northern	0.91	54,087	-44,914	0.83
Silvies River near Burns, OR	Western	0.82	14,069	2,410	0.68
Donner und Blitzen River near Frenchglen, OR	Southern	0.13	—	—	—

Results for Groundwater Recharge from Streams and Floodwater

The mean annual recharge from infiltration of surface water in the Harney Basin lowlands during 1982–2016 totaled 116,000 acre-ft. Most recharge from surface water occurred in the northern region (64,000 acre-ft/yr) with lesser amounts in the southern region (27,000 acre-ft/yr) and western region (25,000 acre-ft/yr) (table 20). Recharge from surface water is about 27 percent of total surface-water inflow to the Harney Basin lowlands but varies spatially by region. Recharge from surface water is 37 percent of surface-water inflow in the northern region, 13 percent of inflow in the southern region, and 46 percent of inflow in the western region.

Streamflow comprised nearly 100 percent of surface-water inflow in northern and western regions and 94 percent of inflow in the southern region. Spring contributions to surface-water inflow were limited to springs near the lowland boundary and excluded springs in Warm Springs Valley, which were assumed to be fully accounted for in lowland ET_g estimates. More than 60 percent of surface-water outflow in northern and western regions is through ET from surface-water irrigated areas. Streamflow to Malheur and Harney Lakes is the second largest component of surface-water outflow in northern and western regions, respectively, followed by ET from naturally flooded areas and evaporation of floodwater, ponds, and reservoirs. Streamflow to Malheur Lake and surface-water ET magnitudes are similar in the southern region, with most ET outflow within the MNWR.

Uncertainties in Recharge from Streams and Floodwater

Estimates of recharge from surface water made in this study were determined from the best available data and likely are accurate to within 15–20 percent. Several factors influence estimate accuracy including measured and estimated streamflow from gaged and ungaged watersheds, ET estimates from irrigated and naturally flooded areas, open-water evaporation estimates from standing floodwater, and pond evaporation estimates (table 20). Measured streamflow used directly in recharge estimates and indirectly to extend records ranged from within 5 to more than 15 percent of the true value based on rating designations of excellent to poor (see section "Accuracy and Limitations of Extended and Estimated Streamflow Records" in app. 4). Extended records using KTRL and OLS methods are more reliable where longer records exist (table 8). In ungaged basins, streamflow estimates are less reliable but typically are small relative to gaged watersheds. Accuracy of ET estimates in irrigated areas are within 10–20 percent of actual values (see section "Irrigation Pumpage"). Estimates of ET from naturally flooded areas likely are underestimated during extremely wet years when shrubland areas are flooded (figs. 7, 9), but these low estimates likely are compensated for by high estimates during extremely dry years when surface-water ET in wet meadow, marsh, and riparian areas likely is overestimated. Evaporation of standing floodwater is based on the maximum extent in 2011 and might not represent the average extent of episodic flooding. Finally, standing floodwater evaporation estimates in seasonally flooded areas might be partially accounted for in ET estimates.

Groundwater Recharge from Malheur and Harney Lakes

About 210 acre-ft/yr of pumping-induced groundwater recharge occurs from Malheur and Harney Lakes. A northward hydraulic gradient provides a driving force for groundwater flow from Harney Lake toward the Weaver Spring/Dog Mountain area (figs. 1, 19; zone A), and westward and eastward hydraulic gradients provide a driving force for groundwater flow away from Malheur Lake toward areas of groundwater decline (zones E and B, respectively). Recharge from Harney Lake is about 150 acre-ft/yr and from Malheur Lake is about 50 acre-ft/yr (table 12; see section "Groundwater Discharge to Malheur and Harney Lakes" for more information).

Groundwater Recharge from Irrigation

Groundwater recharge from surface-water and groundwater irrigation were estimated from estimated ET_{irr} rates and efficiency-loss estimates and are described in the following subsections. See subsection "Irrigation Pumpage" for more information about ET_{irr} estimation methods and results.

Groundwater Recharge from Surface-Water Irrigation

Recharge beneath surface-water irrigated areas is often substantial where flood irrigation is used. Using a water-balance approach, Roark and Healy (1998) estimated that percolation losses below the root zone from flood-irrigated fields in New Mexico accounted for 14 percent of applied irrigation water in poorly drained soils and 43 percent of applied water in well- drained soils. In this study, surface-water irrigation-efficiency estimates of 50 percent were assumed for fields irrigated with surface water only and estimates of 60 percent were assumed for those irrigated with groundwater and surface water (see section "Irrigation Pumpage"). Efficiency losses were equally distributed among surface runoff, groundwater recharge that returns to the stream, and groundwater recharge that does not return to the stream. Under this assumption recharge beneath surface-water irrigated fields that does not return to the stream is 17 percent of applied irrigation water in surface-water irrigated fields and 13 percent of applied irrigation water in fields irrigated with groundwater and surface water.

Recharge estimates from surface-water irrigation that do not return to the stream total about 24,000 acre-ft/yr in the northern region, 26,000 acre-ft/yr in the southern region, and 7,300 acre-ft/yr in the western region (table 22). Estimates in all regions are within or similar to estimates of recharge from streams and floodwater (table 20), indicating that assumed efficiencies are reasonable. The Silvies River and Silver Creek transition to predominantly losing streams as they flow from the uplands to valley lowlands; therefore, groundwater recharge that returns to the stream likely is a smaller proportion of efficiency losses in northern and western regions. An increase in the proportion of recharge that does not return to the stream, from a third to half of all efficiency losses (25 percent of applied water in surface-water irrigated fields and 20 percent of applied water in fields irrigated with groundwater and surface water), also yields reasonable recharge estimates (36,000 and 10,000 acre-ft/yr, respectively) that remain well within recharge estimates from streams and floodwater. In the southern region, nearly all marsh and wet meadow areas

within the GETA are irrigated for habitat restoration by the MNWR; therefore, nearly equal estimates of recharge from surface-water irrigation and from streams and floodwater provide additional confidence in estimated values.

Groundwater Recharge from Groundwater Irrigation

Most pumpage for irrigation returns to the atmosphere as ET, but a small portion of the unconsumed water infiltrates beneath irrigated fields and ultimately returns to the groundwater system. Recharge from percolation beneath the root zone of groundwater-irrigated fields commonly is estimated using published irrigation-efficiency estimates, and efficiency losses in groundwater-irrigated areas are attributed to varying proportions of wind losses, runoff, and percolation below the crop root zone. The volume of water partitioned as runoff and percolation below the root zone depends on soil-hydraulic properties and irrigation practices. An efficiency of 70 percent was estimated for groundwater-irrigated fields, with 5 percent of the loss attributed to percolation below the root zone. An efficiency of 60 percent was used in fields irrigated with groundwater and surface water, with 5 percent of the groundwater loss (where groundwater accounts for half of the total irrigation applied) attributed to percolation below the root zone. Groundwater recharge beneath groundwater-irrigated fields was estimated from mean pumpage during 2017–18 (table 15). Refer to section "Irrigation Pumpage" for more details on determination of irrigation efficiencies. Estimated recharge in the Harney Basin lowlands from groundwater irrigation during 2017–18 totaled 4,700 acre-ft/yr in the northern region, 1,200 acre-ft/yr in the southern region, and 2,200 acre-ft/yr in the western region (table 22).

Groundwater Recharge from Non-Irrigation Use

Most non-irrigation water use for domestic, municipal, industrial, stock water, and other uses is consumed but a small portion returns to the groundwater system. Groundwater recharge from non-irrigation groundwater use reported by Grondin (2021) is used in this study and largely occurs through septic systems from community-systems and rural-domestic uses. Groundwater recharge through septic systems was calculated as 58 percent of household pumpage (table 16; Grondin, 2021). Groundwater return flow from non-irrigation groundwater use in the Harney Basin lowlands during 2000 and 2010 totaled 900 acre-ft/yr (tables 16, 22). Estimates are assumed to remain constant during the 1982–2016 study period.

Table 22.   Estimated mean annual groundwater recharge from surface-water (1982–2016) and groundwater (2017–18) irrigation and non-irrigation groundwater use (2000–10) by region, Harney Basin, southeastern Oregon.

[Regions shown on figure 1. **Type**: 1, groundwater-irrigated fields; 2, groundwater and surface-water irrigated fields; 3, surface-water irrigated fields; 4, non-irrigation water use (table 16). Recharge estimated as 5 percent of pumpage for type 1 and 2, 13 percent of applied surface water for source type 2, and 17 percent of applied surface water for source type 3. Pumpage estimates for irrigation are from table 15]

Recharge source	Type	Mean annual recharge (acre-feet)			
		Northern	**Southern**	**Western**	**Harney Basin**
Surface water	3	22,000	26,000	6,900	54,900
	2	1,900	50	380	2,330
	Total	23,900	26,100	7,280	57,300
Groundwater	1	3,300	1,100	1,900	6,300
	2	800	30	210	1,040
	4	735	86	78	900
	Total	4,840	1,220	2,190	8,250
Total		28,700	27,300	9,470	65,500

Summary of Groundwater Recharge

Mean annual groundwater recharge in the Harney Basin totals about 288,000 acre-ft in the uplands and 172,000 acre-ft in the lowlands (table 23). Upland and lowland recharge are presented separately to prevent double counting water that recharges the uplands, discharges to upland streams, and then recharges the lowlands. More than half of the upland recharge is generated in the southern region (157,000 acre-ft/yr) where higher elevation precipitation catchments are extensive (fig. 2). About 30 percent of upland recharge occurs in the northern region (about 86,000 acre-ft/yr), and less than 20 percent occurs in the western region (about 45,000 acre-ft/yr), which is the driest of the three regions (fig. 2). Recharge to the Harney Basin lowlands is about 77,000 acre-ft/yr in the northern region, 48,000 in the southern region, and 47,000 acre-ft/yr in the western region.

The largest source of lowland recharge is surface water through streams, floodwater, and irrigation (roughly 80 percent in the northern region and about 50 percent in southern and western regions) with lesser contributions from groundwater inflow from upland areas (11 percent in the northern region and about 40 percent in southern and western regions). Estimated recharge from surface-water irrigated areas comprises nearly 40 percent of recharge from streams and floodwater in the northern region and about 30 percent of this recharge in the western region. In the southern region, most (97 percent) recharge from streams and floodwater was estimated to occur beneath irrigated areas. Although recharge from channel losses occurs in the southern region, this recharge is likely balanced by base-flow gains between Frenchglen and Diamond Lane (fig. 35). Recharge from groundwater irrigation and non-irrigation pumpage was minimal and averages about 5 percent across all regions.

Comparisons between current and previous groundwater recharge estimates are reasonable when evaluated over equivalent spatial extents. Robison (1968) estimated 260,000 acre-ft/

yr of recharge from precipitation, which is within 10 percent of current upland recharge estimates. Aquaveo, LLC (2012), estimated 360,000 acre-ft/yr based on deep-percolation of precipitation and irrigation distributed across the basin during 1995–2004. In this study, a comparable estimate of 352,000 acre-ft/yr was computed as the sum of upland recharge from precipitation and lowland recharge from irrigation (surface water and groundwater). Recharge to the northern and southern region lowlands generally is within the range of estimates from Piper and others (1939) (assuming recharge equals discharge). Excluding irrigation from pumpage, which was minimal during the early 1900s, current northern region recharge is about 1.3 times the 57,000 acre-ft/yr estimate from Piper and others (1939). The current southern region estimate is within the range of 0–85,000 acre-ft/yr from Piper and others (1939).

Summary and Discussion of Groundwater Hydrologic Budget

The groundwater hydrologic budget for the Harney Basin consists of natural recharge and discharge components and superimposed anthropogenic modifications to the budget through groundwater pumpage, surface-water management, and irrigation. The budget components presented in this report represent mean annual conditions during 1982–2016, except groundwater pumpage, which uses the most recent data available (2017–18). Distinct upland and lowland water budgets are presented and the relative contribution of anthropogenic effects, most importantly pumpage, on lowland budget estimates is evaluated. Recharge and discharge were estimated assuming: (1) groundwater pumpage is the only notable anthropogenic stress on the system and (2) recharge beneath surface-water irrigated areas is about the same as pre-development conditions. Therefore, natural recharge estimates presented include recharge from surface-water irrigation.

Table 23.   Estimated mean annual groundwater recharge by region, Harney Basin, southeastern Oregon, 1982–2016.

[**Geographic position**: Position of water-bearing units receiving recharge. Regions are shown on figure 1. **Mean annual recharge estimates**: Represent mean of input ranges. Recharge estimates are rounded to two significant figures for values below 100,000 and three significant figures for values above 100,000. Groundwater inflow from uplands is upland recharge that flows through the subsurface and recharges lowland groundwater, computed as upland recharge minus upland base flow and spring flow (table 17). **Abbreviation**: —, not applicable]

Geographic position	Recharge source water	Mean annual recharge by region (acre-feet)			
		Northern	Southern	Western	Harney Basin
Upland	Precipitation and snowmelt	86,000	157,000	45,000	288,000
Lowland	Groundwater inflow from uplands	9,000	20,000	20,000	49,000
	Streams and floodwater (natural) [1,2]	40,000	900	18,000	59,000
	Malheur and Harney Lakes[1]	47	—	160	210
	Surface water (irrigation) [1]	24,000	26,000	7,300	57,000
	Groundwater irrigation and non-irrigation use[3]	4,800	1,200	2,200	8,200
	Total without pumpage	73,000	47,000	45,000	165,000
	Total	78,000	48,000	47,000	173,000

[1]Includes a portion of upland runoff and base flow.

[2]Difference between estimates from tables 20 and 22. In the southern region, recharge from streams and floodwater is mostly accounted for in irrigated areas, and channel losses are assumed to be equally offset by base-flow gains between Frenchglen and Diamond Ln (fig. 1).

[3]Estimate is basin wide, but 99.9 percent occurs either within the lowland boundary or within two miles outside of the lowland boundary.

Upland Groundwater Budget

The upland groundwater budget is minimally affected by groundwater pumpage and is a reasonable representation of the natural system. Recharge to upland areas totals 288,000 acre-ft/yr and discharge totals 239,000 acre-ft/yr, resulting in a net recharge of 49,000 acre-ft/yr (fig. 36; table 24). The net upland recharge represents 17 percent of the total upland recharge and is assumed to migrate as groundwater flow from upland to lowland areas.

The proportion of upland recharge that discharges in upland areas varies regionally and likely reflects differences in hydraulic properties of subsurface hydrostratigraphic units. In the northern and southern regions, about 90 percent of upland recharge discharges in the uplands, whereas in the western region, less than 60 percent of upland recharge discharges in the uplands (table 24). Low-permeability sedimentary, volcanic, and metamorphic rocks in the Blue Mountains of the northern region likely limit groundwater flow at depth, which in turn promotes short flow paths between recharge and discharge areas (Gingerich and others, 2022). On Steens Mountain comprising the southern region uplands, groundwater flow through moderately permeable lava is likely intercepted by the numerous stream channels that dissect upland areas and discharge large quantities of groundwater (fig. 11; table 9). The western region uplands are mostly underlain by low-permeability volcanic rocks, but a portion of the rocks underlying the uplands, such as the Dry Mountain lavas in the Blue Mountains, also have localized higher permeability areas that likely transmit greater proportions of groundwater recharge from upland to lowland areas than in the northern or southern regions (table 24).

Lowland Groundwater Budget

The lowland groundwater budget for the Harney Basin represents post-development conditions as more than 99 percent of groundwater development and use is either inside or within 2 miles of the lowland boundary (fig. 1). Including pumpage, mean (1982–2016) groundwater recharge to lowland areas totals 173,000 acre-ft/yr (table 23) and groundwater discharge totals 283,000 acre-ft/yr (table 17), nearly twice the recharge estimate. Non-pumping components of groundwater recharge and discharge, which exclude discharge to and recharge from pumpage, are much closer in balance and average 165,000 acre-ft/yr and 131,000 acre-ft/yr, respectively, during 1982–2016 (fig. 36; table 24). Annual net pumpage (or the difference between total groundwater pumped from wells and recharge from excess irrigation and other water use) during 2017–18 averaged 144,000 acre-ft (table 24) and is similar to the amount of natural groundwater discharge. The imbalance (or net groundwater budget) between natural recharge and discharge of 34,000 acre-ft/yr (table 24), a 23-percent difference, mostly represents the cumulative uncertainty in the estimates of the various natural recharge and discharge components of the groundwater budget (fig. 36) but also could include a smaller amount of natural groundwater discharge capture by pumpage in some lowland areas.

Table 24.   Estimated mean annual upland and lowland groundwater budgets (1982–2016), Harney Basin, southeastern Oregon.

[Regions are shown on figure 1. **Component**: Recharge (table 23) and discharge (table 17) represent non-pumpage components. Net budget is recharge minus discharge. Net pumpage is total pumpage (table 17) minus recharge from pumpage (table 23). Estimates are rounded to two significant figures for values below 100,000, and three significant figures for values above 100,000]

Region	Component	Mean annual budget components by region (acre-feet)			
		Northern	Southern	Western	Harney Basin
Upland	Recharge	86,000	157,000	45,000	288,000
	Discharge	77,000	137,000	25,000	239,000
	Net recharge[1]	9,000	20,000	20,000	49,000
Lowland	Recharge (no pumpage)	73,000	47,000	45,000	165,000
	Discharge (no pumpage)	64,000	32,000	35,000	131,000
	Net recharge (no pumpage) [2]	9,000	15,000	10,000	34,000
	Net pumpage	82,000	21,000	41,000	144,000
	Net pumpage exceeding net recharge	73,000	6,000	31,000	110,000

[1]Values represent groundwater inflow from upland to lowland areas.

[2]Values mostly represent estimate uncertainty with a smaller proportion attributed to discharge capture by pumpage.

EXPLANATION

→ Mean annual recharge, in acre-feet (inflow)

→ Mean annual discharge, in acre-feet (outflow)
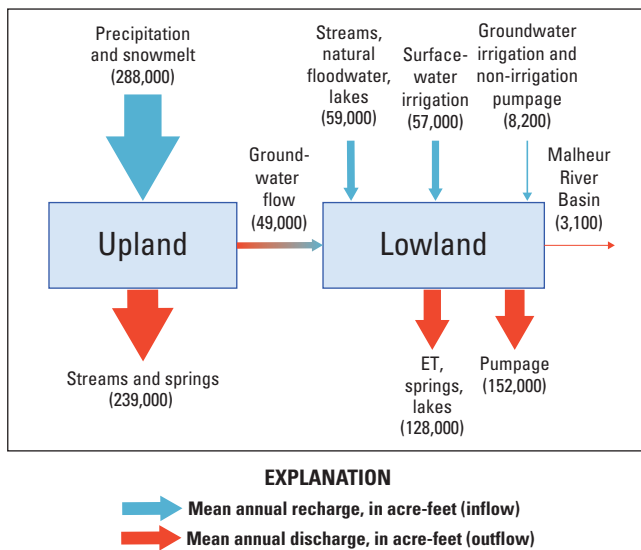
Figure 36.   Estimated mean annual upland and lowland groundwater budgets, Harney Basin, southeastern Oregon, 1982–2016.

Reductions in natural groundwater discharge from capture of discharge by pumpage likely are a small fraction of the imbalance between non-pumping lowland recharge and discharge estimates in northern (9,000 acre-ft/yr) and western regions (10,000 acre-ft/yr). The study-period (1982–2016) ET_g estimate in the northern region lowlands and spring discharge in the western region lowlands (table 17) are similar to estimates made nearly a century ago by Piper and others (1939) and groundwater-level measurements in the northern region indicate low-permeability sediments and shallow recharge from streams and floodwater have likely buffered the response of the shallow water table (and ET) to pumping

at depth (Gingerich and others, 2022). In the western region uplands southwest of Harney Lake hydrologic data are scarce, therefore upland recharge and discharge estimates used to estimate groundwater inflow to lowland areas are minimally constrained. These comparisons support the assumption that biases in northern and western region groundwater budget estimates reflect recharge rather than discharge components. However, with continued pumping of the deeper system, shallow groundwater levels will ultimately decline, thereby reducing groundwater available for ET by shallow-rooted vegetation.

In the southern region, the 15,000 acre-ft/yr imbalance in the non-pumping budget likely results from overestimated recharge and, to a smaller degree, capture of natural discharge by groundwater pumpage in Virginia Valley (fig. 22D). Upland recharge likely was overestimated from the SWB model in the southern region because observed runoff and ET were under-estimated during the simulation period (table 18). Pumpage in the southern region mostly occurs in Virginia Valley where groundwater levels have declined uniformly by about 10 ft (Gingerich and others, 2022). Although groundwater-level declines in Virginia Valley minimally affect groundwater outflow to the Malheur River Basin because of geologic constraints along the flow path (fig. 20), groundwater-level declines and substantial land-use change from phreatophytes to irrigated agriculture (figs. 7, 22C–D) likely have reduced natural groundwater discharge in this part of the southern region.

The net difference between non-pumping recharge and discharge in the Harney Basin lowlands is just over 20 percent of total groundwater pumpage, indicating at least 80 percent of pumpage removes water from aquifer storage if estimate uncertainties in non-pumping components are considered. In the western region, groundwater levels in some pumping areas outside the major discharge areas show substantial

groundwater-level declines indicating that groundwater storage is the primary source of pumped water (fig. 4; Gingerich and others, 2022). Although recent (2017) springflow measurements are within the range of historical measurements in the western region (table 7), the northward hydraulic gradient from Harney Lake toward the Weaver Spring/Dog Mountain area (figs. 1, 19) indicates that some discharge capture by pumpage is likely. In the northern region, substantial groundwater-level declines within and outside the major discharge areas and limited water-table response to pumping at depth indicate most pumpage is removing deeper groundwater from storage (Gingerich and others, 2022). Along the Donner und Blitzen River corridor in the southern region, minimal groundwater development and groundwater-level declines indicate capture of ET_g and spring discharge is unlikely. Although Sodhouse Spring discharge estimates are based on historical measurements prior to the study period, stable isotope data indicate it is sourced from Donner und Blitzen River water (fig. 2.2; Gingerich and others, 2022) and therefore likely fluctuates with multiyear variations in streamflow. In areas where deep pumping is likely drawing down shallow groundwater levels, such as in Virginia Valley in the southern region, pumpage likely captures a fraction of ET_g in addition to aquifer storage.

Although potential capture of natural groundwater discharge is small relative to the total pumpage during the study period, declining groundwater levels and groundwater pumpage volumes that exceed natural discharge from lowland areas indicate future capture will occur. Concerns for ET_g and spring discharge capture by pumping wells are greatest near areas most heavily irrigated with groundwater (fig. 22D) and distant from recharge by streams and floodwater such as along the eastern boundary of the northern region lowlands, near Weaver Spring/Dog Mountain in the western region, and in Virginia Valley in the southern region (fig. 35). Evaluation of the timing and location of potential decreases in natural groundwater discharge in all regions would be best accomplished through the application of a numerical groundwater flow model.

Limitations

The hydrologic groundwater budget developed herein reflects current understanding and provides the best estimate of the Harney Basin system using currently available data. The major components of the budget are constrained by well-quantified inputs of precipitation and well-quantified discharge to the three major stream systems, ET_g by natural vegetation, and ET_g from irrigated crops. The fundamental physics controlling the flux of water in and out of the system are well-understood, but some local parameters are not well-quantified and represent opportunities for future improvements. Future

data collection and novel techniques for data analysis will certainly improve the precision and clarity of certain aspects of the water budget but are unlikely to change the overall balance by more than 10 to 20 percent. The following caveats should be considered when utilizing water-budget information presented herein:

- Estimated discharge to upland streams and springs is more certain in areas where measurements exist. Estimates from ungaged streams and assumptions about unmeasured springs could be refined with additional upland stream- and spring-discharge measurements in the southern part of the western region, in the northern region uplands outside of the Silvies River watershed, and in the southern region uplands within Kiger and Riddle Creek watersheds.

- Upland recharge estimates from the SWB model likely are biased high in ungaged areas. Additional measurements in ungaged watersheds, a more sophisticated snowfall-runoff model on Steens Mountain, and precipitation datasets calibrated to snowpack measurements from snow courses would likely improve these estimates.

- Lowland recharge estimates from infiltration of surface water are based, in part, on extended streamflow data in streamgaged and ungaged basins and naturally flooded areas. Extended records inherently have more uncertainty than measurements. Additional continuous streamflow measurements in ungaged watersheds and in those streamgaged nearly 100 years ago, and a more in-depth evaluation of the extent of natural flooding (beyond irrigated areas) and depth of floodwater could be used to confirm or refine these values.

- Estimated groundwater discharge through ET assumes that sagebrush within the larger GETA uses groundwater for a small fraction of its water needs. Although this was confirmed by plant-water isotopic compositions at one of three sites sampled, additional spatially distributed sampling could confirm this assumption.

Summary

Increased demand for groundwater in the Harney Basin has led to groundwater-level declines, prompting the Oregon Water Resources Department (OWRD) to issue a moratorium on new groundwater permits. Limited knowledge regarding the sustainability of existing groundwater uses and hydraulic connections across the basin led the OWRD to enter into a cooperative agreement with the U.S. Geological Survey

(USGS) to conduct a groundwater-availability study of the Harney Basin. The objectives of this two-phase, 4-year study were to (1) develop a quantitative conceptual understanding of the groundwater-flow system of the Harney Basin and (2) develop numerical hydrologic models to test the conceptualization of the groundwater-flow system and accurately simulate its response to current conditions and potential groundwater management development and scenarios. This report provides a hydrologic budget for the Harney Basin groundwater system resulting from the USGS–OWRD cooperative study. Hydrologic budget estimates of groundwater recharge and discharge are provided for upland areas and lowland areas, where most of the groundwater development occurs. Full, basin-wide accounting of all upland and lowland budget components is useful for numerical simulation of all hydrologic physical processes in the groundwater system. The lowland groundwater budget, which accounts for most groundwater development in the basin, is of practical importance to help resource managers and water users evaluate the outcome of groundwater-management decisions.

The upland groundwater budget is minimally affected by groundwater development and therefore is considered a reasonable representation of current natural conditions. Mean-annual (1982–2016) recharge to upland areas totals 288,000 acre-ft/yr and discharge totals 239,000 acre-ft/yr, resulting in a net groundwater recharge of 49,000 acre-ft/yr. Upland groundwater recharge occurs as infiltration of precipitation and snowmelt and was estimated using the USGS Soil-Water-Balance model calibrated to estimates of runoff, evapotranspiration (ET), base flow, and snow-water equivalent. More than 80 percent of upland recharge discharges to upland streams and springs before reaching the basin fill beneath the valley lowlands. Groundwater discharge to streams as base flow totals 225,000 acre-ft/yr and comprises more than 90 percent of upland discharge. Discharge as base flow to streams represents an average of estimates from graphical hydrograph separation and low-flow techniques computed from streamgaged and estimated streamflow during 1982–2016. Upland discharge to springs, unaccounted for in base-flow estimates, totals 14,000 acre-ft/yr and represents a compilation of current and historical spring-discharge measurements. More than 50 percent of upland spring discharge was measured during 1996–2016 at Page Springs, near the base of the northwestern flank of Steens Mountain. The net upland recharge represents 17 percent of the total upland recharge and is assumed to migrate as groundwater flow from upland to lowland areas. Regionally, groundwater flow from uplands to lowlands increases from 9,000 acre-ft/yr in the northern region to 20,000 acre-ft/yr in the southern and western regions.

The lowland groundwater budget for the Harney Basin represents post-development conditions as more than 99 percent of groundwater development and use is either inside or within 2 miles of the lowland boundary. Mean (1982–2016)

groundwater recharge to lowland areas totaled 173,000 acre-ft/yr, and groundwater discharge totaled 283,000 acre-ft/yr, indicating discharge exceeded recharge by more than 60 percent when including pumpage. Excluding discharge to and recharge from groundwater pumpage, the lowland groundwater recharge and discharge components differed by 23 percent and averaged 165,000 acre-ft/yr and 131,000 acre-ft/yr, respectively during 1982–2016. The imbalance between non-pumping recharge and discharge mostly represents the cumulative uncertainty in the estimates of the various groundwater budget components, but also likely includes a small amount of natural groundwater discharge captured by pumping in some lowland areas.

Most non-pumping lowland groundwater recharge occurs through infiltration of surface water through streams, floodwater, and irrigation (116,000 acre-ft/yr), with a smaller amount through groundwater inflow from uplands (49,000 acre-ft/yr). Recharge from streams and floodwater was estimated from a surface-water balance between surface-water inflow at the upland-lowland boundary through streams and springs and surface-water outflow through ET and streamflow into Malheur and Harney Lakes. A minor amount of recharge through infiltration of lake water (200 acre-ft/yr) was estimated using a hydraulic gradient analysis.

Natural lowland groundwater discharge occurs through ET (ET_g) (119,000 acre-ft/yr), Sodhouse Spring (8,900 acre-ft/yr), and groundwater outflow to the Malheur River Basin (3,100 acre-ft/yr). Estimated ET_g from non-irrigated areas and areas irrigated with spring discharge represents more than 90 percent of discharge from the lowlands and was estimated using two remote-sensing based approaches incorporating ET_g measurements from similar vegetation in other basins and 23 years of Landsat imagery. Despite differences in estimation approaches, ET_g estimates were within 10 percent of one another. Discharge from Sodhouse Spring, 8,900 acre-ft/yr, represents the mean of historical measurements made during 1907–80. An additional 25,000 acre-ft/yr discharges through springs in Warm Springs Valley and surrounding Harney Lake, but this groundwater is ultimately consumed by ET and is represented in ET_g estimates. A hydraulic gradient analysis was used to estimate 3,100 acre-ft/yr of groundwater outflow to the Malheur River Basin and 400 acre-ft/yr of groundwater discharge as seepage to Malheur and Harney Lakes, which is included in ET_g estimates.

Mean annual net groundwater pumpage from the Harney Basin lowlands during 2017–18 was 144,000 acre-ft and represents the amount of groundwater pumped from wells minus recharge beneath groundwater irrigated fields and septic tanks. Groundwater pumpage was estimated in concurrent studies by compiling groundwater-use data and coupling pumpage data from wells with 10 years of remote-sensing-based ET estimates from groundwater-irrigated areas. Net pumpage for irrigation has increased from about 53,000 acre-ft/yr during

1991–94 to 138,000 acre-ft/yr. Regionally, net groundwater pumpage for all uses totals 21,000 acre-ft/yr in the southern region, 41,000 acre-ft/yr in the western region, and 82,000 acre-ft/yr in the northern region.

Under current conditions, mean annual lowland groundwater discharge including pumpage exceeds annual recharge, indicating that the hydrologic budget is out of balance. Current net groundwater pumpage is four times the imbalance between natural lowland recharge and discharge (34,000 acre-ft/yr) across all regions. In northern and western regions, comparisons between net pumpage and the imbalance between recharge and discharge estimates indicate that at least 75 percent of groundwater pumpage is depleting aquifer storage, and the remaining pumpage could be capturing natural discharge through springs and ET. In the southern region most groundwater development occurs east of Malheur Lake and likely represents a combination of storage depletion and capture of ET_g. As pumping continues, aquifer storage depletion will continue until the capture rate of natural discharge to springs and ET is equal to the pumping rate.

References Cited

Abatzoglou, J.T., 2013, Development of gridded surface meteorological data for ecological applications and modelling: International Journal of Climatology, v. 33, no. 1, p. 121–131.

Albano, C.M., Minor, B., Freed, Z., and Huntington, J.L., 2020, Status and trends of groundwater dependent vegetation in relation to climate and shallow groundwater in the Harney Basin, Oregon: Desert Research Institute, Publication no. 41280, 63 p.

Allander, K.K., Smith, J.L., and Johnson, M.J., 2009, Evapotranspiration from the lower Walker River Basin, west-central Nevada, water years 2005–07: U.S. Geological Survey Scientific Investigations Report 2009-5079, 62 p. [Also available at https://pubs.usgs.gov/sir/2009/5079/.]

Allen, R.G., Tasumi, M., and Trezza, R., 2007, Satellite-Based Energy Balance for Mapping Evapotranspiration with Internalized Calibration (METRIC)—Model: Journal of Irrigation and Drainage Engineering, v. 133, no. 4, p. 380–394.

Allen, R.G., Walter, I.A., Elliot, R.L., Howell, T.A., Itenfisu, D., Jensen, M.E., and Snyder, R.L., eds., 2005, The ASCE Standardized Reference Evapotranspiration Equation: Reston, Virginia, American Society of Civil Engineers.

Arnold, J.G., and Allen, P.M., 1999, Automated methods for estimating baseflow and ground water recharge from streamflow records: Journal of the American Water Resources Association, v. 35, no. 2, p. 411–424.

Aquaveo, LLC, 2012, Harney Basin Groundwater Study: Aquaveo, LLC, 104 p.

Aurand, K., 2013, Groundwater recharge estimates for the Lower Tertiary and Upper Cretaceous aquifers in the Williston and Powder River structural basins: Rapid City, South Dakota, South Dakota School of Mines and Technology, M.S. thesis, accessed January, 2015, at https://sd.water.usgs.gov/pubs/theses/Aurand_Thesis.pdf.

Barlow, P.M., and Cunningham, W.L., Zhai, Tong, and Gray, Mark, 2015, U.S. Geological Survey Groundwater Toolbox, a graphical and mapping interface for analysis of hydrologic data (version 1.0)—User guide for estimation of base flow, runoff, and groundwater recharge from streamflow data: U.S. Geological Survey Techniques and Methods, book 3, chap. B10, 27 p. [Also available at https://doi.org/10.3133/tm3B10.]

Bauer, H.H., and Vaccaro, J.J., 1987, Documentation of a deep percolation model for estimating ground-water recharge: U.S. Geological Survey Open-File Report 86-536, 180 p. [Also available at https://doi.org/10.3133/ofr86536.]

Beamer, J.P., Huntington, J.L., Morton, C.G., and Pohll, G.M., 2013, Estimating Annual Groundwater Evapotranspiration from Phreatophytes in the Great Basin Using Landsat and Flux Tower Measurements: Journal of the American Water Resources Association, v. 49, no. 3, p. 518–533.

Beamer, J.P., and Hoskinson, M.D., 2021, Historical irrigation water use and groundwater pumpage estimates in the Harney Basin, Oregon, 1991-2018: Oregon Water Resources Department Open File Report No. 2021-02, 53 p. [Also available at https://www.oregon.gov/owrd/wrreports/OWRD_OFR_2021-02_Harney_Basin_METRIC_Irrigation_Use_Report.pdf.]

Berger, D.L., Mayers, C.J., Garcia, C.A., Buto, S.G., and Huntington, J.M., 2016, Budgets and chemical characterization of groundwater for the Diamond Valley flow system, central Nevada, 2011–12: U.S. Geological Survey Scientific Investigations Report 2016–5055, 83 p. [Also available https://doi.org/10.3133/sir20165055.]

Blaney, H.F., Taylor, C.A., Nickle, H.G., and Young, A.A., 1933, Water losses under natural conditions from wet areas in southern California: California Department of Public Works, Division of Water Resources Bulletin 44, 176 p.

Boschmann, D.E., 2021, Generalized geologic compilation map of the Harney Basin, Oregon Water Resources Department Open File Report 2021-01, 57 p. [Also available at https://www.oregon.gov/owrd/wrreports/OFR_2021-01_report.pdf.]

Burns, D.A., 2002, Stormflow-hydrograph separation based on isotopes—The thrill is gone? what's next?: Hydrological Processes, v. 16, no. 7, p. 1515–1517.

Cannon, H.L., 1960, The development of botanical methods of prospecting for uranium on the Colorado Plateau: Geological Survey Bulletin 1085–A, 50 p. [Also available at https://pubs.usgs.gov/bul/1085a/report.pdf.]

Conlon, T.D., Wozniak, K.C., Woodcock, D., Herrera, N.B., Fisher, B.J., Morgan, D.S., Lee, K.K., and Hinkle, S.R., 2005, Ground-water hydrology of the Willamette basin, Oregon: Scientific Investigations Report 2005–5168. [Also available at http://pubs.er.usgs.gov/publication/sir20055168.]

Cooper, R.M., 2002, Determining surface water availability in Oregon: State of Oregon Water Resources Department Open File Report SW 02-002, 158 p.

Corson-Dosch, N.T., and Garcia, C.A., 2022, Soil-Water-Balance (SWB) model archive used to simulate mean annual upland recharge from infiltration of precipitation and snowmelt in Harney Basin, Oregon, 1982-2016: U.S. Geological Survey data release, https://doi.org/10.5066/P94NH4D8.

Cronshey, R., McCuen, R.H., Miller, N., Rawls, W., Robbins, S., and Woodward, D., 1986, Urban hydrology for small watersheds (2d ed.): Washington, D.C., U.S. Department of Agriculture, Soil Conservation Service, Conservation Engineering Division, Technical Release 55, 164 p.

Cuenca, R., Ciotti, S., and Hagimoto, Y., 2013, Application of Landsat to Evaluate Effects of Irrigation Forbearance: Remote Sensing (Basel), v. 5, no. 8, p. 3776–3802.

Devitt, D.A., and Bird, B., 2016, Changes in groundwater oscillations, soil water content and evapotranspiration as the water table declined in an area with deep rooted phreatophytes: Ecohydrology, v. 9, no. 6, p. 1082–1093.

Dicken, S.N., 1950, Oregon geography—First preliminary edition: Ann Arbor, Michigan, Edwards Brothers, Inc., 104 p.

Dinçer, T., Payne, B.R., Florkowski, T., Martinec, J., and Tongiorgi, E., 1970, Snowmelt runoff from measurements of tritium and oxygen-18: Water Resources Research, v. 6, no. 1, p. 110–124.

Doherty, J., 2010, PEST, Model-independent parameter estimation—User manual (5th ed., with slight additions): Brisbane, Australia, Watermark Numerical Computing, 336 p.

Donovan, L.A., Richards, J.H., and Muller, M.W., 1996, Water Relations and Leaf Chemistry of Chrysothamnus nauseosus ssp. Consimilis (Asteraceae) and Sarcobatus vermiculatus (Chenopodiaceae): American Journal of Botany, v. 83, no. 12, p. 1637.

Dripps, W.R., and Bradbury, K.R., 2007, A simple daily soil–water balance model for estimating the spatial and temporal distribution of groundwater recharge in temperate humid areas: Hydrogeology Journal, v. 15, no. 3, p. 433–444.

Eaton, G.P., 1982, The Basin and Range Province—Origin and Tectonic Significance: Annual Review of Earth and Planetary Sciences, v. 10, no. 1, p. 409–440.

Farm Service Agency, 2008, Common land unit: U.S. Department of Agriculture Farm Service Agency website, accessed June, 2021, at https://www.fsa.usda.gov/programs-and-services/aerial-photography/imagery-products/common-land-unit-clu/index.

Farnsworth, R.K., Thompson, E.S., and Peck, E.L., 1982, Evaporation atlas for the contiguous 48 United States: U.S. Department of Commerce, National Oceanic and Atmospheric Administration, National Weather Service, NOAA Technical Report NWS 33, 26 p., 4 plates. [Also available at https://www.nws.noaa.gov/ohd/hdsc/Technical_reports/TR33.pdf]

Fenelon, J.M., Halford, K.J., and Moreo, M.T., 2016, Delineation of the Pahute Mesa–Oasis Valley groundwater basin, Nevada (ver. 1.1, May 2016): U.S. Geological Survey Scientific Investigations Report 2015–5175, 40 p. [Also available at https://doi.org/10.3133/sir20155175.]

Ferguson, R.I., 1986, River Loads Underestimated by Rating Curves: Water Resources Research, v. 22, no. 1, p. 74–76.

Foken, T., Leuning, R., Oncley, S.R., Mauder, M., and Aubinet, M., 2012, Corrections and data quality control, in Aubinet, M., Vesala, T., and Papale, D., eds., Eddy covariance—A practical guide to measurement and data analysis—Springer Atmospheric Sciences, https://doi.org/10.1007/978-94-007-2351-1_4.

Gannett, M.W., Lite, K.E., Jr., Morgan, D.S., and Collins, C.A., 2001, Ground-water hydrology of the upper Deschutes Basin, Oregon: U.S. Geological Survey Water-Resources Investigations Report 00–4162, 78 p. [Also available at https://pubs.usgs.gov/wri/wri004162/.]

Gannett, M.W., Lite, K.E., Jr., La Marche, J.L., Fisher, B.J., and Polette, D.J., 2007, Ground-Water Hydrology of the Upper Klamath Basin, Oregon and California: Scientific Investigations Report 2007–5050. [Also available at http://pubs.er.usgs.gov/publication/sir20075050]

Gao, B., 1996, NDWI—A normalized difference water index for remote sensing of vegetation liquid water from space: Remote Sensing of Environment, v. 58, no. 3, p. 257–266.

Garcia, C.A., Haynes, J.V., Overstreet, B.T., and Corson-Dosch, N.T., 2022, Supplemental data—Hydrologic budget of the Harney Basin groundwater system, southeastern Oregon, 1982-2016: U.S. Geological Survey data release, https://doi.org/10.5066/P9QABFML.

Garcia, C.A., Huntington, J.M., Buto, S.G., Moreo, M.T., Smith, J.L., and Andraski, B.J., 2015, Groundwater discharge by evapotranspiration, Dixie Valley, west-central Nevada, March 2009–September 2011 (ver. 1.1, April 2015): U.S. Geological Survey Professional Paper 1805, 90 p. [Also available at https://doi.org/10.3133/pp1805.]

Gendaszek, A.S., and Welch, W.B., 2018, Water budget of the upper Chehalis River Basin, southwestern Washington: U.S. Geological Survey Scientific Investigations Report 2018-5084, 17 p. [https://doi.org/10.3133/sir20185084.]

Gingerich, S.B., Johnson, H.M., Boschmann, D.E., Grondin, G.H., and Garcia, C.A., 2022 Groundwater resources of the Harney Basin, Oregon: U.S. Geological Survey Scientific Investigations Report 2020-5103, 116 p. [Also available at https://doi.org/10.3133/sir20215103.]

Glancy, P.A., and Rush, F.E., 1968, Water-resources appraisal of Smoke Creek-San Emidio Desert area, Nevada and California: Nevada Department of Conservation and Natural Resources, Water Resources–Reconnaissance Series Report 44, 57 p.

Gorelick, N., Hancher, M., Dixon, M., Ilyushchenko, S., Thau, D., and Moore, R., 2017, Google Earth Engine—Planetary-scale geospatial analysis for everyone: Remote Sensing of Environment, v. 202, p. 18–27.

Grondin, G.H, 2021, Methods and results for estimating groundwater pumped, returned, and consumed for non-irrigation uses in the Harney Basin, Oregon: Oregon Water Resources Department Open File Report 2021-03, 28 p. [Also available at https://www.oregon.gov/owrd/wrdreports/OWRD_OFR_2021-003_Harney_Basin_non_irrigation_GW_use_report_stamped.pdf.]

Grondin, G.H., Boschmann, D.E., Barnett, H.J., and Scandella, B.P., 2021, Methods and results for estimating the hydraulic characteristics of the subsurface materials in the Harney Basin, Oregon: Oregon water Resources Department Open File Report 2021-04, 63 p. [Also available at https://www.oregon.gov/owrd/wrdreports/OFR_2021-04_Harney_Basin_subsurface_hydraulic_properties.pdf.]

Halford, K.J., and Mayer, G.C., 2000, Problems Associated with Estimating Ground Water Discharge and Recharge from Stream-Discharge Records: Ground Water, v. 38, no. 3, p. 331–342.

Hamilton, D.B., Auble, G.T., Ellison, R.A., and Roelle, J.E., 1986, Effects of flood control alternatives on the hydrology, vegetation, and wildlife resources of the Malheur-Harney Lakes Basin: U.S. Fish and Wildlife Service, National Ecology Center, Fort Collins, Colorado, NEC-86/20, 85 p.

George H. Hargreaves, and the Zohrab A. Samani, 1985, Reference Crop Evapotranspiration from Temperature: Applied Engineering in Agriculture, v. 1, no. 2, p. 96–99.

Helsel, D.R., Hirsch, R.M., Ryberg, K.R., Archfield, S.A., and Gilroy, E.J., 2020, Statistical methods in water resources: U.S. Geological Survey Techniques and Methods, book 4, chapter A3, 458 p. Supersedes USGS Techniques of Water-Resources Investigations, book 4, chapter A3, version 1.1. [Also available at https://doi.org/10.3133/tm4A3.]

Hostetler, S.W., and Bartlein, P.J., 1990, Simulation of lake evaporation with application to modeling lake level variations of Harney-Malheur Lake, Oregon: Water Resources Research, v. 26, no. 10, p. 2603–2612.

Hubbard, L.L., 1975, Hydrology of Malheur Lake, Harney County, Southeastern Oregon: U.S. Geological Survey Water Resources Investigation 21-75, 40 p.

Hubbard, 1989, 1984 Flooding of Malheur-Harney Lake, Harney County, Southeastern Oregon: U.S. Geological Survey Water Resources Investigation: 89-4111, 1 pl. [Also available at https://pubs.er.usgs.gov/publication/wri894111.]

Institute of Hydrology, 1980a, Research report, v. 1 of Low flow studies: Wallingford, United Kingdom, Institute of Hydrology, 42 p.

Institute of Hydrology, 1980b, Catchment characteristic estimation manual, v. 3 of Low flow studies: Wallingford, United Kingdom, Institute of Hydrology, 27 p.

Irmak, S., 2017, Simplified Forms of Deep Percolation Estimation Method below the Crop Root Zone for Silt-Loam Soils: University of Nebraska-Lincoln Nebraska Extension Publications 3015. [Also available at https://extensionpublications.unl.edu/assets/pdf/ec3015.pdf.]

Jackson, T.R., and Fenelon, J.M., 2018, Conceptual framework and trend analysis of water-level responses to hydrologic stresses, Pahute Mesa–Oasis Valley groundwater basin, Nevada, 1966-2016: U.S. Geological Survey Scientific Investigations Report 2018-5064, 89 p. [Also available at https://doi.org/10.3133/sir20185064.]

Jackson, T.R., Halford, K.J., Gardner, P.M., and Garcia, C.A., 2018, Evaluating micrometeorological estimates of groundwater discharge from Great Basin desert playas: Groundwater, v. 56, no. 6, 12 p. [Also available at https://doi.org/10.1111/gwat.12647.]

Johnson, A.G., Engott, J.A., Bassiouni, Maoya, and Rotzoll, Kolja, 2018, Spatially distributed groundwater recharge estimated using a water-budget model for the Island of Maui, Hawai`i, 1978–2007 (ver. 2.0, February 2018): U.S. Geological Survey Scientific Investigations Report 2014–5168, 53 p., [Also available at https://doi.org/10.3133/sir20145168.]

Kagan, J., and Caicco, S., 1992, Manual of Oregon actual vegetation: Portland, Oregon, Biological Resources Division-GAP analysis program, U.S. Fish and Wildlife Service.

Laczniak, R.J., DeMeo, G.A., Reiner, S.R., Smith, J.L., and Nylund, W.E., 1999, Estimates of ground-water discharge as determined from measurements of evapotranspiration, Ash Meadows area, Nye County, Nevada: U.S. Geological Survey Water-Resources Investigations Report 99-4079, 70 p. [Also available at https://pubs.usgs.gov/wri/wri994079/.]

Laczniak, R.J., Flint, A.L., Moreo, M.T., Knochenmus, L.A., Lundmark, K.W., Pohll, G., Carroll, R.W.H., Smith, J.L., Welborn, T.L., Heilweil, V.M., Pavelko, M.T., Hershey, R.L., Thomas, J.M., Earman, S., and Lyles, B.F., 2008, Ground-water budgets, in Welch, A.H., Bright, D.J., and Knochenmus, L.A., eds., Water resources of the basin and range carbonate-rock aquifer system, White Pine County, Nevada, and adjacent areas in Nevada and Utah: U.S. Geological Survey Scientific Investigations Report 2007-5261, p. 43–68. [Also available at https://pubs.usgs.gov/sir/2007/5261/section5.html.]

Lee, K.K., and Risley, J.C., 2002, Estimates of ground-water recharge, base flow, and stream reach gains and losses in the Willamette River Basin, Oregon: U.S. Geological Survey Water-Resources Investigations Report 01–4215, 52 p. [Also available at https://pubs.usgs.gov/wri/2001/4215/wri01-4215.pdf.]

Leonard, A.R., 1970, Ground-water resources in Harney Valley, Harney County, Oregon, Oregon State Engineer Ground Water Report No. 16, 85 p. [Also available at http://digital.osl.state.or.us/islandora/object/osl%3A12093]

Linsley, R. K., Jr., Kohler, M.A., and Paulhus, J. L. H., 1982, Hydrology for engineers: New York, McGraw-Hill, 508 p.

Lovelace, J.K., 2009, Methods for estimating water withdrawals for livestock in the United States, 2005: U.S. Geological Survey Scientific Investigations Report 2009-5041, 7 p [Also available at https://pubs.er.usgs.gov/publication/sir20095041.]

Masbruch, M.D., Heilweil, V.M., Buto, S.G., Brooks, L.E., Susong, D.D., Flint, A.L., Flint, L.E., and Gardner, P.M., 2011, Estimated groundwater budgets, chap. D of Heilweil, V.M., and Brooks, L.E., eds., Conceptual model of the Great Basin carbonate and alluvial aquifer system: U.S. Geological Survey Scientific Investigations Report 2010-5193, 191 p. [Also available at https://pubs.usgs.gov/sir/2010/5193/.]

Mayer, T.M., Roy, R., Hallock, T., Janssen, K., 2007, Hydrology and water quality at Malheur National Wildlife Refute: U.S. Fish and Wildlife Service, 132 p., accessed September 15, 2021, at https://ecos.fws.gov/ServCat/DownloadFile/5535?Reference=5826.

Meinzer, O.W., 1927, Plants as indicators of groundwater: U.S. Geological Survey Water-Supply Paper 577, 95 p. [Also available at https://pubs.usgs.gov/wsp/0577/report.pdf.]

Meyers, T.P., and Baldocchi, D.D., 2015, Current micrometeorological flux methodologies with applications in agriculture, in Micrometeorology in agricultural systems: New York, John Wiley & Sons, Ltd, p. 381–396.

Miller, M.P., Johnson, H.M., Susong, D.D., and Wolock, D.M., 2015, A new approach for continuous estimation of baseflow using discrete water quality data—Method description and comparison with baseflow estimates from two existing approaches: Journal of Hydrology (Amsterdam), v. 522, p. 203–210.

Moreo, M.T., Laczniak, R.J., and Stannard, D.I., 2007, Evapotranspiration rate measurements of vegetation typical of ground-water discharge areas in the Basin and Range carbonate-rock aquifer system, Nevada and Utah, September 2005–August 2006: U.S. Geological Survey Scientific Investigations Report 2007–5078, 36 p. [Also available at https://pubs.usgs.gov/sir/2007/5078/.]

Mozingo, H.N., 1987, Shrubs of the Great Basin, a natural history: Reno, University of Nevada Press, 342 p.

Nagler, P., Glenn, E., Nguyen, U., Scott, R., and Doody, T., 2013, Estimating Riparian and Agricultural Actual Evapotranspiration by Reference Evapotranspiration and MODIS Enhanced Vegetation Index: Remote Sensing (Basel), v. 5, no. 8, p. 3849–3871.

Nash, J.E., and Sutcliffe, J.V., 1970, River flow forecasting through conceptual models part I—A discussion of principles: Journal of Hydrology (Amsterdam), v. 10, no. 3, p. 282–290.

Neff, B.P., Day, S.M., Piggott, A.R., and Fuller, L.M., 2005, Base flow in the Great Lakes Basin: U.S. Geological Survey Scientific Investigations Report 2005–5217, 23 p. [Also available at https://pubs.usgs.gov/sir/2005/5217/pdf/SIR2005-5217.pdf.]

Nichols, W.D., 2000, Regional ground-water evapotranspiration and ground-water budgets, Great Basin, Nevada: U.S. Geological Survey Professional Paper 1628, 3 chaps. + 4 plates, 82 p. [Also available at http://pubs.er.usgs.gov/publication/pp1628.]

Nielsen, M.G., 2019, Soil-Water-Balance (SWB) model archive used to simulate potential annual recharge in Maine, 1991–2015: U.S. Geological Survey data release, https://doi.org/10.5066/P9GRP7DH.

Oregon Health Authority, 2019a, Oregon public health, drinking water data online, inventory by county, Grant County: Oregon Health Authority, accessed November 18, 2019, at https://yourwater.oregon.gov/countyinventory.php?county=Grant&actstat=A&regag=ALL&source=GW&includeNP=y.

Oregon Health Authority, 2019b, Oregon public health, drinking water data online, inventory by county, Harney County: Oregon Health Authority, accessed November 18, 2019, at https://yourwater.oregon.gov/countyinventory.php?county=Harney&actstat=A&regag=ALL&source=GW&includeNP=y.

Oregon Water Resources Board, 1967, Sixth Biennial Report, Various Basin studies completed as of June 30, 1967 including North Coast. Mid Coast, South Coast, Willamette, Umpqua, Rogue, Sandy, Hood, Deschutes, Goose, and Summer Lakes, John Day, Umatilla, Malheur Lake, Grande Ronde, and Powder, 40 p.

Oregon Water Resources Department, 2015, A Work Plan to Investigate the Harney Basin Groundwater Resources with Emphasis in the Greater Harney Valley Area: Draft 3 from Groundwater Hydrology Section, Oregon Water Resources Department, November 2015, Salem, Oregon.

Oregon Water Resources Department, 2016, Rule 690-512-0020—Groundwater use in the Greater Harney Valley Groundwater Area of Concern: Oregon Secretary of State, accessed July 7, 2020, at https://secure.sos.state.or.us/oard/viewSingleRule.action?ruleVrsnRsn=180246.

Oregon Water Resources Department, 2018, Water Availability Reporting System (WARS): Oregon Water Resources Department, https://apps.wrd.state.or.us/apps/wars/wars_display_wa_tables/MainMenu1.aspx.

Oregon Water Resources Department, 2019a, Groundwater information system: Oregon Water Resources Department, accessed August 28, 2019, at https://apps.wrd.state.or.us/apps/gw/gw_info/gw_info_report/Default.aspx.

Oregon Water Resources Department, 2019b, Water use reporting–City of Burns: Oregon Water Resources Department, accessed September 12, 2019, at https://apps.wrd.state.or.us/apps/wr/wateruse_query/wr_wur_entity_report.aspx?directory_id=136206&start_year=&end_year=.

Oregon Water Resources Department, 2019c, Water use reporting–City of Hines: Oregon Water Resources Department, accessed September 12, 2019, at https://apps.wrd.state.or.us/apps/wr/wateruse_query/wr_wur_entity_report.aspx?directory_id=106094&start_year=&end_year=.

Oregon Water Resources Department, 2019d, Water use reporting–City of Seneca: Oregon Water Resources Department, accessed September 12, 2019, at https://apps.wrd.state.or.us/apps/wr/wateruse_query/wr_wur_entity_report.aspx?directory_id=106189&start_year=&end_year=.

Oregon Water Resources Department, 2019e, Well log information system: Oregon Water Resources Department, accessed September 4, 2019, at https://apps.wrd.state.or.us/apps/gw/well_log/Default.aspx.

Oregon Water Resources Department, 2020, Miscellaneous streamflow measurements: Oregon Water Resources Department, accessed September 17, 2020, at https://apps.wrd.state.or.us/apps/sw/misc_measurements_view_only/.

Pinder, G.F., and Jones, J.F., 1969, Determination of the ground-water component of peak discharge from the chemistry of total runoff: Water Resources Research, v. 5, no. 2, p. 438-445.

OSIP (Oregon Statewide Imagery Program), 2017, Oregon Statewide Imagery Program data for eastern Oregon: OSIP, accessed June, 2021, at https://imagery.oregonexplorer.info/arcgis/services/OR_2017/OR_2017_SL/ImageServer/WMSServer?request=GetCapabilities&service=WMS.

Piper, A.M., Robinson, T.W., and Park, C.F., 1939, Geology and ground-water resources of the Harney Basin, Oregon: U.S. Geological Survey Water-Supply Paper 841, 189 p. [Also available at https://pubs.usgs.gov/wsp/0841/report.pdf.]

Philips, K.S., and Van Denburgh, A.S., 1971, Hydrology and geochemistry of Abert, Summer, and Goose Lakes, and other closed-basin lakes in south-central Oregon: U.S. Geological Survey Professional Paper 502-B, 84 p. [Also available at https://pubs.usgs.gov/pp/0502b/report.pdf.]

Portland State University Population Research Center, 2019a, 2010 census profiles, Oregon cities alphabetically A-C: Portland State University Population Research Center, accessed September 17, 2019, at https://www.pdx.edu/population-research/census-2010.

Portland State University Population Research Center, 2019b, 2010 census profiles, Oregon cities alphabetically H-L: Portland State University Population Research Center, accessed September 17, 2019, at https://www.pdx.edu/population-research/census-2010.

Portland State University Population Research Center, 2019c, 2010 census profiles, Oregon cities alphabetically R-S: Portland State University Population Research Center, accessed September 17, 2019, at https://www.pdx.edu/population-research/census-2010.

PRISM Climate Group, 2019, Parameter-elevation Regressions on Independent Slopes Model (PRISM) for 1981–2010: Corvallis, Oregon State University, PRISM database, accessed November 15, 2019, at http://prism.oregonstate.edu.

R Core Team, 2013, R—A Language and Environment for Statistical Computing: R Core Team, http://www.R-project.org/.

Roark, D.M., and Healy, D.F., 1998, Quantification of deep percolation from two flood-irrigated alfalfa fields, Roswell Basin, New Mexico: U.S. Geological Survey Water Resources Investigation Report 98-4096, 33 p. [Also available at https://pubs.er.usgs.gov/publication/wri984096.]

Robinson, T.W., 1958, Phreatophytes: U.S. Geological Survey Water Supply Paper 1423, 84 p. [Also available at http://pubs.er.usgs.gov/publication/wsp1423.]

Robison, J.H., 1968, Estimated existing and potential groundwater storage in major drainage basins in Oregon Open-File Report 68-232, 12 p. + 2 plates. [Also available at https://doi.org/10.3133/wsp78.]

Russell, I.C., 1903, Preliminary report on artesian basins in southwestern Idaho and southeastern Oregon: U.S. Geological Survey Water-Supply Paper 78, 53 p. [Also available at https://doi.org/10.3133/wsp78.]

Sarwar, A., Peters, R.T., Mehanna, H., Amini, M.Z., and Mohamed, A.Z., 2019, Evaluating water application efficiency of low and mid elevation spray application under changing weather conditions: Agricultural Water Management, v. 221, p. 84–91.

Senay, G.B., Bohms, S., Singh, R.K., Gowda, P.H., Velpuri, N.M., Alemu, H., and Verdin, J.P., 2013, Operational Evapotranspiration Mapping Using Remote Sensing and Weather Datasets—A New Parameterization for the SSEB Approach: Journal of the American Water Resources Association, v. 49, no. 3, p. 577–591.

Smith, J.L., Laczniak, R.J., Moreo, M.T., and Welborn, T.L., 2007, Mapping evapotranspiration units in the Basin and Range carbonate-rock aquifer system, White Pine County, Nevada, and adjacent areas in Nevada and Utah: U.S. Geological Survey Scientific Investigations Report 2007–5087, 20 p. [Also available at https://pubs.usgs.gov/sir/2007/5087/.]

Soil Survey Staff, Soil Survey Geographic (SSURGO) Database: Natural Resources Conservation Service, United States Department of Agriculture, accessed March 29, 2018, at https://sdmdataaccess.sc.egov.usda.gov.

Stewart, M., Cimino, J., and Ross, M., 2007, Calibration of Base Flow Separation Methods with Streamflow Conductivity: Ground Water, v. 45, no. 1, p. 17–27.

Stromberg, J.C., 2013, Root patterns and hydrogeomorphic niches of riparian plants in the American Southwest: Journal of Arid Environments, v. 94, p. 1–9.

Trost, J.J., Roth, J.L., Westenbroek, S.M., and Reeves, H.W., 2018, Simulation of potential groundwater recharge for the glacial aquifer system east of the Rocky Mountains, 1980–2011, using the Soil-Water-Balance model: U.S. Geological Survey Scientific Investigations Report 2018–5080, 51 p. [Also available at https://doi.org/10.3133/sir20185080.]

Twine, T.E., Kustas, W.P., Norman, J.M., Cook, D.R., Houser, P.R., Meyers, T.P., Prueger, J.H., Starks, P.J., and Wesely, M.L., 2000, Correcting eddy-covariance flux underestimates over a grassland: Agricultural and Forest Meteorology, v. 103, no. 3, p. 279–300.

U.S. Department of Agriculture, 2016, National Agricultural Imagery Program (NAIP) information sheet: U.S. Department of Agriculture, 2 p., accessed January, 2020, at https://www.fsa.usda.gov/Assets/USDA-FSA-Public/usdafiles/APFO/support-documents/pdfs/naip_infosheet_2016.pdf

U.S. Department of Agriculture, 2018, Livestock report, May 14, 2018–County estimates–Cattle: National Agricultural Statistics Service, U.S. Department of Agriculture, accessed September 16, 2019, at https://www.nass.usda.gov/Statistics_by_State/Oregon/Publications/Livestock_Report/index.php.

U.S. Department of Agriculture, 2019a, National Agricultural Statistics Service, Oregon Field Office, Livestock report, June 14, 2019–County estimates–Cattle: U.S. Department of Agriculture, accessed September 16, 2019, at https://www.nass.usda.gov/Statistics_by_State/Oregon/Publications/Livestock_Report/index.php.

U.S. Department of Agriculture, 2019b, National Agricultural Statistics Service, 2017 Census of agriculture–Oregon State and county data: U.S. Department of Agriculture, Geographic area Series, v. 1, part 37, AC-17-A-37, p. 329. [Also available at https://www.nass.usda.gov/Publications/AgCensus/2017/Full_Report/Census_by_State/Oregon/index.php.]

U.S. Geological Survey, 2016, National hydrography dataset (NHD) best resolution 20161109 for Oregon State or Territory FileGDB 10.1 Model Version 2.2.1: U.S. Geological Survey, accessed November, 2016, at https://www.sciencebase.gov/catalog/item/5136012ce4b03b8ec4025bf7.

U.S. Geological Survey, 2021, USGS National Water Information System: U.S. Geological Survey web interface, https://doi.org/10.5066/F7P55KJN.

Wahl, K.L., and Wahl, T.L., 1995, Determining the flow of Comal Springs at New Braunfels, Texas, *in* Proceedings of Texas Water 95, August 16–17, 1995, San Antonio, Texas: American Society of Civil Engineers, p. 77–86.

Walker, G.W., 1977, Geologic map of Oregon east of the 121st meridian: U.S. Geological Survey Miscellaneous Investigations Series Map I-902. [Also available at https://doi.org/10.3133/i902.]

Waring, G.A., 1908, Geology and water resources of a portion of south-central Oregon: U. S. Geological Survey Water-Supply Paper 220, 86 p. [Also available at https://doi.org/10.3133/wsp220.]

Waring, G.A., 1909, Geology and water resources of the Harney Basin region, Oregon: U.S. Geological Survey Water-Supply Paper 231, 93 p. [Also available at https://doi.org/10.3133/wsp231.]

Washington State Department of Ecology, 2005, Determining irrigation efficiency and consumptive use: Washington State Department of Ecology GUID-1210. [Also available at https://apps.ecology.wa.gov/publications/documents/2011076.pdf.]

Westenbroek, S.M., Kelson, V.A., Dripps, W.R., Hunt, R.J., and Bradbury, K.R., 2010, SWB—A modified Thornthwaite-Mather Soil-Water-Balance code for estimating groundwater recharge: U.S. Geological Survey Techniques and Methods 6–A31, 60 p. [Also available at https://pubs.usgs.gov/tm/tm6-a31/.]

Western Regional Climate Center, 2019, Western U.S. climate historical summaries: Desert Research Institute Web site, accessed November, 2019, at http://www.wrcc.dri.edu/Climsum.html.

Western Regional Climate Center, 2020, Comparison Table of Monthly Average Pan Evaporation or the Western U.S.: Desert Research Institute Web site, accessed December, 2020, at https://wrcc.dri.edu/Climate/comp_tables.php.

Williams, M.W., and Melack, J.M., 1991, Precipitation chemistry in and ionic loading to an Alpine Basin, Sierra Nevada: Water Resources Research, v. 27, no. 7, p. 1563–1574.

Wilson, J.L., and Guan, H., 2004, Mountain-block hydrology and mountain-front recharge, *in* Hogan, J., Phillips, F., and Scanlon, B., eds., Groundwater recharge in a desert environment—The Southwestern United States: Washington, DC, AGU. [Also available at https://agupubs.onlinelibrary.wiley.com/doi/pdf/10.1029/009WSA08.]

Wilson, K., Goldstein, A., Falge, E., Aubinet, M., Baldocchi, D., Berbigier, P., Bernhofer, C., Ceulemans, R., Dolman, H., Field, C., Grelle, A., Ibrom, A., Law, B.E., Kowalski, A., Meyers, T., Moncrieff, J., Monson, R., Oechel, W., Tenhunen, J., Valentini, R., and Verma, S., 2002, Energy balance closure at FLUXNET sites: Agricultural and Forest Meteorology, v. 113, no. 1-4, p. 223–243.

Wolock, D.M., 2003a, Base-flow index grid for the conterminous United States: U.S. Geological Survey Open-File Report 2003–263, accessed April 30, 2015, at https://water.usgs.gov/lookup/getspatial?bfi48grd.

Wolock, D.M., 2003b, Estimated mean annual natural groundwater recharge in the conterminous United States: U.S. Geological Survey Open-File Report 2003–311, digital data set, accessed April 30, 2015, at https://water.usgs.gov/lookup/getspatial?rech48grd.

Young, A.A., and Blaney, H.F., 1942, Use of water by native vegetation: California Department of Public Works, Division of Water Resources, bulletin 50, 160 p.

Appendix 1.   Description of Climate Data and Processing of Satellite Data

Climate Data

Gridded climate data used in this study include PRISM (Parameter-elevation Relationships on Independent Slopes Model; PRISM climate group, 2019) and GridMET (Abatzoglou, 2013) datasets. PRISM is a regression-based model of the conterminous United States that interpolates between precipitation measurements and accounts for physiographically complex landscapes using an 80-meter digital-elevation model (Daly and others, 2008). GridMET is a weather dataset that combines the North American Land Data Assimilation System Phase 2 (NLDAS-2) model and PRISM to improve the temporal accuracy of gridded climate data (with respect to PRISM) while maintaining the spatial accuracy of PRISM. PRISM was used to evaluate the 30-year (yr) mean (1981–2010) precipitation at a spatial resolution of 800-m and long-term (more than 100-yr) precipitation patterns in the basin at a resolution of 4-kilometer (km) (2.5-mile [mi]). GridMET was used to estimate water-budget components 1982–2016. Data obtained from GridMET included (1) precipitation and maximum and minimum air temperature time-series data for recharge estimation, (2) grass-reference ET (ET_o) and precipitation data were acquired for groundwater-discharge estimation, and (3) alfalfa-reference ET (ET_r) and precipitation data were acquired for crop-ET estimation. All climate datasets were projected into the same coordinate system as other datasets prior to use in water-budget estimates. GridMET daily datasets used for recharge estimation were resampled to 1-km resolution and GridMET growing-season and water-year datasets were resampled to 30-m resolution for compatibility with 30-m (98.4-feet [ft]) Landsat imagery.

The accuracy of gridded precipitation from PRISM and GridMET was confirmed by comparison with measurements from meteorological sites in and adjacent to the Harney Basin. Annual precipitation measured at 32 sites with data collected during 1900–2016 was compared with PRISM estimates at the location of the meteorological site (table 1); annual precipitation measured at a subset of 23 sites with data collected during 1979–2016 was compared with the shorter GridMET record (fig. 1.1). Ordinary least squares relations indicate that PRISM and GridMET datasets are within 4 and 6 percent of measurements, respectively. Differences between measured and gridded (PRISM and GridMET) precipitation likely reflect the generalized area of gridded data: 4-km for PRISM and 2.5-mi for GridMET. Both climate models adequately estimate annual precipitation below about 30 in with no appreciable bias; however, at sites where the measured annual precipitation exceeds 30 in, PRISM tends to overestimate annual precipitation and GridMET tends to underestimate annual precipitation. Low-elevation, low-magnitude (less than 11 in/yr) estimates of

precipitation from GridMET were within 2 percent of measurements made at 10 sites within and adjacent to the Harney Basin (figs. 2, 1.1).

Although estimates of ET_o from GridMET often exceed measured values in irrigated areas (Abatzoglou, 2013; see section "Irrigation Pumpage"), no bias is expected in areas of natural vegetation. The overestimation in irrigated areas is caused by two factors: (1) at the scale of an irrigated field, ET_o often is depressed relative to regional values because the increase in the latent-heat flux over irrigated agricultural fields locally decreases the air temperature and ET_o when compared to surrounding non-irrigated areas and (2) GridMET ET_o values are calibrated to regional climate trends and integrated into 4-km grid cells, which may contain irrigated land and natural vegetation. Localized biases that might be observed in irrigated areas likely are not uncharacteristic of natural non-irrigated areas in the Harney Basin groundwater ET area (GETA).
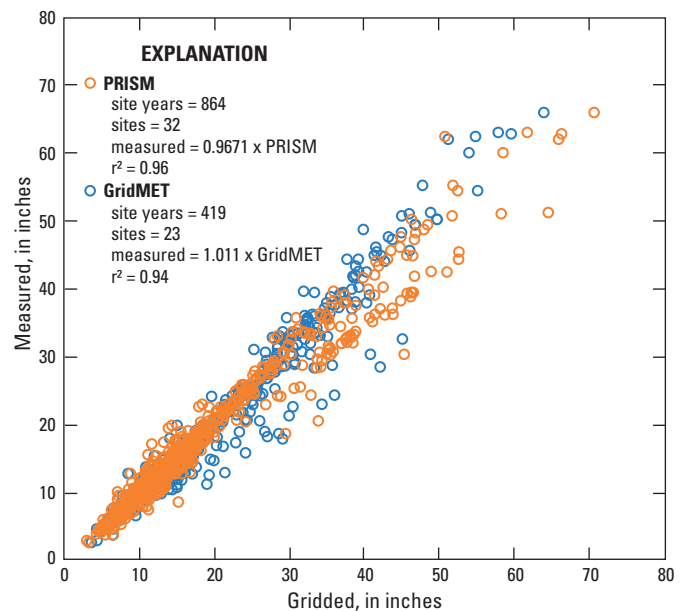
Figure 1.1.   Annual measured and gridded precipitation from PRISM (1900–2016) and GridMET (1979–2016) within and adjacent to the Harney Basin, southeastern Oregon. PRISM is the Parameter-elevation Relationships on Independent Slopes Model (PRISM climate group, 2019) and GridMET combines the North American Land Data Assimilation System Phase 2 model and PRISM (Abatzoglou, 2013). Parameter r^2 is the coefficient of determination from the ordinary least-squares relation.

Satellite Data

Satellite imagery was used to characterize vegetation cover and estimate ET in this study. Vegetation was characterized using vegetation and water indices and landscape texture datasets generated from satellite data. Imagery included reflectance and thermal data from Landsat imagery (30-m resolution) acquired during 1984–2016 and 2016 imagery from the National Agricultural Imagery Program (NAIP; 1-m resolution; U.S. Department of Agriculture, 2016).

Imagery acquired by Landsat 5 Thematic Mapper, Landsat 7 Enhanced Thematic Mapper Plus, and Landsat 8 Operational Land Imager were used for this study. Landsat scene locations are identified using a world reference system 2 (WRS2) path and row number. The areas evaluated in this study are in WRS2 path 43 row 30. All scenes were atmospherically corrected to Surface Reflectance by the U.S. Geological Survey Center for Earth Resources Observation and Science (EROS) data center (Masek and others, 2006; LaSRC; Vermote and others, 2016).

Forty-six Landsat scenes collected over 23 years (spanning 1987–2015) were acquired for ET-unit delineation and ET_g estimation in non-irrigated areas (fig. 1.2). Acquired scenes represent a subset of available scenes (1982–2016) where skies were free of clouds, vegetation canopies were green and active, and little to no antecedent precipitation was measured at nearby weather stations for at least 12 days prior to the Landsat overpass. All scenes were acquired in July and August to represent "growing-season" conditions when phreatophytic vegetation within the GETA is actively transpiring and shrubs have reached maximum growth, but the vigor of early summer annual plants is presumed to be at a minimum. Additional scenes were acquired during 1984–2018 to estimate crop ET and groundwater pumpage (see section "Irrigation Pumpage" and Beamer and others, 2021).

A combination of Landsat bands was used to identify and characterize natural and anthropogenic features within the image. For example, healthy vegetation absorbs light in the red wavelengths for use in photosynthesis and strongly reflects light in the near infrared wavelengths. Vegetation indices, such as the Normalized Difference Vegetation Index (NDVI; Rouse and others, 1974) and Enhanced Vegetation Index (EVI; Huete and others, 1999) use the contrast between these distinct absorption and reflectance features to help identify vegetated areas and to characterize the health and spatial extent of vegetation communities. Standing water strongly reflects light in the short-wave infrared wavelengths and land-surface moisture content is distinguished with short-wave infrared wavelengths. The Modified Normalized-Difference Water Index (MNDWI; Xu, 2006) uses the combination of these wavelengths to distinguish water features and perennially wet vegetation communities from the surrounding dry landscape.

The EVI (Huete and others, 1999) was calculated from each of the 46 scenes selected for ET unit and ET_g analysis. The EVI is a unitless single-band image with valid values ranging between −1 and 1. Index values in vegetated areas are nearly always greater than 0 and, generally, the healthier and denser the vegetation, the closer the vegetation index value is to 1. Open water and salt-covered bare soil commonly have index values between −1 and 0. Spurious values greater than 1 occur where cloud cover exists. In this analysis, negative EVI values were set to zero and spurious values greater than 1 were set to null. Cells with spurious values covered less than 0.05 percent of the area where ET_g occurs. The confounding influence of soil moisture on EVI (Huete and others, 1984; Huete and Jackson, 1987; Karnieli and others, 1996) was minimized by ensuring that nearly 2 weeks had passed between the Landsat overpass and the previous precipitation event.

Various multi-band methods exist for extracting water features from satellite imagery while suppressing the influence of vegetated landscapes (Xu, 2006). The modified normalized-difference water index (MNDWI; Xu, 2006) was used to distinguish wet and dry vegetation and the normalized-difference moisture index (NDMI; Gao, 1996; Wilson and Sader, 2002) was used to identify flood-inundated areas. The MNDWI was calculated from the August 21, 2015, Landsat 8 image and used to distinguish wet ET units such as water features and
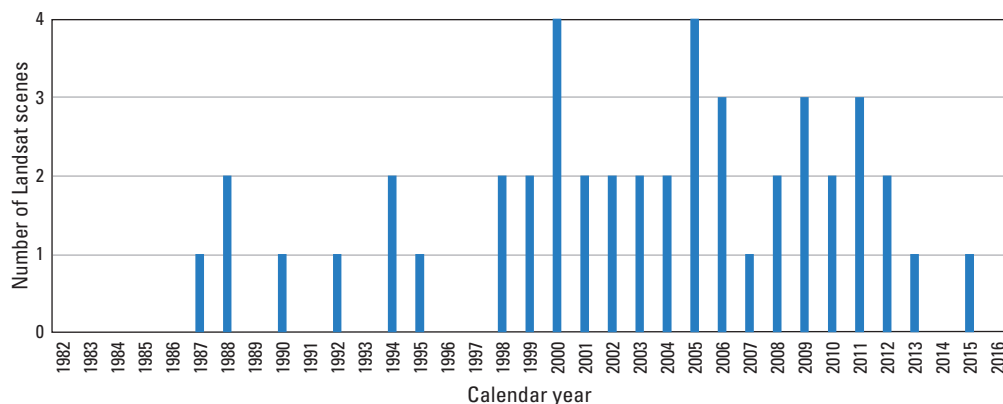
Figure 1.2.   Number of cloud-free and rain-free July and August Landsat scenes acquired each year during 1982–2016, Harney Basin, southeastern Oregon.

perennially wet vegetation communities within the GETA. MNDWI values range between -0.2 and 0.8 where a threshold of 0.09 distinguishes standing water from the surrounding landscape (Xu, 2006). Maximum NDMI distributions from Surface-Reflectance corrected Landsat 5 and seven scenes collected during March–July 2005 and 2011 were obtained from ClimateEngine (Huntington and others, 2017) and used to evaluate variable extents of surface-water flooding within the GETA (see subsection "Groundwater Evapotranspiration Rates for Wet Meadow, Riparian, and Marsh Evapotranspiration Units"). A NDMI threshold of 0.4 was used to distinguish flood-inundated areas on the Harney Basin lowlands (Wilson and Sader, 2002).

Landscape texture derived from high-resolution imagery provides information about vegetation community structure and can be used to distinguish smooth landscapes such as grassland or bare soil from rougher landscapes such as shrublands or forests (Franklin and others, 2000; Herold and others, 2003). Texture represents a comparison of image roughness or smoothness caused by the similarities or differences among individual and neighboring pixels. The texture image used in the random-forest classification (described in app. 3) represents the standard deviation of NDVI, computed from the 2016 NAIP imagery (1-m [3.28-ft] spatial resolution, 4-spectral bands: red, green, blue, near infrared) in Google Earth Engine using neighborhood statistics (Gorelick and others, 2017). The NDVI was first computed for all NAIP tiles within and surrounding the GETA. The standard deviation of NDVI image neighborhoods was computed using a 5-pixel-wide circular sliding window.

References Cited

Abatzoglou, J.T., 2013, Development of gridded surface meteorological data for ecological applications and modelling: International Journal of Climatology, v. 33, no. 1, p. 121–131.

Beamer, J.P., and Hoskinson, M.D., 2021, Historical irrigation water use and groundwater pumpage estimates in the Harney Basin, Oregon, 1991-2018: Oregon Water Resources Department Open File Report No. 2021-02, 53 p. [Also available at https://www.oregon.gov/owrd/wrdreports/OWRD_OFR_2021-02_Harney_Basin_METRIC_Irrigation_Use_Report.pdf.]

Daly, C., Halbleib, M., Smith, J.I., Gibson, W.P., Doggett, M.K., Taylor, G.H., Curtis, J., and Pasteris, P.P., 2008, Physiographically sensitive mapping of climatological temperature and precipitation across the conterminous United States: International Journal of Climatology, 34 p. [Also available at https://doi.org/10.1002/joc.1688.]

Franklin, S.E., Hall, R.J., Moskal, L.M., Maudie, A.J., and Lavigne, M.B., 2000, Incorporating texture into classification of forest species composition from airborne multispectral images: International Journal of Remote Sensing, v. 21, no. 1, p. 61–79.

Gao, B., 1996, NDWI—A normalized difference water index for remote sensing of vegetation liquid water from space: Remote Sensing of Environment, v. 58, no. 3, p. 257–266.

Glenn, E., Huete, A., Nagler, P., and Nelson, S., 2008, Relationship Between Remotely-sensed Vegetation Indices, Canopy Attributes and Plant Physiological Processes—What Vegetation Indices Can and Cannot Tell Us About the Landscape: Sensors (Basel), v. 8, no. 4, p. 2136–2160.

Gorelick, N., Hancher, M., Dixon, M., Ilyushchenko, S., Thau, D., and Moore, R., 2017, Google Earth Engine—Planetary-scale geospatial analysis for everyone: Remote Sensing of Environment, v. 202, p. 18–27.

Herold, M., Liu, X.H., and Clarke, K.C., 2003, Spatial Metrics and Image Texture for Mapping Urban Land Use: Photogrammetric Engineering and Remote Sensing, v. 69, no. 9, p. 991–1001.

Huete, A., Justice, C., and van Leeuwen, W., 1999, MODIS Vegetation Index (MOD 13), version 3. Algorithm Theoretical Basis Document. [Also available at https://modis.gsfc.nasa.gov/data/atbd/atbd_mod13.pdf.]

Huete, A.R., and Jackson, R.D., 1987, Suitability of spectral indices for evaluating vegetation characteristics on arid rangelands: Remote Sensing of Environment, v. 23, no. 2, p. 213–IN8.

Huete, A.R., Post, D.F., and Jackson, R.D., 1984, Soil spectral effects on 4-space vegetation discrimination: Remote Sensing of Environment, v. 15, no. 2, p. 155–165.

Huntington, J.L., Hegewisch, K.C., Daudert, B., Morton, C.G., Abatzoglou, J.T., McEvoy, D.J., and Erickson, T., 2017, Climate Engine—Cloud Computing and Visualization of Climate and Remote Sensing Data for Advanced Natural Resource Monitoring and Process Understanding: Bulletin of the American Meteorological Society, v. 98, no. 11, p. 2397–2410.

Karnieli, A., Shachak, M., Tsoar, H., Zaady, E., Kaufman, Y., Danin, A., and Porter, W., 1996, The effect of microphytes on the spectral reflectance of vegetation in semiarid regions: Remote Sensing of Environment, v. 57, no. 2, p. 88–96.

Masek, J.G., Vermote, E.F., Saleous, N.E., Wolfe, R., Hall, F.G., Huemmrich, K.F., Gao, F., Kutler, J., and Lim, T.-K., 2006, A Landsat Surface Reflectance Dataset for North America, 1990–2000: IEEE Geoscience and Remote Sensing Letters, v. 3, no. 1, p. 68–72.

PRISM Climate Group, 2019, Parameter-elevation Regressions on Independent Slopes Model (PRISM) for 1981–2010: Corvallis, Oregon State University, PRISM database, accessed November 15, 2019, at http://prism. oregonstate.edu.

Rouse, J.W., Haas, R.H., Schell, J.A., and Deering, D.W., 1974, Monitoring vegetation systems in the great plains with ERTS: Proceedings of the third Earth Resources Technology Satellite-1 Symposium, Washington D.C., NASA, Scientific and Technical Information Office, p. 309–317. [Also available at https://ntrs.nasa.gov/citations/ 19740022614.]

U.S. Department of Agriculture, 2016, National Agricultural Imagery Program (NAIP) Information Sheet: 2 p., accessed January, 2020, at https://www.fsa.usda.gov/Assets/USDA-FSA-Public/usdafiles/APFO/support-documents/pdfs/naip_ infosheet_2016.pdf.

Vermote, E., Justice, C., Claverie, M., and Franch, B., 2016, Preliminary analysis of the performance of the Landsat 8/ OLI land surface reflectance product: Remote Sensing of Environment, v. 185, p. 46–56.

Wilson, E.H., and Sader, S.A., 2002, Detection of forest harvest type using multiple dates of Landsat TM imagery: Remote Sensing of Environment, v. 80, no. 3, p. 385–396.

Xu, H., 2006, Modification of normalised difference water index (NDWI) to enhance open water features in remotely sensed imagery: International Journal of Remote Sensing, v. 27, no. 14, p. 3025–3033.

Appendix 2.   Groundwater Use by Phreatophytes in the Harney Basin Lowlands

Identifying Sources of Water Used by Phreatophytes

Stable isotopes of hydrogen and oxygen in water molecules have been used as conservative tracers to investigate water movement in the unsaturated zone (Barnes and Allison, 1988; Walvoord and others, 2004) and to identify water sources contributing to plant growth or total ET (White and others, 1985; Ehleringer and others, 1991; Chimner and Cooper, 2004; Scott and others, 2005). For most species, the stable isotopic composition of soil water remains unaltered during plant-water uptake and stem water reflects the integrated average isotopic composition of water from the various depths of water uptake. Some studies have documented hydrogen-isotope fractionation in halophytic coastal-wetland species (Lin and Sternberg, 1993), but the process has not been documented in desert halophytes.

Stable Isotope Sampling and Analyses

Samples for stable isotope analysis were collected from dominant plant species, shallow soil water, and shallow wells at multiple locations on the Harney Basin lowlands during July 2017 and 2018 when shallow soil moisture from precipitation was depleted and phreatophytes were more likely to be using groundwater (fig. 2.1; table 2.1). Sampling locations include Embree Bridge Rd (EB), N. Newton Rd (NN), S. Newton Rd (NS), north of Mud Lake (ML), near Malheur Field Station (MF), Dog Mountain (DM), and the northeastern valley lowlands (NE) (fig. 2.1). Plant-water samples include xylem water from woody stems in greasewood, rubber rabbitbrush, and big sagebrush and root water in saltgrass and basin wildrye. Saltgrass and basin wildrye roots were sampled rather than aboveground biomass because of the potential for isotopic fractionation in leaves (Gat and others, 2007). Stem and root samples were cut from 4 to 5 plants at each site and combined in a single sample bottle to create a composite sample. Soil samples were collected at three sites from depths of roughly 1.5 and 5 ft below land surface, and replicate samples from two locations at each site were composited into a single sample for analysis. All soil and plant samples were packaged immediately in airtight bottles. At the end of each day, samples were refrigerated until processed by the lab. Soil and plant-stem water were extracted at the lab using azeotropic distillation with toluene (Révész and Woods, 1990).

Groundwater samples were collected from the shallowest wells available near plant and soil collection locations; most samples were collected between the water table (12–20 ft below land surface) and 170 ft below land surface. Time series of stable isotope samples were collected during 2017–19 from Sodhouse Spring, Silvies River, and Donner und Blitzen River. The groundwater, spring, and stream samples are discussed in greater detail in Gingerich and others (2022).

Soil water, plant water, groundwater, and stream water were analyzed for stable isotopes of oxygen (^{18}O, ^{16}O) and hydrogen (^{2}H, ^{1}H) at the USGS Stable Isotope Laboratory in Reston, Virginia. Hydrogen analyses utilized a hydrogen equilibration technique (Coplen and others, 1991; Révész and Coplen, 2008) and oxygen analyses utilized a carbon dioxide equilibration technique (Epstein and Mayeda, 1953). Isotopic ratios of ^{2}H/^{1}H and ^{18}O/^{16}O were expressed as delta values relative to Vienna Standard Mean Ocean Water (in units of permil, ‰), where δ^{2}H is the hydrogen isotopic composition and δ^{18}O is the oxygen isotopic composition (Clark and Fritz, 1997).

Stable Isotopic Composition of Shallow Groundwater at Phreatophyte Study Sites

All groundwater samples plot to the right of the global meteoric water line (GMWL) and reflect local meteoric conditions (fig. 2.2). As water evaporates, heavier isotopes (^{18}O and ^{2}H) are preferentially retained in the residual liquid water and lighter isotopes (^{16}O and ^{1}H) are preferentially lost to the vapor phase. The stable isotopic composition of the residual liquid water has a more positive delta value than its unevaporated source. Increasingly evaporated samples originating from the same water source follow a linear trend having a slope less than slope of unevaporated local meteoric waters, which typically is subparallel to the GWML (Clark and Fritz, 1997). Using age-tracer data to calibrate hydrogen isotopic compositions, Gingerich and others (2022) characterized samples having a δ^{2}H value greater than -119 permil and less than about -105 permil as containing water primarily recharged after 1953, calling them "predominantly modern." Samples having a δ^{2}H value less than -122 permil were identified as having a large proportion of water recharged prior to 1953 and were called "predominantly premodern." Values of δ^{2}H greater than -105 permil likely have been evaporated and values less than -119 permil were recharged under different climate conditions that prevailed thousands or tens of thousands of years ago. This characterization can be useful for distinguishing soil water supplied by modern precipitation from soil water supplied by old groundwater.
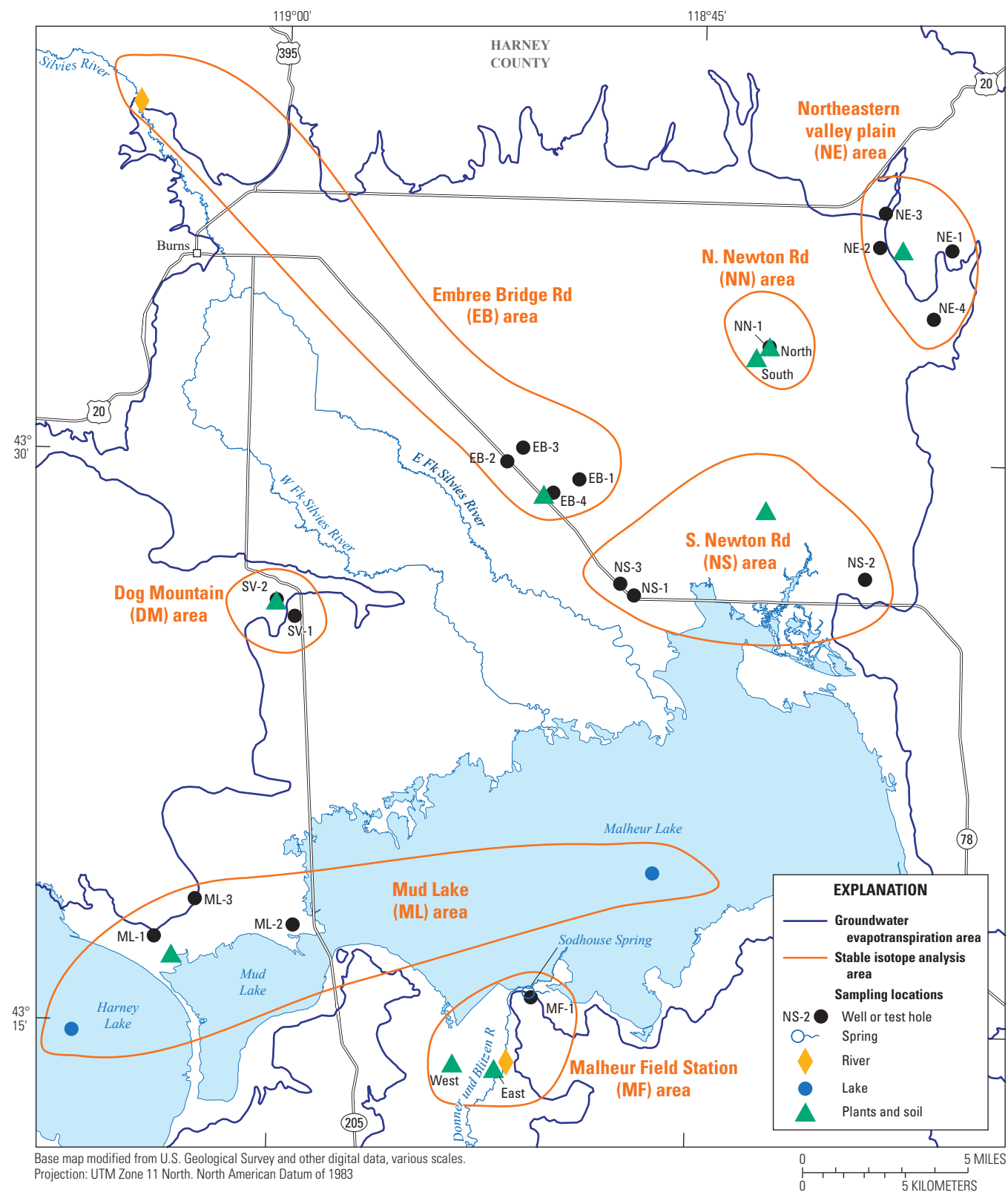
Figure 2.1.   Stable isotope sample locations and analysis areas, Harney Basin, southeastern Oregon. Sample locations and associated site information is provided in table 2.1.

Table 2.1.   Selected stable isotope samples and locations, Harney Basin, southeastern Oregon.

[**Analysis area**: Area used to group samples for analysis including Embree Bridge Rd (EB), N. Newton Rd (NN), north of Mud Lake (ML), near Malheur Field Station (MF), Dog Mountain (DM), S. Newton Rd (NS), and northeastern valley plain (NE). **Report/map ID**: ID discussed in report. **Depth of hole open interval**: Values represented as elevation. **Sample date**: Month/day/year. **Abbreviations**: ft, feet; ft bls, feet below land surface; ID, identifier; δ^2H, ratio of hydrogen-2 (deuterium) to hydrogen-1 in sampled compared to reference standard; $\delta^{18}O$, ratio of oxygen-18 to oxygen-16 in sampled compared to reference standard; permil, parts per thousand; NA, not available; OWRD, Oregon Water Resources Department; USGS, U.S. Geological Survey; WG, groundwater; WM, soil water; WP, plant water; WS, surface water; Unk, unknown; —, not applicable]

Analysis area	Report/map ID	USGS site number	OWRD well log ID	Sample type	Latitude (decimal degrees)	Longitude (decimal degrees)	Elevation (ft)	Depth of hole open interval/soil sample (ft bls) or plant name	Sample date	δ18O (permil)	δ2H (permil)
EB	—	432904118503201	—	WP	43.484417	-118.842194	4,118	Greasewood	7/19/2017	-14.1	-123.5
	—	432904118503201	—	WP	43.484417	-118.842194	4,118	Sagebrush	7/19/2017	-14.7	-124.0
	—	432904118503201	—	WP	43.484417	-118.842194	4,118	Rabbitbrush	7/19/2017	-13.7	-117.0
	EB-1	432928118491501	HARN0052315	WG	43.49125	-118.820944	4,123	Unk-180	4/11/2018	-14.8	-120.0
	EB-2	432954118515201	NA	WG	43.498444	-118.864528	4,124	NA	3/21/2018	-15.8	-127.0
	EB-3	433017118511801	HARN0052671	WG	43.504611	-118.855139	4,128	20–98	3/21/2018	-15.5	-125.0
	EB-4	432907118501101	NA	WG	43.485169	-118.836436	4,115	0–20	8/7/2019	-14.1	-114.0
	Silvies River at Fivemile Dam near Burns	433908119052000	—	WS	43.652444	-119.089611	4,181	—	10/18/2016	-14.8	-117.0
NN	North	433318118422821	—	WP	43.551031	-118.708208	4,129	Sagebrush	7/18/2018	-8.0	-104.7
	South	433246118425521	—	WP	43.546161	-118.716056	4,124	Sagebrush	7/18/2018	-11.8	-111.6
		433246118425520	—	WP	43.546161	-118.716056	4,124	Greasewood	7/18/2018	-15.1	-126.6
		433246118425522	—	WP	43.546161	-118.716056	4,124	Rabbitbrush	7/18/2018	-14.4	-127.6
		433246118425523	—	WP	43.546161	-118.716056	4,124	Saltgrass	7/18/2018	-10.2	-113.5
		433246118425524	—	WP	43.546161	-118.716056	4,124	Wildrye	7/18/2018	-9.5	-114.4
		433246118425510	—	WM	43.546161	-118.716056	4,124	1.5–1.9	7/18/2018	-13.6	-123.0
		433246118425511	—	WM	43.546161	-118.716056	4,124	4.7–5.1	7/18/2018	-16.7	-135.6
	NN-1	433270118385301	NA	WG	43.550919	-118.708244	4,129	0–12	8/7/2019	-15.7	-126.0
ML		431648119033420	—	WP	43.279903	-119.059466	4,109	Greasewood	7/18/2018	-10.3	-90.5
		431648119033422	—	WP	43.279903	-119.059466	4,109	Rabbitbrush	7/18/2018	-10.4	-100.6
		431648119033423	—	WP	43.279903	-119.059466	4,109	Saltgrass	7/18/2018	-8.6	-99.3
		431648119033410	—	WM	43.279903	-119.059466	4,109	1.5–1.8	7/18/2018	-10.1	-108.6
		431648119033411	—	WM	43.279903	-119.059466	4,109	4.6–5.2	7/18/2018	-10.4	-97.0
	ML-1	431715119041201	HARN0050950	WG	43.287417	-119.069861	4,124	40–65	4/26/2018	-12.5	-111.0
	ML-2	431737118591301	HARN0051086	WG	43.293639	-118.986917	4,114	40–60	3/22/2018	-7.9	-83.2
	ML-3	431815119024501	HARN0050399	WG	43.304167	-119.045889	4,176	84–110	3/22/2018	-15.6	-128.0
	Harney Lake	431444119070400	—	WS	43.245556	-119.117778	NA	—	7/20/1988	-2.6	-53.0
	Malheur Lake	431910118462000	—	WS	43.319444	-118.772222	NA	—	7/19/1988	-0.4	-40.0

Table 2.1. Selected stable isotope samples and locations, Harney Basin, southeastern Oregon.—Continued

[**Analysis area**: Area used to group samples for analysis including Embree Bridge Rd (EB), N. Newton Rd (NN), north of Mud Lake (ML), near Malheur Field Station (MF), Dog Mountain (DM), S. Newton Rd (NS), and northeastern valley plain (NE). **Report/map ID**: ID discussed in report. **Depth of hole open interval**: ID discussed in report. **Sample date**: Month/day/year. Values represented as elevation. **Abbreviations**: ft, feet; ft bls, feet below land surface; ID, identifier; δ²H, ratio of hydrogen-2 (deuterium) to hydrogen-1 in sampled compared to reference standard; δ¹⁸O, ratio of oxygen-18 to oxygen-16 in sampled compared to reference standard; permil, parts per thousand; NA, not available; OWRD, Oregon Water Resources Department; USGS, U.S. Geological Survey; WG, groundwater; WM, soil water; WP, plant water; WS, surface water; Unk, unknown; —, not applicable]
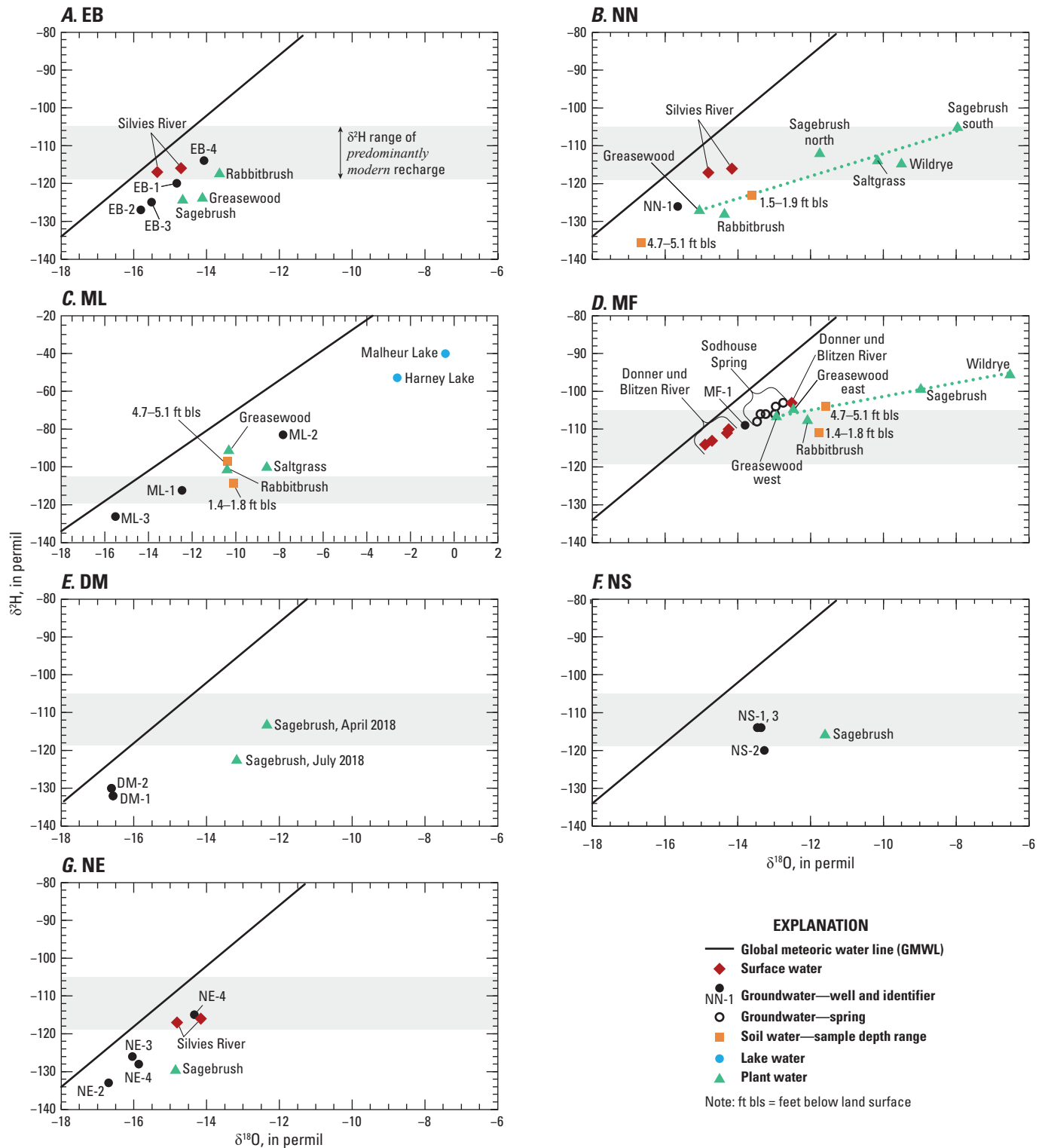
Analysis area	Report/map ID	USGS site number	OWRD well log ID	Sample type	Latitude (decimal degrees)	Longitude (decimal degrees)	Elevation (ft)	Depth of hole open interval/soil sample (ft bls) or plant name	Sample date	δ¹⁸O (permil)	δ²H (permil)
MF	East	431358118515320	—	WP	43.232688	-118.864717	4,109	Greasewood	7/19/2018	-12.5	-104.3
	West	431405118532320	—	WP	43.234716	-118.889757	4,113	Greasewood	7/19/2018	-13.0	-106.3
	—	431405118532321	—	WP	43.234716	-118.889757	4,113	Sagebrush	7/19/2018	-9.0	-99.0
	—	431405118532322	—	WP	43.234716	-118.889757	4,113	Rabbitbrush	7/19/2018	-12.1	-107.3
	—	431405118532324	—	WP	43.234716	-118.889757	4,113	Wildrye	7/19/2018	-6.5	-95.2
	—	431405118532310	—	WM	43.234716	-118.889757	4,113	1.4–1.8	7/19/2018	-11.8	-110.8
	—	431405118532311	—	WM	43.234716	-118.889757	4,113	4.7–5.1	7/19/2018	-11.6	-104.0
	MF-1	431551118503601	HARN0050707	WG	43.264194	-118.843333	4,187	88–111	10/18/2018	-13.8	-109.0
									4/19/2017	-12.8	-103.0
									7/18/2017	-13.4	-106.0
	Sodhouse Spring	10401600		WG	43.266386	-118.845144	4,106	—	10/16/2017	-13.0	-104.0
									4/20/2018	-13.2	-106.0
									7/19/2018	-13.5	-108.0
									1/18/2018	-13.0	-106.0
									5/23/2017	-14.3	-111.0
									7/18/2017	-12.5	-103.0
	Donner und Blitzen River near Voltage	431407118512501		WS	43.2355	-118.857417	4,109	—	10/16/2017	-14.7	-113.0
									1/18/2018	-14.9	-114.0
									4/20/2018	-14.3	-110.0
DM	—	432608119000521	—	WP	43.435449	-119.001376	4,123	Sagebrush	7/19/2018	-13.2	-122.2
									4/17/2018	-12.3	-112.8
	DM-1	432543118592401	HARN001103	WG	43.428722	-118.990028	4,110	18–40	3/21/2018	-16.6	-132.0
	DM-2	432609119000401	HARN0052629	WG	43.435778	-119.001056	4,124	82–105	4/12/2018	-16.6	-130.0
NS	—	432846118423021	—	WP	43.47935	-118.708555	4,114	sagebrush	7/19/2018	-11.6	-115.5
	NS-1	432628118471201	HARN0051276	WG	43.440978	-118.786694	4,112	20–62	4/18/2017	-13.4	-114.0
	NS-2	432700118385301	NA	WG	43.449919	-118.648097	4,115	0–11	8/7/2019	-13.3	-120.0
	NS-3	432646118474201	HARN0052234	WG	43.445972	-118.795028	4,108	52–76	4/11/2018	-13.5	-114.0
NE	—	433538118374421	—	WP	43.594223	-118.62912	4,142	sagebrush	7/19/2018	-14.9	-129.3
	NE-1	433540118355801	HARN0051205	WG	43.594361	-118.599417	4,208	75–165	3/22/2018	-15.9	-128.0
	NE-2	433543118383501	HARN0052411	WG	43.595228	-118.642958	4,136	0–755	10/18/2017	-16.7	-133.0
	NE-3	433637118382401	HARN0052029	WG	43.610269	-118.639889	4,144	48–165	10/18/2017	-16.1	-126.0
	NE-4	433531118363501	NA	WG	43.564278	-118.609806	4,139	NA	5/17/2018	-14.3	-115.0

Figure 2.2.   Stable hydrogen isotope ratios (δ²H) compared to stable oxygen isotope ratios (δ¹⁸O) in plant water, soil water, groundwater, and surface water at seven analysis areas in the Harney Basin, southeastern Oregon. Analysis areas include (*A*) Embree Bridge Rd (EB), (*B*) N. Newton Rd (NN), (*C*) north of Mud Lake (ML), (*D*) near Malheur Field Station (MF), (*E*) Dog Mountain (DM), (*F*) S. Newton Rd (NS), and (*G*) Northeastern valley lowlands (NE). Site and sample information is provided in table 2.1.

Stable isotopes of water in groundwater samples from the Harney Basin lowlands varied spatially and with depth, highlighting differences in recharge sources (Gingerich and others, 2022). In the ML area, the stable isotopic composition of groundwater from two of the wells (ML-1 and ML-3) are similar to other near-lake wells such as those in the MF and NS areas (figs. 2.1, 2.2; table 2.1). However, the isotopic composition of groundwater from ML-2 was considerably more positive and reflects mixing with evaporated water from Malheur Lake (Gingerich and others, 2022). In the MF area, stable isotope samples from Sodhouse Spring and the MF-1 well (fig. 2.1, table 2.1) are similar to samples from the Donner und Blitzen River near Voltage (fig. 2.2), indicating that groundwater in the MF area receives water lost from the river or wetlands (Gingerich and others, 2022). Groundwater stable isotope values in the shallowest EB area well (EB-4) and the most positive groundwater sample in the NE area (NE-4) are similar to modern river water sampled from the Silvies River north of Burns (fig. 2.2). Although Silvies River water does not reach the NE area, it serves as a proxy for other streams issuing from the Blue Mountain uplands and indicates that shallow groundwater in the EB and NE areas is recharged, in part, by infiltration of stream water and floodwater. Stable isotopes of water in groundwater samples from the NN and DM areas, some groundwater samples from the EB area, from deeper wells within the NE area, and from ML-3 in the ML area (fig. 2.1) are more negative than groundwater samples in other areas and reflect a source other than modern river water (Gingerich and others, 2022).

Stable Isotopic Composition of Soil Water at Phreatophyte Study Sites

Stable isotope samples of soil water were collected at three sites: NN, ML, and MF. Soil water originates either as local precipitation or the upward movement of groundwater by capillary forces. The isotopic composition of soil water reflects the evolution and mixing of these two sources. Due to its shallow depth, the stable isotopic composition of soil water sampled from the shallow root zone (1.4–1.9-ft bls) was expected to reflect evaporative fractionation of soil moisture supplied by precipitation, and possibly, of upward moving groundwater. Evaporative fractionation can be observed at the NN area, where the shallow soil-water stable isotope composition (1.5- to 1.9-ft bls) is enriched relative to groundwater (NN-1) and deeper soil water (4.7-5.1-ft bls) but has a δ^2H value, indicating predominantly premodern recharge and indicating a

groundwater source for the soil water (fig. 2.2B). The slope of trend lines connecting groundwater and the shallow soil water or connecting the deep and shallow soil-water samples are considerably less than the GMWL, indicating the shallow soil water has undergone evaporation. The deep soil-water stable isotope composition (4.7–5.1-ft depth) is more negative than groundwater (NN-1), which might be caused by the 0.5-mi distance between groundwater and soil sampling sites.

At the ML area, δ^2H of the shallow soil water was in the range of predominantly modern water, but the considerably more positive value of δ^2H from the deep soil-water sample was indicative of evaporation and could highlight replenishment of the deep soil-water reservoir by more evaporated episodic floodwater (figs. 2.1,2.2C). It is likely that both samples are mixtures of evaporated and unevaporated waters as the samples plot along a trend line connecting the most negative groundwater sample (ML-3) and the most evaporated surface-water sample (Malheur Lake) in the region, which is consistent with mixing of sources falling along the trend line. Evaporated samples would plot to the right of the regional trend. Like the ML-2 groundwater sample, the soil-water samples plot between regional groundwater (ML-1 and ML-3) and lake water, and likely reflect a mixture of those two end-member sources–a mixture containing slightly more regional groundwater and less lake water than ML-2. The soil water in the ML area is consistent with a groundwater source that is a mixture of lake water and regional groundwater and indicates that the capillary fringe above the water table extends to within 2 feet of land surface.

The shallow and deep soil-water compositions at the MF area exhibit the same pattern observed at ML: the shallow soil-water sample was well within the range of predominantly modern recharge whereas the deeper soil-water was more positive and likely had experienced some evaporation (figs. 2.1, 2.2D). Both soil-water samples plot in the range of samples from nearby surface water, groundwater, and spring water, but are shifted to the right of those samples. A shift to the right indicates they are derived from a water source plotting along the same regional trend line but have undergone evaporation. Gingerich and others (2022) demonstrated that the shallow groundwater, spring water, and late-summer surface water in this region are indistinguishable, therefore the soil water at MF could be derived from infiltration of episodic or seasonal floodwater from the lower Donner und Blitzen River or from the upward movement of groundwater by capillary action. Despite the source, the soil water appears to have experienced in situ evaporative fractionation to a depth of 5 feet.

Sources of Water Used by Phreatophytes

At the NN and MF areas, stable isotopes of water from sagebrush, saltgrass (NN only), and basin wildrye were enriched relative to local groundwater, whereas samples from greasewood and rabbitbrush were similar to groundwater (figs. 2.2*B, D*). Plant water in sagebrush, wildrye, and saltgrass was more enriched than the shallowest soil-water sample, indicating root-water uptake likely occurs from depths shallower than 1.5-ft bls where soil water likely is a mixture of groundwater and precipitation or precipitation only. Because area-specific measurements of precipitation were not made, the relative proportion of groundwater and precipitation in shallow soil water could not be determined. The stable isotopes of water from greasewood and rabbitbrush were similar to local groundwater in their respective analysis areas, indicating root-water uptake likely occurs at or just above the water table (figs. 2.2*B, D*).

At the ML area, all plant-water samples have a similar stable isotope composition and plot on the linear trend relating nearby groundwater samples. The similarity of stable isotope compositions among plants and groundwater at ML indicates all plants are transpiring unfractionated groundwater (fig. 2.2*C*).

Like the ML area, all plant-water samples at the EB area have a similar stable isotope composition and plot near the linear trend relating nearby groundwater samples (fig. 2.2*A*). Unlike plants at the ML area, however, all plant water at EB was shifted slightly to the right of nearby groundwater indicating the water is slightly evaporated relative to local groundwater. Greasewood and sagebrush must be utilizing evaporated local groundwater because δ^2H in those samples are more negative than the range of predominantly modern recharge. Soil-water samples were not collected at this location, but they likely are accessing slightly evaporated soil water derived from local groundwater. The δ^2H value from the rabbitbrush sample falls within the range of predominantly modern

recharge and could be derived from recent precipitation or upward moving groundwater, but most likely is utilizing a mixture of both sources.

The source of stem water in sagebrush varied by location and plant association across the basin and indicates that it is an opportunistically phreatophytic shrub. At the EB, NN, and MF areas, sagebrush was collocated with greasewood and rubber rabbitbrush which used groundwater at all sites where they occurred (fig. 2.2). However, the stable isotopic composition of sagebrush stem water was similar to groundwater only at the EB area. At the NN and MF areas, the stable isotopic composition of sagebrush stem water was substantially more positive than local groundwater, often had δ^2H value exceeding the upper range of predominantly modern recharge, and the slope of the line connecting sagebrush stem water and local groundwater was substantially less than the slope of the GMWL. Collectively, this evidence indicates that sagebrush at NN and MF utilizes a highly evaporated water source, which likely is a mixture of precipitation and groundwater. At DM and NS analysis areas where sagebrush was the dominant shrub and other phreatophytes were absent, the stable isotope values of sagebrush water were shifted to the right and more enriched than nearby groundwater samples (figs. 2.2*E, F*), similar to sagebrush water samples at NN and MF analysis areas and indicating opportunistic use of precipitation and evaporated groundwater.

Like the SV and NS areas, sagebrush was the dominant shrub in the NE area and other phreatophytes were absent. The isotopic composition of sagebrush stem water at NE had a similar range but was shifted to the right of local groundwater samples (fig. 2.2). The δ^2H value was much lower than the lower range of predominantly modern recharge, indicating a groundwater source for the stem water. However, the rightward shift in the isotopic composition indicates the groundwater had been evaporated to some degree prior to uptake by the sagebrush. A similar phenomenon was observed in sagebrush at the EB area, and like the EB area, soil-water samples were not collected at this location, so the depth of water uptake is unknown.

References Cited

Barnes, C.J., and Allison, G.B., 1988, Tracing of water movement in the unsaturated zone using stable isotopes of hydrogen and oxygen: Journal of Hydrology (Amsterdam), v. 100, no. 1-3, p. 143–176.

Chimner, R.A., and Cooper, D.J., 2004, Using stable oxygen isotopes to quantify the water source used for transpiration by native shrubs in the San Luis Valley, Colorado U.S.A: Plant and Soil, v. 260, no. 1/2, p. 225–236.

Clark, I., and Fritz, P., 1997, Environmental isotopes in hydrogeology: New York, Lewis publishers, 328 p.

Coplen, T.B., Wildman, J.D., and Chen, J., 1991, Improvements in the gaseous hydrogen-water equilibration technique for hydrogen isotope-ratio analysis: Analytical Chemistry, v. 63, no. 9, p. 910–912.

Ehleringer, J.R., Phillips, S.L., Schuster, W.S.F., and Sandquist, D.R., 1991, Differential utilization of summer rains by desert plants: Oecologia, v. 88, no. 3, p. 430–434.

Epstein, S., and Mayeda, T., 1953, Variation of O18 content of waters from natural sources: Geochimica et Cosmochimica Acta, v. 4, no. 5, p. 213–224.

Gat, J.R., Yakir, D., Goodfriend, G., Fritz, P., Trimborn, P., Lipp, J., Gev, I., Adar, E., and Waisel, Y., 2007, Stable isotope composition of water in desert plants: Plant and Soil, v. 298, no. 1-2, p. 31–45.

Gingerich, S.B., Johnson, H.M., Boschmann, D.E., Grondin, G.H., and Garcia, C.A., 2022, Groundwater resources of the Harney Basin, Oregon: U.S. Geological Survey Scientific Investigations Report 2020-5103, 116 p. [Also available at] https://doi.org/10.3133/sir20215103.

Lin, G., and Sternberg, L. da S.L., 1993, Hydrogen isotopic fractionation by plant roots during water uptake in coastal wetland plants, in Ehleringer, J.R., Hall, A.E., and Farquhar, G.D., eds., Stable isotopes and plant carbon–water relations: San Diego, California, Academic Press, p. 497–510.

Révész, K., and Coplen, T.B., 2008, Determination of the delta (2H/1H) of water—RSIL lab code 1574, chap. C1 of Révész, K., and Coplen, T.B., eds., Methods of the Reston Stable Isotope Laboratory: U.S. Geological Survey Techniques and Methods, book 10, chap. C1, 27 p. [Also available at http://pubs.usgs.gov/tm/2007/tm10c1/.]

Revesz, K., and Woods, P.H., 1990, A method to extract soil water for stable isotope analysis: Journal of Hydrology (Amsterdam), v. 115, no. 1-4, p. 397–406.

Scott, R.L., Williams, D.G., Goodrich, D.C., Cable, W.L., Levick, L.R., McGuire, R., Gazal, R.M., Yepez, E.A., Ellsworth, P., and Huxman, T.E., 2005, Determining the riparian ground-water use within the San Pedro Riparian National Conservation Area and the Sierra Vista subwatershed, Arizona, chap. D of Leenhouts, J.M., Stromberg, J.C., and Scott, R.L., Hydrologic requirements of and consumptive ground-water use by riparian vegetation along the San Pedro River, Arizona: U.S. Geological Survey Scientific Investigations Report 2005–5163, 154 p. [Also available at http://pubs.usgs.gov/sir/2005/5163/.]

Walvoord, M.A., Stonestrom, D.A., Andraski, B.J., and Striegl, R.G., 2004, Constraining the Inferred Paleohydrologic Evolution of a Deep Unsaturated Zone in the Amargosa Desert: Vadose Zone Journal, v. 3, no. 2, p. 502–512.

White, J.W.C., Cook, E.R., Lawrence, J.R., and Wallace S, B., 1985, The ratios of sap in trees—Implications for water sources and tree ring ratios: Geochimica et Cosmochimica Acta, v. 49, no. 1, p. 237–246.

Appendix 3.   Evapotranspiration Unit Delineation and Groundwater Evapotranspiration Data Sources, Adjustments, and Calculations

Evapotranspiration Unit Delineation

Vegetation groupings characterized by plant type and water-use characteristics, called ET units, were identified and mapped in the Harney Basin groundwater ET area (GETA) using a supervised classification model for vegetated areas and Malheur Lake and an imagery-based threshold in Harney Lake. The classification model incorporated a random forest algorithm (Breiman, 2001) to relate 11 observed ET units (table 2) to spectrally derived metrics from the remotely sensed imagery. Harney Lake was classified further using a Landsat-derived water index and 2016 NAIP imagery.

Classification Model

The random forest algorithm was implemented using the "randomForest" package (*v4.6.14*, Liaw and Wiener, 2002). Random forest is a bootstrap method in which an ensemble of decision trees is automatically generated using random samples of the training data for each tree. Training data are sampled with replacement, meaning that some data are used more than once while a fraction of the observations (about one third) are unused. The sampled training data are referred to as the out-of-bag (OOB) sample. Each decision tree consists of a series of branches and nodes developed by identifying the best split of randomly selected variables. At each tree, the OOB sample is used to test model accuracy by comparing the observed classification to the model-predicted classification. Model accuracy is assessed by calculating the proportion of the OOB samples incorrectly classified for all decision trees, herein referred to as the "OOB error." Classification predictions are made on new data, containing the same variables assigned to the training dataset by passing data points, through each tree in the random forest. The final classification assigned to each data point is the model prediction from all classification trees.

The random forest model was developed using land-cover observations paired with Landsat 8 image bands and computed spectral indices and surface texture from 2016 NAIP imagery. Landsat 8 data used in the classification model are from the August 21, 2015, image and include bands 1–7 (ultra blue, blue, green, red, near infrared, shortwave infrared 1, and shortwave infrared 2, respectively), EVI, and MNDWI (see app. 2 for more information about EVI and MNDWI). The raster image used for model development maintained the 30-m spatial resolution of the Landsat data and all spectral metrics were calculated at the same resolution. Image texture was calculated from 1-m (3.28-ft) spatial resolution 2016 NAIP data and resampled to a 30-m (98.4-ft) resolution by calculating the mean of all 1-m pixels within the larger 30-m pixel (see app. 2 for more information about image texture). All raster layers were merged into a single raster stack containing 10 bands (7 Landsat bands, EVI, MNDWI, and texture).

Training and Validation

The random forest image classification was trained and validated using field observations made during this study and vegetation point data collected by the BLM and USFWS (Daniel Craver, U.S. Fish and Wildlife Service, written commun., 2017; Jimmy Kagan, Oregon Biodiversity Information Center, written commun, 2017). Circular areas surrounding field observation points were digitized to represent the area of observation and extended radially to distances of 33–330 ft. Roads and structures were removed from field observation areas to reduce noise in the training and validation dataset. Additionally, manually digitized training areas were created using 2016 NAIP imagery to ensure equal representation among vegetation classes and that sufficient observations exist to build a robust model. A total of 1,454 training polygons representing 11 observed ET units were generated from field and imagery observations. Of the training and validation polygons, 80 percent were used to build the model and 20 percent were used for external model validation. Within each polygon, 50 percent of the pixels were sampled producing a calibration and validation dataset of about 44,000 and 11,500 pixels, respectively.

As described above, random forest uses an aggregate of decision trees to determine the classification output. The ultimate classification is based on the output of numerous decision trees making it difficult to determine the structure of the model and interactions between variables; however, ranking variable importance can provide some insight into model structure. Variable importance was calculated within the randomForest package by comparing OOB error before and after random permutation, or shuffling, of the data for each variable (Liaw and Wiener, 2002). The premise of the permutation approach is that if a variable is of low importance, randomly rearranging the data of that variable, while maintaining the original order of the other variables in the datasets, should result in a smaller increase in OOB error than rearranging the data of a variable with greater importance in the model. To compute variable importance, OOB data for every tree are first classified and the OOB error recorded. Next, for each variable in the OOB dataset, OOB data are randomly permuted while all other variable data are held constant. Each permuted dataset is run through the decision tree and the permuted OOB error is recorded. Finally, the importance of each variable is calculated as the difference between the OOB error for the original dataset and the OOB error for permuted dataset averaged over all decision trees (fig. 3.1).

Random forest uses aggregate bootstrap sampling to build decision trees. For each tree built, the portion of the training data not used to build the tree are used to test the model performance. The mean OOB accuracy is an unweighted metric applied across all ET unit classes. Because this error assessment uses data not included in the model development, it is a robust predictor of model accuracy. In this random forest model, 20 percent of the training polygons were randomly removed from the training dataset and withheld for model validation.

Evapotranspiration Unit Accuracy

The ET units, as defined and delineated, are not intended to be exact but rather generalizations of the long-term average conditions. The accuracy of the final ET-unit classification is
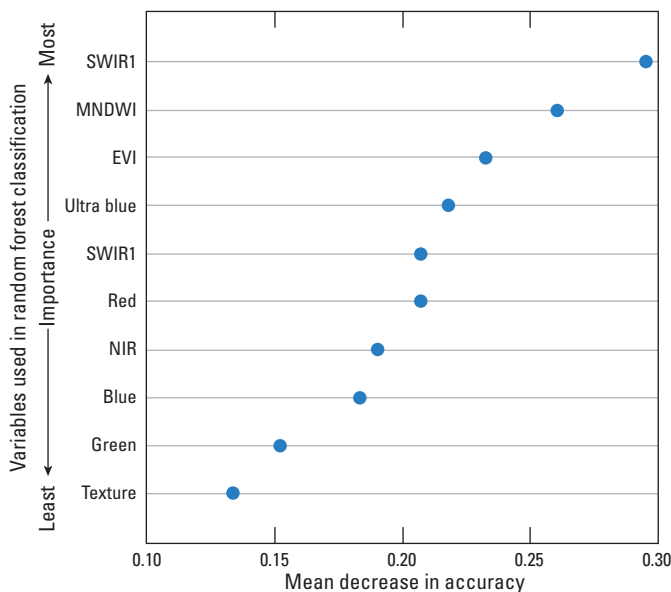
Figure 3.1.   Importance of variables used in random forest classification. Variables on y-axis are ordered top-to-bottom as most-to-least important. Variables from the August 21, 2015, Landsat 8 image include bands 1–7 (ultra blue, blue, green, red, near infrared [NIR], shortwave infrared 1 [SWIR1], and shortwave infrared 2 [SWIR2], respectively), enhanced vegetation index (EVI), and modified normalized difference water index (MNDWI). Texture was calculated from 1-meter (3.28-foot) spatial resolution 2016 National Agricultural Imagery Program (NAIP) data.

difficult to assess because the vegetation and soil conditions throughout the Harney Basin GETA are not homogeneous, and transitions from one condition to the next are not abrupt but rather subtle and often occur over broad zones. Another factor contributing to the difficulty in assessing the accuracy of mapped ET units is that the vegetation understory and soil-surface conditions change within a season and interannually. Despite these difficulties, an assessment of the overall accuracy was made of the ET-unit classification.

The automatically generated mean OOB accuracy for the random forest classification is 91 percent. The confusion matrix, also an output from the random forest model, represents how each OOB sample was classified and the accuracy for each class. Classification accuracy among ET units averaged 82 percent and ranges from 63 percent for riparian to 100 percent in bare soil-playa and open water classes (table 3.1). Riparian areas predominantly were misclassified as sagebrush shrubland, wet meadow, or marsh. Misclassification of riparian areas likely occurs because riparian vegetation exists along narrow stream corridors surrounded by wet meadow and sagebrush and often represent only a small fraction of an image pixel. Classification errors among marsh, wet meadow, and dry meadow ET units were expected as most of the training data for these classes exist within the MNWR (fig. 1), where historical meandering channels along the Donner und Blitzen River have created a heterogeneous patchwork of land covers that often exist within a single 30-m pixel. Misclassification of all classes as big sagebrush also was expected as this shrub is ubiquitous across the Harney Basin lowlands and exists within all land-cover classes. Among mixed shrubland, green rabbitbrush shrubland, and sagebrush shrubland ET units, misclassification is acceptable for the purpose of this study, as green rabbitbrush and sagebrush shrubland ET units are predominantly comprised of xerophytes that use little to no groundwater and several mixed shrubland observations indicate sparse phreatophyte cover.

In addition to the OOB error assessment, model performance was externally validated by comparing observed and modeled ET units. Randomly withheld training polygons were run thorough the random forest model after it was built to generate modeled ET units. The cross-validation method is highly sensitive to the number of pixels and classification of the random sample of training polygons. Because of this sensitivity, classification error varied between roughly 65 and 75 percent depending on the model run. While the OOB approach is a less robust method of error assessment, it serves as an external check on the accuracy of the model.

Table 3.1.   Random forest classification confusion matrix.

	Evapotranspiration units											Class accuracy (percent)
	Bare soil-playa	Marsh	Dry meadow	Wet meadow	Open water	Riparian	Mixed shrubland	Phreatophyte shrubland	Xerophyte shrubland	Sagebrush shrubland	Xerophyte grassland	
Bare soil-playa	3,716	0	0	0	0	0	0	3	0	0	0	100
Marsh	0	310	9	55	4	12	0	6	0	22	0	74
Dry meadow	0	6	2,415	41	0	0	18	124	0	435	4	79
Wet meadow	0	18	39	1,199	3	6	4	22	1	99	2	86
Open water	0	0	0	1	1,761	0	0	0	0	0	0	100
Riparian	0	15	2	18	0	136	1	1	0	44	0	63
Mixed shrubland	0	0	25	6	0	0	2,110	192	19	551	15	72
Phreatophyte shrubland	4	3	37	17	1	2	49	4,953	3	729	3	85
Xerophyte shrubland	0	0	0	2	1	0	16	5	651	227	4	72
Sagebrush shrubland	0	6	52	49	0	15	69	224	35	26,493	84	98
Xerophyte grassland	0	0	1	0	0	0	16	24	1	541	1,995	77

ET units were developed from a single set of Landsat images acquired in August 2015 and a single NAIP image acquired in 2016. Changes in the local vegetation can result from seasonal or annual increases or decreases in precipitation. These changes affect the vigor of the local vegetation, soil-moisture conditions, and the depth to groundwater. Although the imagery acquired is considered reasonable for mapping phreatophytes in the study area, delineations could be improved by using multiple years of imagery and multiple images within years. The inclusion of multiple images would provide more confidence in acreage estimates.

Harney Lake

ET units within Harney Lake were classified using 2016 NAIP imagery and the Landsat-based modified normalized-difference water index (MNDWI; Xu, 2006) because a comparison between random-forest classified ET units within Harney Lake and aerial imagery indicated misclassification of the playa as open water, mixed shrubland, and sagebrush shrubland. Misclassification of the Harney Lake playa likely resulted from variations in the thickness and concentration of surface salts, which in turn, can affect factors such as surface color, temperature, and albedo (Garcia and others, 2015) and lead to misclassification of remotely-sensed surface material. The non-vegetated Harney Lake extent was manually digitized from NAIP imagery. Areas within the lake extent with MNDWI values (derived from the August 21, 2015, Landsat image) greater than or equal to 0.09 were classified as open water based on a threshold analysis by Xu (2006), and the remaining area was classified as bare soil-playa. ET units within Harney Lake were merged with the ET units classified using the random forest model and used to estimate ET_g from non-irrigated areas within the Harney Basin GETA.

Groundwater Evapotranspiration Data Sources, Adjustments, and Calculations

Physics-Based Method

Groundwater ET rates estimated for natural areas with the physics-based method were based on eddy-covariance measurements from 21 sites from within 360 miles of the Harney Basin in north-central Nevada and southern Oregon (areas with similar vegetation and climatic conditions) (Moreo and others, 2007; Allander and others, 2009; Stannard and others, 2013; Garcia and others, 2015; Berger and others, 2016) (table 3). Similarities between the Harney Basin GETA and measurement sites include similar plant species, semi-arid climate with annual precipitation of 2–14 inches, and depth-to-groundwater ranging from less than 1 to more than 30 ft below land surface (tables 2 and 3; see table 3 data sources for more site-specific information).

Selected sites include at least one full year of ET, precipitation, and other meteorological data necessary to compute grass-reference ET (ET_o; Allen and others, 2005). ET_o is the atmospheric ET demand from a uniform grass surface with unlimited water availability and was used to normalize local ET so it could be applied to other basins. Daily mean measurements of air temperature, relative humidity, and wind speed along with station location were used to compute ET_o following the ASCE Standardized Penman-Monteith equation for a grass reference (Allen and others, 2005). Daily precipitation totals for each site-year were collected either at a rain gage at the site or from a nearby weather station. Site instrumentation and data-processing details associated with each site are available in source publications (Moreo and others, 2007; Allander and others, 2009; Stannard and others, 2013; Garcia and others, 2015; Berger and others, 2016).

Prior to computing ET_{net}, site ET estimates were adjusted for energy balance closure (ET_c). Instrumentation used to estimate ET with the eddy-covariance method provides independent measurements of surface energy balance components, but those used to compute ET are consistently underestimated relative to other components. Of the 21 reported site estimates used in the physics-based method, about half were published with consideration of energy balance closure and of those adjusted, only two were modified to reach full energy balance closure. In this study, the Bowen Ratio method (Twine and others, 2000; Foken and others, 2012) was used to adjust site ET estimates used in the physics-based approach to reach full energy balance closure and facilitate comparisons among sites. Energy balance components were adjusted using the energy balance ratio computed over each respective site study period like Stannard and others (2013). ET_c rates were computed from adjusted energy-balance components and summed over the water year for analysis in the physics-based method (table 3).

Empirical Method

Groundwater ET rates estimated with the empirical method (Beamer and others, 2013) are based on ET and micrometeorological data from 26 sites in central and southern Nevada, 10 of which also were used in the physics-based approach (Moreo and others, 2007; Allander and others, 2009). Sites included in the empirical method are arid to semi-arid and contain vegetation like those used in the physics-based approach, except for marsh areas. The empirical method also includes ET measurements from crop areas of pasture grass and alfalfa. The 26 empirical-method sites include measurements made with the eddy-covariance and Bowen-ratio methods. ET rates from eddy-covariance sites also were adjusted upward to achieve full energy balance closure for comparison with estimates from the Bowen-ratio method. Information about site locations, period of record, vegetation type, and rates of ET and precipitation, and source publications can be found in Beamer and others (2013).

References Cited

Allander, K.K., Smith, J.L., and Johnson, M.J., 2009, Evapotranspiration from the lower Walker River Basin, west-central Nevada, water years 2005–07: U.S. Geological Survey Scientific Investigations Report 2009-5079, 62 p. [Also available at https://pubs.usgs.gov/sir/2009/5079/.]

Allen, R.G., Walter, I.A., Elliot, R.L., Howell, T.A., Itenfisu, D., Jensen, M.E., and Snyder, R.L., eds., 2005, The ASCE Standardized Reference Evapotranspiration Equation: Reston, Virginia, American Society of Civil Engineers.

Beamer, J.P., Huntington, J.L., Morton, C.G., and Pohll, G.M., 2013, Estimating Annual Groundwater Evapotranspiration from Phreatophytes in the Great Basin Using Landsat and Flux Tower Measurements: Journal of the American Water Resources Association, v. 49, no. 3, p. 518–533. https://doi.org/10.1111/jawr.12058.

Berger, D.L., Mayers, C.J., Garcia, C.A., Buto, S.G., and Huntington, J.M., 2016, Budgets and chemical characterization of groundwater for the Diamond Valley flow system, central Nevada, 2011–12: U.S. Geological Survey Scientific Investigations Report 2016–5055, 83 p. [https://doi.org/10.3133/sir20165055.]

Breiman, L, 2001, Random forests: Machine Learning, v. 45, p. 5–32.

Foken, T., Leuning, R., Oncley, S.R., Mauder, M., and Aubinet, M., 2012, Corrections and data quality control, in Aubinet, M., Vesala, T., and Papale, D., eds., Eddy covariance—A practical guide to measurement and data analysis—Springer Atmospheric Sciences.

Garcia, C.A., Huntington, J.M., Buto, S.G., Moreo, M.T., Smith, J.L., and Andraski, B.J., 2015, Groundwater discharge by evapotranspiration, Dixie Valley, west-central Nevada, March 2009–September 2011 (ver. 1.1, April 2015): U.S. Geological Survey Professional Paper 1805, 90 p. [https://doi.org/10.3133/pp1805.]

Liaw, A., and Wiener, M., 2002, Classification and regression by randomForest: R News, v. 2/3, p. 18–22.

Maurer, D.K., Berger, D.L., Tumbusch, M.L., and Johnson, M.J., 2006, Rates of evapotranspiration, recharge from precipitation beneath selected areas of native vegetation, and streamflow gain and loss in Carson Valley, Douglas County, Nevada, and Alpine County, California: U.S. Geological Survey Scientific Investigations Report 2005-5288, 70 p. [Also available at https://pubs.usgs.gov/sir/2005/5288/pdf/sir20055288.pdf.]

Moreo, M.T., Laczniak, R.J., and Stannard, D.I., 2007, Evapotranspiration rate measurements of vegetation typical of ground-water discharge areas in the Basin and Range carbonate-rock aquifer system, Nevada and Utah, September 2005–August 2006: U.S. Geological Survey Scientific Investigations Report 2007–5078, 36 p. [Also available at https://pubs.usgs.gov/sir/2007/5078/.]

Stannard, D.I., Gannett, M.W., Polette, D.J., Cameron, J.M., Waibel, M.S., and Spears, J.M., 2013, Evapotranspiration from wetland and open-water sites at Upper Klamath Lake, Oregon, 2008–2010: U.S. Geological Survey Scientific Investigations Report 2013–5014, 66 p. [Also available at https://pubs.usgs.gov/sir/2013/5014/.]

Twine, T.E., Kustas, W.P., Norman, J.M., Cook, D.R., Houser, P.R., Meyers, T.P., Prueger, J.H., Starks, P.J., and Wesely, M.L., 2000, Correcting eddy-covariance flux underestimates over a grassland: Agricultural and Forest Meteorology, v. 103, no. 3, p. 279–300. https://doi..1016/8- 518–533. https://doi.org/10.1111/

Appendix 4.   Streamflow Record Extension and Estimation

Streamflow for Streamgaged Watersheds with Multi-year Records

The Kendall-Theil robust line (KTRL) and ordinary least-squares regression (OLS) methods were used to extend short-term streamflow records and estimate mean annual streamflow during 1982–2016 for many gaged streams in the Harney Basin. Quantitative methods for estimating streamflow at a site of interest based on a longer-term record at an index station generally use some form of linear regression, but each approach has slight variations that provide an advantage for a particular application. Parametric-regression techniques such as OLS regression commonly are applied to hydrologic data and are widely available but might be insufficient where outliers are common or where a single-segment regression does not adequately characterize the data. Helsel and others (2020) featured the KTRL method as a nonparametric alternative to OLS methods for statistical analysis of water-resources data. The KTRL is a multi-segment regression model that allows flexibility where different environmental processes are dominant over different ranges of the explanatory variable(s), such as base flow and snowmelt runoff processes that affect streamflow at a streamgage.

Long-term continuous streamflow measurements are available during 1904–2018 at two sites on the Silvies River (10393500) and Donner und Blitzen River (10396000); these two sites are referred to as "index sites" and used to extend short-term records at other sites. Short-term (months to decades) continuous measurements are available over the previous century for nine additional upland and lowland watersheds. Records for short-term sites were extended using the index sites for comparison. The KTRL method was used to extend daily discharge values to 1982–2016 for short-term records at six sites where correlation coefficients based on daily data with index gages were reasonable (Pearson's r greater than 0.7, except for Bridge Creek sites; table 4.1). At the five sites where daily correlations were poor, annual correlations (with at least 5 years of measurements) notably improved correlation coefficients, therefore OLS was used to extrapolate the annual water-year discharge from these short-term sites. Streamflow from ungaged watersheds, watersheds with less than a full-year record, or watersheds with substantial regulation (Krumbo Creek below Krumbo Reservoir) was determined by scaling streamflow to precipitation distributions of nearby streamgaged watersheds. Detail on the extension and estimation procedures are provided in the following subsections.

Record Extension Methods

KTRL and OLS methods were used to extend short-term streamflow records (Theil, 1950; Conover, 1980). The USGS has developed a suite of software to facilitate the use of KTRL equations. The KTRLine program (Granato, 2006) provides a graphical interface that assists the user in selection of breakpoints for multiple line segments for a single index station. The KTRL equations computed for each line in the multi-segment model are entered in the Streamflow Record Extension Facilitator (SREF) program (Granato, 2009) for computation of the estimated values for the site of interest using each index station.

Index gages on the Silvies River near Burns and Donner und Blitzen River near Frenchglen provided an acceptable range of dates to extend most intermittent streamflow records for water years 1982–2016; records are available for the full 35 years at the Donner und Blitzen River index gage and for 32 years at the Silvies River streamgage. The Silvies River index gage was used to extend short-term records in the northern and western regions and the Donner und Blitzen River index gage was used in the southern region. Although the Silvies River is regulated upstream of the long-term streamgage near Burns, regulated flows represent only a small fraction of total flow within the more than 900-mi^2 drainage area. Additionally, correlations between the Silvies River index gage and most northern and western streamgages provided confidence in its suitability as an index gage (table 4.1). Correlation coefficients (Pearson's r) based on daily comparisons of index sites and short-term streamgages ranged between 0.23 and 0.94 in northern and western regions and from 0.38 to 0.90 in the southern region.

Weak correlations (Pearson's r less than 0.75) at Rock Creek (10395600), Krumbo Creek below Krumbo Reservoir (357009), Donner und Blitzen River near Voltage (10401500), East Fork Silvies River (10395000), and West Fork Silvies River (10395500) streamgages are from differences in watershed size (table 8), upstream water management, and natural flooding from bank overflow. Because correlations notably improved when annual water-year data were compared, OLS was used to extend short-term records at these streamgages (table 4.2).

Table 4.1.   Correlation coefficients and coefficients of determination between logarithms of daily and water-year discharge values at sites of interest and potential index sites for streams in the Harney Basin, southeastern Oregon.

[**Index site**: USGS site numbers are shown in parentheses. **Short-term site number**: Numbers are USGS site numbers unless otherwise noted. Coefficients based on daily log-transformed data. **Abbreviations**: r[2], coefficient of determination]

Index site	Short-term site	Short-term site number	Pearson correlation coefficient	r[2]
Daily				
Donner und Blitzen River near Frenchglen (10396000)	McCoy Creek near Diamond	10400000	0.90	0.81
	Mud Creek near Diamond	10396500	0.87	0.76
	Bridge Creek near Frenchglen - USGS	10397000	0.68	0.48
	Bridge Creek near Frenchglen - USFWS	[1]357004	0.66	0.48
	Donner und Blitzen River near Voltage	[1]357005	0.54	0.23
	Donner und Blitzen River near Sodhouse	10401500	0.47	0.30
	Krumbo Creek Flume below Krumbo Reservoir	[1]357009	0.38	0.14
Silvies River near Burns (10393500)	Silver Creek below Nicoll Creek near Riley	10403400	0.94	0.88
	West Fork Silvies River near Lawen	10395500	0.75	0.56
	East Fork Silvies River near Lawen	10395000	0.73	0.53
	Rock Creek near Burns	10395600	0.23	0.05
Water year				
Donner und Blitzen River near Frenchglen (10396000)	Donner und Blitzen River near Voltage and Donner und Blitzen River near Sodhouse	[1,2]357005 and 10401500	0.87	0.76
	Krumbo Creek Flume below Krumbo Reservoir	[1]357009	0.60	0.36
Silvies River near Burns (10393500)	West Fork Silvies River near Lawen	10395500	0.88	0.78
	East Fork Silvies River near Lawen	10395000	0.99	0.97
	Rock Creek near Burns	10395600	0.72	0.52

[1] U.S. Fish and Wildlife Service, Mayer and others (2007)

[2] Records combined for water-year analysis.

Multiple short-term records at similar streamgages on the Donner und Blitzen River near Voltage and on Bridge Creek were combined prior to record extension. Outflow from the Donner und Blitzen River to Malheur Lake was measured by the USGS during the 1930s, 1940s, and 1970s at the Donner und Blitzen River near Voltage (10401500) and a gage was redeployed by the USFWS in 2001 at the Donner und Blitzen River near Sodhouse (357007), within 100 ft upstream of the USGS streamgage. Likewise, the Bridge Creek near Frenchglen streamgage (10397000), which was measured by the USGS intermittently between 1911 and 1970, was redeployed by the USFWS (357004) in 2004 and measurements there have since been ongoing .

Multi-segment regressions equations were computed for five of the six streamgage pairs used in this study using KTRLine (Granato, 2006). A single-segment regression equation was computed for a single streamgage pair. Log-transformation of streamflow data either improved the linear fit between streamgage pairs or precluded negative streamflow estimation at low flow. Following Curran (2012), initial breakpoints between multi-segment lines were visually determined from the LOWESS-smoothed line on the log-scale scatter plot of daily discharge. Selected breakpoints were input into KTRLine and adjusted until the best fit was obtained with the fewest possible segments. Resulting equations (table 4.2) contained a maximum of three segments. Values from regression equations (table 4.2) for each equation were entered into SREF (Granato, 2009), which computed the extended discharge values and retransformed them from logarithmic values (incorporating bias correction factors; table 4.2) to produce a suite of predicted (estimated values for the period concurrent with the index gage) and extended (estimated values for the nonconcurrent period) daily discharge values for the streamgage of interest. For records extended with OLS, regression equation values were applied to index gage values to compute extended water-year discharge values, and logarithmic values were retransformed and corrected for retransformation bias to produce predicted and extended water-year discharge values for each streamgage of interest.

Table 4.2. Values for variables, discharge input ranges, and measures of error for Kendall–Thiel Robust Line equations used for estimating daily discharge and for ordinary least squares equations used for estimating mean water-year discharge from index gage data at selected streamgages, Harney Basin, southeastern Oregon.

[Estimation variables based on logarithms of daily and mean water-year values. **Index site:** USGS site numbers. **Short-term site numbers:** USGS site numbers unless otherwise noted. **Range of daily and water-year discharge input values:** Values are associated with index sites. **Bias correction factor:** Accounts for bias when untransforming predicted values. **Abbreviations:** ft³/s, cubic feet per second; USGS, U.S. Geological Survey]

Index site	Short-term site	Short-term site number	Root mean squared error (ft³/s)	Segment number	Intercept	Slope	Range of daily and water-year discharge input values		Bias correction factor
							Minimum (ft³/s)	Maximum (ft³/s)	
Kendall–Thiel Robust Line method—Daily estimation									
Donner und Blitzen River near Frenchglen (10396000)	Mud Creek near Diamond	10396500	0.345	1	-3.276	1.757	1.398	2.577	1.527
				2	-1.420	1.037	2.577	3.260	1.059
	Bridge Creek near Frenchglen (USGS; USFWS)	10397000; [1]357004	0.111	1	0.471	0.361	1.041	1.631	1.031
				2	0.899	0.099	1.631	2.176	1.059
				3	-0.133	0.573	2.176	3.396	1.060
	McCoy Creek near Diamond	10400000	0.237	1	-1.785	1.485	1.415	2.526	1.087
				2	1.232	0.291	2.526	3.170	1.022
Silvies River near Burns (10393500)	Silver Creek below Nicoll Creek near Riley	10403400	0.271	1	-1.140	1.495	0.415	1.109	1.256
				2	-0.205	0.652	1.109	1.654	1.102
				3	-1.215	1.263	1.654	3.538	0.996
Ordinary least squares method—Water-year estimation									
Donner und Blitzen River near Frenchglen (10396000)	Donner und Blitzen River near Voltage; Donner und Blitzen River near Sodhouse	10401500; [1,2]357005	0.123	1	-1.465	1.650	1.495	2.581	1.036
	Krumbo Creek Flume below Krumbo Reservoir	[1]357009	0.174	1	-1.332	0.885	0.092	0.920	1.079
Silvies River near Burns (10393500)	East Fork Silvies River near Lawen	10395000	0.114	1	-3.077	1.777	-0.465	2.970	1.018
	West Fork Silvies River near Lawen	10395500	0.395	1	-3.472	1.896	-0.670	1.621	1.538
	Rock Creek near Burns	10395600	0.325	1	-2.745	1.511	-0.082	1.295	1.286

[1]U.S. Fish and Wildlife Service, Mayer and others (2007)

[2]Records combined for water-year analysis.

Record Extension Results

Streamflow data extended with the KTRL method reasonably matched observed values with RMS error between 0.11 and 0.35 log ft³/s (table 4.2). Hydrograph comparisons indicate that extended records captured general high and low-flow trends within a year during measurement periods (fig. 4.1). Extended records at Bridge Creek and Silver Creek matched weekly fluctuations and seasonal trends in observed streamflow. At Silver Creek, extended streamflow slightly underestimated observations during high flow and generally overestimated observations during low flow.

Records extended with OLS reasonably matched observed values at all streamgages considering the differences in watershed characteristics and water management between short-term and index gages (RMS error of 0.11–0.4 log ft³/s, where mean annual streamflow is about 4–120 ft³/s; table 4.2). Streamflow estimates at regulated streamgages near Malheur Lake (East Fork Silvies River, West Fork Silvies River, and Donner und Blitzen River near Voltage) generally matched mean water-year observations but are less certain because upgradient reaches are affected by substantial irrigation diversions and bank overflow during springtime months (see section "Irrigation Pumpage"). Water year OLS streamflow estimates at Krumbo and Rock Creeks have the greatest uncertainty (coefficients of determination of 0.36 and 0.52, respectively; table 4.1). The Krumbo Creek streamgage was established at the outlet of Krumbo Reservoir to measure streamflow into the MNWR and is influenced by reservoir management. The Rock Creek watershed is the smallest one evaluated and exhibits flashy runoff-dominated flow. Despite these uncertainties, extended streamflow data from streamgages evaluated with OLS provide useful means for the water-budget analysis of recharge.

The composite record of observed and extended values for water years 1982–2016 was compiled and used to compute mean annual streamflow (table 4.3). Extended KTRL daily streamflow records for water years 1982–2016 and extended OLS water-year streamflow records for the same period are presented as a data release in Garcia and others (2022). The observed data available for the same period can be obtained from this file for convenience or from the USGS National Water Information System (U.S. Geological Survey, 2021) or OWRD website for the most current version of USGS- and OWRD-operated streamgages.
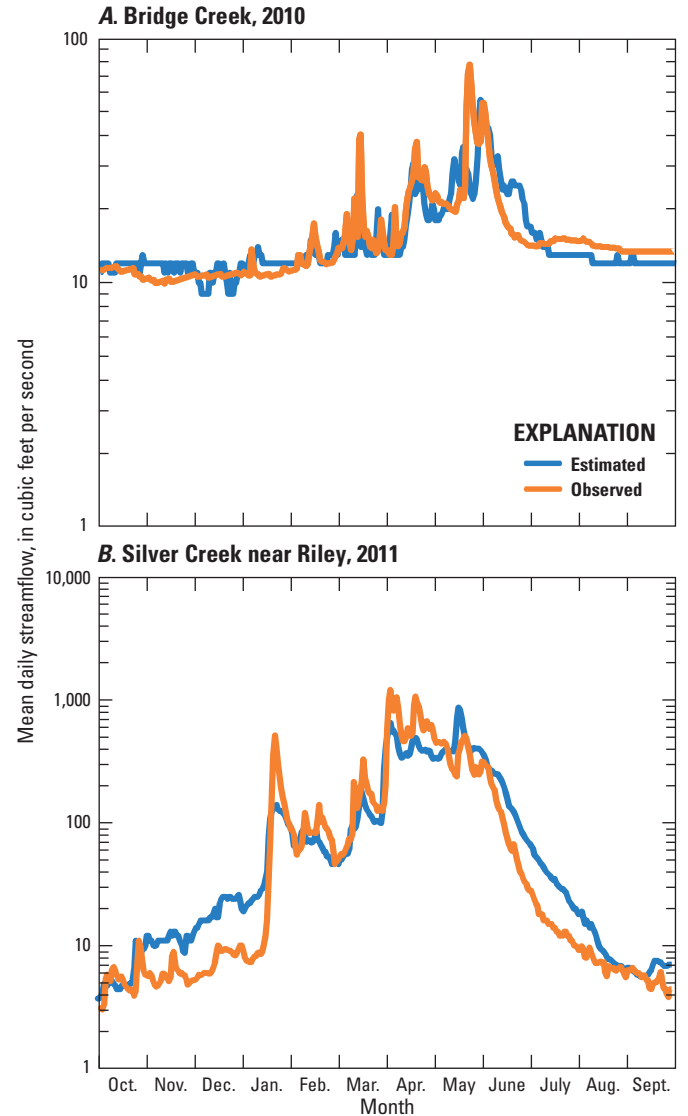
Figure 4.1. Examples of predicted and observed discharge values at (*A*) Bridge Creek (streamgage 10397000) and (*B*) Silver Creek (streamgage 10403400), Harney Basin, southeastern Oregon. Predicted values are independent of discharge at the streamgage of interest based on records for index gages: Silvies River near Burns (streamgage 10393500) and Donner und Blitzen River near Frenchglen (streamgage 10396000).

Table 4.3.   Estimated mean annual streamflow for gaged and ungaged streams during water years 1982–2016, Harney Basin, southeastern Oregon.

[Locations of streamgaged and ungaged watersheds are shown on figure 11. **Mean annual measured and estimated streamflow**: Values represent composites of measurements and estimates where measured during water years 1982–2016. **Estimation method**: Method used to extend measured records or ungaged estimates to the 1982–2016 study period include Kendall-Thiel Robust Line method (KTRL; Helsel and others, 2020), ordinary least squares (OLS), composites of estimated and measured values (KRTL and Meas.; OLS and Meas.), or streamflow-precipitation model (flow-PPT). Streamflow estimates from flow-PPT model represent flow in upland areas only (portion of watershed in lowland area not included in analysis). **Abbreviations**: ft³/s, cubic feet per second; KTRL, Kendall-Thiel Robust Line method; Meas., measured; OLS, ordinary least squares; flow-PPT, streamflow-precipitation model; USGS, U.S. Geological Survey; OWRD, Oregon Water Resources Department; —, not available]

Site name	USGS/OWRD site number (other site number)	Map index number	Mean annual measured and estimated streamflow (ft³/s)	Estimation method	Percentage of measured record in composite estimate
			Gaged watersheds		
Silvies River near Burns, OR	10393500	1	[1]195.1	Meas.	100
Rattlesnake Creek near Harney, OR	10394600	2	[1]5.0	Flow-PPT	0
East Fork Silvies River near Lawen, OR	10395000	—	[1]14.1	OLS	0
West Fork Silvies River near Lawen, OR	10395500	—	[1]17.2	OLS	0
Rock Creek near Burns, OR	10395600	3	[1]8.2	OLS	0
Donner und Blitzen River near Frenchglen, OR	10396000 [2](357010)	4	130.9	Meas.	100
Mud Creek near Diamond, OR	10396500	5	5.5	KTRL	0
Bridge Creek near Frenchglen, OR	10397000 [2](357004)	6	14.9	KTRL & Meas.	34
Krumbo Creek Flume below Krumbo Reservoir [3]	[2](357009)	7	3.7	OLS & Meas.	37
Krumbo Creek Flume below Krumbo Reservoir [3]	[2](357009)	7	11.6	Flow-PPT	0
Kiger Creek near Diamond, OR	10399000	8	61.8	Flow-PPT	0
Mccoy Creek near Diamond, OR	10400000 [2](357007)	9	25.0	KTRL	0
Donner und Blitzen River near Voltage, OR	10401500 [2](357005)	10	124.1	OLS & Meas.	37
Silver Creek below Nicoll Creek near Riley, OR	10403400	11	[1]65.8	KTRL & Meas.	17
Silvies River below Soda Spring near Seneca, OR	10392400	22	[1]67.4	KTRL & Meas.	5
Silvies River near Silvies, OR	10392500	23	[1]82.1	KTRL & Meas.	5
			Ungaged watersheds		
Sagehen Creek at Silvies River	[4](31200202)	14	12.4	Flow-PPT	0
Poison Creek Slough at Ninemile Slough	[4](31200106)	15	21.1	Flow-PPT	0
Malheur Slough above Ninemile Slough	[4](31200107)	16	12.3	Flow-PPT	0
Hot Springs Slough at Malheur Slough	[4](31200102)	17	7.0	Flow-PPT	0
Soldier Creek at Poison Creek Slough	[4](31200105)	18	8.7	Flow-PPT	0

Table 4.3.   Estimated mean annual streamflow for gaged and ungaged streams during water years 1982–2016, Harney Basin, southeastern Oregon.—Continued

[Locations of streamgaged and ungaged watersheds are shown on figure 11. **Mean annual measured and estimated streamflow**: Values represent composites of measurements and estimates where measured during water years 1982–2016. **Estimation method**: Method used to extend measured records or ungaged estimates to the 1982–2016 study period include Kendall-Thiel Robust Line method (KTRL; Helsel and others, 2020), ordinary least squares (OLS), composites of estimated and measured values (KRTL and Meas.; OLS and Meas.), or streamflow-precipitation model (flow-PPT). Streamflow estimates from flow-PPT model represent flow in upland areas only (portion of watershed in lowland area not included in analysis). **Abbreviations**: ft³/s, cubic feet per second; KTRL, Kendall-Thiel Robust Line method; Meas., measured; OLS, ordinary least squares; flow-PPT, streamflow-precipitation model; USGS, U.S. Geological Survey; OWRD, Oregon Water Resources Department; —, not available]

Site name	USGS/OWRD site number (other site number)	Map index number	Mean annual measured and estimated streamflow (ft³/s)	Estimation method	Percentage of measured record in composite estimate
Ungaged watersheds—Continued					
Cucamonga Creek at Kiger Creek	[4](31200303)	19	7.5	Flow-PPT	0
Chickahominy Creek at Silver Creek	[4](31200402)	20	1.8	Flow-PPT	0
Miller Canyon Creek at Silver Creek	[4](31200404)	21	7.7	Flow-PPT	0
Virginia Creek at Silver Creek	[4](31200403)	22	4.8	Flow-PPT	0
Riddle Creek area[5]	—	23	31.4	Flow-PPT	0
Other upland areas[6]					
Northern region	—	—	17.6	Flow-PPT	0
Southern region	—	—	18.5	Flow-PPT	0
Western region	—	—	21.9	Flow-PPT	0

[1]Value excludes streamflow data from water years 2007–08.

[2]U.S. Fish and Wildlife Service, Mayer and others (2007)

[3]Streamgage located downstream of Krumbo Reservoir and measured and OLS-estimated flow likely affected by reservoir management. Estimated flow from flow-PPT model assumed representative of natural unmanaged conditions.

[4]Oregon Water Resources Department, Cooper (2002). Streamflow estimates represent upland watershed area only (fig. 11).

[5]Ungaged area surrounding Riddle Creek, northeast of the Kiger Creek watershed.

[6]Upland areas without delineated watersheds.

Streamflow for Ungaged Watersheds, Watersheds with Sub-Year Records, and Other Upland Areas

Streamflow from ungaged watersheds, watersheds with continuous short-term streamgages with less than a full-year record, and other ungaged areas in the Harney Basin uplands (fig. 11; table 8) was estimated using an empirical streamflow-precipitation model analogous to the Maxey-Eakin recharge-precipitation method for recharge estimation (Maxey and Eakin, 1951; Fenelon and others, 2016). Estimated mean annual streamflow volumes were determined by comparing estimated streamflow and precipitation from four streamgaged watersheds (Silvies River near Burns, 10393500; Silver Creek below Nicoll Creek near Riley, 10403400; Donner und Blitzen River near Frenchglen, 10396000; and Bridge Creek near Frenchglen, 10397000) (table 4.3). Here, streamflow was estimated using the modified Maxey-Eakin method by scaling the mean annual 1981–2010 PRISM precipitation distribution (fig. 2) to match measured and KTRL-estimated streamflow for 1982–2016 in the four watersheds (table 4.3). The scaling factors from the four nearby watersheds were then applied to the precipitation distribution in the areas of interest to estimate streamflow (Garcia and others, 2022).

The Silvies River watershed used to develop the streamflow-precipitation relation was limited to the watershed area and streamflow generated between the Silvies River near Burns (10393500) and Silvies River near Silvies (10392500) streamgages. The relationship was limited to remove the effects of irrigation diversions that occur upstream of the Silvies River near Silvies streamgage. Mean annual 1982–2016 streamflow at the Silvies River near Silvies streamgage (determined from measured and KTRL-estimated flow) was subtracted from measured flow at the Silvies River near Burns streamgage, and the difference was used in the streamflow-precipitation model discussed herein.

The precipitation distribution was divided into zones based on ranges of precipitation fractions and precipitation within each zone was scaled to balance total streamflow. Scaled precipitation within each zone represents the precipitation fraction contributing to streamflow. Precipitation fractions were estimated by multiplying annual precipitation amounts within specified precipitation zones by coefficients that represent the fraction of precipitation that is converted to streamflow (Garcia and others, 2022). Precipitation for the area within each zone is summed over the streamgaged watershed area and multiplied by a fitted coefficient to estimate streamflow. Simulated streamflow was balanced against composite (measured and KTRL-estimated) values by varying the coefficients for each precipitation zone to get a best fit. A rule was applied that requires a precipitation range with a higher precipitation rate to have a coefficient that is equal to or greater than a range with a lower rate. This was done because as precipitation increases, a larger percentage is assumed available

for streamflow. The best fit was measured by minimizing the RMS error of the differences between simulated and composite streamflow using the Microsoft Excel® Solver. A best fit is obtained by manually changing the precipitation ranges, iteratively balancing simulated and composite streamflow, and comparing RMS errors between models with different ranges until the error is minimized.

The best fit had an RMS error of 1.2 ft³/s (860 acre-ft/yr) and required five precipitation ranges: less than 12, 12–19, 19–23, 23–31, and greater than 31 in/yr. The area with the low-precipitation range had 1 percent of precipitation converted to streamflow, the middle three ranges had 20–26 percent converted to streamflow, and the area with the high range had 41 percent of precipitation converted to streamflow.

Calibrated precipitation coefficients were applied to similar precipitation zones in ungaged watersheds and other upland areas to estimate streamflow. Watershed-scale streamflow processes among streamgaged and ungaged watersheds were assumed similar and differences among watershed rates were assumed to result from spatially varying precipitation volumes.

Accuracy and Limitations of Extend and Estimated Streamflow Records

The accuracy of the estimates for daily discharge extended using the KTRLine program is indicated the RMS error of the estimating equations for each index site. The regression-equation model RMS (table 4.2) describes the fit of the multi-segment line to the plot of the logarithms of daily values for every index-short-term site pair. The RMS errors provided describe the fit during the concurrent period but cannot evaluate the uncertainty in the values for the extended period. Refer to table 4.2 for associated logarithms of daily and water-year streamflow values.

In addition to the accuracy of the estimates, users should consider limitations inherent in the data or introduced by the streamflow-extension methods. One source of uncertainty is the streamflow measurements on which they are based. Uncertainty in daily discharge data represent a combination of random and systematic errors (Hamilton and Moore, 2012; McMillan and others, 2017). Random errors typically decrease with increasing integration periods from daily discharge rates to annual and multi-decade periods analyzed in this study, therefore mean-annual discharge estimates used in this study likely are closer to actual values than was reported for daily discharge. Streamflow from the Donner und Blitzen River streamgage at Frenchglen is generally within 10 percent of the measured values. Streamflow from the Silvies River near Burns streamgage generally is within 15 percent of measured values through 1997 and generally greater than 15 percent of measured values for the period 1998–2016. The quality of USFWS streamgage records predominantly were within 15 percent of the measured values.

Periods of observation compared with periods of extension also should be considered a limiting factor for several sites. Record extension over decades to more than half a century requires the underlying assumption that channel and flow characteristics within a watershed have remained stationary over time. The validity of the stationarity assumption is uncertain in many watersheds because limited data exists; however, comparisons between measurements made decades apart by the USGS and USFWS at sites such as Bridge Creek near Frenchglen and Donner und Blitzen River near Voltage and Donner und Blitzen River near Sodhouse support this assumption (app. 5). Annual estimates of extended streamflow records likely are more accurate than sub-annual estimates because estimates are based on streamflow magnitude rather than season (Curran, 2012).

The accuracy of estimated streamflow from ungaged basins and other upland areas determined with a modified Maxey-Eakin method was determined to be within 1,000 acre-ft/yr based on the model RMS error, but the error does not account for additional uncertainties in measured and extended streamflow records used to calibrate the model, which could deviate from actual values by more than 15 percent at some sites. Despite this uncertainty, however, the RMS error likely is a reasonable assessment of error since the Maxey-Eakin based estimate was calibrated using measurements and estimates from several watersheds.

References Cited

Conover, W.J., 1980, Practical nonparametric statistics (2nd ed.): New York, Wiley, 493 p.

Curran, J.H., 2012, Streamflow record extension for selected streams in the Susitna River Basin, Alaska: U.S. Geological Survey Scientific Investigations Report 2012–5210, 36 p. [Also available at https://pubs.usgs.gov/sir/2012/5210/.]

Fenelon, J.M., Halford, K.J., and Moreo, M.T., 2016, Delineation of the Pahute Mesa–Oasis Valley groundwater basin, Nevada (ver. 1.1, May 2016): U.S. Geological Survey Scientific Investigations Report 2015–5175, 40 p. [Also available at https://doi.org/10.3133/sir20155175.]

Garcia, C.A., Haynes, J.V., Overstreet, B.T., Corson-Dosch, N.T., 2022, Supplemental data—Hydrologic budget of the Harney Basin groundwater system, Oregon: U.S. Geological Survey data release, https://doi.org/10.5066/P9QABFML.

Granato, G.E., 2006, Kendall-Theil Robust Line (KTRLine—version 1.0)—A visual basic program for calculating and graphing robust nonparametric estimates of linear-regression coefficients between two continuous variables: U.S. Geological Survey Techniques and Methods, book 4, chap. A7, 31 p. [Also available at https://pubs.usgs.gov/tm/2006/tm4a7/.]

Granato, G.E., 2009, Computer programs for obtaining and analyzing daily mean streamflow data from the U.S. Geological Survey National Water Information System web site: U.S. Geological Survey Open-File Report 2008–1362, 123 p., on CD-ROM, 5 app. [Also available at https://pubs.usgs.gov/of/2008/1362/.]

Hamilton, A.S., and Moore, R.D., 2012, Quantifying Uncertainty in Streamflow Records: Canadian Water Resources Journal, v. 37, no. 1, p. 3–21.

Helsel, D.R., Hirsch, R.M., Ryberg, K.R., Archfield, S.A., and Gilroy, E.J., 2020, Statistical methods in water resources: U.S. Geological Survey Techniques and Methods, book 4, chapter A3, 458 p., https://doi.org/10.3133/tm4A3. [Supersedes USGS Techniques of Water-Resources Investigations, book 4, chapter A3, version 1.1.]

Maxey, G.B., and Eakin, T.E., 1949, Ground water in White River Valley, White Pine, Nye, and Lincoln Counties, Nevada: Nevada State Engineer, Water Resources Bulletin 8, 59 p. [Also available at https://www.nrc.gov/docs/ML0331/ML033140348.pdf.]

McMillan, H., Seibert, J., Petersen-Overleir, A., Lang, M., White, P., Snelder, T., Rutherford, K., Krueger, T., Mason, R., and Kiang, J., 2017, How uncertainty analysis of streamflow data can reduce costs and promote robust decisions in water management applications: Water Resources Research, v. 53, no. 7, p. 5220–5228.

Theil, H., 1992, A Rank-Invariant Method of Linear and Polynomial Regression Analysis: Advanced Studies in Theoretical and Applied Econometrics, v. 23, p. 345–381.

Appendix 5.   Plots of Daily Streamflow and Best-Fit Multi-Segment Kendall-Theil Regression Lines for Sites of Interest and Index Stations for Concurrent Periods, Harney Basin, Southeastern Oregon
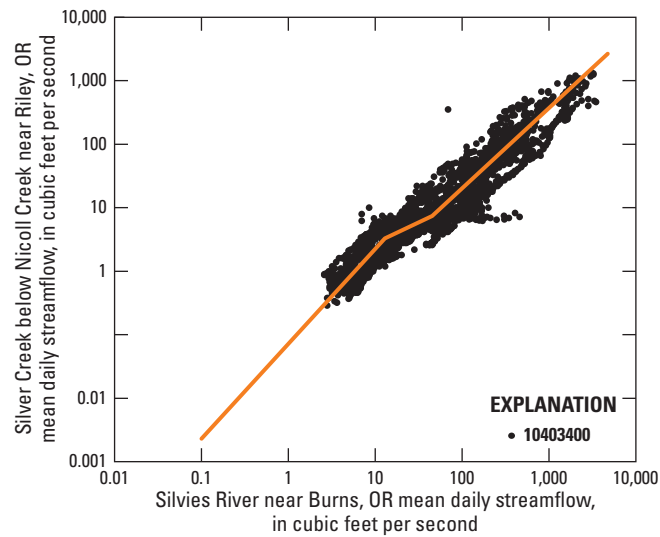
Figure 5.1.   Mean daily streamflow in cubic feet per second and best-fit multi-segment Kendall-Thiel regression line for Silver Creek below Nicoll Creek near Riley, extended using the Silvies River near Burns, OR (streamgage 10393500), index site, Harney Basin, Oregon. Regression equations are provided in table 4.2.
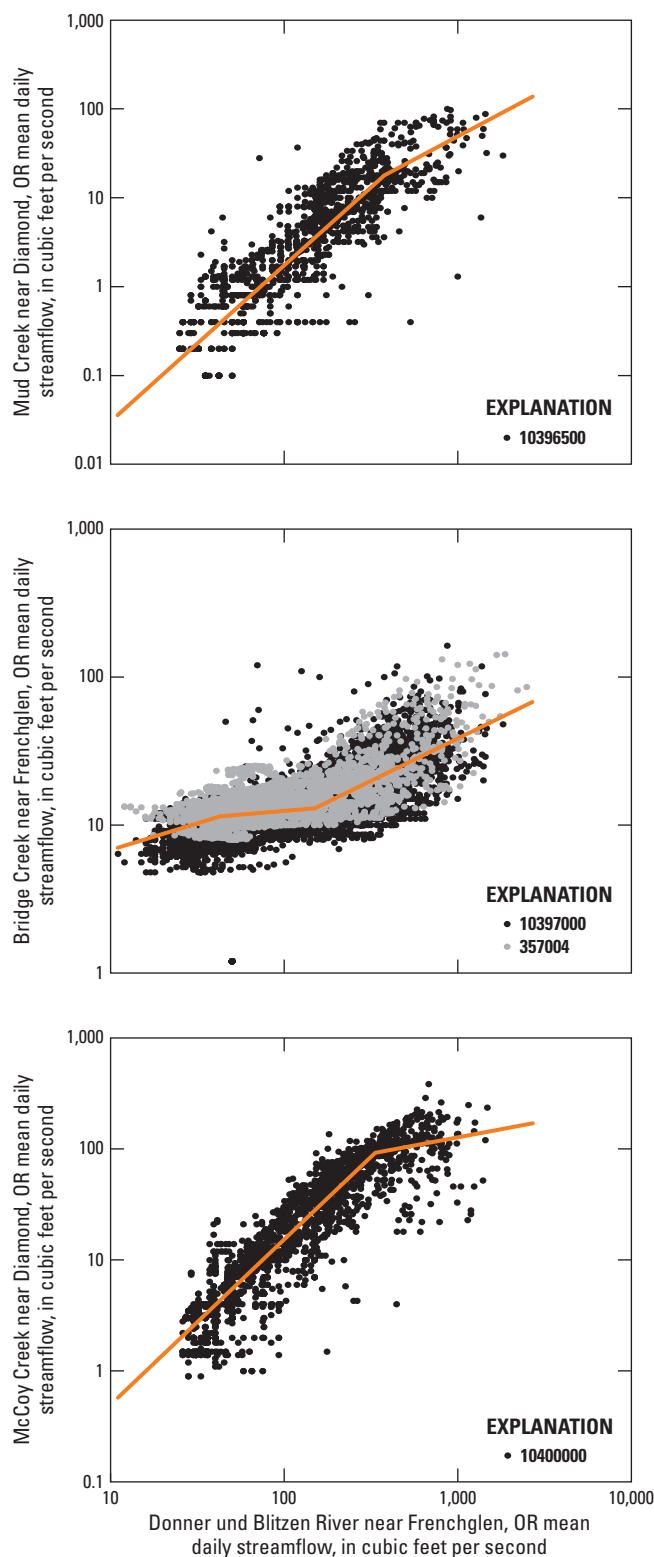
Figure 5.2. Mean daily streamflow in cubic feet per second and best-fit multi-segment Kendall-Thiel regression lines for sites of interest extended using the Donner und Blitzen River near Frenchglen, OR (streamgage 10396000), index site, Harney Basin, Oregon. Multiple sites at the same location are included in a single plot and are distinguished by streamgage site number (table 4.2). Regression equations are provided in table 4.2.
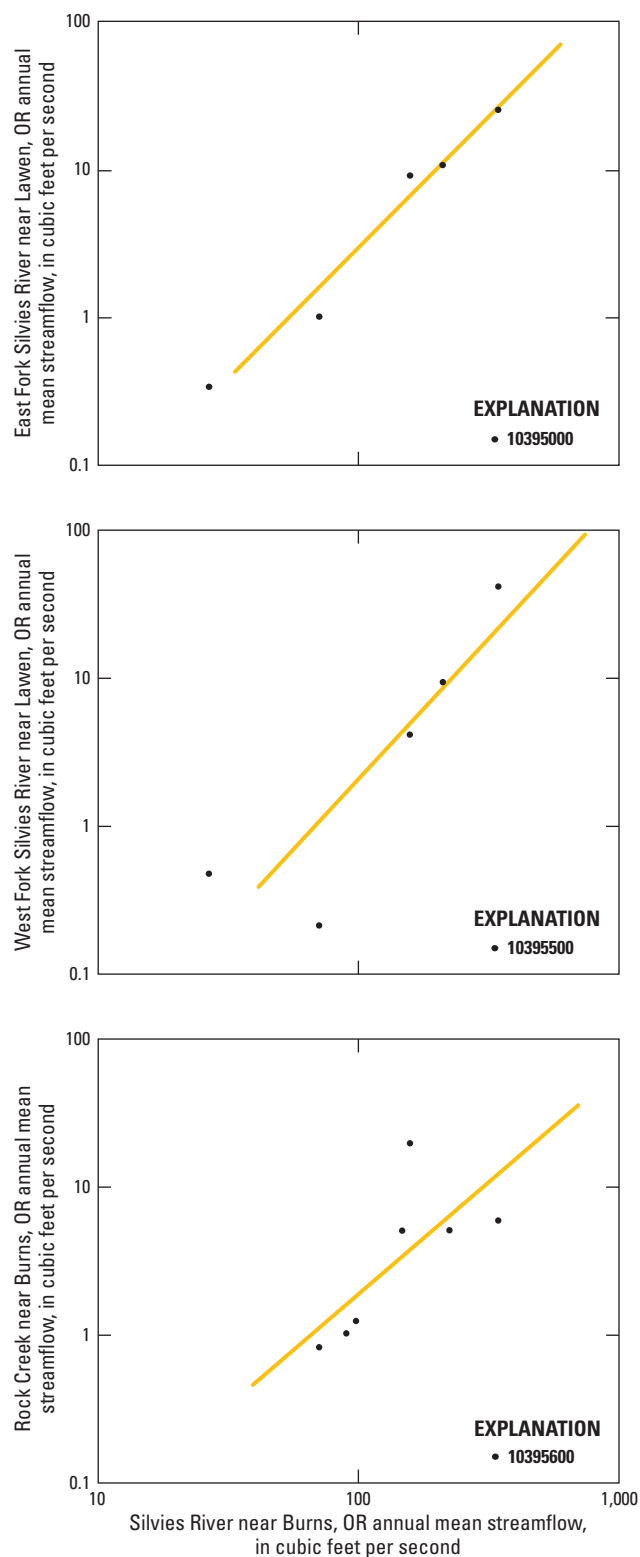
Figure 5.3. Annual (water year) mean streamflow in cubic feet per second and ordinary least-squares regression lines for sites of interest extended using the Silvies River near Burns, OR (streamgage 10393500), index site, Harney Basin, Oregon. Regression equations are provided in table 4.2.
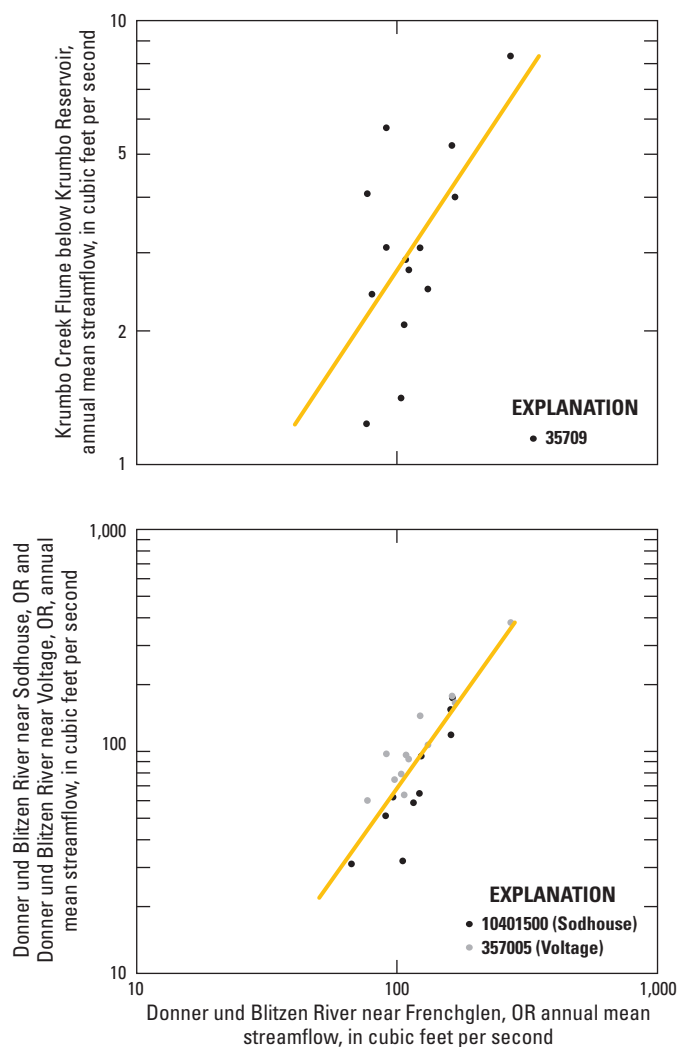
Figure 5.4. Annual (water year) mean streamflow in cubic feet per second and ordinary least-squares regression lines for sites of interest extended using the Donner und Blitzen River near Frenchglen, OR (streamgage 10396000), index site. Multiple sites at the same location are included in a single plot and are distinguished by streamgage site number (table 4.2). Regression equations are provided in table 4.2.

Appendix 6.   Instantaneous Low-Flow and Seepage Measurements from Selected Rivers and Streams in the Harney Basin, Southeastern Oregon

Stream seepage measurements were made on the Silvies River, Silver Creek, Poison Creek, and Rattlesnake Creek to identify changes in streamflow caused by groundwater seepage to or from streams during autumn 2017 (fig. 6.1; table 6.1). Additional seepage and instantaneous low-flow measurements were made during 2017–19 and compiled from measurements made during 1907–2016 for selected streams in the Harney Basin (table 6.1). Measured reaches indicate where streams transition from net gaining to net losing streams. Seepage results provide support for selected boundaries used to distinguish upland recharge areas from lowland recharge areas.
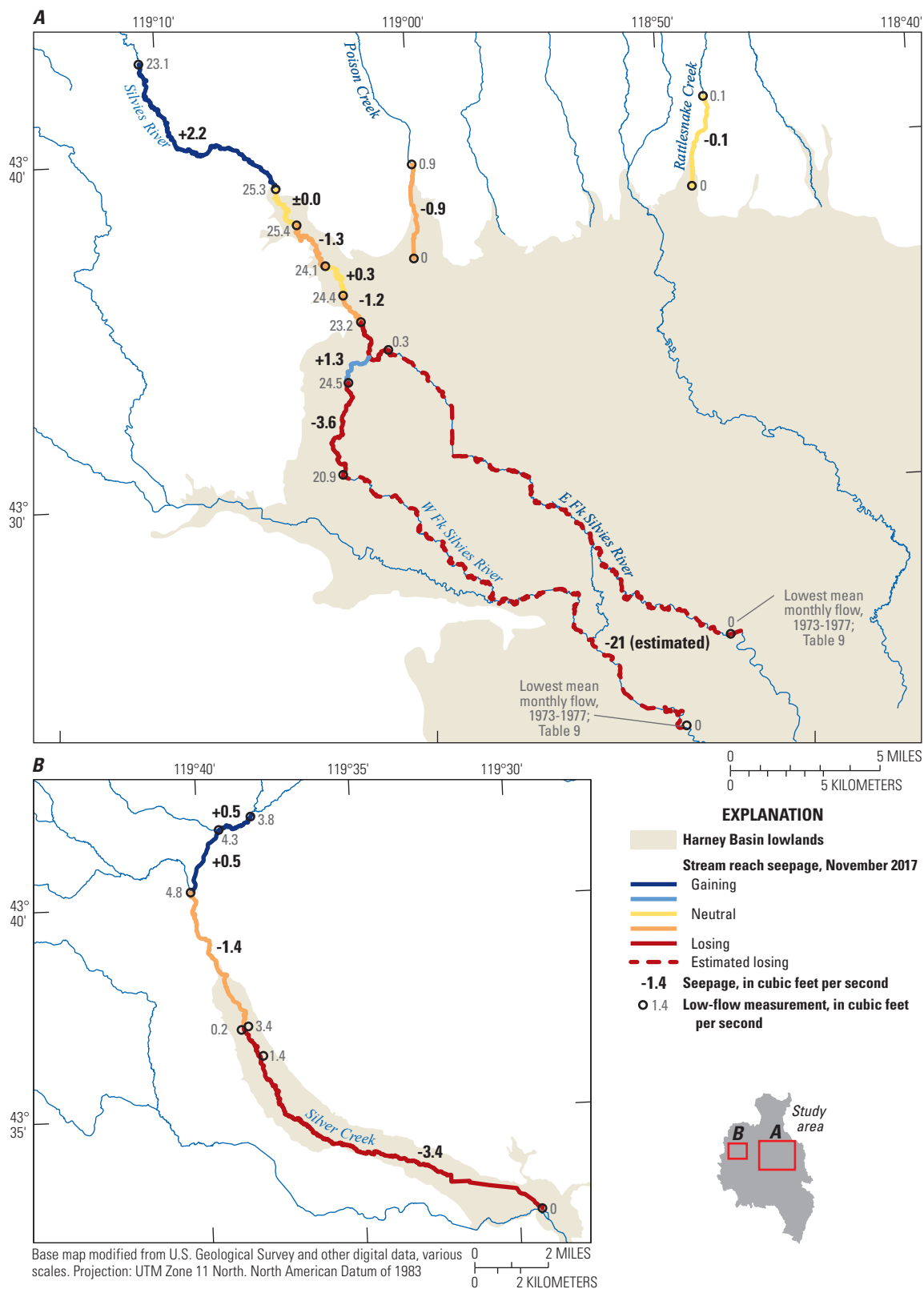
Figure 6.1. Streamflow measurements and locations during seepage runs along streams in (A) northern and (B) western regions of the Harney Basin, southeastern Oregon, 2017.

Table 6.1. Instantaneous low-flow measurements from selected streams in the Harney Basin, southeastern Oregon, 1907–2019.

[Low-flow measurements collected during August through early November in the Harney Basin by the USGS and OWRD. **Latitude and longitude:** Referenced to North American Datum of 1983. **Abbreviations:** ft³/s, cubic feet per second; mi, miles; No., number; OWRD, Oregon Water Resources Department; USGS, U.S. Geological Survey;—, not available]

Site name	USGS/OWRD site number	Latitude (decimal degrees)	Longitude (decimal degrees)	Mean low flow (ft³/s)	Number of measurements	Measurement period (years)
Booner Creek at Diamond Lane	—	43.00871	-118.68823	0.9	1	2018
Bridge Creek near Frenchglen, OR	10397000	42.843772	-118.8502	11.5	2	1907–2018
Cucamonga Creek at Diamond Lane near Diamond, OR	10399500	43.008593	-118.70008	0.0	1	2018
Donner und Blitzen River above Fish Creek	4245471185035000	42.762964	-118.84311	24.2	3	2018
Donner und Blitzen River above Indian Creek	4238151184539000	42.637425	-118.76077	9.9	3	2018
Donner und Blitzen River near Burnt Car Spring	4243251184959000	42.723742	-118.83307	20.9	3	2018
Donner und Blitzen River near Frenchglen, OR	10396000	42.790833	-118.8675	43.3	66	1984–2018
Donner und Blitzen River near Voltage, OR	10401500	43.251264	-118.85798	20.2	1	1978
East Fork Silver Creek above Dry Mountain Ranch near Riley, OR	—	43.618083	-119.63794	3.4	2	2017
East Fork Silver Creek at Dry Mountain Ranch near Riley, OR	—	43.608067	-119.63021	1.4	4	2017
East Fork Silvies River at Hwy 20 near Burns, OR	—	43.571621	-119.02007	0.3	1	2017
East Fork Silvies River near Lawen, OR	10395000	43.426361	-118.80219	0.3	13	1974–1980
East Kiger at Diamond Post Office near Diamond, OR	10399000	43.012233	-118.6685	1.3	1	2018
Emigrant Cr Blw Cricket Cr Nr Burns, OR		43.79821	-119.3063	11.6	1	2019
Fish Creek at Donner und Blitzen River confluence	4245511185032000	42.764072	-118.84232	1.9	3	2018
Indian Creek near Donner und Blitzen River confluence	4238301184532000	42.641803	-118.75899	4.1	3	2018
Kiger Creek at Ham Brown Lane near Diamond, OR	—	43.00869	-118.67203	0.4	1	2018
Kiger Creek near Diamond, OR	10399000	42.988582	-118.63765	2.7	1	2018
Little Blitzen River near Riddle Ranch	4240031184537000	42.66755	-118.76015	2.4	2	2018
McCoy Creek near Diamond, OR	10400000	42.983214	-118.7177	3.2	1	2018
Middle Ditch (or distributary of Trout Cr) at Hwy 395 crossing nr Silvies Valley Ranch	—	43.92315	-118.93245	0.0	1	2019
Mrtyle Cr blw FL Springs	—	43.89215	-119.11436	1.8	1	2019
Mrytle Creek abv Mouth Nr Burnt Mtn, OR	—	43.87437	-119.13361	2.0	1	2019
Mud Creek near Diamond, OR	10396500	42.831005	-118.85052	0.3	2	2018
Nicoll Creek near Riley, OR	—	43.67339	-119.67181	0.2	1	2017
Northern Ditch (or distributary of Trout Cr) at Hwy 395 crossing nr Silvies Valley Ranch	—	43.92497	-118.93244	0.0	1	2019
Poison Creek at HWY 395 near Burns, OR	434053119000700	43.681253	-119.00198	0.4	1	2018

Table 6.1. Instantaneous low-flow measurements from selected streams in the Harney Basin, southeastern Oregon, 1907–2019.—Continued

[Low-flow measurements collected during August through early November in the Harney Basin by the USGS and OWRD. **Latitude and longitude:** Referenced to North American Datum of 1983. **Abbreviations:** ft³/s, cubic feet per second; mi, miles; No, number; OWRD, Oregon Water Resources Department; USGS, U.S. Geological Survey;—, not available]

Site name	USGS/OWRD site number	Latitude (decimal degrees)	Longitude (decimal degrees)	Mean low flow (ft³/s)	Number of measurements	Measurement period (years)
Poison Creek below Gradon Canyon near Burns, OR	—	43.66071	-118.99863	0.9	1	2017
Rattlesnake Creek near Rattlesnake Rd	—	43.68684	-118.80256	0.1	1	2017
Riddle Cr at Coon Town Road Bridge nr Diamond OR	—	43.119291	-118.61132	1.0	1	2019
Riddle Cr blw Canyon and DS of Coon Town Road Bridge nr Diamond OR	—	43.12234	-118.62712	1.0	1	2019
Riddle Cr blw Dry Reservoir Lake at Diamond Craters Rd nr Diamond OR	—	43.130396	-118.65914	4.4	1	2019
Riddle Cr Feed Canal abv Dry Lake Reservoir nr Diamond OR	—	43.12963	-118.62854	0.8	1	2019
Riddle Cr secondary channel abv Dry Lake Reservoir nr Diamond, OR	—	43.128536	-118.63121	0.0	1	2019
Riddle Creek at Pete French Round Barn nr Diamond OR	—	43.133162	-118.64287	0.0	1	2019
Riddle Creek blw Feed Cn nr Diamond OR	—	43.122582	-118.628	0.0	1	2019
Rough Creek near Riley, OR	—	43.69618	-119.65512	0.2	2	2017
Silver Creek above Nicoll Creek near Riley, OR	—	43.67324	-119.67003	0.1	1	2017
Silver Creek above Rough Creek near Riley, OR	—	43.69632	-119.65487	4.3	2	2017
Silver Creek above Silver Creek Spring near Riley, OR	—	43.68275	-119.66661	0.1	2	2017
Silver Creek at Hwy 20 near Riley, OR	—	43.542141	-119.48785	0.0	1	2017
Silver Creek below Wickiup Creek near Riley, OR	—	43.7011	-119.63733	3.8	2	2017
Silvies River at Foley Road near Burns, OR	—	43.61353	-119.05932	24.1	2	2017
Silvies River at 5-mile Dam near Burns, OR	—	43.651833	-119.08989	25.3	5	2017
Silvies River at Hwy 20 near Burns, OR	—	43.59888	-119.04843	24.4	5	2017
Silvies River at Hwy 78 near Burns, OR	—	43.585697	-119.0374	23.2	1	2017
Silvies River at West Loop Road near Burns, OR	—	43.63393	-119.0771	25.4	2	2017
Silvies River near Burns, OR	10393500	43.715148	-119.17744	23.1	1	2017
Skull Creek above Slickear Creek confluence, approximately 2 mi above mouth	—	43.78866	-119.24287	1.5	1	2019
Slickear Creek	—	43.785427	-119.23982	0.0	1	2019
Southern Ditch (or distributary of Trout Cr) at Hwy 395 x-ing nr Silvies Valley Ranch)	—	43.917959	-118.93236	0.0	1	2019
Trout Cr at Hwy 395 crossing nr Silvies Valley Ranch	—	43.92032	-118.93252	0.9	1	2019
Trout Cr blw Roper Spring nr Silvies Valley Ranch	—	43.893166	-118.93169	1.0	1	2019

Table 6.1. Instantaneous low-flow measurements from selected streams in the Harney Basin, southeastern Oregon, 1907–2019.—Continued

[Low-flow measurements collected during August through early November in the Harney Basin by the USGS and OWRD. **Latitude and longitude:** Referenced to North American Datum of 1983. **Abbreviations:** ft³/s, cubic feet per second; mi, miles; No., number; OWRD, Oregon Water Resources Department; USGS, U.S. Geological Survey;—, not available]

Site name	USGS/OWRD site number	Latitude (decimal degrees)	Longitude (decimal degrees)	Mean low flow (ft³/s)	Number of measurements	Measurement period (years)
West Fork Silver Creek above Dry Mountain Ranch near Riley, OR	—	43.618856	-119.64557	0.2	1	2017
West Fork Silvies River at Greenhouse Lane near Burns, OR	—	43.512314	-119.05402	20.9	2	2017
West Fork Silvies River at Hotchkiss Lane near Burns, OR	—	43.55664	-119.04764	24.5	3	2017
West Fork Silvies River near Lawen, OR	10395500	43.383208	-118.83437	1.0	15	1972–1980
West Kiger Creek at Diamond Lane near Diamond, OR	—	43.008603	-118.67689	0.0	1	2018
Silver Creek below Nicoll Creek near Riley, OR	10403400	43.672113	-119.67145	4.8	1	2017

Appendix 7.   Soil-Water-Balance Recharge Model Inputs and Calibration Observations, Weights, and Parameter Estimation Details

Model Inputs

The Soil-Water Balance model (SWB) inputs included spatially distributed and tabular datasets. Spatially distributed inputs included GridMET daily precipitation and daily minimum and maximum air temperature, land-cover data, hydrologic soil group, and available soil-water capacity. Tabular data include parameters that control the water-balance calculations, including runoff curve numbers, maximum potential infiltration rates, rooting depths, and growing- and non-growing season-interception for each combination of land-use class and hydrologic soil type. For each model cell, spatial datasets were resampled to a 1-kilometer-square (0.62-mile [mi]) grid cell size and aligned and projected to a common grid cell for the SWB model.

Daily precipitation and maximum and minimum air temperature from January 1, 1981, to September 30, 2016, were assigned to each model cell and obtained from GridMET (Abatzoglou, 2013) (see app. 2 for more information about GridMET). Land-cover classification data were obtained from the Northwest ReGAP Ecological Systems map of Oregon (ORBIC, 2010). The 100-meter resolution land-cover dataset was clipped to the model extent and resampled to a 1-km-square (0.62-mi) cell size, yielding 24 land-cover classes (table 7.1).

Several land-cover classes were further distinguished to account for differing soil hydrologic and hydrogeologic properties (fig. 7.1; table 7.2). Western juniper was distinguished from the general evergreen forest land-cover class to allow for possible differences in understory, runoff, and infiltration properties. Possible effects of differing volcanic-rock permeability on recharge rates in areas with similar land-cover classes were accounted for by distinguishing land-cover classes in the southern region from northern and western regions. Regionally distinguished land-cover classes include western juniper, low sagebrush and alpine shrubland, big sagebrush shrubland, and sagebrush-bunchgrass steppe in the southern region. Finally, the four classes distinguished in the southern region were differentiated further in upland areas where mean-annual (1981–2010) PRISM precipitation equals or exceeds 20 inches (figs. 2, 7.1). The distinction based on precipitation was made to account for exposed and sparsely vegetated alpine areas on Steens Mountain where substantial snow sublimation is likely to occur.

Hydrologic soil groups and available water capacity data were obtained from the Natural Resources Conservation Service (NRCS) Soil Survey Geographic (SSURGO) database (Soil Survey Staff, 2018), where available. Areas without SSURGO data were filled with the general NRCS State Soil Geographic (STATSGO2) dataset (fig. 7.1; table 7.3). Raster soils data were clipped to the extent of the model and

resampled to the model 1-km-square (0.62-mi) grid size. Soils in SSURGO and STATSGO2 databases are classified into four hydrologic soil groups (A, B, C, and D), which range from group A soils that have a high-infiltration and low-runoff capacity to group D soils that have a low-infiltration and high-runoff capacity (fig. 7.1). SSURGO and STATSGO2 also specify the available water capacity, defined as the amount of water that the soil can hold for each soil series at several soil depths. For the model, the soil-depth weighted average SSURGO and STATSGO2 available water capacity was assigned to each 1-km grid cell (fig. 7.1). Maximum soil-water holding capacity is computed as the product of available water capacity and root-zone depth, where soil moisture exceeding this amount is converted to recharge.

For each unique land cover-hydrologic soil group combination, runoff-curve numbers, vegetation rooting depths, interception rates, and maximum daily recharge values were defined in a lookup table used by SWB. Initial runoff-curve numbers were obtained from the NRCS National Hydrology Handbook (Natural Resources Conservation Service, 2004) and Westenbroek and others (2010), and root-zone depths were obtained from Westenbroek and others (2010) and Tillman (2015). Initial maximum daily infiltration rates were obtained from Westenbroek and others (2010) and Trost and others (2018), and selected land cover-hydrologic soil group combinations in the southern region were adjusted during calibration.

Interception values were applied to mountainous areas in the southern region during the cool season to account for sublimation losses. Sublimation from snow in alpine and forested areas can remove a large fraction of winter precipitation. Previous studies have reported that snow sublimation in mountain catchments can range from about 10 to 20 percent in exposed and alpine areas (Reba and others, 2012; Sextone and others, 2018) and from 30 to 40 percent in forested areas (Pomeroy and Gray, 1995; Sextone and others, 2018). Although above-canopy eddy-covariance ET measurements used to calibrate SSEBop ET observations likely account for sublimation rates in snow-dominated areas of the Harney Basin (Molotch and others, 2007; Reba and others, 2012), ET measurements from alpine areas characteristic of the southern region were not available for ET calibration, therefore SSEBop ET observations likely do not adequately capture sublimation losses in the southern region (Sextone and others, 2018). Interception was not simulated in the SWB model for most land cover-hydrologic soil group combinations because ET observations were assumed to account for interception losses that do not ultimately reach land surface. In alpine areas in the southern region of the Harney Basin, where mean annual precipitation equals or exceeds 20 in, interception was used to account for assumed sublimation losses unaccounted

Table 7.1.   Distribution of land cover in the calibration basins and for the Harney Basin Soil-Water-Balance model domain.

[**Land-cover class**: Based on the 2010 Northwest ReGAP Ecological Systems map of Oregon (ORBIC, 2010), distinguished on Steens Mountain (Steens) and by precipitation rate where the 1981–2010 PRISM precipitation normal (PRISM Climate Group, 2018) equals or exceeds 20 inches per year. **Calibration watersheds**: Include watersheds 1, 4, 5, 6, 11, 22, and 23 shown in figure 11 and table 8. **Upland area**: Model areas between the Harney Basin boundary and the Harney Basin lowlands shown in figure 1]

Land-cover class	Land-cover description	Land-cover distribution (percent)			Difference between calibration watersheds and upland area (percent)
		Calibration watersheds	Upland area	Harney Basin	
111	Open water	0.03	0.05	0.39	-0.02
210	Developed (open space)	0.05	0.05	0.31	0.01
220	Developed (low intensity)	0.00	0.08	0.22	-0.08
230	Developed (medium intensity)	0.05	0.05	0.05	0.01
240	Developed (high intensity)	0.00	0.00	0.00	0.00
311	Playa	0.00	0.42	1.10	-0.42
5258	Salt desert scrub	0.00	0.15	0.60	-0.15
312	Cliff (canyon/volcanic rock/cinder land)	0.13	0.48	0.45	-0.35
313	Ash bed	0.00	0.00	0.02	0.00
314	Inland sand dune	0.00	0.02	0.04	-0.02
360	Recently burned	0.89	1.37	1.13	-0.48
410	Quaking aspen	3.57	1.44	1.14	2.14
420	Evergreen forest	41.84	15.84	12.59	26.00
4204	Western juniper	17.24	12.36	9.85	4.89
42040	Western juniper (Steens)	1.07	1.38	1.13	-0.31
42041	Western juniper (Steens [≥20 in precipitation])	7.33	4.83	3.84	2.49
430	Mixed forest	0.37	0.14	0.11	0.23
440	Harvested forest (tree regeneration)	0.00	0.00	0.00	0.00
510	Low sagebrush/subalpine shrubland	6.36	13.94	11.39	-7.57
5100	Low sagebrush/subalpine shrubland (Steens)	3.83	2.62	2.15	1.21
5101	Low sagebrush/subalpine shrubland (Steens [≥20 in precipitation])	1.82	0.95	0.76	0.87
520	Big sagebrush shrubland	0.65	11.73	10.83	-11.07
5200	Big sagebrush shrubland (Steens)	0.34	2.37	2.52	-2.04
5201	Big sagebrush shrubland (Steens [≥20 in precipitation])	0.83	0.34	0.27	0.49
530	Grassland steppe (foothill-canyon shrubland/mountain mahogany)	3.42	1.53	1.36	1.89
540	Sagebrush (bunchgrass steppe)	4.83	17.88	16.00	-13.06
5400	Sagebrush (bunchgrass steppe—Steens	0.99	5.55	4.97	-4.56
5401	Sagebrush (bunchgrass steppe—Steens [≥20 in precipitation])	3.07	2.06	1.64	1.01
710	Foothill (canyon/semi-desert/montane—alpine/subalpine grassland)	1.02	0.79	0.63	0.23
720	Introduced upland vegetation (annual and perennial grassland)	0.10	0.11	0.36	-0.01
810	Agriculture (hay/pasture)	0.05	0.85	7.11	-0.80
820	Agriculture (irrigated)	0.08	0.18	0.52	-0.10
916	Lowland (foothill, montane, or subalpine riparian)	0.05	0.02	0.01	0.03
920	Freshwater mudflat (alkaline wetland/arid land marsh)	0.00	0.44	6.50	-0.44

A

B

C

D
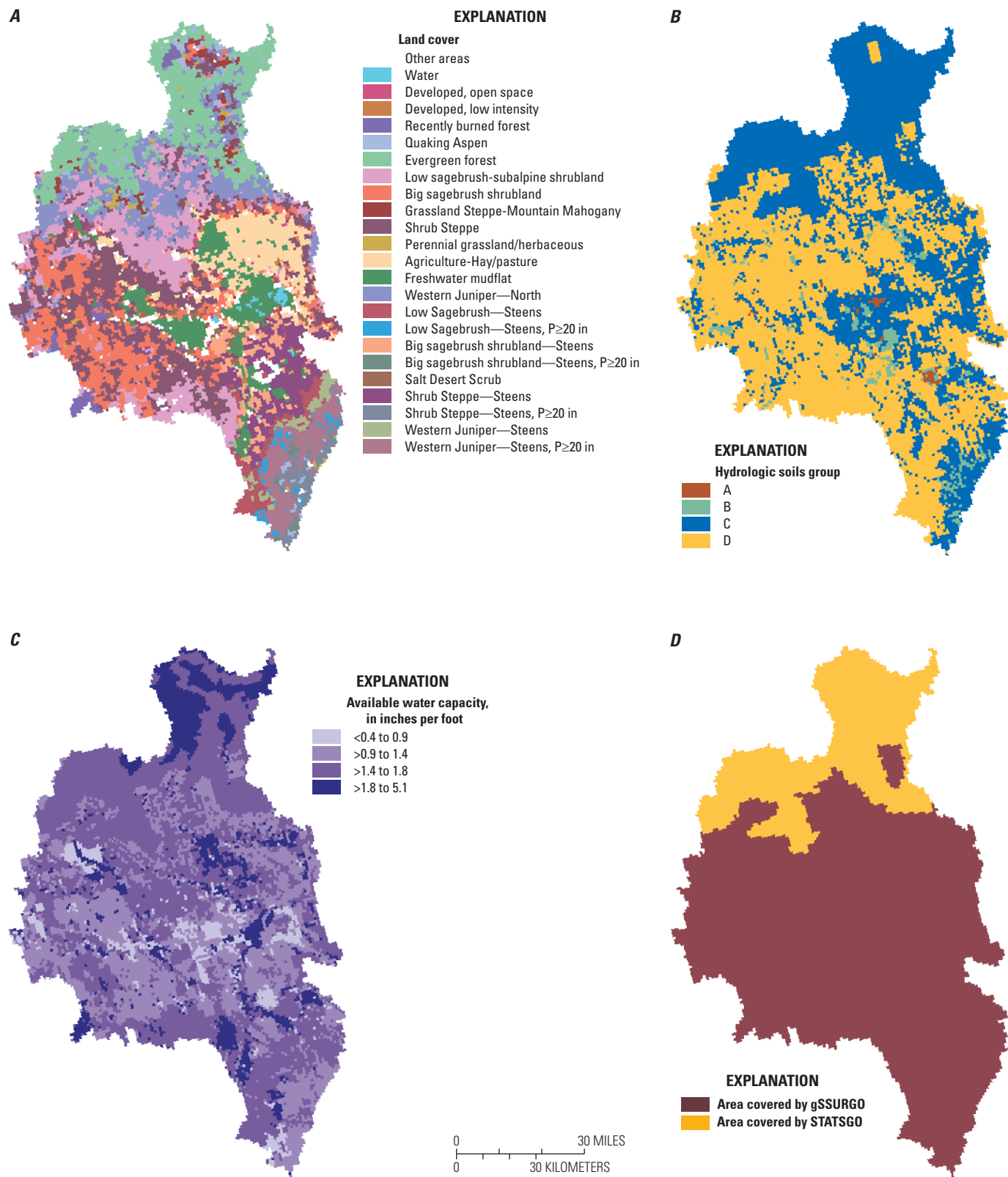
Figure 7.1.   Distribution of (*A*) land cover, (*B*) hydrologic soils group, and (*C*) available water capacity, along with (*D*) the coverage extent of USDA gSSURGO and STATSGO2 soils-information datasets in the Harney Basin, southeastern Oregon. Land cover includes classes representing more than one percent of the Harney Basin. Land cover distinguished between Steens Mountain and other areas, and on Steens Mountain where annual precipitation (P) equals or exceeds 20 inches.

Table 7.2. Calibrated Soil-Water-Balance model lookup table corresponding land cover to runoff curve number (by hydrologic soil group), maximum recharge rate (by hydrologic soil group), interception storage (dormant season), and root-zone depth (by hydrologic soil group).

[Land cover and hydrologic soil group distributions are shown in figure 7.1. Hydrologic soil groups include A–D (table 7.3). **Dormant season interception:** Represents unaccounted for snow loss through sublimation or wind redistribution out of the basin. **Abbreviations:** NA, not applicable]

Land-cover class	Land-cover description	Assumed imperviousness (percent)	Curve number				Maximum recharge rate (inches per day)				Growing season interception	Dormant season interception	Root zone depth (feet)			
			A	B	C	D	A	B	C	D	(inches per day)		A	B	C	D
111	Open water	NA	100	100	100	100	0.0	0.0	0.0	0.00	0	0	0	0	0	0
210	Developed (open space)	NA	49	69	79	84	4.0	1.5	0.5	0.25	0	0	3.0	3.0	1.5	1.0
220	Developed (low intensity)	30	70	80	87	92	4.0	1.5	0.5	0.25	0	0	3.0	3.0	1.5	1.0
230	Developed (medium intensity)	60	82	90	95	97	4.0	1.5	0.5	0.25	0	0	3.0	3.0	1.5	1.0
240	Developed (high intensity)	90	89	92	94	97	4.0	1.5	0.5	0.25	0	0	3.0	3.0	1.5	1.0
311	Playa	NA	90	93	95	96	4.0	1.5	0.5	0.25	0	0	1.0	1.0	1.0	1.0
5258	Salt desert scrub	NA	55	72	81	86	4.0	1.5	0.5	0.25	0	0	10.0	10.0	10.0	10.0
312	Cliff (canyon/volcanic rock/cinder land)	NA	90	93	95	96	4.0	1.5	0.5	0.25	0	0	1.0	1.0	1.0	1.0
313	Ash bed	NA	90	93	95	96	4.0	1.5	0.5	0.25	0	0	1.0	1.0	1.0	1.0
314	Inland sand dune	NA	90	93	95	96	4.0	1.5	0.5	0.25	0	0	1.0	1.0	1.0	1.0
360	Recently burned	NA	90	93	95	96	4.0	1.5	0.5	0.25	0	0	1.0	1.0	1.0	1.0
410	Quaking aspen	NA	48	48	74	75	4.0	1.5	0.5	0.25	0	0	3.0	2.5	4.79	1.01
420	Evergreen forest	NA	55	65	92	96	4.0	1.5	0.5	0.25	0	0	3.0	2.5	5.99	4.39
4204	Western juniper	NA	55	65	84	86	4.0	1.5	0.5	0.25	0	0	3.0	2.5	1.02	1.44
42040	Western juniper (Steens)	NA	55	65	72	95	4.0	1.5	0.5	1.46	0	0	3.0	2.5	0.64	1.75
42041	Western juniper (Steens [≥20 in precipitation])	NA	55	65	74	97	4.0	1.5	0.5	1.46	0	0.105	3.0	2.5	0.64	1.75
430	Mixed forest	NA	55	65	75	61	4.0	1.5	0.5	0.25	0	0	3.0	2.5	1.5	1.0
440	Harvested forest (tree) regeneration	NA	55	65	70	75	4.0	1.5	0.5	0.25	0	0	3.0	2.5	1.5	1.0
510	Low sagebrush/subalpine shrubland	NA	50	55	68	88	4.0	1.5	0.5	0.25	0	0	3.0	2.5	3.43	4.4
5100	Low sagebrush/subalpine shrubland (Steens)	NA	50	55	76	93	4.0	1.5	0.5	1.50	0	0	3.0	2.5	0.79	0.25
5101	Low sagebrush/subalpine shrubland (Steens [≥20 in precipitation])	NA	50	55	76	93	4.0	1.5	0.5	1.50	0	0.105	3.0	2.5	0.79	0.25
520	Big sagebrush shrubland	NA	55	77	95	96	4.0	1.5	0.5	0.25	0	0	5.0	5.0	5.0	1.0
5200	Big sagebrush shrubland (Steens)	NA	40	50	60	75	4.0	1.5	0.5	0.25	0	0	5.0	5.0	2.0	1.0
5201	Big sagebrush shrubland (Steens [≥20 in precipitation])	NA	40	50	60	75	4.0	1.5	0.5	0.25	0	0.105	5.0	5.0	2.0	1.0

Table 7.2. Calibrated Soil-Water-Balance model lookup table corresponding land cover to runoff curve number (by hydrologic soil group), maximum recharge rate (by hydrologic soil group), interception storage (dormant season), and root-zone depth (by hydrologic soil group).—Continued

[Land cover and hydrologic soil group distributions are shown in figure 7.1. Hydrologic soil groups include A–D (table 7.3). **Dormant season interception:** Represents unaccounted for snow loss through sublimation or wind redistribution out of the basin. **Abbreviations**: NA, not applicable]

Land-cover class	Land-cover description	Assumed imperviousness (percent)	Curve number				Maximum recharge rate (inches per day)				Growing season interception	Dormant season interception	Root zone depth (feet)			
			A	B	C	D	A	B	C	D	(inches per day)		A	B	C	D
530	Grassland steppe (foothill-canyon shrubland/mountain mahogany)	NA	50	55	60	65	4.0	1.5	0.5	0.25	0	0	3.0	2.0	1.5	1.0
540	Sagebrush (bunchgrass steppe)	NA	55	77	95	96	4.0	1.5	0.5	0.25	0	0	3.0	2.0	3.68	2.8
5400	Sagebrush (bunchgrass) steppe (Steens)	NA	55	77	84	88	4.0	1.5	0.5	0.25	0	0	3.0	2.0	1.2	5.6
5401	Sagebrush (bunchgrass) steppe (Steens [≥20 in precipitation])	NA	55	77	86	90	4.0	1.5	0.5	0.25	0	0.105	3.0	2.0	1.2	5.6
710	Foothill (canyon/semi-desert/montane - alpine/subalpine grassland)	NA	39	50	60	70	4.0	1.5	0.5	0.25	0	0	3.0	2.0	1.5	1.0
720	Introduced upland vegetation (annual and perennial grassland)	NA	39	50	60	70	4.0	1.5	0.5	0.25	0	0	3.0	2.0	1.5	1.0
810	Agriculture (hay/pasture)	NA	49	69	79	84	4.0	1.5	0.5	0.25	0	0	3.0	2.0	1.5	1.0
820	Agriculture (irrigated)	NA	49	69	79	84	4.0	1.5	0.5	0.25	0	0	3.0	2.0	1.5	1.0
916	Lowland (foothill, montane, or subalpine riparian)	NA	60	60	60	60	4.0	1.5	0.5	0.25	0	0	3.0	2.0	1.5	1.0
920	Freshwater mudflat (alkaline wetland/arid land marsh)	NA	60	60	60	60	4.0	1.5	0.5	0.25	0	0	3.0	2.0	1.5	1.0

Table 7.3.   Hydrologic soil groups used in the Harney Basin Soil-Water-Balance model.

[**Hydrologic soil group**: Distribution is shown on figure 7.1. **Percentage of upland area**: Upland area represents model areas between the Harney Basin boundary and the Harney Basin lowlands shown in figure 1]

Soil Group Number	Hydrologic soil group	Description	Percentage of Harney Basin	Percentage of upland area
1	A	Low runoff potential when wet; water is transmitted freely though the soil	0.5	0.4
2	B	Moderately low runoff potential when wet; water transmission is unimpeded	3.4	3.0
3	C	Moderately high runoff potential when wet; water transmission is somewhat restricted	43.2	42.9
4	D	High runoff potential when wet; water movement is restricted	51.6	53.7
0	Water	Open water; no runoff	1.3	0.0

for in ET observations. Interception values were specified during the non-growing season only and are about 30 percent of winter precipitation. Interception is simulated with a bucket-model approach in SWB where a specified amount of precipitation is intercepted each day that precipitation occurs (Westenbroek and others, 2010). The amount of interception applied to each grid cell within the applicable sublimation area (0.105 in/d) is an average of 30 percent of winter precipitation during 1982–2016. Final calibrated parameters are presented in table 7.2.

Model Calibration

Runoff and Base-flow Observations

Runoff and base-flow observations were compiled for water years 1982–2016 for comparison with SWB-simulated runoff and recharge. Observations made during water years 2001–16 were used for automated calibration, and those made during 1982–2000 were used for validation. Annual water-year base flow was estimated as the mean of lowest monthly flow within the year and total BFI base flow, and runoff was estimated as the difference between total water-year streamflow and mean base flow (see section "Methods for Estimating Groundwater Discharge to Streams").

Runoff and base-flow observations were compiled from six watersheds during the calibration period (watersheds 1, 4, 6, 7, 11, 22, and 23; fig. 11; table 9) and two watersheds during the validation period (watersheds 1 and 4; fig. 11). Six of the seven watersheds are predominantly unregulated; observations from the regulated watershed (7) were given a low weight and used for comparison with other nearby watersheds. Watersheds ranged in size from 30 to 934 square miles (table 7). Observations used for model calibration and validation totaled 101 for annual runoff and 100 for annual base flow.
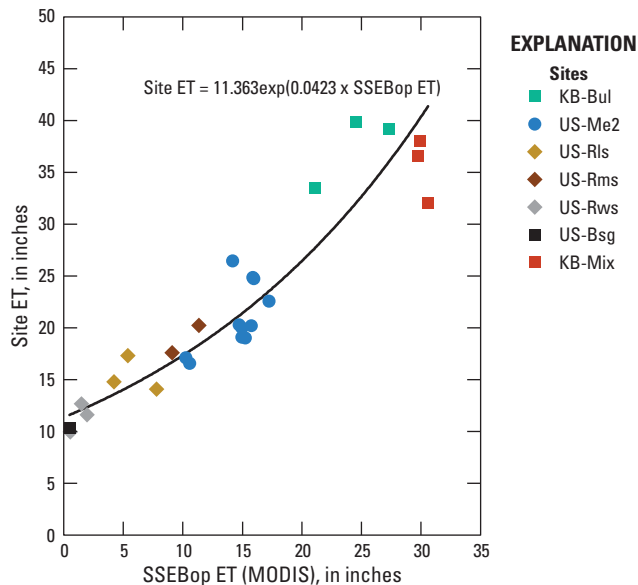
Evapotranspiration Observations

Annual water-year ET observations were computed from 1-km-resolution (0.62-mi) operational Simplified Surface Energy Balance (SSEBop) ET datasets (Senay and others, 2013) calibrated to site-based ET measurements made in Oregon and Idaho for similar land-cover types (table 7.4). The SSEBop ET datasets computed from MODIS (Moderate Resolution Imaging Spectroradiometer) imagery were compiled monthly from January 2000 through September 2017 and summed to compute annual water-year and calendar-year ET datasets. Annual calendar-year SSEBop datasets were related to 26 site years of measurements using an exponential relation (fig. 7.2), and the relation was applied to water-year ET datasets to compute ET observations for SWB calibration. To maximize the number of site-years available, calendar years, rather than water years, were used for site-SSEBop comparisons. The final ET observations represent total ET from all water sources including precipitation and snowmelt, and groundwater and surface water if any.

Site-based eddy-covariance ET measurements were compiled over 26 site years using data from five AmeriFlux and two USGS sites. Sites included two marsh sites measured over 6 site years in Klamath Basin, Oregon (Stannard and others, 2013), one pine forest site measured over 11 years in Metolius, Oregon (Law, 2002), and four shrubland sites measured over 9 site years in the Harney Basin, Oregon (B. Law, Oregon State University, written commun., 2018), and the Reynolds Creek Critical Zone Observatory Cooperative, Idaho (Flerchinger, 2014a,b,c) (table 7.4). AmeriFlux site measurements contained considerable gaps during winter months and days with 48 half-hour measurements within a year ranged from 250 to 365. Gaps in daily ET were filled using a simplified approach; daily ET gaps were assigned values equal to mean daily ET within the same month. Mean daily ET within a month was computed using days with 48 half-hour measurements only. Gap-filled daily ET datasets were summed over the calendar year for comparison with SSEBop ET datasets (table 7.4).

Table 7.4.   Measured and remotely sensed SSEBop evapotranspiration at seven eddy-covariance sites in Oregon and Idaho, 2002–17.

[**Latitude and longitude**: Referenced to the North American Datum of 1983. **Elevation**: Referenced to the North American Vertical Datum of 1988. **ET**: Sum of daily eddy-covariance evapotranspiration measurements within the calendar year. **Days measured**: Number of days with ET measurements per calendar year. *ETc*: Annual evapotranspiration gapfilled using linear extrapolation of monthly mean values; *ETc* is equal to ET when 365 days were measured within a year. **Source**: 1, Law (Oregon State University, written commun., 2018); 2, Law (2002); 3, Flerchinger (2014a); 4, Flerchinger (2014c); 6, Stannard and others (2013). **Abbreviations**: ET, evapotranspiration; MODIS, Moderate Resolution Imaging Spectroradiometer; SSEBop, 1-km MODIS-based operational Simplified Surface-Energy Balance ET (Senay and others, 2013)]

Site	Vegetation type	Latitude (decimal degrees)	Longitude (decimal degrees)	Elevation (feet)	Calendar year	ET measured (inches)	Days measured	*ETc* (inches)	SSEBop ET (inches)	Source
US-Bsg	Sagebrush	43.4712	-119.6909	4,587	2014	10.28	365	10.28	0.47	1
US-Me2	Mature ponderosa pine	44.4523	-121.5574	4,111	2002	15.95	322	17.12	10.24	2
					2004	17.21	295	20.00	14.96	
					2005	13.09	274	16.57	10.55	
					2009	21.35	284	24.75	15.94	
					2010	21.06	286	24.87	15.87	
					2012	21.63	283	26.44	14.17	
					2013	15.76	304	19.10	14.96	
					2014	16.77	251	22.58	17.24	
					2015	17.44	327	19.04	15.24	
					2016	20.00	357	20.19	15.75	
					2017	20.00	350	20.29	14.72	
US-Rls	Low sagebrush	43.1439	-116.7356	5,276	2016	12.85	307	14.79	4.21	3
					2017	15.44	305	17.32	5.39	
					2018	12.65	251	14.06	7.80	
US-Rms	Mountain big sagebrush	43.0645	-116.7486	6,926	2016	14.63	254	17.60	9.09	4
					2017	17.43	264	20.23	11.34	
US-Rws	Wyoming big sagebrush	43.167545	-116.713205	4,675	2015	9.34	259	11.60	1.97	5
					2016	7.26	292	9.94	0.55	
					2017	10.80	297	12.67	1.50	
KB-Bul	Bulrush	42.513578	-122.034692	4,140	2008	39.17	365	39.17	27.28	6
					2009	39.88	365	39.88	24.53	
					2010	33.46	365	33.46	21.10	
KB-Mix	Bulrush, cattail, wocus	42.476889	-122.068347	4,141	2008	38.03	365	38.03	29.92	6
					2009	36.57	365	36.57	29.76	
					2010	32.05	365	32.05	30.59	

Figure 7.2. Relation between measured and remotely sensed SSEBop evapotranspiration (ET) at seven eddy-covariance sites in Oregon and Idaho, 2002–17. Site information is provided in table 7.4. Abbreviations include SSEBop, operational simplified surface energy balance model and MODIS, Moderate Resolution Imaging Spectroradiometer.

Annual site-based ET was considerably higher than 1-km (0.62-mi) MODIS-based SSEBop ET and accuracy in SSEBop ET degraded with decreasing vegetation density and increasing water limitations. At marsh sites (KB-Bul and KB-Mix), site-based ET was about 1.4 times SSEBop-ET estimates, whereas in sagebrush shrubland areas site-based ET was about 7 times SSEBop-ET estimates (fig. 7.2; table 7.4). Substantial underestimation of SSEBop ET in shrubland areas could be from the large differences in spatial resolution or in SSEBop input datasets. Regardless, calibrated SSEBop ET provides a substantially more reliable dataset to use for calibration of the SWB model, especially since the Harney Basin recharge area is largely comprised of sagebrush land cover (fig. 7.1).

Snow-Water Equivalent Observations

Continuous daily precipitation, air temperature, and SWE data were compiled for Rock Springs SNOTEL site in the northern region and Fish Creek SNOTEL site in the southern region. Continuous daily precipitation, air temperature, and SWE data were compiled for Rock Springs SNOTEL site in the northern region and Fish Creek SNOTEL site in the southern region for water years 2011–16 to evaluate the volume and timing of SWB-simulated snowpack and snowmelt. The Rock Springs site (fig. 2) is within the Silvies River

near Burns watershed (watershed 1; fig. 11), where streamflow measurements have been ongoing since 1904. Similarly, the Fish Creek site is within the Donner und Blitzen River near Frenchglen watershed (watershed 4; fig. 11), where continuous streamflow data has been collected since 1939. Daily SWE and streamflow measurements were summarized into monthly observations and used to manually calibrate the SWB model during water years 2011–16. SWB-simulated SWE data were extracted from the 1-km-resolution (0.62-mi) model cells intersecting SNOTEL sites and simulated streamflow was summarized over watersheds corresponding with streamflow measurements. Monthly rather than daily data were used to evaluate snowmelt and runoff to compensate for the timing of snowmelt to travel across the watershed from SNOTEL sites to downgradient streamgages. Differences in snow accumulation measured by snow pillows at SNOTEL sites and computed with measured precipitation and air temperature measurements (as is done by SWB) were evaluated.

Parameter Estimation

Parameter estimation was done using manual and automated methods. Parameters were manually adjusted to match simulated to observed SWE time series during 2011–16 and improve comparisons between mean-annual (1982–2016) simulated recharge and estimated natural groundwater discharge. Automated calibration using the Parameter ESTimation (PEST) software (Doherty and Hunt, 2010) was used to fit simulated and observed runoff and ET and ensure that simulated recharge was equal to or exceeded base-flow estimates.

Weights were assigned to each of the observations used for automatically evaluating model fit. The "observation groups" including runoff, ET, and base flow were weighted so that effects on the overall objective function varied. The objective function is the sum of the weighted squared differences between simulated recharge and observed base flow and simulated and observed runoff and ET values in inches per year over the basin. The weights were assigned so that the initial combined total sum of squares from observations were nearly equal among basins. Within each basin, runoff observations were weighted highest and base-flow observations were generally weighted lowest. In the northern region ET observations were weighted lowest of the three observation groups because precipitation inputs were insufficient to match runoff, base-flow, and ET observations (see section "Model Fit"). Weights were adjusted iteratively so all observation groups affected model calibration to a preferred level. Mismatches in scatter plots of simulated recharge and observed base flow and simulated and observed runoff and ET; spatial distributions of associated residuals, and hydrographs of runoff, ET, recharge, and base flow informed relative importance of observations on model calibration.

A total of 51 parameters were adjusted during varying calibration periods from 2001 to 2016 to fit simulated to observed time-series datasets. Of the 51 adjusted parameters, 1 was a global parameter that affected recharge computations in every active model cell and 50 were parameters applied to specific combinations of land cover-hydrologic soil group combinations. The global parameter is the snowmelt index that controls the amount of snowpack that melts when air temperature exceeds the freezing point (Westenbroek and others, 2010). Additional calibration parameters include curve number, maximum daily recharge, rooting depth, and interception values in the SWB lookup table.

A 15-year calibration period (water years 2001–16) was selected to coincide with the largest streamflow and ET observation dataset. A 21-month model initialization period from January 1999 to September 2000 was completed prior to calibration to stabilize soil-moisture and snow-cover conditions that were initialized at 100 percent cover. The SWB model simulated 1982–2016 using parameters calibrated to time-series data during 2001–16 and parameters were further modified following comparison between mean-annual regionally simulated recharge and estimated natural groundwater discharge. The SWB then simulated 1982–2016 using the final calibrated parameters to estimate upland recharge across the Harney Basin.

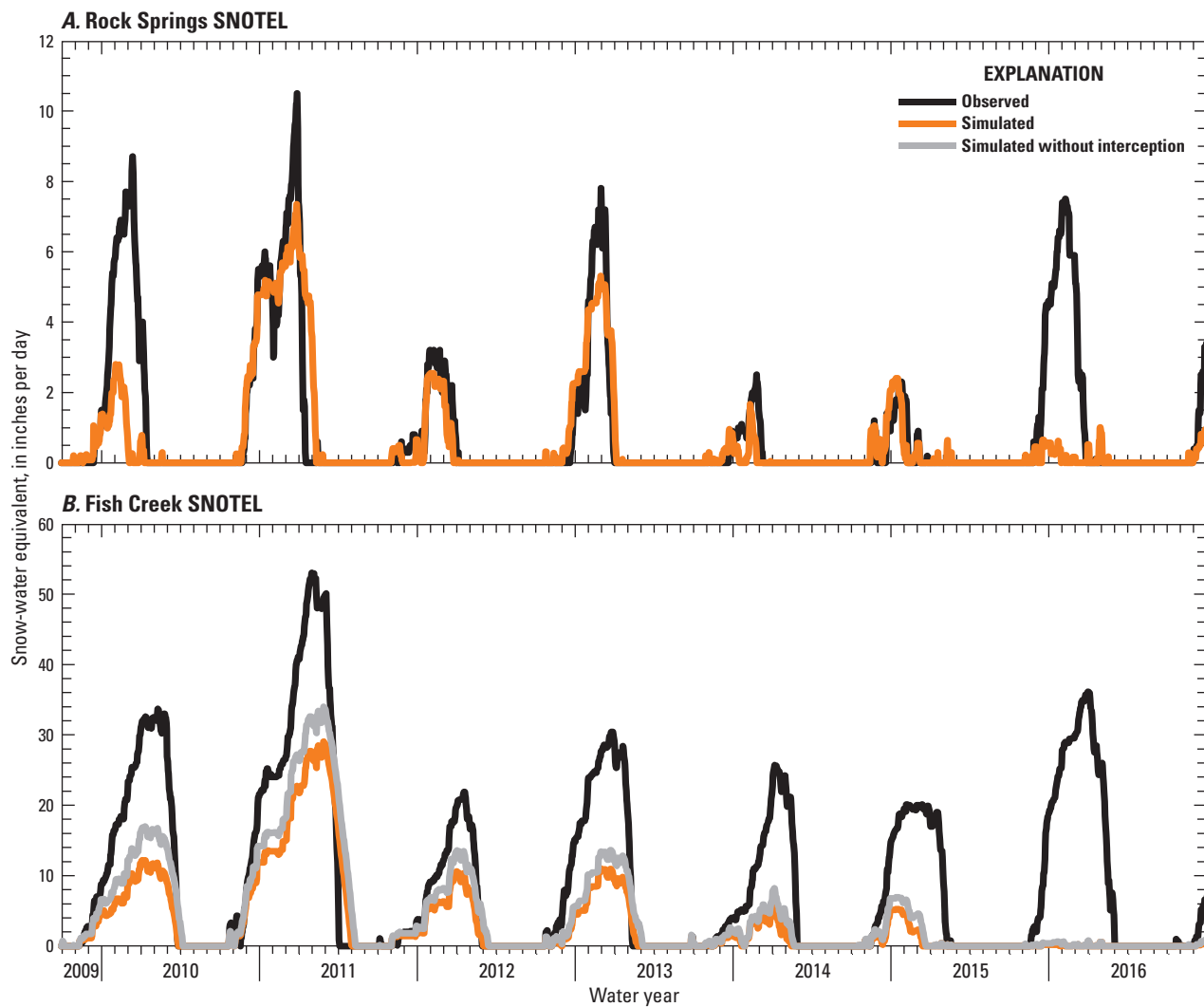# Model Fit—Comparison to Snow-Water-Equivalent Observations

Data from two SNOTEL sites were used to guide the calibration of the runoff and snowpack accumulation in the SWB model: Rock Springs SNOTEL site in the northern region and Fish Creek SNOTEL site in the southern region of the Harney Basin (fig. 2; table 1). The best fit between timing of snowpack accumulation, SWE magnitude, and runoff was achieved using an index value of 0.026 in (0.65 mm; fig. 7.3).

This value was reduced from the default value of 0.059 in (1.5 mm) to better match the measured data and represents a compromise. As the fit between simulated and observed SWE magnitude improved, the lag between observed and simulated snowmelt runoff increased to the point where the simulated snowpack never completely melted.

Differences between simulated and observed SWE (fig. 7.3) could reflect differences in scale between point measurements and the 1-square-kilometer (0.62-mi^2) model grid cells, but most likely are related to the simplified representation of the complex physics controlling snowpack accumulation and melt in the SWB model. For example, in SWB, precipitation falls as snow when the snow factor (the sum of daily minimum temperature and two-thirds the difference between daily maximum and minimum temperature) is below 32 °F (Westenbroek and others, 2010). If the SWB snow factor equation is applied to daily precipitation and temperature measured at Rock Springs and Fish Creek SNOTEL, about half of the days with a measured increase in SWE correspond with a snow factor above 32 °F. Therefore, the SWB snow factor equation in Westenbroek and others (2010) could, in part, be a limiting factor when simulating snowpack accumulation and melt.

In addition to limitations inherent in the SWB model, the precipitation measurements used to produce GridMET (and other gridded climate datasets) might contain data discrepancies in snow-dominated areas. For example, although measured daily precipitation and cool temperatures (below 50 °F) at Rock Springs and Fish Creek sites were nearly equal to 4-kilometer estimates from GridMET during 1982–2016, discrepancies between the measured daily accumulations of SWE and precipitation during winter months of water years 2010–16 were observed at Rock Springs and Fish Creek SNOTEL sites. The comparison indicates that GridMET accurately represents the measured precipitation and temperature at these sites, but an issue with internal consistency in the measurements from the SNOTEL sites themselves might be propagated into the GridMET data.

Figure 7.3. Comparison of measured and Soil-Water-Balance model simulated snow-water equivalent at two SNOTEL sites in (*A*) northern and (*B*) southern regions of the Harney Basin, southeastern Oregon.

References Cited

Abatzoglou, J.T., 2013, Development of gridded surface meteorological data for ecological applications and modelling: International Journal of Climatology, v. 33, no. 1, p. 121–131.

Flerchinger, G., 2014a, AmeriFlux US-Rls RCEW low sagebrush: U.S. Department of Agriculture Agricultural Research Service, accessed October 24, 2019, at https://doi.org/10.17190/AMF/1418682.

Flerchinger, G., 2014b, AmeriFlux US-Rms RCEW mountain big sagebrush: U.S. Department of Agriculture Agricultural Research Service, accessed October 24, 2019, at https://doi.org/10.17190/AMF/1375202.

Flerchinger, G., 2014c, AmeriFlux US-Rws RCEW Wyoming big sagebrush: U.S. Department of Agriculture Agricultural Research Service, accessed October 24, 2019, at https://doi.org/10.17190/AMF/1375201.

Law, B., 2002, AmeriFlux US-Me2 Metolius mature ponderosa pine, accessed October 24, 2019, at https://doi.org/10.17190/AMF/1246076.

Molotch, N.P., Blanken, P.D., Williams, M.W., Turnipseed, A.A., Monson, R.K., and Margulis, S.A., 2007, Estimating sublimation of intercepted and sub-canopy snow using eddy covariance systems: Hydrological Processes, v. 21, no. 12, p. 1567–1575.

ORBIC (Oregon Biodiversity Information Center), 2010, Ecological systems map of Oregon: Oregon Biodiversity Information Center, accessed November 19, 2021 at https://spatialdata.oregonexplorer.info/geoportal/details;id=776e6118422b429c8c3024f289f9f192.

Pomeroy, J.W., and Gray, D.M., 1995, Snow accumulation, relocation and management—National Hydrology Research Institute Science Rep. 7, Saskatchewan, Canada: Saskatoon, Environment Canada.

Reba, M.L., Pomeroy, J., Marks, D., and Link, T.E., 2012, Estimating surface sublimation losses from snowpacks in a mountain catchment using eddy covariance and turbulent transfer calculations: Hydrological Processes, v. 26, no. 24, p. 3699–3711.

Senay, G.B., Bohms, S., Singh, R.K., Gowda, P.H., Velpuri, N.M., Alemu, H., and Verdin, J.P., 2013, Operational Evapotranspiration Mapping Using Remote Sensing and Weather Datasets—A New Parameterization for the SSEB Approach: Journal of the American Water Resources Association, v. 49, no. 3, p. 577–591.

Sexstone, G.A., Clow, D.W., Fassnacht, S.R., Liston, G.E., Hiemstra, C.A., Knowles, J.F., and Penn, C.A., 2018, Snow Sublimation in Mountain Environments and Its Sensitivity to Forest Disturbance and Climate Warming: Water Resources Research, v. 54, no. 2, p. 1191–1211.

Soil Survey Staff, Natural Resources Conservation Service, United States Department of Agriculture, Soil Survey Geographic (SSURGO) Database, accessed March 29, 2018, at https://sdmdataaccess.sc.egov.usda.gov.

Stannard, D.I., Gannett, M.W., Polette, D.J., Cameron, J.M., Waibel, M.S., and Spears, J.M., 2013, Evapotranspiration from wetland and open-water sites at Upper Klamath Lake, Oregon, 2008–2010: U.S. Geological Survey Scientific Investigations Report 2013–5014, 66 p. [Also available at https://pubs.usgs.gov/sir/2013/5014/.]

Tillman, F.D., 2015, Documentation of input datasets for the soil-water balance groundwater recharge model of the Upper Colorado River Basin: U.S. Geological Survey Open-File Report 2015–1160, 17 p. [Also available at https://doi.org/10.3133/ofr20151160.]

Trost, J.J., Roth, J.L., Westenbroek, S.M., and Reeves, H.W., 2018, Simulation of potential groundwater recharge for the glacial aquifer system east of the Rocky Mountains, 1980–2011, using the Soil-Water-Balance model: U.S. Geological Survey Scientific Investigations Report 2018–5080, 51 p. [Also available at https://doi.org/10.3133/sir20185080.]

Westenbroek, S.M., Kelson, V.A., Dripps, W.R., Hunt, R.J., and Bradbury, K.R., 2010, SWB—A modified Thornthwaite-Mather Soil-Water-Balance code for estimating groundwater recharge: U.S. Geological Survey Techniques and Methods 6–A31, 60 p. [Also available at https://pubs.usgs.gov/tm/tm6-a31/.]